

2014-01-30

Energy Efficient Bipedal Locomotion

Hasaneini, Seyed Javad

Hasaneini, S. J. (2014). Energy Efficient Bipedal Locomotion (Doctoral thesis, University of Calgary, Calgary, Canada). Retrieved from <https://prism.ucalgary.ca>. doi:10.11575/PRISM/25886
<http://hdl.handle.net/11023/1351>

Downloaded from PRISM Repository, University of Calgary

UNIVERSITY OF CALGARY

Energy Efficient Bipedal Locomotion

by

Seyed Javad Hasaneini

A THESIS

SUBMITTED TO THE FACULTY OF GRADUATE STUDIES
IN PARTIAL FULFILLMENT OF THE REQUIREMENTS FOR THE
DEGREE OF DOCTOR OF PHILOSOPHY

DEPARTMENT OF ELECTRICAL AND COMPUTER ENGINEERING

CALGARY, ALBERTA

January, 2014

© Seyed Javad Hasaneini 2014

Abstract

In this research, dynamic optimization of a minimally constrained bipedal model (free to exhibit almost any arbitrary gait) is used to find the characteristics of energy efficient gaits. I find that using a work-based cost yields gait optimization that automatically predicts many features of human locomotion. This includes the optimality of walking and running at their respective speeds. The results show the determinant energetic factors are: (i) the cost of stance-leg work to make up for energy loss during downward-to-upward redirection of body motion at each step; and (ii) the cost to move the swing leg forward and prepare it for support transfer. To minimize the net energetic cost, the calculations discover various strategies. For energy-effective walking the critical control actions are identified as: (i) a burst extension force along the support leg just before heel-strike; (ii) a burst hip torque at the start of leg-swing to accelerate the swing leg motion; and (iii) a decelerating burst torque at the end of swing to reduce foot velocity at landing, leading to less energy loss at support transfer between the legs. The burst hip torques at the beginning and end of the swing phase are also used in energy-efficient running. However, exploiting an extension force before heel-strike is not possible in running as there is no support leg during flight. Instead, energy-loss at heel-strike can be minimized by landing on a near-vertical leg.

Swing-leg retraction in walking is also investigated in depth. The approach focuses on simple closed-form analytic solutions. The three principal control actions identified in my gait optimizations are replaced by impulsive forces and torques. With this simplified model it was shown analytically that: (i) it is energetically favorable to delay the retracting hip torque until the end of the pre-emptive push-off; (ii) swing-leg retraction torque reduces the push-off force; and also (iii) increases the maximum possible walking speed; and (iv) the energetic advantage of active swing-leg retraction depends on the step length, average walking speed, ratio of actuator efficiencies for positive and negative work, and percentage

of active work done during heel-strike.

Acknowledgements

First and foremost, I must thank God, the Most Gracious and the Most Merciful, for giving me the opportunity to live, the ability to think, and guiding me throughout my life.

I would like to thank my parents, my mother Akhtar Pirsyavash and my father Seyed Kazem Hasaneini, for their love, support, encouragement, care, and for letting me find my own way.

I am deeply indebted to my lovely and beautiful wife, Zahra Ghadimi, for her constant love, joy, patience, and support. She kindly took care of all household chores since the first day of our marriage, and provided a nice atmosphere at home so I could focus on my work. Without her I would have never taken the opportunity to come to Calgary for my PhD. I will never forget the days and nights she worked part-time to support the family, while I was a PhD student and did not have a work permit.

Thanks to my lovely daughter, Seyedeh Fatemeh Hasaneini, for her joy and patience. She always shares her joy with me, and provides me relief from the pressures of work.

My sincere gratitude to my supervisor, Dr. Chris Macnab, and my co-supervisors, Dr. John Bertram and Dr. Henry Leung, for giving me the opportunity to study at the University of Calgary and supporting me throughout my thesis. My special thanks to Dr. Macnab for not giving me complete freedom to work whenever, wherever, and on whatever I would like.

Two people have been very influential in my PhD program: my co-supervisor Dr. John Bertram (Faculty of Medicine, University of Calgary), and Prof. Andy Ruina (Cornell University, USA). I owe them a great deal of thanks for all the support they have provided me. Most of the ideas and techniques in this thesis have been inspired by them. Dr. Bertram supported me throughout my PhD program. He has always kindly offered me his help, support, and encouragement. He introduced me to Andy Ruina, and provided me funding to

visit Ruina's Lab in Cornell University for six months. Although Andy Ruina did not have any official role in my program, he was always available for help and discussion. On many occasions he spent his personal time with me via videoconference discussing or editing my papers for several hours at a time, even during weekends or until midnight. He even paid \$600 per year out of his pocket just to provide me the opportunity to remotely participate in his Lab's weekly meetings via videoconference. He edited my papers, posters, and my NSERC application, and treated me like one of his own students.

I learned the fundamentals of effective numerical optimization from Dr. Manoj Srinivasan during a lunch date, when I was introduced to him and Andy Ruina by Dr. John Bertram. The techniques that Manoj taught me during that historic lunch and his reading recommendation (Practical Methods for Optimal Control Using Nonlinear Programming, by John Betts) had a substantial impact on my progress.

I could not have completed my research without the support of all these wonderful people!

Table of Contents

| | |
|--|-----------|
| Abstract | ii |
| Acknowledgements | iv |
| Table of Contents | vi |
| List of Tables | xii |
| List of Figures | xiii |
| List of Symbols | xxii |
| List of Abbreviations | xxxvi |
| 1 INTRODUCTION | 1 |
| 1.1 Objective of This Thesis | 2 |
| 1.2 Review of the Relevant Literature | 2 |
| 1.2.1 Minimalistic Models for Legged Locomotion | 2 |
| 1.2.2 Inverted Pendulum Model | 3 |
| 1.2.3 Spring-Mass Model | 4 |
| 1.2.4 Inverted Pendulum-Based Simple Model | 4 |
| 1.3 Swing-Leg Retraction | 10 |
| 1.4 Problems Studied in This Thesis | 16 |
| 1.5 Acknowledgement and Permission for Reproduction of the Text | 17 |
| 1.6 Thesis Outline | 18 |
| 2 A DYNAMIC OPTIMIZATION FRAMEWORK TO STUDY LEGGED LO- COMOTION | 20 |
| 2.1 Biped and Gait Model | 20 |
| 2.1.1 Details of the Gaits | 22 |
| 2.1.2 Energetic Cost of the Gait | 23 |
| 2.2 Mathematical Description of the Biped | 25 |
| 2.2.1 Equations of Motion of the Unpinned Biped | 26 |
| 2.2.2 Single-Support Phase | 27 |
| 2.2.3 Double-Support Phase | 28 |
| 2.2.4 Flight Phase | 29 |
| 2.2.5 Touch-Down Map | 29 |
| 2.3 Optimal Control Problem | 32 |
| 2.3.1 Constraints | 32 |

| | | |
|-------|--|----|
| 2.3.2 | Numerical Optimization | 35 |
| 2.4 | Summary | 37 |
| 3 | ENERGY-OPTIMAL GAITS OF THE MINIMALLY CONSTRAINED BIPEDAL MODEL | 39 |
| 3.1 | Optimization and Simulation Parameters | 39 |
| 3.2 | Optimal Continuous-Support Gait | 42 |
| 3.2.1 | Optimal Continuous-Support Gait on Level-Ground | 44 |
| 3.2.2 | Optimal Continuous-Support Gait to Climb Ramps or Staircases | 47 |
| 3.2.3 | Optimal Continuous-Support Gaits for Stepping Down the Ramps or Staircases | 50 |
| 3.3 | Optimal Intermittent-Support Gait | 52 |
| 3.4 | Discussion | 56 |
| 3.4.1 | General Characteristics of the Optimal Gaits | 56 |
| 3.4.2 | Comparison of Optimization Generated Gaits and Normal Human Gaits | 59 |
| 3.4.3 | Walking and Running; Different Solutions of the Same Problem | 61 |
| 3.4.4 | Determinant Factors in Effective Legged Locomotion | 62 |
| 3.4.5 | Applications to Understanding Human Locomotion | 64 |
| 3.5 | Summary | 64 |
| 4 | WALKING AND RUNNING IN REDUCED GRAVITY | 66 |
| 4.1 | Reduced Gravity Effects on Human Gait Energetics | 66 |
| 4.2 | Predictions of the Minimally Constrained Bipedal Model | 69 |
| 4.2.1 | Predictions of Gait Energetics | 69 |
| 4.2.2 | Gait Kinematics | 70 |
| 4.3 | Discussion | 72 |
| 4.3.1 | Energy Storage and Recovery Is Helpful, But Not Determinant | 72 |
| 4.3.2 | An Alternate Perspective | 73 |
| 4.4 | Summary | 75 |
| 5 | A SIMPLE BIPEDAL MODEL TO STUDY SWING-LEG RETRACTION | 76 |
| 5.1 | Bipedal Model | 77 |
| 5.1.1 | Some Mathematical Properties of the Model | 79 |
| 5.2 | Energy-Optimal Gaits | 80 |
| 5.2.1 | Observations of Energy Optimal Gaits | 81 |
| 5.2.2 | Simplification to Impulsive Forces and Torques | 82 |
| 5.2.3 | Parameterization by Impulses | 83 |

| | | |
|-------|---|-----|
| 5.2.4 | Impulsive Heel-Strike and Instantaneous Support Transfer | 83 |
| 5.2.5 | Gait Cycle | 84 |
| 5.3 | Details of The Dynamics | 86 |
| 5.3.1 | Continuous Dynamics | 87 |
| 5.3.2 | Impulsive Transitions | 90 |
| 5.4 | Periodic Walking | 95 |
| 5.4.1 | Periodic Gait as a Cyclic Sequence of Discrete Velocity Transitions | 95 |
| 5.4.2 | Periodicity Restricts the Actuator Impulses | 96 |
| 5.4.3 | Maximum Retraction Impulse | 97 |
| 5.4.4 | Admissible Combinations of Step Length and Speed | 97 |
| 5.5 | Summary | 101 |
| 6 | ENERGETICS OF IMPULSIVE WALKING GAITS | 103 |
| 6.1 | Work-Based Energetic Cost of Step | 103 |
| 6.2 | Energetic Cost of Isolated Impulsive Swing Thrust Torque | 105 |
| 6.3 | Energetic Cost of Impulsive Push-off Force and Retraction Torque | 106 |
| 6.3.1 | Net Swing-Leg Retraction Work | 107 |
| 6.3.2 | Positive and Negative Swing-Retracton Work | 110 |
| 6.3.3 | Net Push-Off Work | 111 |
| 6.3.4 | Positive and Negative Push-Off Work | 112 |
| 6.3.5 | Energetic Cost of Impulsive Push-Off and Swing-Leg Retraction | 112 |
| 6.4 | Optimal Relative Timing of Impulsive Push-off and Retraction | 113 |
| 6.4.1 | Range of Overlap Parameter for a Non-Contracting Stance Leg | 114 |
| 6.4.2 | Optimal Overlap Parameter for Gaits With a Non-Contracting Stance Leg | 115 |
| 6.4.3 | Optimal Overlap Parameter With Leg Contraction Allowed | 121 |
| 6.4.4 | Optimal Relative Timing of Impulsive Push-off and Retraction | 128 |
| 6.4.5 | Intuitive Justification of the Optimal Relative Timing | 129 |
| 6.4.6 | Generality of the Optimal Relative Timing Result | 130 |
| 6.4.7 | Application for Practical Non-Impulsive Systems | 131 |
| 6.5 | Energy Optimal Swing Retraction Impulse | 132 |
| 6.6 | Summary | 135 |
| 7 | APPROXIMATE ANALYTIC ANALYSIS OF THE IMPULSIVE WALKING MODEL | 137 |
| 7.1 | Small-Leg Mass Approximation | 138 |

| | | |
|-------|--|-----|
| 7.2 | Approximate Dynamics in Passive Single Stance | 139 |
| 7.3 | Approximate Analytic Solution of Passive Single Stance | 141 |
| 7.3.1 | Stance Leg Motion | 141 |
| 7.3.2 | Swing Leg Motion | 142 |
| 7.4 | Approximate Swing-Thrust and Push-Off Impulses | 145 |
| 7.5 | Approximate Minimum and Maximum Retraction Impulse | 147 |
| 7.5.1 | Ensuring Heel-Strike and the Minimum Required Retraction Impulse | 147 |
| 7.5.2 | Approximate Maximum Allowed Retraction Impulse | 148 |
| 7.6 | Approximate Condition for Instantaneous Support Transfer | 149 |
| 7.7 | Approximate Admissible Region | 150 |
| 7.7.1 | Approximate Minimum Allowed Average Walking Speed | 150 |
| 7.7.2 | Approximate GRF-Based Maximum Average Walking Speed | 151 |
| 7.7.3 | Approximate Admissible Region | 152 |
| 7.7.4 | Approximate Maximum Walking Step Angle | 153 |
| 7.8 | Approximate Velocities Before and After the Impulsive Actions | 154 |
| 7.8.1 | Approximate Angular Rates Before and After the Impulsive Swing- Thrust Torque | 154 |
| 7.8.2 | Approximate Velocities Before and After the Impulsive Push-Off Force | 155 |
| 7.8.3 | Approximate Velocities Before and After the Impulsive Retraction Torque | 156 |
| 7.9 | Approximate Work and Energetic Costs | 157 |
| 7.9.1 | Approximate Work and Energetic Cost of Impulsive Swing Thrust Torque | 158 |
| 7.9.2 | Approximate Work and Energetic Cost of Impulsive Push-Off Force . | 158 |
| 7.9.3 | Approximate Work and Energetic Cost of Impulsive Swing Retraction Torque | 159 |
| 7.10 | Extensional Retraction Torque Is Not Energetically Efficient in the Admissible Region | 160 |
| 7.11 | Approximate Energy Optimal Swing-Retracton Impulse | 162 |
| 7.12 | Approximate Energy-Optimal Swing Retraction Rates | 167 |
| 7.13 | Summary | 168 |
| 8 | ADVANTAGES OF SWING-LEG RETRACTION | 169 |
| 8.1 | Less Push-Off Force Is Required With Swing-Leg Retraction | 170 |
| 8.2 | Swing-Leg Retraction Enables Faster Walking Speeds and Shorter Steps . . . | 173 |
| 8.3 | Does Swing-Leg Retraction Reduce the Net Energetic Cost of Walking? . . . | 175 |

| | | |
|-------|---|-----|
| 8.3.1 | Energy-Optimal Retraction Impulse | 175 |
| 8.3.2 | Energy-Optimal Retraction Rates | 181 |
| 8.3.3 | Effect of Doing Active Negative Work During Heel-strike | 181 |
| 8.3.4 | Swing Retraction Can Reduce the Net Energetic Cost of Walking | 186 |
| 8.4 | Summary | 187 |
| 9 | CONCLUSIONS | 189 |
| 9.1 | Insights From Energy-Optimal Gaits of a Minimally Constrained Model | 189 |
| 9.2 | Swing-Leg Retraction | 193 |
| 9.3 | Future Works | 196 |
| 9.3.1 | Gait Optimization with More Realistic Models: | 196 |
| 9.3.2 | Experimental Verification of Model Predictions: | 196 |
| 9.3.3 | Energy-Efficient Closed-Loop Control: | 197 |
| | Bibliography | 199 |
| A | Equations of Motion of the Biped With Torso | 209 |
| A.1 | Equations of Motion of the Unpinned Biped | 209 |
| A.1.1 | Inertia Matrix | 209 |
| A.1.2 | Coriolis, Centrifugal, and Gravity Vector | 209 |
| A.1.3 | Jacobian Matrices | 210 |
| A.1.4 | Torque-Influence Matrix | 210 |
| A.2 | Equations of Motion in Single Support Phase | 210 |
| A.2.1 | Mass-Inertia Matrix | 211 |
| A.2.2 | Coriolis, Centrifugal, and Gravity Vector | 211 |
| A.2.3 | Torque-Influence Matrix | 212 |
| A.3 | Equations of Motion in Double-Support Phase | 212 |
| A.3.1 | Mass-Inertia Matrix | 213 |
| A.3.2 | Coriolis, Centrifugal, and Gravity Vector | 214 |
| A.3.3 | Torque-Influence Matrix | 215 |
| A.4 | Equations of Motion in Flight Phase | 215 |
| A.4.1 | Coriolis and Centrifugal Vector | 215 |
| A.4.2 | Torque-Influence Matrix | 216 |
| A.5 | Jacobian Matrices | 216 |
| B | Simple Bipedal Model Without Torso | 218 |
| B.1 | Details of the Dynamics | 218 |

| | | |
|-------|---|-----|
| B.1.1 | Equations of Motion in Passive Single Stance | 218 |
| B.1.2 | Velocity Mapping of Impulsive Push-off and Retraction | 218 |
| B.1.3 | Heel-Strike Velocity Map | 221 |
| B.1.4 | Swing Thrust Velocity Map | 223 |
| B.2 | Required Swing-Thrust and Push-Off Impulse for Periodic Walking | 223 |
| C | Copyright Permissions | 224 |

List of Tables

| | | |
|-----|---|----|
| 3.1 | Model Parameters for the Biped in Fig. 2.1 | 40 |
| 3.2 | Simulation and Optimization Constants | 41 |
| 5.1 | Model Parameter Values of The Biped in Fig. 5.1 | 78 |

List of Figures and Illustrations

| | | |
|-----|---|----|
| 1.1 | Simple mechanical models of the stance phase in walking and running. a) Inverted pendulum model, b) Spring-mass model, also known as the spring-loaded inverted pendulum (SLIP) model. In both models the body is reduced to a point mass m at the center of mass. In the inverted pendulum model the CoM is supported by a massless rigid leg, whereas in the SLIP model it is supported by a massless spring. | 3 |
| 1.2 | Rimless wheel. Gravity compensates for collision loss, and the rimless wheel exhibits a steady downhill ‘walking’. | 6 |
| 1.3 | Synthetic wheel rolls forward just like an ordinary wheel. The radius of the semi-circular feet is equal to the stance-leg length. The swing leg (solid thick red) swings forward to ‘synthesize’ a continuous rim. For clarity, the swing leg (solid thick red) has been plotted slightly shorter than the stance (dashed thin black) leg. | 6 |
| 1.4 | Passive dynamic walking model. If the radius of the feet is smaller than the leg length or the foot arc is not long enough to synthesize a continuous rim, collision loss occurs at each heel-strike, and the biped cannot exhibit a passive gait on level ground. If the biped is launched with proper initial conditions on a shallow slope, gravity can compensate for the heel-strike collision loss, and the walking gait will converge to a stable limit cycle. | 7 |
| 1.5 | Simplest walking model; an irreducibly simple bipedal model that exhibits stable passive walking on a shallow ramp. | 8 |
| 1.6 | The stabilizing effect of swing-leg retraction in walking. Swing-leg retraction starts at a fixed time in the step cycle, <i>e.g.</i> Δt after mid-swing. With a retraction strategy, the step length will be a decreasing function of the step period (or retraction period). a) If the biped is perturbed to go faster than nominal, heel-strike will occur earlier-than-nominal, and the shorter-than-nominal retraction time will cause the swing leg take a longer-than-nominal step. This longer step causes more collisional dissipation, which with the nominal push-off force (energy input) results in a slowing towards the nominal gait. b) If the biped is disturbed to walk slower than nominal, the longer retraction time causes a reduced step length, a smaller collisional dissipation, and thus a speeding of the biped to return toward its nominal gait. | 13 |
| 2.1 | The biped model with torso. The legs and the torso have distributed mass, with their center of mass, G_{leg} and G_{trs} , located b and a distances from the hips. Feet are massless and always stay parallel to the ground. Thus the ankle actuators can apply torque only when the feet are on the ground. Each legs is equipped with a telescoping actuator that can change the leg length. The lower part of the legs, between the telescoping actuators and the feet, are massless. | 21 |

| | | |
|-----|---|----|
| 2.2 | Biped on different terrains. Panel (a) shows different forces and torques acting on the biped. Panels (b)-(d) show different terrains with the associated reference frames. Panel (e) shows the force components associated with leg _i for i=1,2. $F_{\text{leg}_{1a}}$ and $F_{\text{leg}_{2a}}$ are the leg actuator forces along each leg, while $F_{\text{leg}_{1p}}$ and $F_{\text{leg}_{2p}}$ are the constraint forces perpendicular to each leg. | 25 |
| 2.3 | Multiple shooting method and the defects at interval borders. Each phase of the motion is divided into a few intervals. The state variables on interval borders are determined by optimization <i>via</i> an iterative process. At each iteration, the optimization procedure uses the current value of the state variables at interval borders, <i>e.g.</i> y_k , and y_{k+1} , to integrate the equations of motion over the subsequent interval. The differences between the resulting states at the end of each segment and the states at the beginning of the next, <i>e.g.</i> $\hat{y}_{k+1} - y_{k+1}$, are called the defects. Constraining defects to be zero guarantees state continuity at interval borders. | 36 |
| 3.1 | Leg forces in double support phase. Leg force profiles for two steps of a sample continuous-support gait with no axial impulsive leg force, $T_{\text{ds},\text{min}} = 10\% T$, $N_{\text{ds}} = 3$, and $N_{\text{ss}} = 7$. The dashed and solid vertical lines indicate the touch-down (TD) and toe-off (TO) instants, respectively. | 43 |
| 3.2 | Stick diagram and gait parameters of two steps of the optimal level-ground continuous-support gait generated for $V = 1.38$ m/s with instantaneous DS. Axial impulsive GRFs are <i>not</i> allowed. In the first step, leg ₁ (the solid blue lines in 3.2a) is the stance leg. In 3.2a the asterisks indicate the CoM position. The dashed vertical lines in 3.2b-3.2g indicate the TD instant. In 3.2e the subscripts <i>axial</i> and <i>perp</i> denote the foot velocity components along and perpendicular to the corresponding leg. In 3.2f the stance leg's axial force ($F_{\text{leg}_{1a}}$ and $F_{\text{leg}_{2a}}$) and GRFs in normal and tangential directions (F_{F1x} and F_{F1y}) are all scaled with body weight $m_{\text{tot}} g$. Note that foot scuffing can be avoided by decreasing the length of the swing leg's massless portion. | 45 |
| 3.3 | Stick diagram and gait parameters of two consecutive steps of the optimal uphill continuous-support gait generated for $\gamma = 10^\circ$, and $V = 0.9$ m/s. DS is instantaneous, and unbounded axial leg forces at TD are allowed. In the first step leg ₁ (the solid blue lines in 3.3a) is the stance leg. The asterisks in 3.3a indicate the CoM position. The dashed vertical lines in 3.3b-3.3g indicate the TD instant. In 3.3e the subscripts <i>axial</i> and <i>perp</i> denote the foot velocity components along and perpendicular to the corresponding leg. In 3.3f the stance leg's axial force ($F_{\text{leg}_{1a}}$ and $F_{\text{leg}_{2a}}$) and GRFs in normal and tangential directions (F_{F1x} and F_{F1y}) are all scaled with body weight $m_{\text{tot}} g$. Also the arrows in 3.3f represent the GRF impulses at TD. | 49 |

| | | |
|-----|--|----|
| 3.4 | <p>Two consecutive steps of the optimal downstairs continuous-support gait generated for $H_{\text{step}} = -10$ cm and $L_{\text{step}} = 50$ cm. Other conditions are similar to Fig. 3.3. In the first step leg₁ (the solid blue lines in 3.4a) is the stance leg. The asterisks in 3.4a indicate the CoM position. The dashed vertical lines in 3.4b-3.4g indicate the TD instant. In 3.4e the subscripts <i>axial</i> and <i>perp</i> denote the foot velocity components along and perpendicular to the corresponding leg. In 3.4f the stance leg’s axial force ($F_{\text{leg}_{1a}}$ and $F_{\text{leg}_{2a}}$) and GRFs in normal and tangential directions (F_{F1x} and F_{F1y}) are all scaled with body weight $m_{\text{tot}} g$. Also the arrows in 3.4f represent the GRF impulses at TD.</p> | 51 |
| 3.5 | <p>Two consecutive steps of the optimal intermittent-support gait on level ground generated for $V = 5$ m/s. Unbounded axial leg forces at TD are allowed. In the first step leg₁ (the solid blue lines in 3.5a) is the stance leg. The asterisks in 3.5a indicate the CoM position. The dashed black and solid green vertical lines in 3.5b-3.5g denote the touch-down (TD) and take-off (TK) instants, respectively. In 3.5e the subscripts <i>axial</i> and <i>perp</i> denote the foot velocity components along and perpendicular to the corresponding leg. In 3.5f the stance leg’s axial force ($F_{\text{leg}_{1a}}$ and $F_{\text{leg}_{2a}}$) and GRFs in normal and tangential directions (F_{F1x} and F_{F1y}) are all scaled with body weight $m_{\text{tot}} g$. Also the arrows in 3.5f represent the GRF impulses at TD.</p> | 53 |
| 4.1 | <p>Reduced gravity apparatus used by Farley and McMahon [87]. It consists of “a series of springs (Sp), which applied a nearly constant upward force to the body through a bicycle saddle (S). Magnitude of force was increased by stretching springs with a winch (W). Motorized treadmill included a strain gauge force platform (F) under the tread”. The figure and the quoted text are reproduced from [87] with permission.</p> | 67 |
| 4.2 | <p>Dimensional metabolic cost of transport (DMet-COT) of walking and running in partially reduced gravity conditions (<i>i.e.</i> reduced effective gravity only on the CoM), measured by Farley and McMahon [87]. They calculated the DMet-COT (in the original work it is called the cost of transport) as the net metabolic energy consumption per unit body mass and unit distance travelled. As the figure shows, the DMet-COT in running declines with decreases in gravity faster than in walking.</p> | 68 |
| 4.3 | <p>Dimensional mechanical cost of transport (DMec-COT) of energy-optimal gaits of the model. The optimal gaits were obtained by minimizing the mechanical COT \mathcal{C}_{mt} (see Section 2.1.2) for given speed V and gravity level g_{red}. DMec-COT was then calculated from $\mathcal{C}_{\text{mt}} g_{\text{red}}$. No curve fitting is used in this figure (lines connect the raw data points), but for more clarity some of data points are not marked. The gait optimization correctly predicts the cost trends of human gaits shown in Fig. 4.2.</p> | 69 |

| | | |
|-----|---|----|
| 4.4 | Step length changes with gravity , as predicted by energy-optimal gaits of the minimally constrained bipedal model presented in Chapter 2. For both walking and running, step length increases with reduced gravity, but the changes for running are substantially greater than for walking. The red line (running) corresponds to the $1/g_{\text{red}}$ trend, where g_{red} is the reduced gravity acceleration. The step length data in this figure correspond to the optimal gaits in Fig. 4.3. For more clarity, the results for walking at the other speeds used in Fig. 4.3 are not shown. | 71 |
| 5.1 | Biped model without torso . Two rigid legs with lengths ℓ and distributed mass m_{leg} . The leg center of mass is at G_{leg} located at distance b from the hip. The leg moment of inertia about the hip is $I_{\text{leg/H}} = \delta m_{\text{leg}} \ell b$. A point mass at the hip m_{H} represents the upper body. There is a motor at the hip applying torque τ between the legs, and a prismatic actuator that extends and applies push-off force F along the stance leg. | 77 |
| 5.2 | A single gait cycle . The initial swing leg is <i>thick</i> red, the initial stance leg is <i>thin</i> black. The four phases of one walking step are as follows. a) Just after the thick leg has lifted from the ground at toe-off, the impulsive <i>swing thrust</i> \mathcal{S} starts the swing with proper initial swing velocity; b) The passive swing of the thick leg continues until $\phi = 2\alpha$. During passive swing the thin leg's extension actuator (not shown) is locked; c) Then, nearly simultaneously the <i>thin</i> black leg has an impulsive push-off \mathcal{P} and the hip has an impulsive swing retraction \mathcal{R} . The thin leg's extension actuator is unlocked only at this phase; Finally, immediately after retraction and push-off, d) the thick leg collides with the ground with a sticking (heel-strike) collision. | 84 |
| 5.3 | Four phases of a gait cycle . The phase and the leg labelings are in accordance with Fig. 5.2. 'thick' = swing leg, 'thin' = stance leg. | 85 |
| 5.4 | Labels of the time instants between the phases . In phase (c) the impulsive push-off and retraction can have any (specified) order or overlap. | 86 |
| 5.5 | Symmetric and asymmetric solutions of passive swing . The three numerical solutions of the hip angle ϕ for $V = 1$ m/s and $\alpha = 40^\circ$. For the sake of visibility, the stance leg angle is not plotted here. One of the solutions (thin green) is symmetric and the other two (thick red and dashed blue) are asymmetric but cross-symmetric with each other. | 89 |

| | | | |
|-----|--|--|-----|
| 5.6 | Contour lines of the normalized angular rates at both ends of the symmetric passive swing | for some range of step angle and average walking speed. Panel (a) represents the stance-leg angular rate, and panel (b) represents the hip-joint angular rate. In both panels, angular velocities are normalized relative to $\omega_n = V_n/\ell$, where V_n is the GRF-based maximum walking speed at $\alpha = 0$ and is defined in (5.36). This maximum speed is also used to normalize the vertical axis. For the numerical values used for this figure (Table 5.1) $V_n = 3.18$ m/s, and $\omega_n = 3.53$ rad/s. Above the dashed line no walking is feasible without a pull from the ground (the gait switches to a run on non-sticking surfaces). The shaded region represents the ‘admissible region’, defined in Section 5.4.4. This region constitutes the parameter space and is the focus of this study. Panel (b) shows that the hip rate is positive (extending) for all α and V inside the admissible region. | 90 |
| 5.7 | Velocity transitions in a periodic gait cycle. | A gait cycle can be considered as a sequence of continuous and impulsive phases (blue arrows). This phase sequence can be replaced with a sequence of <i>discrete</i> velocity transitions (black circles) relating the velocities at the beginning of each phase to the velocities at the end of that phase (the beginning of the next phase). The velocity mapping of phase (a) is given by (5.23), and of phase (b) is given by (5.12) and (5.13). Equation (5.14) corresponds to the velocity mapping of phase (c), while (5.19) and (5.22) give the velocities at the end of phase (d). The symmetry in this figure does not imply the symmetry of the gait, though the passive swing is considered to be symmetric. | 96 |
| 5.8 | Admissible region. | The shaded region corresponds to the <i>admissible combinations of step angle and speed</i> . Above this region, walking is not feasible as the calculated centripetal GRF during passive swing becomes negative, which requires an unrealistic sucking foot-ground contact to avoid a flight. Below the shaded region the swing-thrust impulse is applied backwards (pushes the swing leg backward) opposite to that seen in human-like gaits. The lower boundary of the region is set by (5.29), and the upper boundary is calculated using (5.31). The vertical axis is normalized relative to $V_n = V_{\max}(0)$, which is the GRF-based maximum walking speed at $\alpha = 0$, defined in (5.36). For the numerical values used for this figure (see Table 5.1), $V_n = 3.18$ m/s. | 100 |
| 6.1 | Partial impulses. | The partial retraction impulse \mathcal{R} and the partial push-off impulse \mathcal{P} as the partial area under the force/torque curves for the arbitrary impulsive retraction torque and push-off force profiles. The timing between the two impulses is also arbitrary. The length of the periods over which the impulsive push-off force and retraction torque are applied is infinitesimal, but is exaggerated here for clarity of illustration. | 107 |

| | | |
|-----|---|-----|
| 6.2 | Visualization of the overlap parameter s. (a) As the impulsive push-off force F moves relative to the impulsive retraction torque τ , the overlap parameter s changes from 0 to 1. (b) The overlap parameter s can be considered as the area under the cross-plot of p vs. r . Different paths in (b) correspond to different episodes in (a). Impulsive F and τ are ‘synchronous’ if they are proportional, and thus $s = 0.5$ | 109 |
| 6.3 | The partial overlap parameter s_{t_0}. The path i and ii determine the upper and lower bounds of the total overlap parameter s , respectively. | 120 |
| 6.4 | Instantaneous stance leg extension rate during an arbitrary scenario of impulsive extensional push-off force and impulsive extending retraction torque ($\mathcal{R} < 0$). The extending retraction torque tends to decrease the leg extension rate, and results in $\dot{l}(t) < 0$ for $t_1 \leq t \leq t_2$. During this period the impulsive push-off force does negative work. | 122 |
| 6.5 | The partial overlap parameter s_{t_2} and the minimum net overlap parameter s for an arbitrary scenario. The area of the shaded (solid gray) region corresponds to s_{t_2} . Given s_{t_2} , the net overlap parameter s becomes minimum if the push-off impulse completeness parameter $p(t)$ does not change during (t_2, t_r^+) , <i>i.e.</i> from t_2 until $r(t) = 1$. In this case s is given by the area of the hatched region. | 125 |
| 6.6 | Two bipedal models with torso. Each model has two hip actuators, each acting between the torso and the corresponding thigh. The swing retraction torque, quantified by the impulse \mathcal{R} , decreases ϕ and pushes the swing leg toward the stance leg. (a) The straight-leg model: the push-off impulse \mathcal{P} is provided by a prismatic actuator along the stance leg. (b) The articulated-leg model: the resultant push-off is provided by the knee and ankle torques, quantified by their impulses \mathcal{K} and \mathcal{A} , which tend to extend the corresponding angles (consequently extending the leg). | 131 |
| 7.1 | Stance-leg and hip-joint angles for walking at $V = 1.24$ m/s and $\alpha = 31.61^\circ$. The model parameters are those listed in Table 5.1. The evident accuracy of the approximate analytical solution in this figure holds also for almost all other step angles and speeds in the admissible region (defined in Section 5.4.4).142 | |

- 7.2 **Comparison of the approximate (analytic) and the accurate (numerical) angular rates** at the beginning of the passive swing for different step angles and average walking speeds in the admissible region (see Fig. 5.8). The approximate angular rates $\tilde{\theta}_0$ and $\tilde{\phi}_0$ are calculated from the analytic solutions in (7.7) and (7.14). The non-approximate angular rates $\hat{\theta}_0$ and $\hat{\phi}_0$ are calculated using the numerical solution of the original EoM, given by (5.11). For clarity, the results for only four selected average speeds are shown. The calculations are based on the numerical values listed in Table 5.1. V_n is the maximum GRF-based speed limit, given by (5.36). For the respecting parameter set $V_n = 3.18$ m/s. The figures show that the accuracy of the approximate solutions is very good at small step angles, but it degrades at long steps and slow speeds. 144
- 7.3 **Contour lines of the approximate minimum retracting impulse, $\tilde{\mathcal{R}}_{\min}$, required to enforce heel-strike.** The shaded area is the approximate admissible region, defined in Section 7.7.3. The approximate solution predicts that for step angles and speeds above the contour line $\tilde{\mathcal{R}}_{\min} = 0$ a retracting hip torque ($\mathcal{R} > 0$) is required at the end of swing phase to ensure heel-strike. The vertical axis is the normalized average walking speed $\hat{V} = V/\tilde{V}_n$, where \tilde{V}_n is given by (7.32). The model parameter values are those in Table 5.1. . . 148
- 7.4 **Comparison of the approximate and non-approximate admissible regions.** The shaded area corresponds to the numerically calculated admissible region, defined in Section 5.4.4. The hatched area is the approximate admissible region defined by (7.26) and (7.30). The vertical axis is the normalized average walking speed. For the non-approximate numerical solution, the normalizing speed \tilde{V}_n is given by (5.36). For the approximate solution, the normalizing speed \tilde{V}_n is given by (7.32). For the numerical values used for this figure (see Table 5.1), $V_n = 3.18$ m/s, and $\tilde{V}_n = 2.97$ m/s 153
- 8.1 **Percentage variations of the required swing thrust impulse \mathcal{S} and push-off impulse \mathcal{P} with the retracting impulse \mathcal{R} .** The graph is plotted for the average walking speed and the step period of $V = 1.38$ m/s and $T = 0.54$ s. The variation of each impulse is calculated relative to its corresponding value at $\mathcal{R} = 0$. The model data are those in Table 5.1. The numerical results are calculated using the non-approximate equations in (5.26) and (5.27), whereas the approximate analytic results are calculated using (7.15) and (7.16). Consistent with the predictions of approximate analytic solutions, the exact numerical results show that the push-off impulse \mathcal{P} decreases with the retraction impulse \mathcal{R} , whereas the swing thrust impulse \mathcal{S} has a small dependency in \mathcal{R} which has been ignored in the approximate analytic solution. 171

| | | |
|-----|---|-----|
| 8.2 | Retraction torque and its reaction on the hip. The hip applies a retracting force (torque) on the swing leg and pushes it back. In reverse, a reaction force is applied to the hip by the swing leg. This reaction force pulls the hip forward and reduces the required push-off force for given step length and walking speed. | 172 |
| 8.3 | Contour lines of the minimum retracting impulse, \mathcal{R}_{\min}, required to enforce heel-strike. The shaded area is the admissible region, defined in Section 5.4.4. In the lower shaded area (light color) <i>retracting</i> hip torque ($\mathcal{R} > 0$) is not necessary for periodic walking, and walking is feasible even with an extensional torque ($\mathcal{R} < 0$). In the darker area, however, walking is not feasible without a <i>retracting</i> hip torque prior to heel-strike. The vertical axis is the normalized average walking speed $\hat{V} = V/V_n$, where V_n is given by (5.36). The numerical values of model parameters are taken from Table 5.1. . | 174 |
| 8.4 | Contour maps of the energy optimal retraction impulse \mathcal{R}^*, calculated numerically using the minimization problem stated in (6.73). Each panel corresponds to a different set of c_1 and c_2 , <i>i.e.</i> the cost of unit positive and negative work: a) $c_1 \neq 0$ and $c_2 = 0$, b) $c_1 = 4$ and $c_2 = 5/6$ as for human muscles, and c) $c_1 = c_2$. In all three panels, the vertical axis is the average walking speed V normalized with V_n given by (5.36). The shaded area is the admissible region, defined in Section 5.4.4. The cyan ① area (marked with $\mathcal{R}^* = \mathcal{R}_1^*$) corresponds to the set of α and V combinations for which retraction is energetically optimal (energy minimization freely chooses to exploit retraction). \mathcal{R}_1^* is where the derivative of the net energetic cost E_{step} becomes zero (stationary point). The gray ② region (marked with $\mathcal{R}^* = \mathcal{R}_{\min}$) is where the energy minimization would prefer not to apply any retraction torque, but ensuring heel-strike requires the application of at least \mathcal{R}_{\min} (see Fig. 8.3). The blue ③ region corresponds to the zero optimal retraction impulse, <i>i.e.</i> $\mathcal{R}^* = 0$. | 177 |
| 8.5 | Different retraction impulses and their energetic cost corresponding to the cost coefficients $c_1 = c_2$ and average walking speed $V = 1.6$ m/s (equivalent to $\hat{V} = 0.5$ in Fig. 8.4c). The optimal retraction impulse \mathcal{R}^* and its energetic cost are shown with red dots. The vertical lines represent the step angles at which \mathcal{R}^* switches from \mathcal{R}_{\min} to $\mathcal{R} = 0$ and then to \mathcal{R}_1^* . Exactly on each switching line, the two cost curves associated with \mathcal{R}^* before and after the transition are equal, and the optimal retraction impulse has two solutions. Note that although $\mathcal{R} = 0$ results in the least energetic cost for step angles before the first vertical line, ensuring heel-strike in this region results in $\mathcal{R}^* = \mathcal{R}_{\min}$ | 179 |
| 8.6 | The zoomed version of Fig. 8.5. | 180 |

- 8.7 **Optimality region of a retracting hip joint at heel-strike**, corresponding to the optimal retraction impulse \mathcal{R}^* found for Fig. 8.4. Each panel corresponds to a different set of c_1 and c_2 , *i.e.* the cost of unit positive and negative work: **a)** $c_1 \neq 0$ and $c_2 = 0$ (free negative work), **b)** $c_1 = 4$ and $c_2 = 5/6$ as for human muscles, and **c)** $c_1 = c_2$. A retracting hip joint (*i.e.* $\dot{\psi}_{\text{hip}}^* > 0$) is energetically optimal only in the hatched region, which is where $\mathcal{R}^* = \mathcal{R}_1^*$. In all three panels, the vertical axis is the average walking speed V normalized with V_n given by (5.36). The shaded area is the admissible region, defined in Section 5.4.4. 182
- 8.8 **Optimality region of a retracting *swing leg* at heel-strike**, corresponding to the optimal retraction impulse \mathcal{R}^* found for Fig. 8.4. Each panel corresponds to a different set of c_1 and c_2 , *i.e.* the cost of unit positive and negative work: **a)** $c_1 \neq 0$ and $c_2 = 0$ (free negative work), **b)** $c_1 = 4$ and $c_2 = 5/6$ as for human muscles, and **c)** $c_1 = c_2$. A retracting swing leg (*i.e.* $\dot{\psi}_{\text{leg}}^* > 0$) is energetically optimal only in the hatched region, which is where $\mathcal{R}^* = \mathcal{R}_1^*$ and for most of the area corresponding to $\mathcal{R}^* = 0$. In all three panels, the vertical axis is the average walking speed V normalized with V_n given by (5.36). The shaded area is the admissible region, defined in Section 5.4.4. 183

List of Symbols

| Symbol | Definition |
|---|--|
| a | Distance between the torso center of mass and the hip joint, see Fig.2.1 and Fig. 5.1. |
| A_1, A_2 | Ankle joint of leg ₁ and leg ₂ (model with torso), see Fig. 2.1. |
| b | Distance between the leg center of mass and the hip joint, see Fig. 2.1 and Fig. 5.1. |
| \mathbf{B} | Torque-influence matrix in the equations of motion. |
| $\mathbf{B}_{ss}, \mathbf{B}_{ds}, \mathbf{B}_{fl}$ | Matrix \mathbf{B} in single support (SS), double support (DS), and flight (FL) phases, given by (A.31), (A.62), and (A.65), respectively. |
| c_1 | Energetic cost of unit positive work = Inverse of the actuator efficiency for doing positive work. |
| c_2 | Energetic cost of unit negative work = Inverse of the actuator efficiency for doing negative work. |
| \check{c}_1, \check{c}_2 | Modified c_1 and c_2 , given by (8.11) and (8.12) = Modified costs of unit positive and negative work for indirectly taking into account the cost of active work at heel-strike. |
| \mathbf{c} | A column vector containing the Coriolis, centrifugal, and gravity terms in the equations of motion. |
| $\mathbf{c}_{ss}, \mathbf{c}_{ds}, \mathbf{c}_{fl}$ | Vector \mathbf{c} in single support (SS), double support (DS), and flight (FL) phases, given by (A.23), (A.46), and (A.64), respectively. |
| \mathcal{C}_{et} | Specific cost of transport, defined in (2.2); total energetic cost per unit distance traveled and per unit body weight. |
| \mathcal{C}_{mt} | Mechanical cost of transport; total positive mechanical work per unit distance traveled and per unit body weight; given by \mathcal{C}_{et} when $c_1 = 1$ and $c_2 = 0$. |
| d | Distance between two points. |
| $d_{\Delta m/H}$ | Distance between the hip joint H and the point-mass Δm . |
| $d_{G_{leg}/H}$ | Distance between the hip joint H and the center of mass of the leg. |
| D_{step} | Step length = Distance between two consecutive foot places = d_{A_1/A_2} when both feet are on the ground. |

| | |
|--|---|
| E_1, E_2 | Telescoping joints of leg ₁ and leg ₂ (model with torso), see Fig. 2.1. |
| E | Energetic cost of an actuator, given by (6.1). |
| E_{step} | Total energetic cost per step, given by (2.1) or in a simpler form by (6.2). |
| $E_{\text{step,metabolic}}$ | Metabolic energetic cost per step, measured indirectly using the rate of Oxygen consumption. |
| E_S | Energetic cost of impulsive swing thrust torque, given by (6.6). |
| E_P | Energetic cost of impulsive push-off force, given by (6.21). |
| E_R | Energetic cost of impulsive swing retraction torque, given by (6.22). |
| E_H | Energetic cost of actuator work during heel-strike, given by (8.7). |
| E_{PR} | $E_P + E_R$ |
| \tilde{E} | Modified energetic cost based on the modified cost coefficients \check{c}_1 and \check{c}_2 ; given by (8.13). |
| \tilde{E}_{step} | Modified E_{step} which includes the cost of active work at heel-strike; given by (8.6). |
| $\tilde{E}_S, \tilde{E}_P, \tilde{E}_R, \tilde{E}_{\text{step}}$ | Approximate $E_S, E_P, E_R,$ and E_{step} , given by (7.51), (7.53), (7.58), and (7.64), respectively. |
| \tilde{E}_{PR} | Approximate E_{PR} , given by $\tilde{E}_{PR} = \tilde{E}_P + \tilde{E}_R$. |
| \dot{E} | Rate of the energy expenditure = Power consumption. |
| $\mathbf{f}_{F1}, \mathbf{f}_{F2}$ | 2×1 vectors expressing the ground reaction force vectors \vec{F}_{F1} and \vec{F}_{F2} in the reference frame; $\mathbf{f}_{F1} = [F_{F1x}, F_{F1y}]^T$ and $\mathbf{f}_{F2} = [F_{F2x}, F_{F2y}]^T$. |
| F | Force of the stance leg's prismatic actuator (model without torso), see Fig. 5.1. |
| $F_{\text{leg1a}}, F_{\text{leg2a}}$ | Forces applied by the leg prismatic actuators along leg ₁ and leg ₂ (model with torso); See Fig. 2.2e. |
| $F_{\text{leg1p}}, F_{\text{leg2p}}$ | Constraint forces applied perpendicular to leg ₁ and leg ₂ = The perpendicular component of the total force applied on each leg (model with torso); See Fig. 2.2e. |
| $\vec{F}_{F1}, \vec{F}_{F2}$ | Ground reaction force vectors applied on leg ₁ and leg ₂ . |

| | |
|--|---|
| F_{F1}, F_{F2} | Magnitude of ground reaction forces on leg ₁ and leg ₂ (model with torso); $F_{F1} = \vec{F}_{F1} $, and $F_{F2} = \vec{F}_{F2} $. |
| F_{F1x}, F_{F2x} | Tangential (along the floor) components of the ground reaction forces on leg ₁ and leg ₂ (model with torso), see Fig. 2.2e. |
| F_{F1y}, F_{F2y} | Normal (perpendicular to the floor) components of the ground reaction forces on leg ₁ and leg ₂ (model with torso), see Fig. 2.2e. |
| F_{\max} | Actuator force limit used in numerical optimizations (model with torso); see Table 3.2. |
| g | Gravitational acceleration = 9.81 m/s ² . |
| g_{red} | Reduced gravitational acceleration. |
| \mathbf{g} | Gravitational acceleration vector expressed in the reference frame; $\mathbf{g} = -[\sin(\gamma), \cos(\gamma)]^T g$, where γ is the terrain slope. |
| G_{leg} | Leg center of mass; see Fig. 2.1 and Fig. 5.1. |
| G_{trs} | Torso center of mass; see Fig. 2.1. |
| GRF_a | Centripetal (along the stance leg) ground reaction force, given by (5.30). |
| h_{tot} | Total body height (model with torso); see Table 3.1. |
| h_{trs} | Torso height; ; see Table 3.1. |
| H | Hip joint; see Fig. 5.1. |
| H_1, H_2 | Hip joints between leg ₁ or leg ₂ and the torso; see Fig. 2.1. |
| H_{step} | Step height; see Fig. 2.2c. |
| $\mathbf{i}_{F1}, \mathbf{i}_{F2}$ | Vectors of the TD impulse on leg ₁ and leg ₂ expressed in the reference frame; $\mathbf{i}_{Fi} = \int_{t_d^-}^{t_d^+} \mathbf{f}_{Fi}(t) dt = [\mathcal{I}_{Fi_x}, \mathcal{I}_{Fi_y}]^T$ for $i = 1, 2$. |
| $\mathcal{I}_{F1x}, \mathcal{I}_{F1y}$ | Tangential (along the surface) and normal (perpendicular to the surface) components of the TD impulse on leg ₁ . |
| $\mathcal{I}_{F2x}, \mathcal{I}_{F2y}$ | Tangential (along the surface) and normal (perpendicular to the surface) components of the TD impulse on leg ₂ . |
| $I_{\text{leg}/G_{\text{leg}}}$ | Leg moment of inertia relative to the leg center of mass G_{leg} . |
| $I_{\text{leg}/H}$ | Leg moment of inertia relative to the hip joint H. |

| | |
|--|--|
| $I_{\text{trs}/G_{\text{trs}}}$ | Torso moment of inertia relative to its center of mass G_{trs} . |
| $I_{\text{trs}/H}$ | Torso moment of inertia relative to the hip joint H. |
| $J_{\dot{\theta}/\mathcal{P}}, J_{\dot{\theta}/\mathcal{R}}, J_{\dot{\theta}/\mathcal{S}}$ | Step-angle dependent scalars quantifying the influence of the push-off impulse \mathcal{P} , retraction impulse \mathcal{R} , and swing-thrust impulse \mathcal{S} on the stance-leg angular rate $\dot{\theta}$. |
| $J_{\dot{\phi}/\mathcal{P}}, J_{\dot{\phi}/\mathcal{R}}, J_{\dot{\phi}/\mathcal{S}}$ | Step-angle dependent scalars quantifying the influence of the push-off impulse \mathcal{P} , retraction impulse \mathcal{R} , and swing-thrust impulse \mathcal{S} on the hip-joint angular rate $\dot{\phi}$. |
| $J_{\dot{\ell}/\mathcal{P}}, J_{\dot{\ell}/\mathcal{R}}$ | Step-angle dependent scalars quantifying the influence of the push-off impulse \mathcal{P} , and retraction impulse \mathcal{R} on the stance-leg extension rate $\dot{\ell}$. |
| $J_{\mathcal{S}/\mathcal{R}}$ | Step-angle dependent scalar quantifying the influence of retraction impulse \mathcal{R} on the swing-thrust impulse \mathcal{S} ; given by (B.33). |
| $J_{\mathcal{P}/\mathcal{R}}$ | Step-angle dependent scalar quantifying the influence of retraction impulse \mathcal{R} on the push-off impulse \mathcal{P} ; given by (B.33). |
| $\mathbf{J}_{1\theta}, \mathbf{J}_{2\theta}, \mathbf{J}_{21\theta}$ | Jacobian of the position vectors $\mathbf{r}_{A_1/G_{\text{tot}}}$, $\mathbf{r}_{A_2/G_{\text{tot}}}$, and \mathbf{r}_{A_2/A_1} relative to $\mathbf{q}\theta$; $\mathbf{J}_{1\theta} = \partial\mathbf{r}_{A_1/G_{\text{tot}}}/\partial\mathbf{q}\theta$, $\mathbf{J}_{2\theta} = \partial\mathbf{r}_{A_2/G_{\text{tot}}}/\partial\mathbf{q}\theta$, and $\mathbf{J}_{21\theta} = \partial\mathbf{r}_{A_2/A_1}/\partial\mathbf{q}\theta$. These Jacobians are expanded in (A.66), (A.67), and (A.70). |
| $\mathbf{J}_{1\ell_1}, \mathbf{J}_{21\ell_1}$ | Jacobian of the position vectors $\mathbf{r}_{A_1/G_{\text{tot}}}$, and \mathbf{r}_{A_2/A_1} relative to ℓ_1 ; $\mathbf{J}_{1\ell_1} = \partial\mathbf{r}_{A_1/G_{\text{tot}}}/\partial\ell_1$, and $\mathbf{J}_{21\ell_1} = \partial\mathbf{r}_{A_2/A_1}/\partial\ell_1$. These Jacobians are expanded in (A.68), and (A.71). |
| $\mathbf{J}_{21\ell_2}$ | Jacobian of the position vectors \mathbf{r}_{A_2/A_1} relative to ℓ_2 ; $\mathbf{J}_{21\ell_2} = \partial\mathbf{r}_{A_2/A_1}/\partial\ell_2$. It is expanded in (A.72) |
| k | Fraction of the heel-strike energy dissipation that takes place actively via negative actuator work, given in (8.5); $0 \leq k \leq 1$. |
| ℓ | Leg length; see Fig. 2.1 and Fig. 5.1. |
| ℓ_1, ℓ_2 | Lengths of leg ₁ and leg ₂ (model with torso); see Fig. 2.1. |
| ℓ_0 | Length of the landing leg at touch-down, used in numerical optimizations of the model with torso, see Table 3.2. |
| ℓ_u | Length of the upper (non-massless) segment of the telescoping leg in the biped model in Fig. 2.1, see Table 3.1. |
| ℓ_{\min}, ℓ_{\max} | Minimum and maximum leg length used in numerical optimizations of the model with torso, see Table 3.2. |

| | |
|--|--|
| $\dot{\ell}, \dot{\ell}_1, \dot{\ell}_2$ | Leg extension rate; $\dot{\ell} = d\ell/dt$, $\dot{\ell}_1 = dl_1/dt$, and $\dot{\ell}_2 = dl_2/dt$. |
| $\dot{\ell}_1^-, \dot{\ell}_1^+$ | Extension rates of leg ₁ just before and just after the TD event at t_{td} . |
| $\dot{\ell}_2^-, \dot{\ell}_2^+$ | Extension rates of leg ₂ just before and just after the TD event at t_{td} . |
| $\dot{\ell}_{t_{pr}}^-, \dot{\ell}_{t_{pr}}^+$ | Leg extension rates at t_{pr}^- and t_{pr}^+ , <i>i.e.</i> just before and just after both the push-off and retraction impulses. |
| $\tilde{\dot{\ell}}_{t_{pr}}^+$ | Approximate $\dot{\ell}_{t_{pr}}^+$, given by (7.43). |
| $\tilde{\dot{\ell}}_{t_r}^+$ | Approximate $\dot{\ell}_{t_r}^+$, given by (7.47). |
| $\ddot{\ell}, \ddot{\ell}_1, \ddot{\ell}_2$ | Leg extension acceleration; $\ddot{\ell} = d^2\ell/dt^2$, $\ddot{\ell}_1 = d^2l_1/dt^2$, and $\ddot{\ell}_2 = d^2l_2/dt^2$. |
| L_{step} | Tangential distance (parallel to the surface) between the two consecutive foot-falls; see Fig. 2.2b-2.2d. |
| m_{leg} | Leg mass; see Fig. 2.1 and Fig. 5.1. |
| m_{tot} | Total mass of the biped. |
| m_{trs} | Torso mass; see Fig. 2.1 and Fig. 5.1. |
| m_H | Point-mass at the hip (model without torso); see Fig. 5.1. |
| \mathbf{M} | Mass-inertia matrix. |
| $\mathbf{M}_{ss}, \mathbf{M}_{ds}$ | Mass-inertia matrix \mathbf{M} in single support (SS) and double support (DS) phases. |
| N_{ss}, N_{ds}, N_{fl} | Number of equal-length intervals (grids) in single support (SS), double support (DS), and flight (FL) phase. The duration of each grid (interval) is T_{ss}/N_{ss} , T_{ds}/N_{ds} , and T_{fl}/N_{fl} . Within each interval, the actuator forces and torques are approximated by a piecewise-linear function for numerical optimization. |
| p | Push-off impulse completeness parameter (non-dimensional), defined in (6.8); specifies the portion of the push-off impulse that has been applied so far. |
| p_t | $p(t)$ |
| $p_{t_1}, p_{t_2}, p_{t_{pr}}^+, p_{t_r}^+$ | $p(t_1), p(t_2), p(t_{pr}^+), p(t_r^+)$ |
| $p_{t_1}^*, p_{t_2}^*$ | Optimal values of p_{t_1} and p_{t_2} . |

| | |
|---|--|
| p_{\min} | Lower bound on the impulse completeness parameter p that satisfies $\dot{\ell} > 0$. |
| \mathcal{P} | Push-off impulse, defined in (5.10). |
| \mathcal{P} | Partial push-off impulse, defined in (6.8). |
| $\tilde{\mathcal{P}}$ | Approximate \mathcal{P} , given by (7.16). |
| \mathbf{q} | Biped configuration vector (model without torso); $\mathbf{q} = [\theta, \phi]^T$. |
| \mathbf{q}_θ | A 3×1 vector containing the link angles θ_1 , θ_2 , and θ_3 (model with torso); $\mathbf{q}_\theta = [\theta_1, \theta_2, \theta_3]^T$. |
| \mathbf{q}_ℓ | A 2×1 vector containing the leg lengths ℓ_1 , and ℓ_2 (model with torso); $\mathbf{q}_\ell = [\ell_1, \ell_2]^T$. |
| $\mathbf{q}_{G_{\text{tot}}}$ | A 2×1 vector containing the cartesian coordinates of the biped center of mass G_{tot} ; $\mathbf{q}_{G_{\text{tot}}} = [x_{G_{\text{tot}}}, y_{G_{\text{tot}}}]^T$. |
| \mathbf{q}_{ss} | A 4×1 vector expressing the biped configuration in single support (SS) phase (biped with torso); $\mathbf{q}_{\text{ss}} = [\ell_1, \mathbf{q}_\theta^T]^T$. |
| \mathbf{q}_{ds} | A 4×1 vector expressing the biped configuration in double support (DS) phase (biped with torso); $\mathbf{q}_{\text{ds}} = [\ell_1, \mathbf{q}_\theta^T]^T$. |
| \mathbf{q}_{fl} | A 5×1 vector expressing the biped configuration in flight (FL) phase (biped with torso); $\mathbf{q}_{\text{fl}} = [\mathbf{q}_{G_{\text{tot}}}^T, \mathbf{q}_\theta^T]^T$. |
| \dot{q} | Joint velocity (general case). |
| \dot{q}^-, \dot{q}^+ | Joint velocities just before and just the impulse \mathcal{I} ; used for formulating the work of an isolated impulse in (6.3). |
| $\dot{\mathbf{q}}_\theta, \dot{\mathbf{q}}_\ell, \dot{\mathbf{q}}_{G_{\text{tot}}}$ | First-derivative (with respect to time) of \mathbf{q}_θ , \mathbf{q}_ℓ , and $\mathbf{q}_{G_{\text{tot}}}$. |
| $\dot{\mathbf{q}}_{\text{ss}}, \dot{\mathbf{q}}_{\text{ds}}, \dot{\mathbf{q}}_{\text{fl}}$ | First-derivative (with respect to time) of \mathbf{q}_{ss} , \mathbf{q}_{ds} , and \mathbf{q}_{fl} . |
| $\ddot{\mathbf{q}}_\theta, \ddot{\mathbf{q}}_\ell, \ddot{\mathbf{q}}_{G_{\text{tot}}}$ | Second-derivative (with respect to time) of \mathbf{q}_θ , \mathbf{q}_ℓ , and $\mathbf{q}_{G_{\text{tot}}}$. |
| $\ddot{\mathbf{q}}_{\text{ss}}, \ddot{\mathbf{q}}_{\text{ds}}, \ddot{\mathbf{q}}_{\text{fl}}$ | Second-derivative (with respect to time) of \mathbf{q}_{ss} , \mathbf{q}_{ds} , and \mathbf{q}_{fl} . |
| $\dot{\mathbf{q}}_\theta^-, \dot{\mathbf{q}}_\theta^+$ | $\dot{\mathbf{q}}_\theta$ just before and just after the TD event at t_{td} . |
| $\dot{\mathbf{q}}_{G_{\text{tot}}}^-, \dot{\mathbf{q}}_{G_{\text{tot}}}^+$ | $\dot{\mathbf{q}}_{G_{\text{tot}}}$ just before and just after the TD event at t_{td} . |

| | |
|--|--|
| r | Retraction-impulse completeness parameter (non-dimensional), defined in (6.7); specifies the portion of the retraction impulse that has been applied so far. |
| r_t | $r(t)$ |
| $r_{t_1}, r_{t_2}, r_{t_{pr}^+}$ | $r(t_1), r(t_2), r(t_{pr}^+)$ |
| $r_{t_1}^*, r_{t_2}^*$ | Optimal values of r_{t_1} , and r_{t_2} . |
| \mathbf{r} | Position vector expressed in the reference frame. |
| \mathbf{r}_{A_2/A_1} | Position vector of the ankle joint A_2 relative to the ankle joint A_1 . |
| $\mathbf{r}_{A_1/G_{tot}}, \mathbf{r}_{A_2/G_{tot}}$ | Position vectors of the ankle joints A_1 and A_2 relative to the biped's center of mass G_{tot} . |
| $\mathbf{r}_{G_{tot}/A_1}, \mathbf{r}_{G_{tot}/A_2}$ | Position vectors of the biped's center of mass G_{tot} relative to the ankle joints A_1 and A_2 . |
| $\dot{\mathbf{r}}_{G_{tot}/A_1}, \dot{\mathbf{r}}_{A_2/A_1}$ | First-derivative (relative to time) of \mathbf{r}_{G_{tot}/A_1} , and \mathbf{r}_{A_2/A_1} . |
| $\ddot{\mathbf{r}}_{G_{tot}/A_1}, \ddot{\mathbf{r}}_{A_2/A_1}$ | Second-derivative (relative to time) of \mathbf{r}_{G_{tot}/A_1} , and \mathbf{r}_{A_2/A_1} . |
| \mathcal{R} | Swing retraction impulse, defined in (5.9). |
| \mathcal{R} | Partial retraction impulse, defined in (6.7). |
| \mathcal{R}_{min} | Minimum retraction impulse required to ensure heel-strike, given by (8.2). |
| \mathcal{R}_{max} | Maximum retraction impulse for a non-negative push-off impulse, defined in (5.28). |
| \mathcal{R}^* | Optimal swing retraction impulse that minimizes the total energetic cost per step. |
| \mathcal{R}_1^* | Swing retraction impulse at which $\partial E_{step}/\partial \mathcal{R} = 0$. |
| $\tilde{\mathcal{R}}_{min}$ | Approximate \mathcal{R}_{min} , given by (7.21). |
| $\tilde{\mathcal{R}}_{max}$ | Approximate \mathcal{R}_{max} , given by (7.22). |
| $\tilde{\mathcal{R}}^*$ | Approximate \mathcal{R}^* , calculated by minimizing \tilde{E}_{step} ; given by (7.76). |
| $\tilde{\mathcal{R}}_1^*$ | Approximate \mathcal{R}_1^* ; the retraction impulse for which $\partial \tilde{E}_{step}/\partial \mathcal{R} = 0$; given by (7.71). |

| | |
|---|---|
| $\tilde{\mathcal{R}}^\ddagger$ | For $0 \leq \mathcal{R} \leq \tilde{\mathcal{R}}^\ddagger$, $\tilde{W}_{\mathcal{R}}^+ = 0$, whereas for $\mathcal{R} > \tilde{\mathcal{R}}^\ddagger$ the impulsive retraction torque does some positive work. Its approximate solution is given by (7.56). |
| s | Quantifies the relative timing of impulsive push-off force and the impulsive retraction torque; a non-dimensional parameter given by (6.15). |
| s^* | Optimal overlap parameter s . |
| s_t | Partial overlap parameter, defined in (6.12). |
| $s_{t_{\text{pr}}}^+, s_{t_1}, s_{t_2}$ | s_t at t_{pr}^+ , t_1 , and t_2 . |
| $s_{t_1}^*, s_{t_2}^*$ | Optimal partial overlap parameters s_{t_1} and s_{t_2} . |
| s_{min} | Lower bound on overlap parameter s that satisfies $\dot{\ell} > 0$. |
| \mathcal{S} | Swing thrust impulse, defined in (5.8). |
| $\tilde{\mathcal{S}}$ | Approximate \mathcal{S} ; given by (7.15). |
| t | Time |
| t_{td} | Time instant corresponding to the TD event. |
| t_{s}^- | Time instant just before the impulsive swing thrust torque = just after toe-off; it is also equivalent to $t = 0^-$, see Fig. 5.4. |
| t_{s}^+ | Time instant just after the impulsive swing thrust torque = the beginning of passive swing; it is also equivalent to $t = 0^+$; see Fig. 5.4. |
| t_{pr}^- | Time instant just before both the impulsive push-off force and retraction torque = the end of passive swing $\equiv \min(t_{\text{r}}^-, t_{\text{p}}^-)$; see Fig. 5.4. |
| t_{pr}^+ | Time instant just after both the impulsive push-off force and retraction torque = just before heel-strike $\equiv \max(t_{\text{r}}^+, t_{\text{p}}^+) \equiv t_{\text{h}}^-$; see Fig. 5.4. |
| $t_{\text{r}}^-, t_{\text{r}}^+$ | Time instants just before and just after the impulsive retraction torque; see Fig. 5.4. |
| $t_{\text{p}}^-, t_{\text{p}}^+$ | Time instant just before and just after the impulsive push-off force; see Fig. 5.4. |
| t_{h}^- | Time instant just before the collisional heel-strike $\equiv t_{\text{pr}}^+$; see Fig. 5.4. |
| t_{h}^+ | Time instant just after the collisional heel-strike = just after toe-off; see Fig. 5.4. |

| | |
|---|---|
| T | Step period. |
| T^- | $T^- \equiv t_{\text{pr}}^-$ |
| $T_{\text{ss}}, T_{\text{ds}}, T_{\text{fl}}$ | Duration of single support (SS), double support (DS), and flight (FL) phase. |
| $T_{\text{ds,min}}$ | Lower bound on T_{ds} used in numerical optimization (model with torso). |
| V | Average walking speed. |
| V_{min} | Minimum average walking speed for which the calculated swing thrust impulse is non-negative; defined in (5.29). |
| V_{max} | Maximum average walking speed for which GRF along the stance leg is non-negative during passive single stance; defined in (5.31). |
| V_n | Normalizing speed = $\max V_{\text{max}}(\alpha)$ for all α , given by (5.36). |
| V_{tr} | Transition speed above which the optimal gait switches to a new pattern, <i>i.e.</i> from continuous-support to intermittent-support. |
| $V_{\text{F1axial}}, V_{\text{F2axial}}$ | Velocities of foot ₁ and foot ₂ along their corresponding leg. |
| $V_{\text{F1perp}}, V_{\text{F2perp}}$ | Velocities of foot ₁ and foot ₂ perpendicular to their corresponding leg. |
| \hat{V} | Normalized average walking speed; $\hat{V} = V/V_n$. |
| V^\dagger | Maximum speed for which ω_2 exists and is given by (7.11). |
| \tilde{V}_n | Approximate V_n , given by (7.32). |
| \tilde{V}_{min} | Approximate V_{min} ; defined in (7.26). |
| \tilde{V}_{max} | Approximate V_{max} ; defined in (7.30). |
| W, W^+, W^- | Net, positive, and negative mechanical work performed by a given force or torque. |
| $W_{\mathcal{P}}$ | Net mechanical work done by impulsive the push-off force, given by (6.19). |
| $W_{\mathcal{P}}(t)$ | Partial push-off work = net work done by the impulsive push-off force from its beginning until an arbitrary instant t in $(t_{\text{p}}^-, t_{\text{pr}}^+)$, defined in (6.18). |
| $W_{\mathcal{P}}^+, W_{\mathcal{P}}^-$ | Positive and negative mechanical work performed by the impulsive push-off force. |

| | |
|--|--|
| W_S, W_S^+, W_S^- | Net, positive, and negative mechanical work performed by the impulsive swing thrust torque. |
| $W_{\mathcal{R}}$ | Net mechanical work performed by the impulsive swing retraction torque, given by (6.14). |
| $W_{\mathcal{R}}(t)$ | Partial retraction work = the work performed by the impulsive retraction torque from its beginning until t , defined in (6.10), and given by (6.11). |
| $W_{\mathcal{R}}^+, W_{\mathcal{R}}^-$ | Positive and negative mechanical work performed by the impulsive swing retraction torque. |
| $W_{\mathcal{P}\mathcal{R}}$ | $W_{\mathcal{P}} + W_{\mathcal{R}}$ |
| $W_{\mathcal{H}}$ | Energy dissipation at heel-strike, given by (8.4). |
| $W_{\mathcal{H},\text{active}}$ | The portion of energy dissipation at heel-strike that takes place actively, <i>i.e.</i> by actuator work. |
| $W_{\mathcal{H},\text{passive}}$ | The portion of energy dissipation at heel-strike that takes place passively, <i>i.e.</i> through energy loss at collision. |
| $\tilde{W}_{\mathcal{P}}$ | Approximate $W_{\mathcal{P}}$, given by (7.52). |
| \tilde{W}_S | Approximate W_S , given by (7.49) or (7.50). |
| $\tilde{W}_{\mathcal{R}}$ | Approximate $W_{\mathcal{R}}$, given by (7.55). |
| $\tilde{W}_{\mathcal{R}}^+, \tilde{W}_{\mathcal{R}}^-$ | Approximate $W_{\mathcal{R}}^+$ and $W_{\mathcal{R}}^-$; where $\tilde{W}_{\mathcal{R}}^+$ is given by (7.57) and $\tilde{W}_{\mathcal{R}}^- = \tilde{W}_{\mathcal{R}} - \tilde{W}_{\mathcal{R}}^+$. |
| \dot{W} | Mechanical power of an actuator. |
| \dot{W}_i | Mechanical power of the i^{th} actuator. |
| x | Tangential (along the ground surface) component of a position vector. |
| $x_{G_{\text{tot}}}$ | Tangential (along the ground surface) coordinate of the biped center of mass (G_{tot}) in the reference frame. |
| y | Normal (perpendicular to the ground surface) component of a position vector. |
| $y_{G_{\text{tot}}}$ | Normal (perpendicular to the ground surface) coordinate of the biped center of mass (G_{tot}) in the reference frame. |
| $\dot{y}_{f_{\text{swing}}}$ | Vertical component of the swing-foot velocity. |

| | |
|--|--|
| $\dot{y}_{f_{\text{trailing}}}$ | Vertical component of the trailing-foot velocity. |
| α | Step angle; the angle of the stance leg relative to the vertical at heel-strike; see Fig. 5.2. |
| α_{max} | Maximum step angle for which walking is feasible. |
| γ | Ground slope relative to horizontal. |
| δ | Nondimensional coefficient representing the spread of the leg mass relative to the leg center of mass. It is used to calculate the leg moment of inertia about the hip, as $I_{\text{leg}/H} = \delta m_{\text{leg}} \ell b$. |
| ϵ | Smoothing parameter used to approximate the non-smooth positive-value function with a smooth function, as $[x]^+ \approx (x + \sqrt{x^2 + \epsilon^2})/2$. |
| η | Nondimensional parameter given by $\eta = \omega_2^2 / (\omega_1^2 + \omega_2^2)$. It is used to calculate $\tilde{\phi}$ and $\tilde{\phi}_0$. |
| θ | Stance leg angle relative to vertical (model without torso), see Fig. 5.1. |
| $\theta_1, \theta_2, \theta_3$ | Angles of, respectively, leg ₁ , torso, and leg ₂ relative to vertical (model with torso), see Fig. 2.1. |
| $\tilde{\theta}$ | Approximate θ , given by (7.5). |
| $\dot{\theta}, \ddot{\theta}$ | Stance-leg angular rate and angular acceleration (model without torso). |
| $\dot{\theta}_0$ | Stance leg angular velocity at the start of passive swing = $\dot{\theta}_{t_s^+}$; it is a simpler notation for $\dot{\theta}_{0^+}$. |
| $\dot{\theta}_{0^+}$ | Stance leg angular rate at the start of passive swing = $\dot{\theta}_{t_s^+}$; for simplicity it is denoted by $\dot{\theta}_0$. |
| $\dot{\theta}_{t_s^-}, \dot{\theta}_{t_s^+}$ | Stance leg angular rates at t_s^- and t_s^+ , <i>i.e.</i> just before and just after the swing-thrust impulse. |
| $\dot{\theta}_{t_{\text{pr}}^-}, \dot{\theta}_{t_{\text{pr}}^+}$ | Stance leg angular rates at t_{pr}^- and t_{pr}^+ , <i>i.e.</i> just before and just after both the push-off and swing-retraction impulses. |
| $\dot{\theta}_{t_{\text{p}}^-}, \dot{\theta}_{t_{\text{p}}^+}$ | Stance leg angular rates at t_{p}^- and t_{p}^+ , <i>i.e.</i> just before and just after the push-off impulse. |
| $\dot{\theta}_{t_{\text{r}}^-}, \dot{\theta}_{t_{\text{r}}^+}$ | Stance-leg angular rates at t_{r}^- and t_{r}^+ , <i>i.e.</i> just before and just after the swing-retraction impulse. |

| | |
|--|--|
| $\dot{\theta}_{t_h^-}, \dot{\theta}_{t_h^+}$ | Stance-leg angular rates at t_h^- and t_h^+ , <i>i.e.</i> just before and just after the collisional heel-strike. |
| $\hat{\theta}_0$ | Normalized $\dot{\theta}_0$, given by $\hat{\theta}_0 = \dot{\theta}_0/\omega_n$. |
| $\tilde{\theta}, \tilde{\ddot{\theta}}$ | Approximate $\dot{\theta}$ and $\ddot{\theta}$. |
| $\tilde{\theta}_0$ | Approximate $\dot{\theta}_0$; given by (7.7). |
| $\tilde{\theta}_{t_s^-}, \tilde{\theta}_{t_s^+}$ | Approximate $\dot{\theta}_{t_s^-}$ and $\dot{\theta}_{t_s^+}$, given by (7.37) and (7.35). |
| $\tilde{\theta}_{t_p^+}$ | Approximate $\dot{\theta}_{t_p^+}$, given by (7.41). |
| $\tilde{\theta}_{t_r^-}, \tilde{\theta}_{t_r^+}$ | Approximate $\dot{\theta}_{t_r^-}$ and $\dot{\theta}_{t_r^+}$. When the push-off impulse is applied before the retraction impulse, $\tilde{\theta}_{t_r^-} = \tilde{\theta}_{t_p^+}$, and $\tilde{\theta}_{t_r^+}$ is given by (7.45). |
| λ | A nondimensional parameter quantifying the influence of swing-leg motion on stance-leg dynamics; given by (7.1). |
| μ | Friction coefficient, see Table 3.2. |
| ρ | Average angular rate of the stance leg, given by (7.8). |
| τ | Hip torque (biped model without torso), see Fig. 5.1. |
| τ_1 | Stance leg's ankle torque applied from the foot to the leg (biped model with torso), see Fig. 2.2a. |
| τ_2 | Stance leg's hip torque applied from the torso to the leg (biped model with torso), see Fig. 2.2a. |
| τ_3 | Swing leg's hip torque applied from the torso to the leg (biped model with torso), see Fig. 2.2a. |
| τ_4 | Swing leg's ankle torque applied from the foot to the leg (biped model with torso), see Fig. 2.2a. |
| τ_{\max} | Upper bound of the joint torque used in numerical optimizations (model with torso); see Table 3.2. |
| $\boldsymbol{\tau}$ | Torque vector; $\boldsymbol{\tau} = [\tau_1, \tau_2, \tau_3, \tau_4]^T$. |
| $\boldsymbol{\tau}_{\text{ss}}$ | Actuation vector in single stance (single support) phase; $\boldsymbol{\tau}_{\text{ss}} = [F_{\text{leg1a}}, \tau_1, \tau_2, \tau_3]^T$. |

| | |
|--|---|
| $\boldsymbol{\tau}_{\text{ds}}$ | Actuation vector in double stance (double support) phase; $\boldsymbol{\tau}_{\text{ds}} = [F_{\text{leg}_{1a}}, F_{\text{leg}_{2a}}, \tau_1, \tau_2, \tau_3, \tau_4]^T$. |
| $\boldsymbol{\tau}_{\text{fl}}$ | Actuation vector in flight phase; $\boldsymbol{\tau}_{\text{fl}} = [\tau_2, \tau_3]^T$. |
| ϕ | Hip-joint angle (model without torso), see Fig. 5.1. |
| $\tilde{\phi}$ | Approximate ϕ , given by (7.12). |
| $\dot{\phi}, \ddot{\phi}$ | Hip-joint angular rate and angular acceleration. |
| $\dot{\phi}_0$ | Hip-joint angular rate at the start of passive swing $\equiv \dot{\phi}_{t_s^+}$; it is a simpler notation for $\dot{\phi}_{0+}$. |
| $\dot{\phi}_{0+}$ | Hip-joint angular rate at the start of passive swing $\equiv \dot{\phi}_{t_s^+}$; for simplicity it is denoted by $\dot{\phi}_0$. |
| $\dot{\phi}_{t_s^-}, \dot{\phi}_{t_s^+}$ | Hip-joint angular rates at t_s^- and t_s^+ , <i>i.e.</i> just before and just after the swing-thrust impulse. |
| $\dot{\phi}_{t_{\text{pr}}^-}, \dot{\phi}_{t_{\text{pr}}^+}$ | Hip-joint angular rate at t_{pr}^- and t_{pr}^+ , <i>i.e.</i> just before and just after both the push-off and swing-retraction impulses. |
| $\dot{\phi}_{t_{\text{p}}^-}, \dot{\phi}_{t_{\text{p}}^+}$ | Hip-joint angular rates at t_{p}^- and t_{p}^+ , <i>i.e.</i> just before and just after the push-off impulse. |
| $\dot{\phi}_{t_{\text{r}}^-}, \dot{\phi}_{t_{\text{r}}^+}$ | Hip-joint angular rates at t_{r}^- and t_{r}^+ , <i>i.e.</i> just before and just after the swing-retraction impulse. |
| $\dot{\phi}_{t_{\text{h}}^-}, \dot{\phi}_{t_{\text{h}}^+}$ | Hip-joint angular rates at t_{h}^- and t_{h}^+ , <i>i.e.</i> just before and just after the collisional heel-strike. |
| $\hat{\phi}_0$ | Normalized $\dot{\phi}_0$, given by $\hat{\phi}_0 = \dot{\phi}_0/\omega_n$. |
| $\tilde{\dot{\phi}}, \tilde{\ddot{\phi}}$ | Approximate $\dot{\phi}$ and $\ddot{\phi}$. |
| $\tilde{\dot{\phi}}_0$ | Approximate $\dot{\phi}_0$; given by (7.14). |
| $\tilde{\dot{\phi}}_{t_s^-}, \tilde{\dot{\phi}}_{t_s^+}$ | Approximate $\dot{\phi}_{t_s^-}$ and $\dot{\phi}_{t_s^+}$; given by (7.38) and (7.36). |
| $\tilde{\dot{\phi}}_{t_{\text{p}}^+}$ | Approximate $\dot{\phi}_{t_{\text{p}}^+}$, given by (7.42) or (7.44). |
| $\tilde{\dot{\phi}}_{t_{\text{r}}^-}, \tilde{\dot{\phi}}_{t_{\text{r}}^+}$ | Approximate $\dot{\phi}_{t_{\text{r}}^-}$ and $\dot{\phi}_{t_{\text{r}}^+}$, where $\tilde{\dot{\phi}}_{t_{\text{r}}^-} = \tilde{\dot{\phi}}_{t_{\text{p}}^+}$ and $\tilde{\dot{\phi}}_{t_{\text{r}}^+}$ is given by (7.46) or (7.48). |

| | |
|-------------------------------------|---|
| $\dot{\psi}_{\text{hip}}$ | Hip-joint retraction rate, given by (7.78). |
| $\dot{\psi}_{\text{leg}}$ | Swing-leg retraction rate, given by (7.79). |
| $\dot{\psi}_{\text{hip}}^*$ | Energy-optimal hip-joint retraction rate, calculated by evaluating $\dot{\psi}_{\text{hip}}$ at $\mathcal{R} = \mathcal{R}^*$. |
| $\dot{\psi}_{\text{leg}}^*$ | Energy-optimal swing-leg retraction rate, calculated by evaluating $\dot{\psi}_{\text{leg}}$ at $\mathcal{R} = \mathcal{R}^*$. |
| $\tilde{\dot{\psi}}_{\text{hip}}^*$ | Approximate $\dot{\psi}_{\text{hip}}^*$, given by (7.80). |
| $\tilde{\dot{\psi}}_{\text{leg}}^*$ | Approximate $\dot{\psi}_{\text{leg}}^*$, given by (7.81). |
| ω_1 | Stance leg's approximate natural frequency, given by (7.6). |
| ω_2 | Swing leg's approximate oscillation frequency, given by (7.10). |
| ω_n | Normalizing angular rate = $\max(\dot{\theta}_0)$ for all α and V , given by (5.35). |
| $\tilde{\omega}_n$ | Approximate ω_n ; its analytic solution is given by (7.31). |
| $\tilde{\Omega}$ | Approximate change in the hip-joint angular rate due to the swing thrust impulse; given by (7.17). |

List of Abbreviations

| Abbreviation | Definition |
|---------------------|---|
| CoM | center of mass, |
| COT | cost of transport, |
| DC | direct current, |
| DMec-COT | dimensional mechanical cost of transport, |
| DMet-COT | dimensional metabolic cost of transport, |
| DoF | degree of freedom, |
| DS | double support (stance) phase |
| EoM | equations of motion |
| FL | fligh phase |
| GRF | ground reaction force |
| SLIP | spring loaded inverted pendulum |
| SP | support (stance) phase |
| SS | single support (stance) phase |
| TD | touch-down |
| TK | take-off |
| TO | toe-off |
| TPBV | two point boundary value |
| NLP | nonlinear programming |
| w.r.t. | with respect to |
| ZMP | zero moment point |

Chapter 1

INTRODUCTION

Humans and animals can achieve movement from one place to another, or *locomotion*, using a variety of strategies. Legs are arguably the most appropriate and versatile mode when moving on uneven terrain [1]. Because of the strong connection of walking and running with our daily life, and due to potential applications such as replacing humans with functional robots in hazardous environments and the restoration of motion in the disabled with dynamically-controlled lower-limb prostheses, legged locomotion has attracted substantial interest from different fields such as Biology, Kinesiology, Neuroscience, Computer Science, Control Engineering, Mechanical Engineering, and Robotics.

While walking and running have been well described, the governing principles determining effective legged locomotion are not well understood [2, 3, 4]. Despite the advancements in the design and manufacturing of high performance sensors and actuators, to date there has been no bipedal robot exhibiting both the dexterity and efficiency of human locomotion [3, 5, 6]. Although Honda's ASIMO [7, 8] and Boston Dynamics' PETMAN [9] and ATLAS [10] robots have impressive versatility and robustness, they still fall far short of human performance. Also, scaled for weight and speed, their energy consumption is roughly 10 times more than that of humans [11]. Conversely, the Cornell Ranger robot [12] is energy stingy, but all it can do is to walk on flat ground. But there are no known reasons why a robot should not be able to nearly match human efficiency, versatility, and robustness. Available actuators, sensors, and components seem good enough; the problem seems to be in the design of the control system, which in turn is caused by the lack of our understanding of the principles for effective and robust legged locomotion.

Although legged robots might be significantly different from their biological counterparts,

both groups are subject to the same mechanics principles governing their motions. Therefore, understanding biological legged locomotion can contribute to better designs of walking and running robots - improving performance, robustness, and energy efficiency. Experimental robots and computer-based models can, in turn, improve our knowledge of legged locomotion by serving as a means to evaluate theories of how, and why, humans and animals move the way that they do [4].

1.1 Objective of This Thesis

I intend to develop a better understanding of energy efficient legged locomotion using simulation and optimization of computer models of robots and humans. My eventual goal is to develop a simple and tractable theory of effective legged locomotion and balance control in bipedal models comparable to humans. Such a functional theory will indicate the origin of stability and define features of energy economy that are hallmarks of biological locomotory capacity. It will also reliably predict how humans and animals choose special gait parameters, such as stride length and frequency at a given forward speed and other specified conditions.

1.2 Review of the Relevant Literature

In the following, I provide a brief review of the most important work relevant to the analysis of legged locomotion.

1.2.1 Minimalistic Models for Legged Locomotion

One approach to study legged locomotion is to model a legged organism as a machine described by Newtonian mechanics. Although organisms are generally multi-purpose and highly complex systems, describing them using simple models can provide insight into the factors influencing their fundamental behavior. Simple models are more amenable to in-

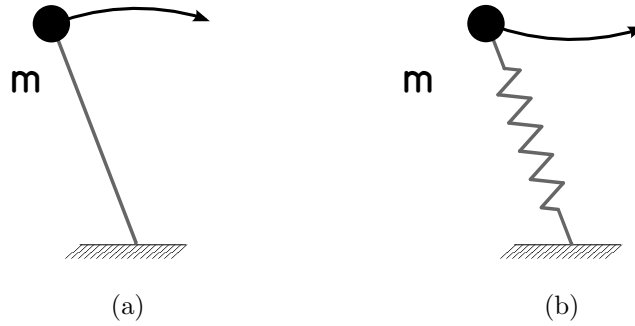


Figure 1.1: **Simple mechanical models** of the stance phase in walking and running. **a)** Inverted pendulum model, **b)** Spring-mass model, also known as the spring-loaded inverted pendulum (SLIP) model. In both models the body is reduced to a point mass m at the center of mass. In the inverted pendulum model the CoM is supported by a massless rigid leg, whereas in the SLIP model it is supported by a massless spring.

terpretation and are computationally fast, while comprehensive models have complexities that can obscure the underlying principles responsible for their observed behavior. If more elaborate models are required, it is advantageous to add complexities step-by-step to track their influence on model behavior.

Among different models proposed to study legged locomotion, the two simplest ones are the inverted pendulum model [13, 14], and the spring-mass model [15, 16, 17, 18]. The latter is also known as the spring-loaded inverted pendulum (SLIP) model [19]. These models are shown in Fig. 1.1. In both cases, the body is reduced to a point-mass located at the center of mass (CoM). In the inverted pendulum model the CoM is supported by a massless rigid stance leg, whereas in the spring-mass model it is supported by a massless spring. In the following, these models and their modified versions are briefly explained.

1.2.2 Inverted Pendulum Model

The inverted pendulum model is shown in Fig. 1.1a. This model was first proposed to study bipedal walking [13, 20]. This was based on the observation that walking seems to resemble a ‘compass gait’ where the CoM vaults over a rigid stance leg, and follows an almost arc-shape trajectory between two consecutive foot falls [13, 21]. Later, this model showed good success

in explaining some aspects of human and animal locomotion. For example, this model can in part explain the transfer of potential and kinetic energy during walking [20, 22]. It also correctly predicts that the speed at which animals and humans prefer to switch from walking to running is solely a function of gravitational acceleration and leg length [23, 24]. Although this model was first proposed to study walking, some modified versions of this model have also been used to study running, galloping, and trotting as well [25, 26].

1.2.3 Spring-Mass Model

This model is shown in Fig. 1.1b. The point-mass m , representing the total body mass, is supported by a massless spring. The SLIP model was originally proposed to model running [15, 16]. This was based on the observation that in human and animal running elastic energy can be stored and released by passive compliant structures such as tendons, ligaments, and even muscles [27, 28]. More recently, a modified version of this model with two massless springs has been used to generate stable walking gaits [3, 29].

One of the main features of this model is that it can correctly predict the ground reaction force (GRF) profiles in both walking and running [3, 29, 30]. Due to this feature and also the smooth behavior of this model at foot-ground contacts, the SLIP model has recently enjoyed substantial attention. However, the original SLIP model is completely energy conservative, so it cannot be used to study the energetics of locomotion, the subject of this thesis. Furthermore, it has been shown that many features of running can be correctly predicted using fully rigid models [2, 26, 31, 32]. Therefore, in the rest of the thesis I focus on rigid models.

1.2.4 Inverted Pendulum-Based Simple Model

Ballistic Walking Model:

Inspired from the observation of relatively low muscle activities during the swing phase of human walking [33], and that the sum of kinetic plus potential energies of the body CoM

changes relatively little during the swing phase of a walking step [34], Mochon and McMahon [35, 36] developed the ‘ballistic walking’ model with a stiff stance leg and a segmented swing leg. They showed that by choosing a realistic leg-mass distribution, and with proper initial conditions provided by muscle activities prior to swing, the model can move forward with no muscle activity during swing. Moreover, the model could produce swing times, joint angles, and reaction forces similar to those in normal human gait (during the swing phase).

The term ‘ballistic walking’ is used to emphasize that the motion of the swing leg is driven only by gravity and the momentum established by the initial velocities (like a projectile moving through space). In other words, no continuous energy investment (muscle work) or control is required during leg swing. This was an important step toward understanding effective legged locomotion.

The ballistic walking model was only a partial model of the step cycle, since it was limited to just the swing portion of the gait cycle. Therefore, it was limited in the insights it could provide on effective gaits, and more elaborate models were required to study the complete step cycle. The next important step in understanding the governing principles of legged locomotion was taken by Tad McGeer.

McGeer’s Passive Dynamic Walking Models:

Motivated by the results of the ballistic walking model, McGeer followed a systematic approach to study a series of two-dimensional passive gait models and walking mechanisms [37, 38, 39, 40, 41, 42]. His pioneering work proceeded with an evolution of models of increasing complexity combined with the development of physical robots to validate his theoretical models.

He first studied the ‘rimless wheel’ and the ‘synthetic wheel’ as simple models of walking [37, 38, 39]. The rimless wheel, shown in Fig. 1.2, consists of a mass at the center and n equally spaced struts extending outwards, like a wagon wheel without an outer rim. Once

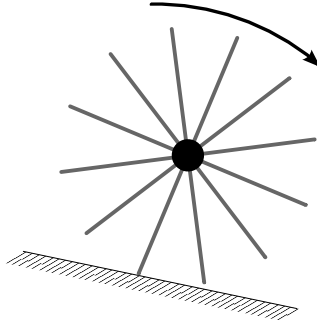


Figure 1.2: **Rimless wheel**. Gravity compensates for collision loss, and the rimless wheel exhibits a steady downhill ‘walking’.

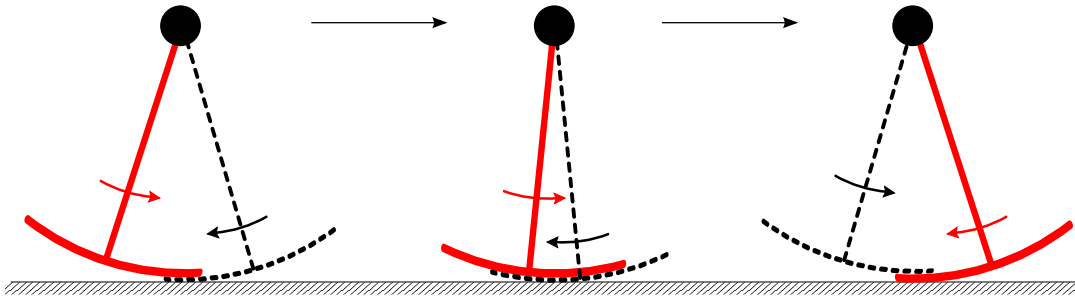


Figure 1.3: **Synthetic wheel** rolls forward just like an ordinary wheel. The radius of the semi-circular feet is equal to the stance-leg length. The swing leg (solid thick red) swings forward to ‘synthesize’ a continuous rim. For clarity, the swing leg (solid thick red) has been plotted slightly shorter than the stance (dashed thin black) leg.

started, this device will settle into a steady downhill ‘walk’, with gravity balancing the angular momentum lost on each support-strut transfer. The simplicity of the model allows for analytic proof of stability of the motion and the calculation of the steady state speed.

The other model studied by McGeer, the synthetic wheel shown in Fig. 1.3, has two straight legs and a large mass at the hip. It also has semi-circular feet with a radius equal to the leg length. Like a true wheel, the stance leg of this model rolls at constant speed along a flat surface. Meanwhile, the swing leg passively swings forward and makes the new support to ‘synthesize’ a continuous rim. Because there is no collision loss, in the absence of friction this model could exhibit a steady walking gait on level ground [37, 38, 39].

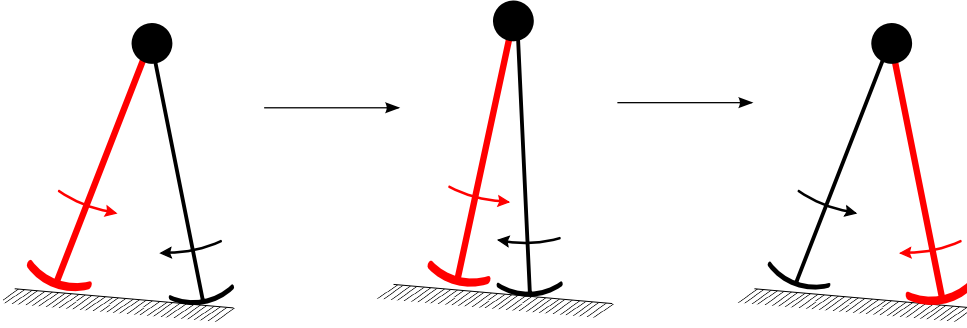


Figure 1.4: **Passive dynamic walking model.** If the radius of the feet is smaller than the leg length or the foot arc is not long enough to synthesize a continuous rim, collision loss occurs at each heel-strike, and the biped cannot exhibit a passive gait on level ground. If the biped is launched with proper initial conditions on a shallow slope, gravity can compensate for the heel-strike collision loss, and the walking gait will converge to a stable limit cycle.

By combining the rimless wheel and the synthetic wheel, McGeer developed more-realistic bipedal models that could passively walk down a shallow ramp [39, 40, 41]. A knee-less version of these models is shown in Fig. 1.4. Using mathematical gait models and linearized stability analysis, he showed that these models can have a stable limit cycle motion, provided that a proper mass distribution and link dimensions are used. He also built several physical models (with and without knee joints) that exhibit stable passive dynamic walking in two dimensions, *e.g.* [43].

Inspired by McGeer’s significant work, Collins *et. al.* built a three dimensional passive dynamic walker with knees [44]. Using the ideas of passive dynamic walking, and by adding a powered ankle and minimalistic control, Collins *et. al.* also built the Cornell Biped [45], a very efficient powered bipedal robot that could walk on level ground. Scaled for weight and speed, Cornell Biped matched human energy use.

Passive Simplest Walking Model:

Following McGeer, Garcia *et. al.* [46] studied the simplest passive walking model, an irreducible bipedal model exhibiting passive walking on a ramp (see Fig. 1.5). This model consists of two rigid legs connected at the hip by a frictionless joint. All the biped mass is

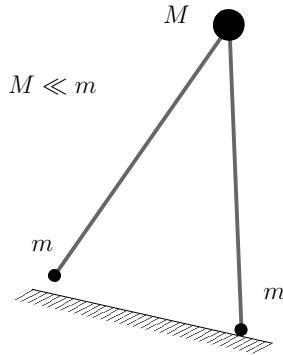


Figure 1.5: **Simplest walking model**; an irreducibly simple bipedal model that exhibits stable passive walking on a shallow ramp.

concentrated at either the feet or the hip. The hip mass is much larger than those at the feet. This allows for simplification of the stance leg dynamics, so an approximate analytic solution can be calculated for the stance leg motion. However, the authors did not simplify (approximate) the swing leg motion. Using numerical methods and linearized stability analysis of the type used by McGeer [39], they showed that this model can have stable limit cycles for some range of slopes.

The ballistic walking model and the passive dynamic walking models and robots show that the walking gait does not need high-bandwidth control, and during most of the step cycle the biped can move passively by its own natural dynamics. In other words, the low-bandwidth effective gait control can be achieved by properly exploiting the interaction between the biped's natural dynamics and its environment (gravity and the substrate); an important observation that should be noted in understanding effective legged locomotion.

Powered Simplest Walking Model:

The simplest walking model is completely passive, and therefore can only walk on a ramp to make up for the energy lost at heel-strike. To study the energetics of walking, Kuo [47] modified this model to walk on level ground. Powered walking was realized using either a torque applied to the stance leg, or an impulsive force applied along the stance leg immediately before heel strike. Using analytic analyses and a work-based energetic cost, Kuo showed that

for powered walking the pre-emptive impulsive push-off force is four times less costly than the torque on the stance leg. The reason for this substantial energetic cost improvement is that the pre-emptive push-off force reduces the collision loss at heel-strike.

The above result emphasizes the importance of the interaction between the biped and its substrate for an efficient gait. In fact, collision loss at heel-strike is the direct outcome of this interaction, so an effective control action is the one that interferes with this interaction to reduce the loss [2]. Furthermore, the powered simplest walking model predicts that for efficient walking, work is not needed within each step, but rather between steps where the CoM is redirected from moving downward to moving upward (step-to-step transitions). This prediction was later verified experimentally with human subjects [48, 49, 50].

By adding a spring at the hip to tune the step frequency and step length with no propulsive energy to the gait, Kuo also studied the effect of a hip torque on gait energetics [47]. At a given average walking speed, increasing the step frequency results in a shorter step length and less heel-strike loss (energy loss at foot-ground impact). Consequently, less push-off work is required to compensate for the loss.

Collisional Model, Leg Sequencing in Walking, and Pseudo-Elasticity in Running:

Ruina *et. al.* [26] also studied the energetics of legged locomotion using a simple collisional inverted pendulum model. With a work-based energetic cost, in which both positive and negative work contribute to the net cost through their respective efficiencies, they analytically showed that the relative timing of push-off and heel-strike impulses can substantially change the gait energetics. In fact, when push-off is applied before heel-strike the cost is 66% less than when push-off follows heel-strike. This, again, indicates the importance of the interaction between the biped's CoM motion (biped dynamics) and the substrate (the ground) for an efficient gait.

Ruina *et. al.* [26] also showed that to reduce the energetic cost in running the legs should

actively behave like purely elastic springs even in the absence of elastic elements in the legs (‘pseudo elasticity’). This indicates that the advantage of bouncing motion in running is more fundamental than just being produced by passive elastic elements in the body. In other words, the bouncing motion in running is effective by itself, regardless of how it is implemented (by either specific actuator force-position profiles, or passive springs), but the use of passive springs makes it more effective.

Walking and Running: the Optimal Gaits at Slow and Fast Speeds:

Using computer optimization of a simple bipedal model (massless rigid legs and a point-mass at the hip), Srinivasan and Ruina [25] found that among an infinite number of possible gaits, the classic inverted-pendulum walk is the most energy efficient gait at slow speeds. Furthermore, at high speeds a bouncing run is the optimal gait even without springs, verifying the optimality of the pseudo elasticity concept [26].

So far, I reviewed the main background relevant to simple bipedal models and energy efficient gaits. In the next section, I review the work related to one of the common, and surprisingly influential, characteristics among many different gaits, the specific motion of the swing leg prior to foot-ground contact.

1.3 Swing-Leg Retraction

When people walk or run their swing leg rotates forwards during most of the swing phase in preparation for the next step. However, just before the swing foot hits the ground (heel-strike), it decelerates rapidly and generally moves backwards slightly (e.g. [51, 52, 53, 54]). This late-swing rotation reversal, known as *swing-leg retraction*, is easily seen in running. In walking the retraction period is short and the final retracting leg angular velocity is small, so retraction in walking is difficult to see by eye, or even on videos. However, it can be easily seen as a sign change in the slope of the measured joint angles (velocities) and in

muscle activity recordings (e.g. [55]). The swing leg retraction is also observed in some animals (e.g. [52, 56, 57]). Why do many legged organisms use this swing leg retraction? Previous studies, using theoretical models and physical robots, have shown several benefits of swing-leg retraction.

Advantage 1: Increased Stability Regions in Running:

In the context of some particularly simple control policies (e.g. [58]), Seyfarth *et. al.* [59] showed that a retracting swing-leg angular velocity can increase the range of parameters (e.g. average speed, apex height) over which stable periodic running is possible. Here, stability is defined as whether the model returns to a periodic gait after a small deviation (caused by a disturbance or incorrect initial conditions) from the nominal periodic gait. In this context, stability is evaluated in terms of the eigenvalues of the Jacobian matrix of a periodic gait's Poincare map [60]; a gait is stable if all eigenvalues are inside the unit circle, otherwise not.

In walking, however, retracting the swing leg *decreases* the range of parameters (e.g. slope, step length) for a stable periodic gait, at least for a simple inverted pendulum model with massless legs [61]. In this model the parameter space for stable periodic walking is largest at zero retraction speed. However, walking with zero retraction (like a rimless wheel) would make the walker operate very close to instability, as the resulting eigenvalues are very close to the unit circle. Retracting the leg with a mild retraction speed will decrease the eigenvalues for a more reliable gait.

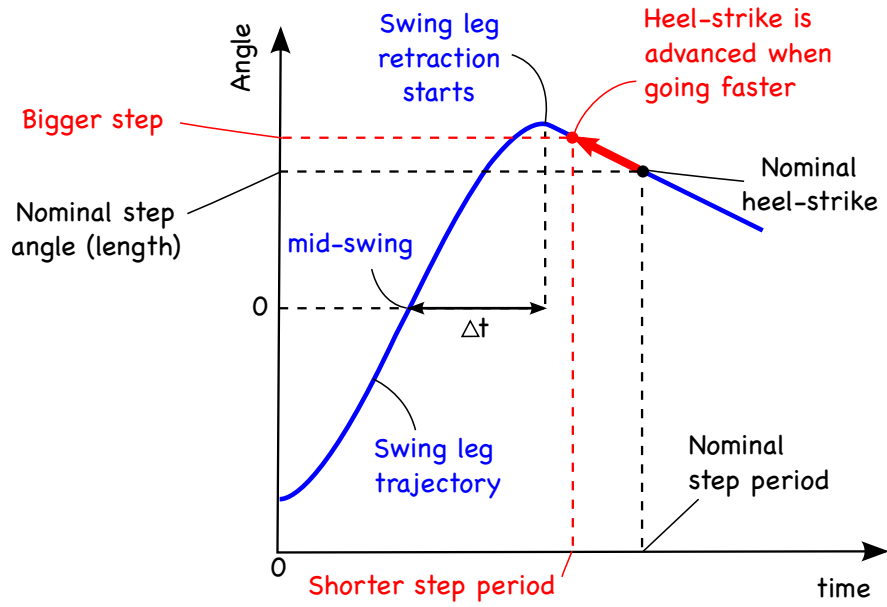
Advantage 2: Improved Disturbance Rejection:

For given gait parameters, a retracting swing-leg angular velocity prior to heel-strike can also improve the disturbance rejection. This improvement is characterized by either a faster recovery after a small disturbance, or a greater disturbance magnitude that can be tolerated without falling [62, 63]. For small disturbances the improved disturbance rejection is because the retraction reduces the magnitude of the eigenvalues of the Poincare Map's Jacobian

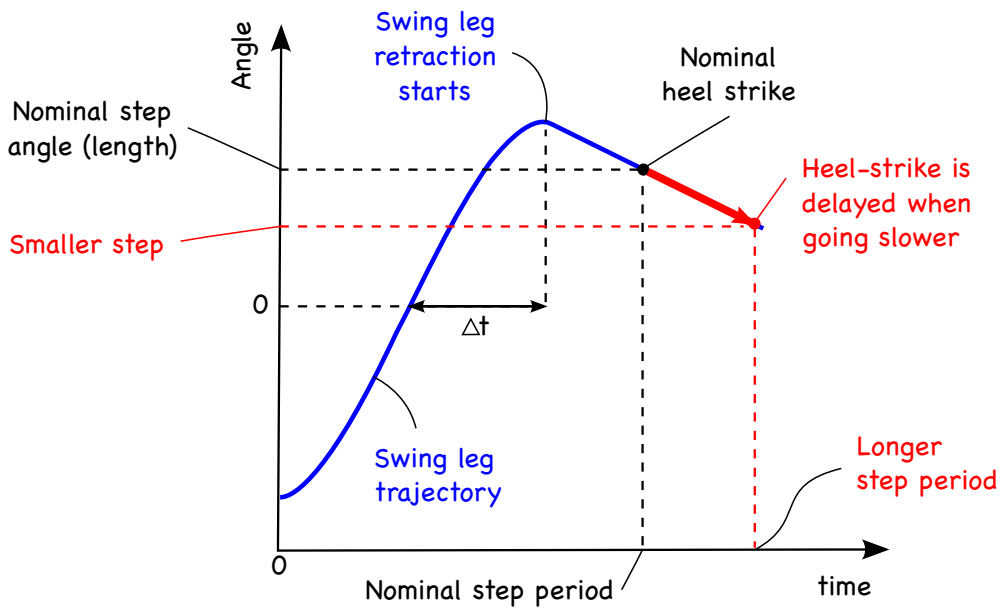
matrix, speeding the decay of transients after disturbances. Using a mild retraction speed, the fastest recovery from an arbitrary disturbance can be achieved when the eigenvalue with the largest magnitude is minimum.

How does this work? In the simplest walking model the full control strategy is to program the leg angle as a function of time [61], an open-loop motor program, starting with a trigger (*e.g.* the previous heel-strike or the instance of mid-stance). If such an open-loop motor program uses a retraction strategy, the hip angle (the inter-leg angle) will be decreasing at the time of impact. If the gait is perturbed, the time to heel-strike will depend on the perturbations. With a retraction strategy, the step length will be a decreasing function of the step period (or time from trigger until heel-strike). In this case, if the robot is pushed forward after the leg swing program is begun, then heel-strike will happen sooner than for the nominal (the undisturbed case), as shown in Fig. 1.6a, and the shorter-than-nominal retraction time will cause the lead leg take a longer-than-nominal step. This longer step causes more collisional dissipation and thus causes a slowing and return toward the nominal gait. If the robot is disturbed to walk slower than nominal, the longer retraction time causes a reduced step length (see Fig. 1.6b), a smaller collisional dissipation, and thus a speeding of the robot back towards its nominal gait. For spring-mass models [59] which conserve energy at heel-strike, the explanation is different in detail, having to do with the partitioning of energy into forwards and vertical parts, but the resulting response to perturbations, that a forwards push leads to slowing and *vice versa*, is the same.

For larger disturbances, Hobbelen and Wisse [62] found, using two theoretical models and a physical bipedal robot, that the magnitude of a random step-height disturbance that makes a walker fall is increased by using mild feed-forward leg retraction. That is to say, in the absence of real-time feedback control, an open-loop trajectory with some retraction gives more robustness to disturbances (larger basin of attraction and faster decay) than a trajectory without retraction. A similar result is verified by Karssen [63] for a simple



(a)



(b)

Figure 1.6: **The stabilizing effect of swing-leg retraction in walking.** Swing-leg retraction starts at a fixed time in the step cycle, *e.g.* Δt after mid-swing. With a retraction strategy, the step length will be a decreasing function of the step period (or retraction period). **a)** If the biped is perturbed to go faster than nominal, heel-strike will occur earlier-than-nominal, and the shorter-than-nominal retraction time will cause the swing leg take a longer-than-nominal step. This longer step causes more collisional dissipation, which with the nominal push-off force (energy input) results in a slowing towards the nominal gait. **b)** If the biped is disturbed to walk slower than nominal, the longer retraction time causes a reduced step length, a smaller collisional dissipation, and thus a speeding of the biped to return toward its nominal gait.

spring-mass running model.

Advantage 3: Improved State Estimation:

In closed loop control, state estimation is key. Because the relative timing between heel-strike and push-off highly influences the energetics of walking [26, 47], accurately predicting the heel-strike time can improve the push-off timing and amplitude. In the presence of sensor noise or physical disturbances, this increased determinacy can improve both gait energetics and also the determination of the walker states at the next step, resulting in increased controllability. Swing leg retraction might increase the accuracy of predicting when the swing foot will hit the ground. Why? Appropriate retraction leads to a more vertical foot velocity at heel-strike and thus a more determinate heel-strike time in the presence of uncertainties introduced by modeling errors, floor irregularities, and *etc.* [12].

Advantage 4: Improved Foot Clearance:

In order to avoid foot scuffing, especially in the presence of, or absence of knowledge about, ground obstacles, during swing the swing foot should be as high as possible. Given the need to straighten the leg before heel-strike, and the inability of the human knee to bend forward, swing-leg retraction allows for higher foot-swing while still ensuring heel-strike. This facilitates adequate ground clearance.

Advantage 5: Reducing the Tangential Collision at Heel-Strike:

A tangential heel-strike collision, one where the foot has substantial velocity tangent to the ground before heel-strike, can be harmful by causing foot slippage. Leg retraction, to the extent that it slows down swing-leg forward motion, can minimize or eliminate this tangential collision [63]. The scuffing of one foot can also cause an undesirable (Yaw/steer) torque about the vertical axis [64].

Note, a faster-than-passive swing can help walking in terms of stability regions or ener-

getics, as discussed by [47] and also later in this dissertation. However, that faster swing does not have to be decelerated by retraction; it could be braked by a scuffing foot collision. So, the desirability of a faster-than-passive swing, in itself, does not explain active, *versus* scuffing-collision, contraction. Thus, I do not count the benefits of a fast swing as a reason, in itself, for swing leg retraction.

Other Advantages for Swing-Leg Retraction?

There are further possible energetic benefits of swing-leg retraction. For example, retraction can reduce the collision loss by reducing the relative foot-ground speed at heel-strike. But this collisional saving comes at the extra effort spent to decelerate and reaccelerate the swing leg in the rearward direction. For a special running model, in which the axial (along the leg) GRF impulse at touch-down is avoided by the leg spring, it is shown in [65] that swing-leg retraction can reduce the net energetic cost of the gait. In the absence of the axial impulse, the optimal retraction rate is the one that nulls the tangential foot speed, and thus avoids any collisions at heel-strike [65, 66]. However, this optimal retraction rate may not be valid for gaits with non-negligible axial impulse, *e.g.* walking with rigid legs. The change in retraction rate changes the cost of retraction torque and collision loss, as well as the trade-off between them.

On the other hand, in walking, pre-emptive push-off and retraction occur at the same phase of the gait cycle (at the end of the swing phase). In a multi-body mechanism forces and/or torques at different joints are mechanically coupled, so their relative timing potentially influences the gait energetics. For example, the energetic cost of step-to-step transitions in walking (transition from one stance leg to the other) changes substantially when the order of impulses on leading and trailing legs is changed from (a) heel-strike followed by push-off to (b) push-off then heel-strike [26]. Therefore, the energetics of retraction and its potential cost improvement can be influenced by the interaction between the hip torque and the

push-off force, as well as by their relative timing.

The above discussion raises the questions of whether the energetic advantage of active swing-leg retraction still holds for walking, and if it does, for which step size, walking speed, and retraction rate? What is the best (energetically optimum) relative timing of the pre-emptive push-off force and the retraction hip torque to achieve a given swing-leg retraction rate prior to heel-strike? Should the retraction torque be just after, just before, or synchronous with the pre-emptive push-off force? Does the actuator efficiency have any effect on the results? If it does, what are the influences?

1.4 Problems Studied in This Thesis

As discussed above, minimal analytical and numerical models have shown good success in explaining some aspects of human and animal locomotion. Combining optimization with computer models [25, 67] holds substantial promise for interpreting the dynamics responsible for the locomotion strategies observed in the natural world. However, the capability of the minimal models is restricted, and thus at this stage it is reasonable to use more realistic (more complex) models to test a broader range of hypotheses.

In this thesis, I investigate some aspects of bipedal locomotion using two simple models probed with numerical and analytic techniques. The models are slightly more elaborate than the minimalistic ones previously used by other researchers. This increased complexity allows the inclusion of key features of the dynamic interaction of components that are not included in the simpler models, opening the possibility of discovering new insights into the system's dynamic opportunities.

The first model is used with numerical optimization to study the energy-optimal gaits at different speeds and terrains. Due to the limitations inherent in minimal models, extra constraints are required to achieve practical gaits (for instance minimum step length constraint

in [25]), whereas in this work the constraints are mostly limited to those imposing the laws of physics for the motion. The results of this study will help to find the main determinant factors in effective legged locomotion, as well as the control strategies for efficient walking and running.

The second model, which is simpler than the first one, is used to study swing-leg retraction in walking. The simplicity of the model allows the use of approximate analytic analyses to achieve more insight into how different gait parameters are influenced by each other. With this model I discover some new aspects of swing-leg retraction that can better explain the advantages of using leg retraction in effective legged locomotion.

1.5 Acknowledgement and Permission for Reproduction of the Text

Some of the text and graphs in this thesis are taken with permission from the following papers I have published.

- Hasaneini, S.J., Macnab, C.J.B., Bertram, J.E.A., and Leung, H., “The dynamic optimization approach to locomotion dynamics: human-like gaits from a minimally-constrained biped model”, *Advanced Robotics*, vol. 27, pp. 845-859, 2013.
- Hasaneini, S.J., Macnab, C.J.B., Bertram, J.E.A., and Ruina, A., “Eight reasons to brake leg swing just before heel strike”, *Online Proceedings of Dynamic Walking 2013*, June 2013.
- Hasaneini, S.J., Macnab, C.J.B., Bertram, J.E.A., and Leung, H., “Optimal relative timing of stance push-off and swing-leg retraction”, in *proceedings of 2013 IEEE/RSJ International Conference on Intelligent Robots and Systems*, pp. 3616-3623, Nov. 2013.

Hereby, I express my gratitude to the corresponding publishers for their kind cooperation in letting me reproduce the material here.

1.6 Thesis Outline

In Chapter 2, I introduce the bipedal model used to investigate gait optimization in a variety of circumstances. The governing dynamics of the model are described in detail. Also, a gait optimization algorithm that imposes a minimum set of realistic constraints is formulated. This serves as the mathematical background to the analyses in Chapters 3 and 4.

In Chapter 3, the gait optimization results of the minimally-constrained model is presented. The details of the resulting optimal gaits at different speeds and terrains are explained. Based on these results, the insights achieved on the determinant factors of walking and running are explained.

In Chapter 4, bipedal walking and running under reduced gravity conditions are investigated using the optimal gaits of the minimally constrained model introduced in Chapter 2. The results of the numerical optimization are compared to the experimental observations of human gaits. This study serves as a verification of the hypothesis that the same determinant factors discovered in Chapter 3 influence human gait coordination.

In Chapter 5, I introduce another simple model to study swing-leg retraction in walking. After explaining the governing dynamics and the constraints for a periodic gait, all gait parameters are formulated as a family of solutions parameterized by the step angle, average walking speed and the retraction impulse. This result will be used in the rest of the thesis to find the bounds or optimal value of the retraction impulse associated with different criteria.

In Chapter 6, the energetics of the impulsive walking gait of the model are studied, and the energy-optimal relative timing of the impulsive push-off force and retraction torque is analytically calculated.

In Chapter 7, approximate analytic solutions are derived for almost all gait parameters, including the energy-optimal retraction impulse and retraction rates. These solutions provide useful insights into the dominant behavior of different gait parameters and their dependency to each other.

In Chapter 8, three new model-based advantages of swing-leg retraction are discovered. These advantages are motivated by the approximate analyses in Chapter 7. Accurate numerical studies are also performed to verify the accuracy of the predictions of the approximate solutions. Furthermore, detailed analyses of the energetics of swing-leg retraction and its dependency on the step length, speed, actuator efficiency, and active negative work at heel-strike are presented.

Finally, I conclude the thesis in Chapter 9 by summarizing the main contributions of this research.

Chapter 2

A DYNAMIC OPTIMIZATION FRAMEWORK TO STUDY LEGGED LOCOMOTION

This chapter formulates the gait optimization problem of the first bipedal model studied in this thesis. It serves as the mathematical background to the analyses in Chapters 3 and 4, where bipedal locomotion is studied from energy efficiency point of view. Section 2.1 describes the biped model and the two types of gait considered here. In Section 2.2 the mathematical description of the governing dynamics is presented. The gait optimization is then formulated as an optimal control problem with a set of constraints discussed in detail in Section 2.3. The resulting optimal control problem is highly nonlinear, so the use of numerical techniques for optimization is inevitable. An efficient technique to numerically solve this problem is presented in the last section. Finally, the chapter is summarized in Section 2.4.

2.1 Biped and Gait Model

The planar articulated biped in Fig. 2.1 consists of seven rigid links: two flat feet, two telescoping legs (with upper and lower segments), and a torso. Six actuated one degree-of-freedom (DoF) frictionless rigid joints connect the links. The ankle joints A_1 and A_2 , and the hip joints H_1 and H_2 revolve, *i.e.* they are rotational joints, whereas the telescoping joints E_1 and E_2 serve to change the total leg length, *i.e.* prismatic joints. The telescoping actuators can only carry compressive (extensional) forces, and serve to model, in a simpler kinematic form, the human ankle's ability to push-off.

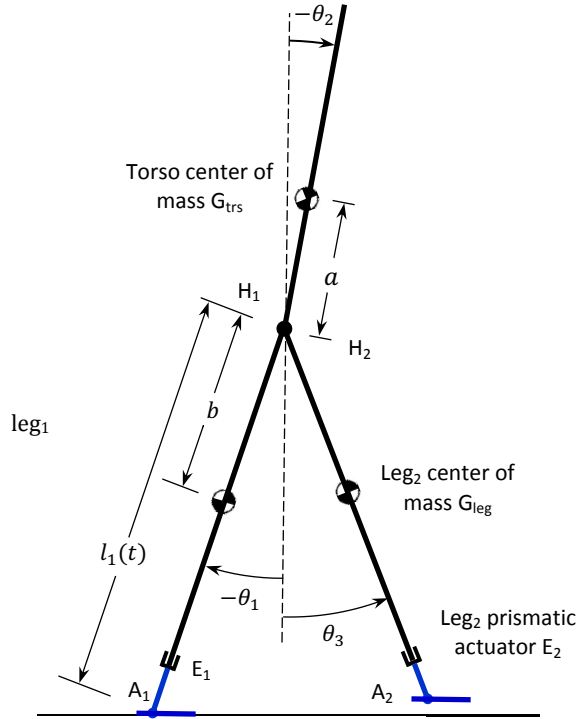


Figure 2.1: **The biped model with torso.** The legs and the torso have distributed mass, with their center of mass, G_{leg} and G_{trs} , located b and a distances from the hips. Feet are massless and always stay parallel to the ground. Thus the ankle actuators can apply torque only when the feet are on the ground. Each legs is equipped with a telescoping actuator that can change the leg length. The lower part of the legs, between the telescoping actuators and the feet, are massless.

In this study the feet and lower legs are treated as massless. The torso mass m_{trs} and the upper-leg mass m_{leg} are distributed about their individual CoM, G_{trs} and G_{leg} , located at distances a and b , respectively, from the hip. The biped's total mass is $m_{\text{tot}} = m_{\text{trs}} + 2 m_{\text{leg}}$. The moment of inertia of the torso, $I_{\text{trs}/G_{\text{trs}}}$, and of the upper leg, $I_{\text{leg}/G_{\text{leg}}}$, are taken about their individual CoM. While the upper legs have fixed length, the lower-leg lengths fluctuate independently. At time t the total length of each leg is $\ell_i(t)$ for $i=1,2$, and always $\ell_{\min} \leq \ell_i(t) \leq \ell_{\max}$. It is assumed that the foot length is enough to satisfy the gait requirements. The required minimum foot length thus follows from the resulting zero moment point (ZMP) [68] locations, verified after the gait is generated.

For simplicity it is assumed that the feet remain flat and parallel to the surface when on the ground. With this assumption ankle torque can *only* change the angular momentum (of the biped about the ankle joint). The ankle’s contribution in push-off and leg-length fluctuation is incorporated in the leg’s axial actuator. This configuration results in faster convergence of the optimal gait synthesis. Although the simulation results (see Chapter 3) show that a point foot is sufficient for gait optimization, an eventual closed-loop control can benefit from extended feet in order to reject disturbances.

When a leg is on the ground it is labeled as a *stance* leg, otherwise it is a *swing* leg. The focus of this study is on gaits where the stance foot does not slide. To let the stance leg’s length fluctuate in both directions it is assumed that the leg length at landing is $\ell_0 > \ell_{\min}$, where ℓ_{\min} is the minimum leg length. Because the massless lower segment of the swing leg can contract instantaneously, foot scuffing (stubbing) in mid-stance can be avoided without any cost. Except for possible instantaneous foot-ground collisions, all forces and torques remain bounded, causing velocities to vary continuously.

2.1.1 Details of the Gaits

The stance or *support* (SP) phase is the portion of a gait during which at least one leg is a stance leg. Depending on the number of stance legs involved, the SP can be either *single-support* (SS) or *double-support* (DS). In some literatures these phases are called single-stance and double-stance. The biped is in the *flight* (FL) phase when both legs are swing legs. Some gaits can have zero-duration DS and/or FL phases. For example in human walking there is no FL, while in running DS is of zero duration. The transition from SP to FL is called *take-off* (TK), and that from DS to SS is called *toe-off* (TO). At the end of FL and also in transition from SS to DS, the touch-down (TD) event occurs where a swing leg lands on the ground. This event is also known as heel-strike. The focus here is on gaits where the landing foot neither rebounds nor slides at TD. I do not assume either a collisional or

collision-less foot-ground contact *a priori*. Instead, the optimization procedure discovers the strategy leading to the *optimal gait*. The optimal gait minimizes energy expenditure subject to a set of physical and desired-motion constraints (see Section 2.3.1).

Among many possible phase sequences, two special periodic ones are of focus here:

- *Continuous-support gait*: a *step* has one DS, followed by one SS, followed by a TD event, or
- *Intermittent-support gait*: a *step* has one SP with SS, followed by one FL, followed by a TD event.

This study only considers the gaits where the individual legs' roles alternate between steps. Normal human walking and running or their impulsive approximations (pendular walk and impulsive run [25]) are special cases of the above gaits. However, this should not imply that for optimal gait synthesis the study here is limited to these special gaits. For a set of pre-determined gait parameters, like forward speed or step height, the implemented optimization routine is free to search among an infinite number of possible force and torque profiles (some of this spectrum of gaits may appear quite unlikely, reminiscent of the Monty Python skit "Ministry of Silly Walks" [69], but all are evaluated as potential options for optimization). Thus, part of the significance of the current study is comparing the resulting computer-generated optimal gaits to those normally used by humans, *i.e.* determining how *human-like* the optimal gaits are. From the hypothesis that humans choose their gait parameters based on minimum effort [14, 26, 70, 71], the algorithm selects the gait, among all valid periodic gaits, that minimizes an energy expenditure index subject to physical constraints.

2.1.2 Energetic Cost of the Gait

Researchers have addressed the effort demanded of locomotion in biological systems as the total metabolic cost per unit distance traveled [14, 26, 67, 71, 72]. Srinivasan [67] has shown that for different simple bipedal models, and many different metabolic cost models,

the qualitative behavior of energy-minimizing gaits is not highly sensitive to the choice of metabolic cost model. Hence, I choose a simple mechanical-work based model [25, 26] where a muscle’s metabolic energy expenditure rate \dot{E} is proportional to its mechanical power \dot{W} . The proportionality constant is the energetic cost of unit work (or equivalently the inverse of the muscle efficiency), and in general, is different for positive and negative work¹ [26, 73]. If c_1 and c_2 are the energetic costs of unit positive and negative work, the work-based cost model estimates the total energetic cost of the whole body as

$$E_{\text{step}} = \int_{t_0}^{t_0+T} \sum_{i \in \{\text{muscles}\}} \left(c_1 \dot{W}_i^+(t) - c_2 \dot{W}_i^-(t) \right) dt. \quad (2.1)$$

Here t_0 is an arbitrary instant, T is the step period, and $\dot{W}_i^+(t)$ and $\dot{W}_i^-(t)$ are the instantaneous positive and negative muscle (actuator) powers. Using the positive-part function $[x]^+$, where $[x]^+$ is x for $x \geq 0$ and 0 for $x < 0$, the positive and negative muscle powers follow $\dot{W}_i^+(t) = [\dot{W}_i(t)]^+$, and $\dot{W}_i^-(t) = \dot{W}_i(t) - \dot{W}_i^+(t)$. Energy storage and recovery provides no contribution in the above work-based cost model, consistent with the fully rigid model used here. For the bipedal model, the summation in (2.1) should be taken over all actuators.

Using the above equations, the total energetic cost per unit distance traveled and per unit body weight, or specific *cost of transport* (COT), is given by

$$\mathcal{C}_{\text{et}} = \frac{E_{\text{step}}}{m_{\text{tot}} g D_{\text{step}}}, \quad (2.2)$$

where g is gravity, and D_{step} is the step length: the distance travelled by the CoM during the step period T (between two consecutive TD events). In this work, a gait is energetically most efficient if its specific COT (\mathcal{C}_{et}) is minimum for given cost coefficients c_1 and c_2 . Typical human locomotion results in 25% and 120% positive and negative work efficiencies, respectively [26, 73]. Consequently, for the analysis in Chapters 2 and 3, $c_1 = 1/0.25$ and $c_2 = 1/1.2$ are used to calculate \mathcal{C}_{et} . An alternative performance measure in legged robots

¹When an actuator accelerates [decelerates] its corresponding joint it does positive [negative] work. In mathematical terms, if force/torque $F(t)$ is acting on a joint whose instantaneous velocity is $v(t)$, the actuator does positive work when $\dot{W}(t) = F(t)v(t) > 0$, and negative work when $\dot{W}(t) = F(t)v(t) < 0$.

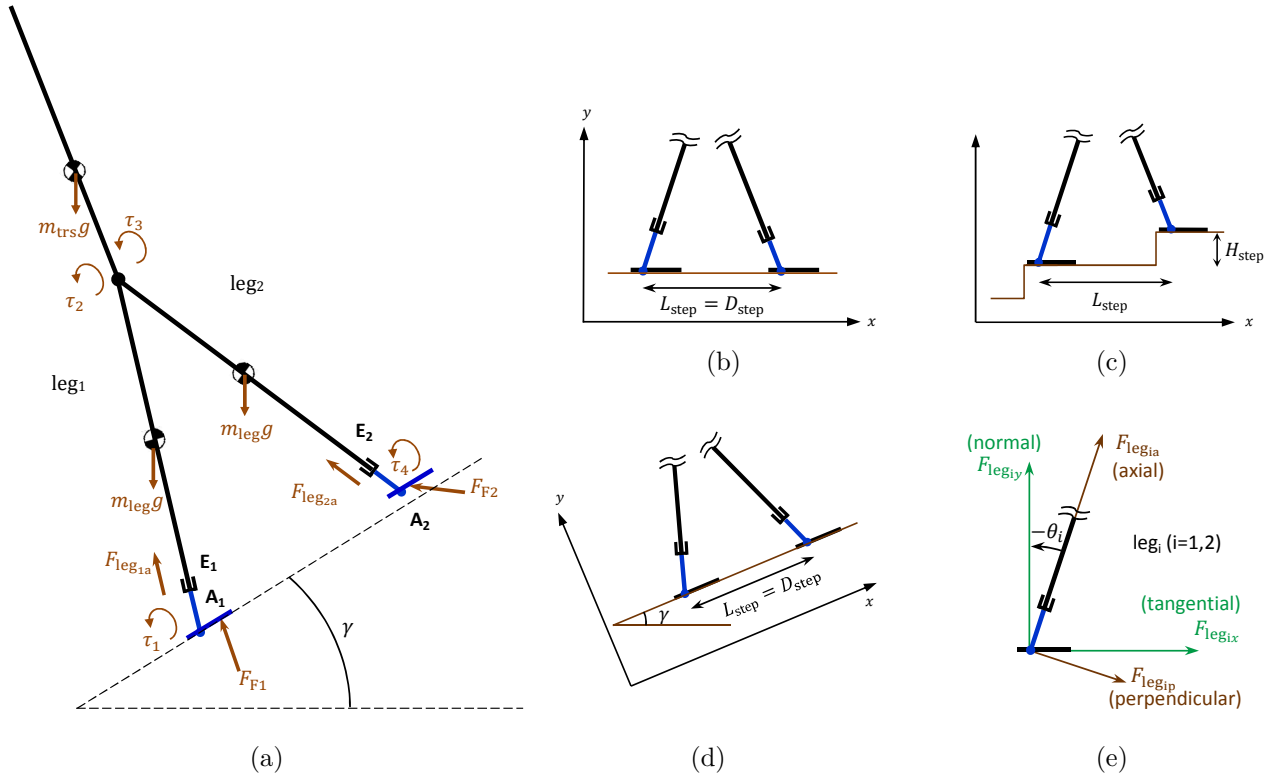


Figure 2.2: **Biped on different terrains.** Panel (a) shows different forces and torques acting on the biped. Panels (b)-(d) show different terrains with the associated reference frames. Panel (e) shows the force components associated with leg_{*i*} for $i=1,2$. $F_{\text{leg}_{1a}}$ and $F_{\text{leg}_{2a}}$ are the leg actuator forces along each leg, while $F_{\text{leg}_{1p}}$ and $F_{\text{leg}_{2p}}$ are the constraint forces perpendicular to each leg.

is known as the *mechanical* COT (C_{mt}) [45] which is calculated from (2.2) with $c_1 = 1$ and $c_2 = 0$ (only positive work).

2.2 Mathematical Description of the Biped

Consider three stepping surfaces: level ground, flight of stairs, and inclined (see Fig. 2.2b-2.2d). In all three cases the reference frame has its x -axis parallel to the ground surface, in the *tangential* direction. In this thesis, *tangential* and *normal* indicate directions with respect to (w.r.t.) the ground surface (Fig. 2.2e), whereas *vertical* and *horizontal* directions are defined along and perpendicular to gravity, respectively. If the ground surface has no inclination, *normal* and *vertical* are equivalent, and so are *tangential* and *horizontal*. The terms *axial* and *perpendicular* denote directions along and normal to a leg, respectively. A

motion or vector is considered *forward* if it has a positive component in the desired direction of the biped’s motion (otherwise it is *backward* or *rearward*).

The biped moves forward along the positive x -axis. For stepping down a slope (or stairs) the inclination angle γ and step height H_{step} are negative. A generalized formula can incorporate all three cases in Fig. 2.2b-2.2d: in level-ground locomotion $H_{\text{step}} = \gamma = 0$, whereas for inclined surfaces $\gamma \neq 0$ and $H_{\text{step}} = 0$. Choosing $\gamma = 0$ with $H_{\text{step}} \neq 0$ represents stepping on a flight of stairs. The step length is always given by $D_{\text{step}} = \sqrt{L_{\text{step}}^2 + H_{\text{step}}^2}$ where L_{step} is the tangential distance between consecutive footsteps.

Fig. 2.2a illustrates the general forces and torques acting on the biped. Ground reaction forces \vec{F}_{F1} and \vec{F}_{F2} affect the feet, and F_{Fi_x} and F_{Fi_y} ($i = 1, 2$) are the components of \vec{F}_{Fi} along the x and y axes. Axial leg forces $F_{\text{leg}_{1a}}$ and $F_{\text{leg}_{2a}}$ are the compressive forces applied by the telescoping actuators on legs. Ankle torques τ_1 and τ_4 from the feet affect the corresponding legs. The torso applies torques τ_2 and τ_3 to the legs. The orientation of the i^{th} link ($i = 1, 2, 3$) is given by the absolute angles θ_i measured from the normal to the surface (Fig. 2.1). Because the foot and the lower leg segment are massless, the swing foot orientation and the swing leg length can vary instantaneously without any cost. For simplicity, assume a constant leg length (ℓ_0) and flat foot orientation for the swing leg.

2.2.1 Equations of Motion of the Unpinned Bipod

In this study, a Newton-Euler formulation is used to provide insight into how forces and torques affect the motion. First, the equations of motion (EoM) are derived for the general case of the unpinned (unconstrained) bipod model (Fig. 2.2a), and then constraints are added to define each phase. In the general case, the coordinates of all points on the bipod follow from the coordinates of the bipod’s CoM in the reference frame, $\mathbf{q}_{\text{Gtot}} = [x_{\text{Gtot}}, y_{\text{Gtot}}]^T$, the orientation of the links, $\mathbf{q}_{\theta} = [\theta_1, \theta_2, \theta_3]^T$, and leg extensions, $\mathbf{q}_{\ell} = [\ell_1, \ell_2]^T$. For the unpinned bipod, angular momentum balance equations of the individual leg₂, torso, and leg₁

about H_1 , H_2 , and A_1 , respectively, and the linear momentum balance equations of the whole biped along the x and y directions provide a set of five equations:

$$\mathbf{M}(\mathbf{q}_\theta) \ddot{\mathbf{q}}_\theta - m_{\text{tot}} \mathbf{J}_{1\theta}^T(\mathbf{q}_\theta, \mathbf{q}_\ell) \ddot{\mathbf{q}}_{\text{Gtot}} + \mathbf{c}(\mathbf{q}_\theta, \dot{\mathbf{q}}_\theta, \mathbf{q}_\ell, \gamma) = \mathbf{B} \boldsymbol{\tau} + \mathbf{J}_{21\theta}^T(\mathbf{q}_\theta, \mathbf{q}_\ell) \mathbf{f}_{\text{F2}}, \quad (2.3)$$

$$m_{\text{tot}} \ddot{\mathbf{q}}_{\text{Gtot}} = \mathbf{f}_{\text{F1}} + \mathbf{f}_{\text{F2}} + m_{\text{tot}} \mathbf{g}, \quad (2.4)$$

where \mathbf{M} is the inertia matrix, the vector \mathbf{c} contains the Coriolis, centrifugal, and gravity terms, \mathbf{B} is the torque-influence matrix, $\mathbf{g} = -[\sin(\gamma), \cos(\gamma)]^T g$ is the gravity acceleration vector expressed in the reference frame, $\mathbf{f}_{\text{F1}} = [F_{\text{F1}_x}, F_{\text{F1}_y}]^T$, $\mathbf{f}_{\text{F2}} = [F_{\text{F2}_x}, F_{\text{F2}_y}]^T$, $\boldsymbol{\tau} = [\tau_1, \tau_2, \tau_3, \tau_4]^T$, and $\mathbf{J}_{1\theta}$ and $\mathbf{J}_{21\theta}$ are the Jacobian matrices (defined below). All the above matrices and vectors are expressed in Appendix A.1. Using the virtual work principle, or simply by inspection, one can verify that in (2.3)

$$\mathbf{J}_{21\theta} = \frac{\partial \mathbf{r}_{\text{A2/A1}}}{\partial \mathbf{q}_\theta}, \quad (2.5)$$

$$\mathbf{J}_{1\theta} = \frac{\partial \mathbf{r}_{\text{A1/Gtot}}}{\partial \mathbf{q}_\theta}, \quad (2.6)$$

where $\mathbf{r}_{\text{A2/A1}}$ is the position vector of A_2 relative to A_1 , and $\mathbf{r}_{\text{A1/Gtot}}$ is the position vector of A_1 relative to the biped's CoM. These Jacobians are provided in Appendix A.5.

2.2.2 Single-Support Phase

Without loss of generality, consider leg_1 and leg_2 as the stance and swing legs, respectively. In this case, $\mathbf{f}_{\text{F2}} = 0$, and because the swing leg's distal links are massless $\tau_4 = F_{\text{leg}_{2a}} = 0$. With the swing leg's prismatic joint locked, four inputs $\boldsymbol{\tau}_{\text{ss}} = [F_{\text{leg}_{1a}}, \tau_1, \tau_2, \tau_3]^T$ control the biped in SS. This fully actuated system has four DoF, determined by $\mathbf{q}_{\text{ss}} = [\ell_1, \mathbf{q}_\theta^T]^T$. Because A_1 is fixed, $\dot{\mathbf{q}}_{\text{Gtot}}$ and $\ddot{\mathbf{q}}_{\text{Gtot}}$ are related to the joint velocities and accelerations as below:

$$\dot{\mathbf{q}}_{\text{Gtot}} = \dot{\mathbf{r}}_{\text{Gtot/A1}} = -\mathbf{J}_{1\theta} \dot{\mathbf{q}}_\theta - \mathbf{J}_{1\ell_1} \dot{\ell}_1, \quad (2.7)$$

$$\ddot{\mathbf{q}}_{\text{Gtot}} = \ddot{\mathbf{r}}_{\text{Gtot/A1}} = -\mathbf{J}_{1\theta} \ddot{\mathbf{q}}_\theta - \mathbf{J}_{1\ell_1} \ddot{\ell}_1 + \mathbf{h}_1, \quad (2.8)$$

where $\mathbf{J}_{1\ell_1} = \partial \mathbf{r}_{A_1/G_{\text{tot}}} / \partial \ell_1$, and \mathbf{h}_1 collects the second-order and cross-product derivative terms. The details of these quantities are provided in Appendix A.5. Substituting (2.8) into (2.3) yields three equations in terms of four generalized coordinates. The force balance equation on the massless foot₁ and lower leg₁, combined with (2.4), gives a fourth:

$$F_{\text{leg}_{1a}} = [-\sin \theta_1, \cos \theta_1] \mathbf{f}_{F1} = [-\sin \theta_1, \cos \theta_1] m_{\text{tot}} (\ddot{\mathbf{q}}_{G_{\text{tot}}} - \mathbf{g}). \quad (2.9)$$

The resulting four equations can be rearranged in the compact form:

$$\mathbf{M}_{\text{ss}}(\mathbf{q}_{\text{ss}}) \ddot{\mathbf{q}}_{\text{ss}} + \mathbf{c}_{\text{ss}}(\mathbf{q}_{\text{ss}}, \dot{\mathbf{q}}_{\text{ss}}, \gamma) = \mathbf{B}_{\text{ss}} \boldsymbol{\tau}_{\text{ss}}, \quad (2.10)$$

where the details of the above matrices are provided in Appendix A.2.

2.2.3 Double-Support Phase

In this phase both legs are on the ground, implying non-zero \mathbf{f}_{F1} and \mathbf{f}_{F2} . All six actuators are potentially active, but the biped has only four DoF. The vector $\mathbf{q}_{\text{ds}} = [\ell_1, \mathbf{q}_\theta^T]^T$ determines the biped configuration. Since both feet must be stationary on the ground with proper distance between, we should have

$$\mathbf{r}_{A_2/A_1} = [-L_{\text{step}}, -H_{\text{step}}]^T, \quad (2.11)$$

$$\dot{\mathbf{r}}_{A_2/A_1} = [\mathbf{J}_{21\ell_1}, \mathbf{J}_{21\theta}, \mathbf{J}_{21\ell_2}] \begin{bmatrix} \dot{\ell}_1 \\ \dot{\mathbf{q}}_\theta \\ \dot{\ell}_2 \end{bmatrix}^T = \mathbf{0}, \quad (2.12)$$

$$\ddot{\mathbf{r}}_{A_2/A_1} = [\mathbf{J}_{21\ell_1}, \mathbf{J}_{21\theta}, \mathbf{J}_{21\ell_2}] \begin{bmatrix} \ddot{\ell}_1 \\ \ddot{\mathbf{q}}_\theta \\ \ddot{\ell}_2 \end{bmatrix}^T + \mathbf{h}_{21} = \mathbf{0}, \quad (2.13)$$

where $\mathbf{J}_{21\ell_i} = \partial \mathbf{r}_{A_2/A_1} / \partial \ell_i$ for $i = 1, 2$, and \mathbf{h}_{21} collects the second-order and cross-product derivative terms. These Jacobian and derivative matrices are expressed in Appendix A.5. The length and extension rate of leg₂, *i.e.* ℓ_2 and $\dot{\ell}_2$, are not free in this phase and can be calculated from (2.11) and (2.12).

Equations (2.7) and (2.8) also apply in DS. By canceling $\ddot{\ell}_2$ between the two rows of (2.13), and substituting (2.8) into (2.3) we get four equations in terms of six unknown

variables: $\ddot{\mathbf{q}}_{\text{ds}}, \mathbf{f}_{\text{F}_2}$. Force balance equations on the massless parts of leg₂ relate \mathbf{f}_{F_2} to the known actuator force $F_{\text{leg}_{2a}}$ and the unknown constraint force $F_{\text{leg}_{2p}}$ (Fig. 2.2e). Finally, we can remove $F_{\text{leg}_{2p}}$ from the equations by calculating it in terms of $\ddot{\mathbf{q}}_{\text{ds}}, F_{\text{leg}_{1a}}$, and $F_{\text{leg}_{2a}}$ using the force balance equation along the massless lower leg₁ (equivalent to (2.9) with non-zero \mathbf{f}_{F_2}). The four simplified equations constitute the EoM in DS, and can be rearranged in the compact form:

$$\mathbf{M}_{\text{ds}}(\mathbf{q}_{\text{ds}}) \ddot{\mathbf{q}}_{\text{ds}} + \mathbf{c}_{\text{ds}}(\mathbf{q}_{\text{ds}}, \dot{\mathbf{q}}_{\text{ds}}, \gamma) = \mathbf{B}_{\text{ds}} \boldsymbol{\tau}_{\text{ds}}, \quad (2.14)$$

where $\boldsymbol{\tau}_{\text{ds}} = [F_{\text{leg}_{1a}}, F_{\text{leg}_{2a}}, \tau_1, \tau_2, \tau_3, \tau_4]^T$, and the other matrices and vectors are expanded in Appendix A.3.

2.2.4 Flight Phase

In this phase both GRFs, \mathbf{f}_{F_1} and \mathbf{f}_{F_2} , are zero, and gravity acts as the only external force, simplifying (2.4) to $\ddot{\mathbf{q}}_{\text{Gtot}} = \mathbf{g}$. Having unconstrained massless links gives zero $\tau_1, \tau_4, F_{\text{leg}_{1a}}$, and $F_{\text{leg}_{2a}}$, and reduces the torque vector to $\boldsymbol{\tau}_{\text{fl}} = [\tau_2, \tau_3]^T$. With both leg-lengths locked, the biped exhibits five DoF in FL with vector $\mathbf{q}_{\text{fl}} = [\mathbf{q}_{\text{Gtot}}^T, \mathbf{q}_{\theta}^T]^T$ fully determining the biped configuration. In this case the general-case EoM in (2.3) simplify to

$$\mathbf{M}(\mathbf{q}_{\theta}) \ddot{\mathbf{q}}_{\theta} + \mathbf{c}_{\text{fl}}(\mathbf{q}_{\theta}, \dot{\mathbf{q}}_{\theta}) = \mathbf{B}_{\text{fl}} \boldsymbol{\tau}_{\text{fl}}, \quad (2.15)$$

where the mass matrix \mathbf{M} is the one appeared in (2.3). The matrix \mathbf{B}_{fl} and the vector \mathbf{c}_{fl} are expanded in Appendix A.4.

2.2.5 Touch-Down Map

The optimization procedure allows both collision-less and collisional TDs. A collisional TD will be an instantaneous inelastic rigid impact, in which the ground exerts passive impulsive forces on the stance leg(s) [74], and joint velocities change discontinuously. Positive impulsive work at TD is not allowed. This imposes hard limits on post-TD extension/shortening rate

of the stance legs: the new stance leg cannot be extending immediately after TD; also in continuous-support gaits with extended double-support, the former stance leg cannot extend immediately after TD if it was shortening just before TD, or if it was lengthening its extension rate cannot increase.

In collision-less contacts the GRF remains bounded, and joint velocities are continuous. The optimization procedure also has the option of locking the linear leg actuators for a passive transfer of the impulsive axial leg forces to the rest of the body, or allowing them to try to actively *absorb* some of the impact in an active control.

In order to find the optimum gait without considering the type of TD *a priori*, the algorithm requires an algebraic mapping for TD that is independent of the type of foot-ground contact. Here I derive the TD map for both gaits without using a matrix-inversion operation (unlike previous studies including [1]), and without assuming a zero-duration DS phase in the continuous-support gait. Assume that leg₁ is going to land at time t_{td} , making $\mathbf{f}_{F1}(t_{td})$ either impulsive or bounded (based on the relative foot-ground velocity). In intermittent-support gaits leg₂ is above the ground at TD, making $\mathbf{f}_{F2}(t_{td}) = 0$, but in continuous-support gaits $\mathbf{f}_{F2}(t_{td})$ can be unbounded. During TD the configuration of the mechanism remains unchanged, so the terms in the left hand side of (2.3), with the possible exception of the first and the second terms, remain bounded. Therefore, integrating the general-case EoM in (2.3) and (2.4) over the infinitesimal duration of TD gives

$$\mathbf{M} \cdot (\dot{\mathbf{q}}_{\theta}^+ - \dot{\mathbf{q}}_{\theta}^-) - m_{tot} \mathbf{J}_{1\theta}^T \cdot (\dot{\mathbf{q}}_{G_{tot}}^+ - \dot{\mathbf{q}}_{G_{tot}}^-) = \mathbf{J}_{21\theta}^T \mathbf{i}_{F2}, \quad (2.16)$$

$$m_{tot} (\dot{\mathbf{q}}_{G_{tot}}^+ - \dot{\mathbf{q}}_{G_{tot}}^-) = \mathbf{i}_{F1} + \mathbf{i}_{F2} = \begin{bmatrix} \mathcal{I}_{F1_x} + \mathcal{I}_{F2_x} \\ \mathcal{I}_{F1_y} + \mathcal{I}_{F2_y} \end{bmatrix}, \quad (2.17)$$

where \mathbf{M} and $\mathbf{J}_{1\theta}$ are evaluated at t_{td} , and the superscripts $-$ and $+$ denote the time instants immediately before, and immediately after t_{td} . Also, $\mathbf{i}_{Fi} = \int_{t_{td}^-}^{t_{td}^+} \mathbf{f}_{Fi}(t) dt$ is the TD impulse on leg _{i} ($i = 1, 2$) with the tangential and normal components \mathcal{I}_{Fi_x} and \mathcal{I}_{Fi_y} , respectively. In

intermittent-support gaits $\mathbf{i}_{F2} = \mathbf{0}$. If in FL, $\dot{\mathbf{q}}_{G_{tot}}^-$ follows from both the CoM velocity at TK and the duration of FL. If in SS, $\dot{\mathbf{q}}_{G_{tot}}^-$ follows from $\dot{\mathbf{q}}_\theta^-$ and $\dot{\ell}_2^-$, as

$$\dot{\mathbf{q}}_{G_{tot}}^- = -\mathbf{J}_{2\theta} \dot{\mathbf{q}}_\theta^- - \mathbf{J}_{2\ell_2} \dot{\ell}_2^-, \quad (2.18)$$

where $\mathbf{J}_{2\theta} = \partial \mathbf{r}_{A_2/G_{tot}} / \partial \mathbf{q}_\theta$ and $\mathbf{J}_{2\ell_2} = \partial \mathbf{r}_{A_2/G_{tot}} / \partial \ell_2$ are evaluated at t_{td} . In both cases, the landing foot (foot₁) becomes motionless immediately after foot-ground contact, and $\dot{\mathbf{q}}_{G_{tot}}^+$ can be calculated as a function of $\dot{\mathbf{q}}_\theta^+$ and $\dot{\ell}_1^+$ using (2.7). To produce the TD-map for continuous-support gaits, substitute (2.7) and (2.18) in (2.16) to get

$$\begin{aligned} \begin{bmatrix} m_{tot} \mathbf{J}_{1\theta}^T \mathbf{J}_{1\ell_1} & \mathbf{M} + m_{tot} \mathbf{J}_{1\theta}^T \mathbf{J}_{1\theta} \end{bmatrix} \begin{bmatrix} \dot{\ell}_1^+ \\ \dot{\mathbf{q}}_\theta^+ \end{bmatrix} = \\ \begin{bmatrix} m_{tot} \mathbf{J}_{1\theta}^T \mathbf{J}_{2\ell_2} & \mathbf{M} + m_{tot} \mathbf{J}_{1\theta}^T \mathbf{J}_{2\theta} \end{bmatrix} \begin{bmatrix} \dot{\ell}_2^- \\ \dot{\mathbf{q}}_\theta^- \end{bmatrix} + \mathbf{J}_{21\theta}^T \mathbf{i}_{F2}. \end{aligned} \quad (2.19)$$

Equivalent substitutions for intermittent-support gaits result in the following TD-map:

$$\begin{bmatrix} m_{tot} \mathbf{J}_{1\theta}^T \mathbf{J}_{1\ell_1} & \mathbf{M} + m_{tot} \mathbf{J}_{1\theta}^T \mathbf{J}_{1\theta} \end{bmatrix} \begin{bmatrix} \dot{\ell}_1^+ \\ \dot{\mathbf{q}}_\theta^+ \end{bmatrix} = \begin{bmatrix} -m_{tot} \mathbf{J}_{1\theta}^T & \mathbf{M} \end{bmatrix} \begin{bmatrix} \dot{\mathbf{q}}_{G_{tot}}^- \\ \dot{\mathbf{q}}_\theta^- \end{bmatrix}, \quad (2.20)$$

where all matrices are evaluated at t_{td} . Due to the non-instantaneous DS in continuous-support gaits, A_2 must remain motionless immediately after TD. Canceling $\dot{\ell}_2^-$ between the two rows of (2.12) results in

$$\mathbf{J}_{21\ell_2}^T \begin{bmatrix} 0 & 1 \\ -1 & 0 \end{bmatrix} \begin{bmatrix} \mathbf{J}_{21\ell_1} & \mathbf{J}_{21\theta} \end{bmatrix} \begin{bmatrix} \dot{\ell}_1^+ \\ \dot{\mathbf{q}}_\theta^+ \end{bmatrix} = 0. \quad (2.21)$$

Summarizing, in intermittent-support gaits six unknown variables $\dot{\mathbf{q}}_\theta^+$, $\dot{\ell}_1^+$, \mathcal{I}_{F1_x} , \mathcal{I}_{F1_y} appear in five equations: two in (2.17) and three in (2.20). In continuous-support gaits two extra unknown variables, \mathcal{I}_{F2_x} and \mathcal{I}_{F2_y} , add up to eight unknowns appearing in six equations: two in (2.17), three in (2.19), and one in (2.21). For gaits with no axial impulsive GRF, conservation of the linear momentum along the stance leg(s) at TD equalizes the number

of unknowns and equations, otherwise unknown active impulse(s) of the stance leg actuator(s) leaves extra D(s)oF in TD mapping for optimization. Note, the direct calculation of the post-TD joint velocities from the pre-TD kinematic information involves inverse matrix calculations and, even with efficient decomposition methods, is computationally expensive. Instead, in a computationally efficient approach the optimization can find a set of joint velocities on both sides of TD that satisfy the TD-map.

2.3 Optimal Control Problem

The goal of this study is to minimize the specific COT \mathcal{C}_{et} , given by (2.2), subject to the functional constraints. In the language of Optimization theory, this is a constrained nonlinear optimal control problem. The objective here is to produce a *quasi-global* (global within the parameter range) solution by maintaining as many free parameters as possible, *via* imposing the minimum number of constraints. Specifically, only natural phenomena defining the physical system as well as the desired (pre-determined) parameters defining the general objective of the locomotion task (*e.g.* speed, step height) constitute constraints.

2.3.1 Constraints

For a physically consistent system, the EoM and the defined phase sequence (see Section 2.1.1) must be satisfied throughout the entire step². Assume that the step starts ($t=0$) when foot₁ lands at $\mathbf{r}=\mathbf{0}$. The TD-map equations (previous section) serve as a set of constraints that can be evaluated for a given set of pre- and post-TD joint velocities, and GRF impulses. To satisfy the zero-slip condition at TD and during the entire SP phase, the normal and tangential GRFs and possible TD impulses on each stance leg must lie in or on

²In this work the phase sequence is assumed *a priori*, and therefore it should be imposed by the constraints. After writing and defending this thesis, I learned that there are some studies (*e.g.* [75, 76]) that have considered the gait optimization problem without imposing the phase sequence. In fact, in those studies the optimal phase sequence is also determined by the optimization.

the friction cone, with the normal components directed upward. If a bound on axial leg force at TD is required, the axial (and only axial) GRF impulse at TD has to be zero, otherwise proper limits on post-TD leg extension rates are required to prevent impulsive positive work by the telescoping actuators:

$$\dot{\ell}_1(0^+) \leq 0, \quad (2.22)$$

$$\dot{\ell}_2(0^+) \leq \begin{cases} 0 & \text{if } \dot{\ell}_2(0^-) \leq 0 \\ \dot{\ell}_2(0^-) & \text{if } \dot{\ell}_2(0^-) \geq 0 \end{cases} \quad (2.23)$$

The latter equation is valid in continuous-support gaits only.

For the DS phase, the position and velocity of foot₂ become other constraints. With the zero foot-acceleration equation, given by (2.13), as part of the EoM in DS, imposing (2.11) and (2.12) at the beginning of DS ($t=0$) is sufficient. Since the projection of (2.12) along leg₂ has already been used to calculate $\dot{\ell}_2$ for use in (2.13), one only needs to impose the constraint of zero perpendicular velocity for foot₂ at $t=0$.

In continuous-support gaits $F_{\text{leg}_{2a}}$, τ_4 , and \mathbf{f}_{F_2} must be zero at TO as leg₂ leaves the ground. For intermittent-support gaits equivalent constraints must hold for $F_{\text{leg}_{1a}}$, τ_1 , and \mathbf{f}_{F_1} at TK. Note that this does not require both (tangential and normal) GRF components of the transitioning leg to become zero simultaneously; while the normal must stay positive until TO or TK, the tangential can vanish earlier.

At $t=T$ the gait cycle ends just before foot₂ lands at $[L_{\text{step}}, H_{\text{step}}]^T$. This is ensured by imposing (2.11) and the periodicity constraints below. In order to have a physically admissible solution, the foot must land from above the surface, requiring another constraint for a non-upward foot velocity just before TD.

The periodicity of the gait implies that the orientations and velocities of leg₁ and leg₂ must be mutually symmetric-identical at the beginning and end of the step. The same is

applied for the torso itself. These symmetry constraints can be formulated as:

$$\theta_i(T) = \theta_j(0), \quad \dot{\theta}_i(T^-) = \dot{\theta}_j(0^-), \quad \dot{\theta}_i(T^+) = \dot{\theta}_j(0^+), \quad i, j = 1, 3, \quad i \neq j, \quad (2.24)$$

$$\theta_2(T) = \theta_2(0), \quad \dot{\theta}_2(T^-) = \dot{\theta}_2(0^-), \quad \dot{\theta}_2(T^+) = \dot{\theta}_2(0^+), \quad (2.25)$$

$$l_m(T) = l_n(0), \quad \dot{l}_m(T^-) = \dot{l}_n(0^-), \quad \dot{l}_m(T^+) = \dot{l}_n(0^+), \quad m, n = 1, 2, \quad m \neq n. \quad (2.26)$$

Assuming a desired speed V has been specified, the step length and step period must satisfy

$$V = \frac{D_{\text{step}}}{T}. \quad (2.27)$$

Ensuring all points of the biped remain above ground merely requires enforcing bounds on θ_1 . Desiring an upright torso (anthropomorphic configuration), bounds are enforced on θ_2 as well (so it does not fall up-side down). θ_3 and all joint velocities are free. Finally, lower and upper bounds on actuator torques/forces and the lower leg length can be enforced to create a realistic solution:

$$l_{\min} \leq l_1, l_2 \leq l_{\max}, \quad (2.28)$$

$$-\infty < \dot{l}_1, \dot{l}_2 < \infty, \quad (2.29)$$

$$0 < \theta_1, \theta_2 < \pi, \quad (2.30)$$

$$-\infty < \theta_3 < \infty, \quad (2.31)$$

$$-\infty < \dot{\theta}_1, \dot{\theta}_2, \dot{\theta}_3 < \infty, \quad (2.32)$$

$$T > 0, \quad (2.33)$$

$$-\tau_{\max} \leq \tau_1, \tau_2, \tau_3, \tau_4 \leq \tau_{\max}, \quad (2.34)$$

$$0 \leq F_{\text{leg}_{1a}}, F_{\text{leg}_{2a}} \leq F_{\max}. \quad (2.35)$$

Some constraints have been imposed at either end of the phases or gait cycle, defining a two-point-boundary-value (TPBV) problem. The remaining constraints (the differential

equations and some algebraic constraints) are continuous-time equations that must be satisfied during the entire length of a phase or the whole gait cycle. In a computationally efficient approach most of the inequality constraints are not included in the optimization, but rather checked afterward (and each constraint that is not satisfied is then explicitly added into the optimization for the next run).

2.3.2 Numerical Optimization

The resulting nonlinear optimal control problem is infinite-dimensional due to the continuous-time states, actuation functions, and constraints. For the numerical approach, we can create a finite number of nonlinear-programming (NLP) variables and constraints (transcription technique [77]) by discretizing the DS, SS, and FL phases separately into a sequence of N_{ds} , N_{ss} , and N_{fl} equal length intervals, with the optimization itself determining interval durations T_{ds}/N_{ds} , T_{ss}/N_{ss} , T_{fl}/N_{fl} (see the next chapter for the number of intervals used to generate different gaits). Each (implemented) continuous-time constraint becomes a set of discrete-time constraints evaluated on the grid points (interval borders), or only in a subset of them for faster convergence. The optimization control variables, *i.e.* joint torques and forces, are approximated by continuous piecewise-linear functions, except at impulsive TDs where continuity is not required by assumption.

Due to the high degree of nonlinearity of the problem, the use of the direct (single) shooting method to solve the TPBV will likely cause the “tail wagging the dog” problem [77]. Instead, I use the multi-shooting method with only one interval per shooting segment. The state variables at interval borders are defined as NLP variables. In each segment, using the current guess for the NLP variables, the EoM are integrated forward in time from the beginning to the end of the segment. Constraining the *defects*, differences between the resulting states at the end of each segment and the states at the beginning of the next, to be zero guarantees state continuity at interval borders (see Fig. 2.3).

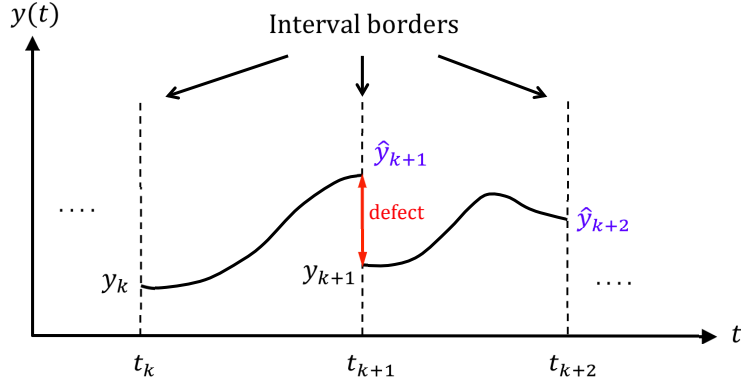


Figure 2.3: **Multiple shooting method and the defects at interval borders.** Each phase of the motion is divided into a few intervals. The state variables on interval borders are determined by optimization *via* an iterative process. At each iteration, the optimization procedure uses the current value of the state variables at interval borders, *e.g.* y_k , and y_{k+1} , to integrate the equations of motion over the subsequent interval. The differences between the resulting states at the end of each segment and the states at the beginning of the next, *e.g.* $\hat{y}_{k+1} - y_{k+1}$, are called the defects. Constraining defects to be zero guarantees state continuity at interval borders.

To prevent singularities during numerical optimization, small non-zero lower bounds on the duration of each phase are enforced. If the actual optimal gait for a given desired gait parameter involves the complete removal of a phase, the lower bound on the duration of that phase becomes an active constraint in the resulting optimal solution regardless of how small the bound. In this case, we can remove the related phase from the problem formulation in order to achieve the true optimal gait in the admissible space.

Non-smooth functions create difficulties for numerical optimization when the optimal solution is at, or very close to, the singular (non-smooth) point. Unfortunately, this is the case for gait optimization with the work-based cost function in (2.2), which contains non-smooth positive-value functions. To overcome the numerical difficulty, we can use the approximation $[x]^+ \approx (x + \sqrt{x^2 + \epsilon^2}) / 2$ with a small ϵ (square-root smoothing technique [78, 79]) to remove the singularity.

The resulting finite-dimensional NLP problem is solved using numerical parameter optimization. For given values of the state and control variables, the state equations are

numerically integrated forward in time over each interval separately. Then the objective function and constraint violations are evaluated. The parameter optimization algorithm iteratively updates the NLP variables to minimize the cost function and satisfy constraints within defined tolerances. The accuracy of the optimal solution is assessed with the original continuous-time problem, and if necessary the discretization and optimization procedure is repeated.

The optimal solution found using numerical optimization is a local optimum. To increase the chance of converging to the global minimum for each set of pre-determined gait parameters, we can repeat the optimization with many initial guesses chosen randomly within the parameter range. Another technique to escape from local optimums is to run the optimization with initial guesses obtained from perturbing the last optimal solution with different perturbation magnitudes.

2.4 Summary

In this chapter I presented a framework for gait optimization of a simple bipedal model. The model includes a torso, flat feet, and telescoping legs equipped with rotational hip and ankle joints. Two general types of gaits are considered in this framework: with and without a flight phase. The support surface can be level ground, a slope, or a staircase. The optimal gaits at different circumstances are achieved by minimizing a work-based energetic cost subject to a minimal set of realistic physical constraints. In order to let the model exhibit its natural behavior, any *a priori* assumptions on kinetic and kinematic parameters, such as extended or instantaneous double-support, collisional or collision-less foot-ground contact, step length, and step period, are avoided. Since the resulting optimal control problem is highly nonlinear, an efficient technique was discussed to numerically solve the optimization problem. The mathematical formulation and numerical technique presented here will be used

in the following chapters to study bipedal locomotion from the energy efficiency perspective.

Chapter 3

ENERGY-OPTIMAL GAITS OF THE MINIMALLY CONSTRAINED BIPEDAL MODEL

The biped model and gait optimization algorithm described in the previous chapter can be used to study energy-optimal bipedal locomotion. Since the formulated gait optimization problem is minimally constrained, the optimization will use the most effective strategies available to achieve an efficient gait on a given terrain. Studying these strategies can help us find the determinant factors for effective gait coordination. Moreover, comparison of the optimization-generated gaits with those of humans may lead to a better understanding of human and animal locomotion. For example, the possible similarities between the human gaits and those determined by optimization may imply that the human gait coordination is governed by the same determinant factors responsible for the optimization-generated gaits.

Motivated by the above possible outcomes, I investigated the optimal gaits of the model. The optimization results are presented in this chapter. First, the optimization and simulation parameters are presented in Section 3.1. The optimal continuous-support gaits on different terrains are described in Section 3.2. Then optimal intermittent-support gait is discussed in Section 3.3. Finally, the insights achieved from the analysis and results presented in this chapter will be discussed in Section 3.4. The chapter is summarized in Section 3.5.

3.1 Optimization and Simulation Parameters

The numerical results presented in this chapter are based on the bipedal model in Fig. 2.1. Although the results are qualitatively similar for a very wide range of model parameter values,

those presented here are based on the values listed in Table 3.1. These values are calculated from the estimated anthropomorphic data [80] of a subject with total mass of $m_{\text{tot}} = 75$ Kg and body height of $h_{\text{tot}} = 170$ cm. Upper leg length l_u is calculated from Greater Trochanter (hip) to Medial Malleolus (ankle). In accordance with Fig.2.1, the torso represents the head, arms, and trunk, so its height is calculated from Greater Trochanter (hip) to the top of the head.

The optimization and simulation constants are listed in Table 3.2. Upper bounds for actuator force and torques, F_{max} and τ_{max} , are chosen high enough so that they do not qualitatively affect the results. Note that the maximum leg force F_{max} is not applicable for possible impulsive leg forces at idealized impacts.

To make sure that the results are independent of the value of the friction coefficient μ , simulations have been repeated for three different typical values $\mu = 0.3, 0.7, \text{ and } 1.0$. Because the results for all three cases are very similar, only those for $\mu = 1.0$ are shown here.

To avoid numerical difficulty, the positive-value function, used in (2.1) to calculate the positive and negative actuator power, is approximated by $[x]^+ \approx (x + \sqrt{x^2 + \epsilon^2}) / 2$ with two

Table 3.1: Model Parameters for the Biped in Fig. 2.1

| Parameter Description | Symbol | Value |
|---|---------------------------------|--|
| total body mass | m_{tot} | 75 Kg |
| torso mass | m_{trs} | 0.68 m_{tot} |
| leg mass | m_{leg} | 0.16 m_{tot} |
| total body height | h_{tot} | 170 cm |
| torso height | h_{trs} | 0.47 h_{tot} |
| upper leg length (massive part) | l_u | 0.48 h_{tot} |
| torso CoM proximal distance | a | 0.42 h_{trs} |
| leg CoM proximal distance | b | 0.45 l_u |
| torso moment of inertia about the torso CoM | $I_{\text{trs}/G_{\text{trs}}}$ | 0.1084 $m_{\text{trs}} h_{\text{trs}}^2$ |
| leg moment of inertia about the leg CoM | $I_{\text{leg}/G_{\text{leg}}}$ | 0.1063 $m_{\text{leg}} l_u^2$ |

Table 3.2: Simulation and Optimization Constants

| Parameter Description | Symbol | Value |
|------------------------------------|---------------|-----------------------------|
| minimum leg length | l_{\min} | $0.48 h_{\text{tot}} = l_u$ |
| maximum leg length | l_{\max} | $0.58 h_{\text{tot}}$ |
| leg length at landing | l_0 | $0.53 h_{\text{tot}}$ |
| maximum hip and ankle torque | τ_{\max} | 500 Nm. |
| maximum leg force | F_{\max} | $3 m_{\text{tot}} g$ |
| gravity acceleration | g | 9.81 m/s^2 |
| friction coefficient | μ | 1.0 |
| smoothing parameter | ϵ | 1.0 |
| cost of unit positive work (power) | c_1 | 4 |
| cost of unit negative work (power) | c_2 | 5/6 |

different values of $\epsilon = 1, 0.1 \text{ W}$. In fact, decreasing ϵ by 10 fold reduces the COT by only about 10%, with small changes in the value, but the same qualitative behavior, of resulting gait parameters. Due to the negligible differences in the results, only those results produced by $\epsilon = 1 \text{ W}$ are presented.

Different combinations of the number of grid points (see Section 2.3.2) are examined to check the effect of piecewise-linear approximation of the control variables. In general, by increasing the number of grid points the minimum achievable COT slightly decreases (favoring impulsive actuation), but the overall behavior of the optimal solutions does not change. The number of grid points used for each gait will be provided when presenting different synthesized optimal gaits in Sections 3.2 and 3.3.

The constraints and the objective function are implemented in MATLAB, with ODE113 used for integrating the state equations with absolute tolerance of 10^{-12} and relative tolerance of 10^{-9} . The MATLAB interface SNOPT [81] provides the optimization routine.

The accuracy of the optimal solution is verified afterwards by numerically integrating the state equations continuously over the entire step with a small maximum step size and

with initial conditions specified only at the beginning of the step (in contrast to the multiple shooting method used for optimization). At this verification stage the TD maps in (2.19) and (2.20) are replaced by a root finding procedure that searches for TD impulses and post-TD joint velocities that directly satisfy the conservation of angular momentum at TD. Besides checking that all constraints are satisfied, the total mechanical energy and angular momentum of the system are also inspected as a means of validating the entire procedure, including modeling, simulation, and numerical integration.

For each set of pre-determined gait parameters the optimization procedure was repeated with many initial guesses chosen randomly within the parameter range. Escaping from local optimums was ensured by perturbing the obtained optimal solutions with different perturbation magnitudes. In almost all cases more than 80% of trials converged to the same solution which was then accepted as, or to be very close to, the global optimum in the parameter range defined by (2.28)-(2.35).

In the following sections, the input gait parameter for level-ground and uphill gaits is the forward velocity V , and for going down a stairway the inputs are both the step height H_{step} and tangential step length L_{step} .

3.2 Optimal Continuous-Support Gait

Regardless of the lower bound on the DS duration, and as long as the upper bound on leg force is greater than total body weight, all optimal continuous-support gaits at different circumstances take the minimum allowed DS duration. Fig. 3.1 shows leg force profiles for an optimal level-ground gait for which DS is not allowed to be less than 10% of the step period, *i.e.* $T_{\text{ds}} \leq 10\% T$ (see the figure caption for other gait parameters). The resulting DS duration is exactly 10% T . Moreover, the resulting overlap of the leading and trailing leg forces (where both leg forces are non-zero) only takes one grid-interval of the enforced

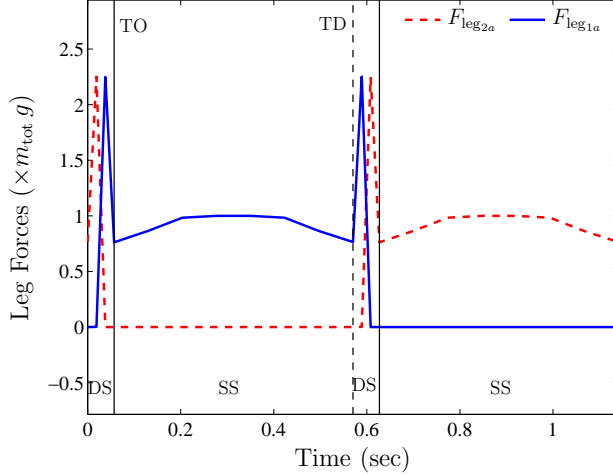


Figure 3.1: **Leg forces in double support phase.** Leg force profiles for two steps of a sample continuous-support gait with no axial impulsive leg force, $T_{\text{ds,min}} = 10\% T$, $N_{\text{ds}} = 3$, and $N_{\text{ss}} = 7$. The dashed and solid vertical lines indicate the touch-down (TD) and toe-off (TO) instants, respectively.

extended DS phase, independent of the number of grid points used. This profile is typical for all ground slopes and step heights, as well as for all speeds for which continuous-support gait is feasible. This implies that for the chosen objective function (see Section 2.1.2), and without imposing extra constraints, the optimum continuous-support gait has an instantaneous DS (*i.e.* $T_{\text{ds}} = 0$). Therefore, we can use $N_{\text{ds}} = 0$ for all optimal continuous-support gaits.

The non-optimality of an extended DS phase can be intuitively justified as follows: a non-instantaneous DS would require simultaneous negative and positive work performed by the leading and trailing legs, respectively. While these simultaneous works almost cancel each other and have no energetic benefit for the system (the net energy level of the system remains almost unchanged as the velocities and the CoM height do not change much during DS), active production of both forms of work is costly for the system.

In spite of the energetic benefit of an instantaneous DS for the model, normal human walking has extended DS phases of about 20% of the gait cycle [50], perhaps due to the extra constraints acting on the human body or its actuators (muscles) [67].

3.2.1 Optimal Continuous-Support Gait on Level-Ground

At slow speeds, and independent of whether the impulsive axial GRF at TD are allowed or not, a special type of continuous-support gait, known as the ‘pendular walk’ [25], is energetically favorable. In this gait, which more or less resembles normal human walking, the stance-leg length is constant over most of the SP phase, providing an inverted-pendulum-like trajectory for the CoM.

A sample optimal gait synthesized for the average forward speed $V = 1.38$ m/s with instantaneous DS and no axial impulsive leg forces is shown in Fig. 3.2. This gait is synthesized with $N_{ss} = 7$ and $N_{ds} = 0$ (optimal DS is instantaneous; see the first paragraph in Section 3.2). The resulting optimal step period and step length are $T = 0.33$ s and $D_{step} = 0.455$ m. Also, the specific and mechanical COT are $\mathcal{C}_{et} = 0.335$ and $\mathcal{C}_{mt} = 0.069$. This cost is almost evenly distributed between the stance leg’s linear actuator (51%) and the swing hip (48.6%), and the other joints have negligible contributions.

Optimal Leg Forces, Collisional Foot-Ground Contact, and the Pre-Emptive Push-Off:

As shown in Fig. 3.2f (and also in Fig. 3.1), each leg force exhibits two peaks that take place at support transfer between the legs. The first peak occurs on the leading leg immediately after the foot-ground contact. This burst force activity quickly stops the leg shortening (Fig. 3.2d) and causes energy dissipations (negative work) in a short period of time. These characteristics represent a collisional foot-ground contact [25]. Because the impulsive axial leg forces are prohibited in the sample gait shown in Fig. 3.2, the resulting TD collisions are not the idealized instantaneous ones, but rather extended over a short period of time with large (but finite) leg forces involved. For this reason they can be called *extended collisions*. By increasing the number of grid points and the upper bound on the leg force, these extended collisions occur in a shorter period of time and thus converge to instantaneous collisions.

The second peak leg-force occurs on the trailing leg at the end of single support phase.

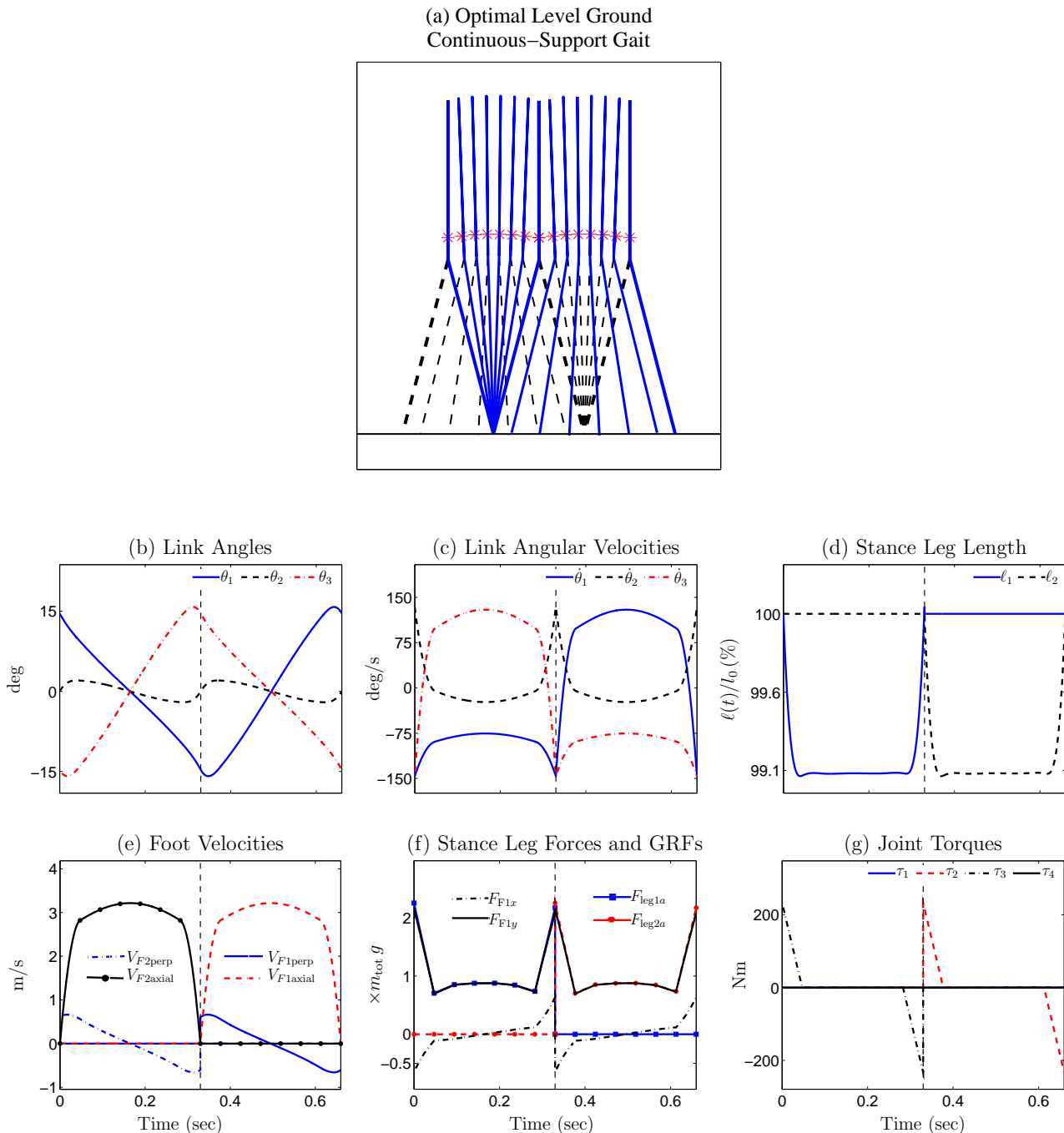


Figure 3.2: **Stick diagram and gait parameters of two steps of the optimal level-ground continuous-support gait** generated for $V = 1.38$ m/s with instantaneous DS. Axial impulsive GRFs are *not* allowed. In the first step, leg₁ (the solid blue lines in 3.2a) is the stance leg. In 3.2a the asterisks indicate the CoM position. The dashed vertical lines in 3.2b-3.2g indicate the TD instant. In 3.2e the subscripts *axial* and *perp* denote the foot velocity components along and perpendicular to the corresponding leg. In 3.2f the stance leg’s axial force ($F_{leg_{1a}}$ and $F_{leg_{2a}}$) and GRFs in normal and tangential directions (F_{F1x} and F_{F1y}) are all scaled with body weight $m_{tot} g$. Note that foot scuffing can be avoided by decreasing the length of the swing leg’s massless portion.

Approaching touch-down, and while the CoM has a downward motion, the trailing leg begins pushing off with its linear actuator, effectively adding energy to the system. This action redirects the linear momentum vector of the biped, reducing the momentum that is going to be lost at the following TD collision [26]. Interestingly, this cost-reducing strategy (referred to as *preemptive push-off*) is a well-known characteristic of human walking [26, 50].

As a consequence of the above actions, the resultant vertical GRF (Fig. 3.2f) in the optimal gait has a double-hump profile, another well-recognized characteristic of the human walk [29, 82]. The horizontal component of the GRF also has a profile similar to that of human walking. It consists of negative and positive halves corresponding to deceleration and acceleration of the CoM before and after mid-stance.

In the optimization routine associated with the gait shown in Fig. 3.2 the impulsive GRFs at TD are allowed in the normal to the leg direction, but not along the leg. Notwithstanding, the optimal gait does not include any impulsive forces in any direction. In other words, when the axial GRFs at TD are enforced to stay bounded, impulsive perpendicular GRFs are not energetically advantageous. This will be justified later in Section 3.4.1.

Optimal Hip Torque Profile:

Experimental observations of human walking show that the swing hip has burst activities at both ends of the swing phase: just after toe-off, and just before heel-strike [47]. As can be seen in Fig. 3.2g, the energy optimization model automatically discovers the advantage of this strategy as well, and activates the swing hip in a ‘bang-coast-bang’ manner: Immediately after toe-off the swing leg is rotating rearward (negative $\dot{\theta}_3$ at the beginning of the first step in Fig. 3.2c) due to its angular momentum prior to toe-off. To quickly redirect the swing leg’s rotation and to increase the step frequency above the leg’s natural frequency, the swing hip applies a burst torque to the leg. After that, the leg swings passively in the forward direction until shortly before TD, when the swing hip applies another burst torque

to stop the forward leg-swing and reverse its rotation. This late-swing rotation reversal is called *swing-leg retraction* and can reduce the energy dissipation at foot-ground contact (see Section 3.4.1). For slower forward speeds, peak swing-hip activity occurs with short offsets from toe-off and TD.

Contribution of the Revolute Stance-Ankle:

In Fig. 3.2g the revolute stance-ankle and the stance-hip torques (τ_1 and τ_2 in the first step) have very small activities which are not visible in the figure. The peak ankle and hip torques are 0.127 Nm and 0.6 Nm, respectively. This yields a maximum ZMP displacement of 0.3 mm from the ankle joint, supporting the argument in Section 2.1 that for optimization purposes the biped can be simplified to a point-foot model. See Section 3.4.2 for the comparison of this result with human gaits.

Optimal Continuous-Support Gait at Fast Speeds

At adequately fast speeds (close to 2 m/s) the peak push-off force occurs slightly earlier than the following support transfer. By further increasing the average speed, the separation of push-off and termination of the support transfer increases, and GRF components stay on the boundary of the friction cone. By letting the friction coefficient tend to infinity the vertical post-push-off GRF becomes zero with a negligible horizontal GRF, demonstrating the optimality of having a flight phase (intermittent-support gait) at higher speeds.

3.2.2 Optimal Continuous-Support Gait to Climb Ramps or Staircases

The optimal continuous-support gait for climbing a staircase or a ramp has much in common with the optimal gait on a level surface, but also some important differences.

A sample optimal gait for climbing a 10° slope at $V = 0.9$ m/s is shown in Fig. 3.3. For this optimal gait $N_{ss} = 7$, $N_{ds} = 0$ (optimal DS is instantaneous; see the first paragraph in

Section 3.2), and axial impulsive GRFs at TD are allowed. The resulting gait parameters are: step period $T = 0.49$ s, step length $D_{\text{step}} = 0.44$ m, mechanical COT $\mathcal{C}_{\text{mt}} = 0.1737$, and specific COT $\mathcal{C}_{\text{et}} = 0.694$. The COT is distributed over different actuators as: stance leg's linear actuator: 25%, revolute ankle: 3.5%, stance hip: 49.5%, and swing hip: 22%.

For the same progression slope the optimal stair-climbing gait and the optimal uphill gait are similar. In both cases foot stubbing (scuffing) can be avoided by contracting or re-orienting the massless parts of the swing leg.

Optimal Gait Strategies:

As for the level-ground case, foot-ground contacts in this case are collisional. Because for the optimal gait in Fig. 3.3 the leg forces are allowed to be unbounded at the foot-ground contact, the TD collisions are instantaneous and include dissipative impulsive GRFs (Fig. 3.3f) that instantaneously redirect the CoM and avoid the stance leg from shortening (Fig. 3.3d). To reduce the energy dissipation at these collisions, a burst pre-TD push-off force (preemptive push-off) is also applied in this case, as seen in Fig. 3.3d and Fig. 3.3f.

At equal speeds the optimal step length on uphill is shorter than on level ground, resulting in less dissipations at TD collisions [26].

Compared to the level-ground gait, here the activity of the stance hip has substantially increased (Fig. 3.3g). In going uphill/upstairs the stance hip applies a significant torque to vault the CoM over the stance leg. This torque pushes the torso back, and can potentially cause instability. To overcome this problem the torso leans forward, as seen in Fig. 3.3a. The leaning angle increases with the ground slope.

Similar to the level-ground case, the swing-hip motor and the stance-leg's telescoping actuator have almost equal cost contributions. As seen in Fig. 3.3g, the major burst activity of the swing hip is limited to the beginning of the swing, since the pre-TD swing-leg retraction is mostly done passively by gravity.

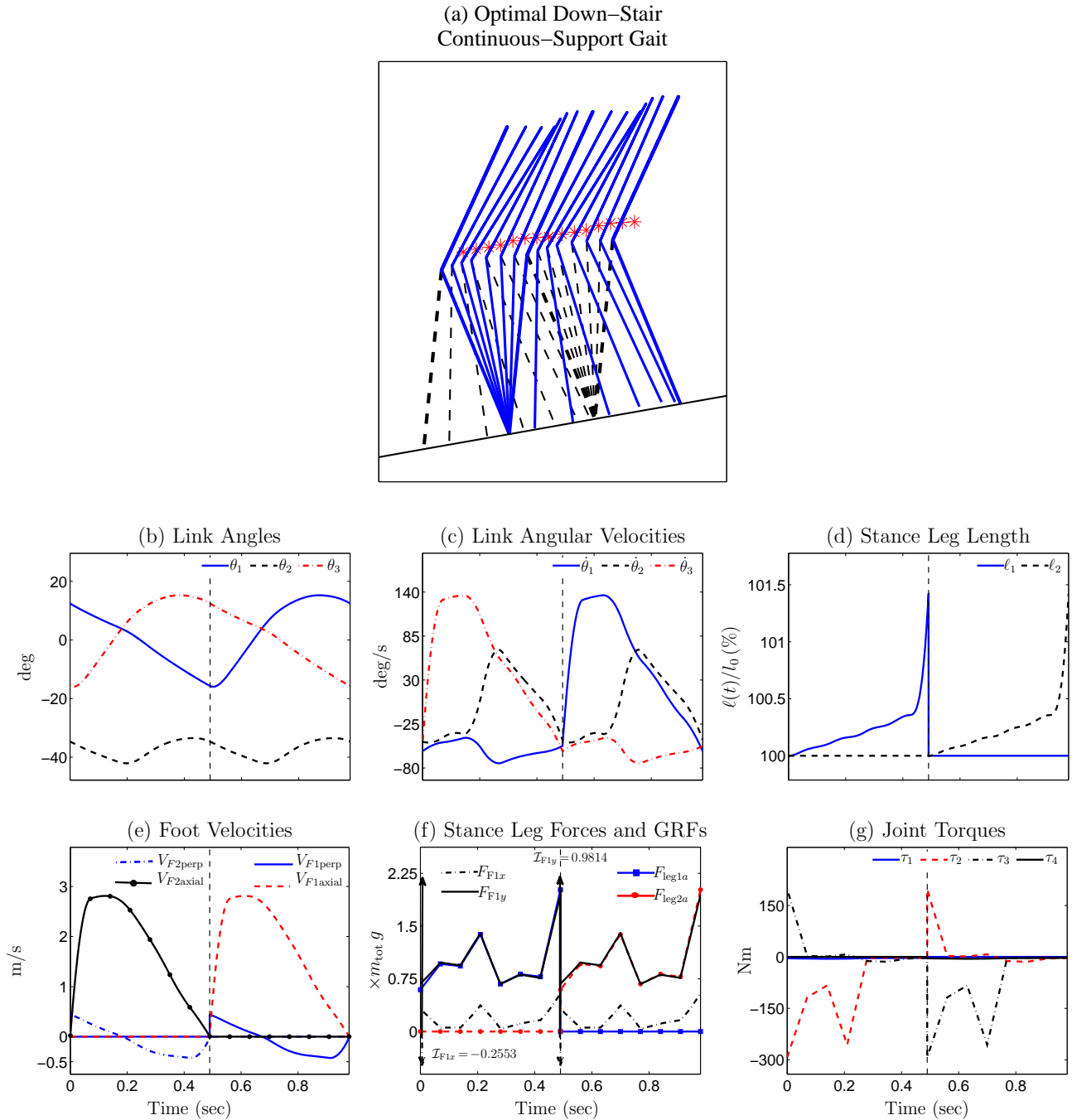


Figure 3.3: **Stick diagram and gait parameters of two consecutive steps of the optimal uphill continuous-support gait** generated for $\gamma = 10^\circ$, and $V = 0.9$ m/s. DS is instantaneous, and unbounded axial leg forces at TD are allowed. In the first step leg₁ (the solid blue lines in 3.3a) is the stance leg. The asterisks in 3.3a indicate the CoM position. The dashed vertical lines in 3.3b-3.3g indicate the TD instant. In 3.3e the subscripts *axial* and *perp* denote the foot velocity components along and perpendicular to the corresponding leg. In 3.3f the stance leg’s axial force ($F_{\text{leg}1a}$ and $F_{\text{leg}2a}$) and GRFs in normal and tangential directions (F_{F1x} and F_{F1y}) are all scaled with body weight $m_{\text{tot}} g$. Also the arrows in 3.3f represent the GRF impulses at TD.

The minimum achievable \mathcal{C}_{mt} in climbing a slope of angle γ is $\sin\gamma$ – equivalent to the case when there is no dissipation or negative actuator work, and all the positive actuator work is spent to increase the potential energy. The specific COT for the optimal gait shown in Fig.3.3 ($\mathcal{C}_{\text{et}} = 0.1737$) is very close to the associated theoretical minimum ($\sin\gamma = \sin 10^\circ = 0.1736$), showing that most of the actuator work is positive.

3.2.3 Optimal Continuous-Support Gaits for Stepping Down the Ramps or Staircases

For downhill/downstair gaits a different behavior is observed (see below). A sample optimal gait for stepping down a stairway with $H_{\text{step}} = -10$ cm and $L_{\text{step}} = 50$ cm is shown in Fig. 3.4. The resulting gait parameters with $N_{\text{ds}} = 0$ (optimal T_{ds} is zero) and $N_{\text{ss}} = 7$ are: step period $T = 0.537$ s, specific COT $\mathcal{C}_{\text{et}} = 0.014$, and mechanical COT $\mathcal{C}_{\text{mt}} = 0$. The distribution of \mathcal{C}_{et} over different joints is: stance leg’s telescoping actuator: 59%, revolute ankle: 13%, stance hip: 16%, and swing hip: 12%. Because the mechanical COT is calculated using only positive actuator work, $\mathcal{C}_{\text{mt}} = 0$ implies that the actuators are doing only negative work, and all the positive work is done by gravity. By decreasing the slope of progression the actuators will start doing positive work.

Optimal Gait Strategies:

Similar to the previous two cases, the foot-ground contacts are collisional here. In the sample gait provided, the axial impulsive leg forces at TD are allowed, so the collisions are instantaneous.

Unlike the previous two optimal gaits, in this case the length of the stance leg continuously decreases (Fig. 3.4d), and the peak of the leg force occurs around mid-stance, as seen in Fig. 3.4f. No pre-TD push-off force is observed in this case. Consequently, the collision loss is noticeable (it is 11 times greater than the total negative work done by all the actuators). This strategy is observed in all downhill/downstair gaits and is justified in Section 3.4.1.

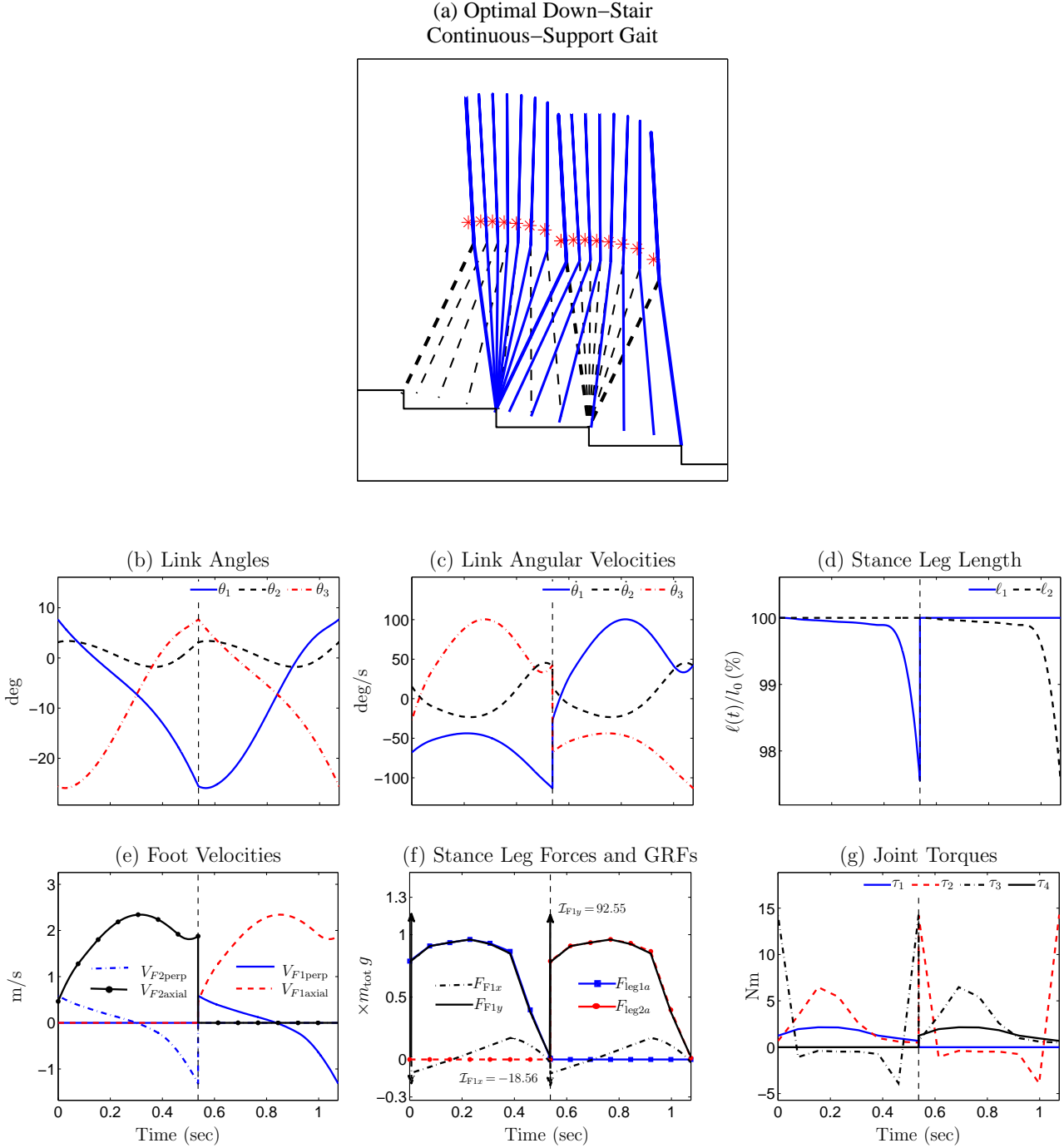


Figure 3.4: **Two consecutive steps of the optimal downstair continuous-support gait** generated for $H_{\text{step}} = -10$ cm and $L_{\text{step}} = 50$ cm. Other conditions are similar to Fig. 3.3. In the first step leg₁ (the solid blue lines in 3.4a) is the stance leg. The asterisks in 3.4a indicate the CoM position. The dashed vertical lines in 3.4b-3.4g indicate the TD instant. In 3.4e the subscripts *axial* and *perp* denote the foot velocity components along and perpendicular to the corresponding leg. In 3.4f the stance leg’s axial force ($F_{\text{leg}1a}$ and $F_{\text{leg}2a}$) and GRFs in normal and tangential directions (F_{F1x} and F_{F1y}) are all scaled with body weight $m_{\text{tot}} g$. Also the arrows in 3.4f represent the GRF impulses at TD.

In contrast to uphill gaits, in downstairs gaits the stance hip applies a decelerating torque (Fig. 3.4g) to achieve the optimal step period. In reaction to this torque, and to avoid falling forward, the torso leans backward.

Although the swing hip exhibits a bang-coast-bang torque profile (Fig. 3.4g), its pre-TD activity is not to retracting the swing leg, but to push the leg forward (in Fig. 3.4c the swing-leg angular rate has increased before TD). This enforced forward motion of the leg at the end of swing increases the foot velocity at TD (Fig. 3.4e), and therefore results in more collision loss (see Section 3.4.1 for the justification).

The required foot length (based on ZMP) of 1.2 cm and the revolute ankle joint activity do not seem to be an important requirement for energy efficiency, since the corresponding gait with forced zero-ankle-torque (point-feet biped) has $\mathcal{C}_{et} = 0.012$; practically not different from $\mathcal{C}_{et} = 0.014$ for the gait in Fig. 3.4. See Section 3.4.2 for the comparison of this result with human gaits.

3.3 Optimal Intermittent-Support Gait

For adequately fast speeds (approximately above 3 m/s) a special type of intermittent-support gait is optimal. This gait is known as *impulsive running* [25] and more or less resembles normal human running.

Fig. 3.5 shows a sample of this gait at $V = 5$ m/s. For this sample gait $N_{ss} = 5$, $N_{fl} = 10$, and the impulsive axial leg forces at TD are allowed. The optimal step period, step length, and duty factor (the fraction of step period that a foot is in stance) are 0.22 s, 0.97 m, and 30%, respectively. Also the mechanical and specific COT are $\mathcal{C}_{mt} = 0.11$ and $\mathcal{C}_{et} = 0.48$. The contribution of each actuator in \mathcal{C}_{et} is: stance-leg telescoping actuator: 73%, stance hip: 18%, and swing hip: 9%. The revolute ankle joint has negligible contribution.

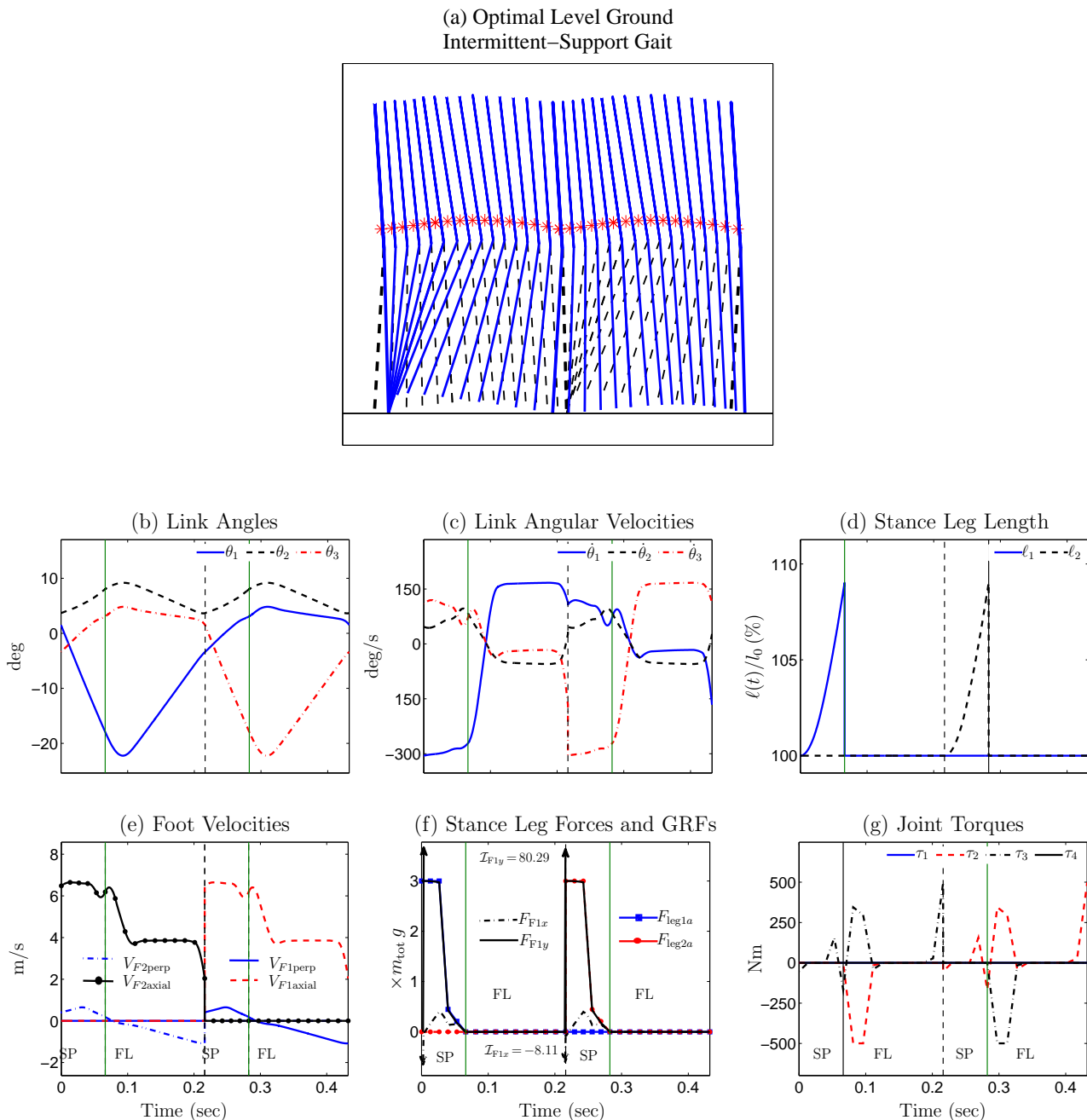


Figure 3.5: **Two consecutive steps of the optimal intermittent-support gait on level ground** generated for $V = 5$ m/s. Unbounded axial leg forces at TD are allowed. In the first step leg₁ (the solid blue lines in 3.5a) is the stance leg. The asterisks in 3.5a indicate the CoM position. The dashed black and solid green vertical lines in 3.5b-3.5g denote the touch-down (TD) and take-off (TK) instants, respectively. In 3.5e the subscripts *axial* and *perp* denote the foot velocity components along and perpendicular to the corresponding leg. In 3.5f the stance leg’s axial force (F_{leg1a} and F_{leg2a}) and GRFs in normal and tangential directions (F_{F1x} and F_{F1y}) are all scaled with body weight $m_{tot}g$. Also the arrows in 3.5f represent the GRF impulses at TD.

Optimal Leg Force and Center of Mass Motion:

In contrast to the continuous-support gait, where the axial leg force falls below body weight for most of the step period, here the leg force stays at its maximum over most of the support phase (Fig. 3.5f). The large leg forces at early support phase quickly stop leg shortening and the downward motion of the CoM (collisional TD). For the sample gait presented, this deceleration phase is compressed at the TD instant due to the idealized impulsive axial leg forces at TD (arrows in Fig. 3.5f). After this deceleration, large leg forces increase the leg length and provide the required upward velocity for the CoM at take-off.

As a result of the above actions, the CoM has a bouncing-type trajectory which reaches its lowest point in the middle of SP, while the CoM has its minimum speed. At this point the kinetic and potential energy are at their minimum. The highest point of the CoM trajectory occurs in FL where the CoM speed is about maximum, and so are the kinetic and potential energy. Therefore, the kinetic and potential energy change in-phase with each other, a well-known characteristic of running-type gaits in biological systems.

Interestingly, the optimal bouncing motion of the CoM and in-phase changes in kinetic and potential energy occur without having any elasticity in the biped. This shows that the advantage of this motion is more fundamental than being dependent mainly on elastic energy recovery, a fact that has been largely overlooked [26].

Ground Reaction Force Profiles:

As shown in Fig. 3.5f, the resulting vertical GRF has a pulse shape that approximates the bell-shaped GRF of human running [83].

Swing Leg Motion and Hip Torque Activity:

Regardless of the average forward speed, the swing leg is rotating forward at off-side TD ($\dot{\theta}_1 > 0$ at the vertical dashed line in Fig. 3.5c, *i.e.* at TD on leg₂). This forward rotation

continues after TD, and brings the swing leg in front of the body in the second half of the stance phase (θ_1 becomes positive after some t between the dashed and solid vertical lines in Fig. 3.5b, *i.e.* after TD and TK on leg₂). Shortly before take-off the hip applies a decelerating burst to reduce the swing leg's angular velocity. This reduces the GRF and helps prepare the conditions required for take-off (zero GRF). At the end of the FL, and while the landing leg has reached a near-vertical orientation, hip torque applies a burst to slow down the rotation of the leg and prepare it for landing (swing-leg retraction). Unlike the continuous-support gait, there is no ground contact, so the pre-emptive push-off strategy is not available in this gait. Instead, landing with the leg as vertical as possible reduces the horizontal-momentum loss at TD.

At the beginning of the FL the new swing leg (which was the stance leg before take-off) is rotating rearward with a high angular rate due to its angular momentum prior to take-off. Immediately after take-off the new swing hip applies a burst to decelerate the leg rotation, as seen in Fig. 3.5f. Around the mid-flight, and almost simultaneously with the landing leg, the rotation of the rear leg is reversed (at about $t = 0.1$ sec in Fig. 3.5c), and the leg is prepared for the next step.

Contribution of Ankle Torque:

Similar to the continuous-support gaits, the ankle torque during the support phase is too small (maximum 0.05 Nm) to be seen in Fig. 3.5g. As a result, the ZMP has a negligible offset (0.3 mm) from the ankle. Although this might be counter intuitive, it indicates that the main contribution of the ankle joint (the complex ankle includes both the telescoping joint along the leg and the revolute joint between the foot and the leg) is to push off and provide the required linear momentum for step transition. Section 3.4.2 compares the ankle torques in human gaits and the optimization generated gaits.

Optimal Intermittent-Support Gait at Slow Speeds

Note that at velocities close to 2 m/s the optimization converges to the so-called *pendular running* gait [25], with a mixture of a pendular SP and a short FL. Further decrease in speed eliminates the FL, implying the optimality of continuous-support gait over intermittent-support gait at slower speeds. Because the optimization has been formalized in a way that converges to the quasi-global optimal gait at any given speed, generating gaits with non-zero flight phase requires an extra constraint on the minimum flight time at these low speeds.

3.4 Discussion

In this section, some aspects of the optimal gaits found in the previous sections are discussed. Also, the insights that can be achieved from them are provided.

3.4.1 General Characteristics of the Optimal Gaits

Collisional Foot-Ground Contact:

Consistent with findings of [25] with a simpler bipedal model than the one used in this work (Fig. 2.1), the implemented optimization routine for all types of gait converged to solutions that include collisional foot-ground contacts. When axial impulsive GRFs at TD were permitted, these TD collisions were *idealized instantaneous* impacts. Otherwise, they were *extended collisions*, which involve high (but finite) dissipating leg forces that quickly stop the leg shortening after a new foot-ground contact (step-to-step transitions). By increasing the number of grid points and the maximum allowed leg force in the optimization routine, these high leg forces converge to instantaneous impulses. These results are valid for a large range of models when a work-based energetic cost is used as the optimization objective function (*e.g.* [25, 67]).

Strategies to Reduce Collision Loss in Level-Ground:

Although it may appear, from an energy-efficiency point of view, that dissipative collisions are not desirable, eliminating them requires extra actions and effort and thus may increase the net energetic cost. For example, in continuous-support gaits collision energy loss could be avoided completely by, say, moving the CoM in a horizontal path and taking steps with zero foot-velocity at TD. Unfortunately, such motion requires more work from the legs, simultaneously shortening an extending, than is saved in reducing energy loss at collisions [2, 25].

In fact, the optimal solution uses different strategies to reduce the collision loss, but *only to the extent that results in a net energy saving*. Some of these strategies are gait specific. In continuous-support gaits a burst push-off force is applied along the stance leg just before TD to reduce the CoM momentum along the leading leg. This reduces the energy that should be dissipated to quickly stop the leg shortening and redirect the CoM motion. In running, however, there is no support leg during flight to apply the pre-TD push-off. Instead, landing with the leg as vertical as possible reduces the momentum loss at TD (CoM momentum is directed mainly in the horizontal direction rather than the vertical).

Another strategy in reducing collision loss is *swing-leg retraction*: the late-swing rotation reversal of the swing leg prior to TD. Interestingly, swing-leg retraction has been also observed in human and animal locomotion [47, 51, 52, 54, 56]. This rearward limb rotation, while the hip is moving forward, reduces the TD impact by reducing the relative foot-ground velocity (Fig. 3.2e, Fig. 3.3e, Fig. 3.5e). In level-ground gaits, swing-leg retraction is achieved actively by applying a hip torque to the leg to stop its forward swing and force it to rotate backward. Therefore, depending on the balance between the energy it saves via collision reduction and the cost it takes to brake/accelerate the leg, swing-leg retraction can potentially reduce the net energetic cost of the gait. It is shown in Chapter 8 that the energetic benefit of active leg retraction depends on different factors, including the step length and speed.

Optimal Cost Reduction Strategies for Gaits on Ramps or Stairways:

When climbing stairs or a ramp, the potential energy of the biped increases at each step. Therefore, the net work done at each step must be positive (unlike the periodic gaits on a level ground for which the net work done in each step must be zero to keep the mechanical energy of the biped at the same level after each step). In an efficient gait, the positive net work is achieved in part by decreasing the negative work and dissipations. As a result, for climbing stairs or a ramp, the intensity of TD impact decreases with slope by increasing the preemptive burst push-off force and/or taking shorter steps. Also, to further decrease the negative work, the swing-leg retraction is mostly done passively by gravity, eliminating the active negative work required to stop the forward leg-swing.

In downhill/downstair gaits not only the stance-leg preemptive push-off and swing-leg retraction are not observed, but also opposite actions are taken. In fact, as can be seen in Fig. 3.4, the stance-leg length is reduced prior to TD (opposite to pre-TD leg extension) and an extending (opposite to retracting) torque is applied at the swing hip that increases the foot velocity at TD. Consequently, the TD impact and its associated loss is maximum. This is because in downhill gaits the system gains net kinetic energy during each step, and increasing collision loss is a cost-effective way to dissipate this extra energy.

Effect of Bounded Axial Leg Forces on Swing-Leg Retraction:

Another factor that determines the optimal scenario of TD collision and swing-leg retraction at foot-ground contacts is whether *axial* GRF impulses are allowed at TD or not. When these *axial* forces are allowed, the *perpendicular* impulsive GRFs at TD may also exist in the optimal gait. However, when TD impulses are allowed *only in the perpendicular* direction, the TD becomes completely non-impulsive for *all* optimal gaits found (*e.g.* see the optimal gait in Fig.3.2). In other words, when the *axial* impulsive forces are avoided, the best strategy is to avoid the *perpendicular* ones as well.

The above result can be explained as follows: In the absence of axial impulsive forces at TD, the unilateral foot-ground contact (the foot cannot penetrate to the surface) restricts the permissible perpendicular impulses to the non-downward direction. Due to the orientation of the landing leg at TD (the landing foot is usually ahead of the hip) the non-downward perpendicular impulses are possible only if the perpendicular foot velocity at TD is either zero (avoiding instantaneous impact), or directed downward. The latter demands more positive work from the swing hip and also dissipates more energy at impact; thus is not energetically favorable.

Because of the forward motion of the hip, the zero perpendicular foot velocity at TD is possible almost only by applying a retracting hip torque at the end of swing phase. This torque brakes the forward leg-swing and accelerates its backward rotation to cancel the effect of the perpendicular hip velocity. Thus, when axial impulses are prohibited a retracting hip torque is required to have a physically meaningful model, otherwise a suctional contact (pulling force from the ground) is required to stop the foot at landing. A side implication of this result is that the models with an axial spring in the leg (avoiding the axial impulsive forces at TD) will spontaneously have leg retraction and are not appropriate to examine whether leg-retraction has any net energetic advantages; a fact that is neglected in [65].

3.4.2 Comparison of Optimization Generated Gaits and Normal Human Gaits

Many of the identified characteristics of the optimization generated gaits are similar to those of human gaits, including the burst preemptive push-off in walking, landing on a near-vertical leg in running, bang-coast-bang hip torque profile of the swing hip, swing-leg retraction, collisional foot-ground contacts, torso leaning on ramps, GRF profiles, etc. However, there are some differences as well.

In all the optimal gaits identified, the contribution of the stance ankle torque is negligible, implying that for optimization purposes the extended feet can be reduced to point feet.

However, in humans feet are extended and ankle torque is not negligible. This difference comes from the difference between the ankle joints of humans and the model. In humans the ankles are purely revolute joints and the push-off is provided mainly by ankle joint extension and foot rotation. In contrast, the model has compound ankle joints consisting of a linear joint along the leg and a revolute joint between the leg and the foot. As explained in Section 2.1, this is meant to simplify the model dynamics and increase the optimization convergence rate. With this compound ankle, the push-off is provided by the telescoping joint, and the ankle torques can only change the angular momentum of the biped. The resulting negligible ankle torques in the optimal gaits imply that the main contribution of the ankle is to push off and provide the required linear momentum for step transition.

Typical human walking has a specific COT of $\mathcal{C}_{\text{et}} \approx 0.2$, estimated by the volume of Oxygen consumed (VO_2), and a mechanical COT of $\mathcal{C}_{\text{mt}} \approx 0.05$ [45]. The associated preferred step period and step length, when walking at the preferred speed $V = 1.3 \text{ m/s}$, are $T \approx 0.55 \text{ s}$ and $D_{\text{step}} \approx 0.72 \text{ m}$ [84]. For the current bipedal model with the sample optimal gait shown in Fig. 3.2 the specific and mechanical COT (0.335 and 0.069, respectively) are close to those of humans walking at the same speed, but with shorter step length and step period. By letting the optimization use impulsive axial leg forces at TD, the optimal \mathcal{C}_{et} and \mathcal{C}_{mt} become closer to human costs (0.22 and 0.055, respectively), but the step period and step length become even smaller. These results may show that the dominant factor in metabolic energy expenditure of human walking is the mechanical work done by muscles. The shorter step period and step length can be explained by the fact that the optimization does not face any cost or limiting upper bound in using high torques, as the goal here is to study the optimal gaits under minimal constraints. Adding actuation cost in the energetic cost equation in (2.1), such as the force-over-time cost suggested in [85], resolves the problem of fast steps.

For treadmill running at the same speed as for the sample optimal gait in Fig. 3.5 humans

have $\mathcal{C}_{\text{et}} \approx 0.43$ (extracted from non-athlete running data in [73]) with a duty factor of 33%. Relative step length with respect to the leg length is $D_{\text{step}}/\ell = 1.67$ (extracted from [86]). Scaled for the human subject of Table 3.1, this corresponds to $D_{\text{step}} \approx 1.5$ m. Comparing these values with those corresponding to the optimal gait of Fig. 3.5 ($\mathcal{C}_{\text{et}} = 0.48$ and $D_{\text{step}} = 0.97$ m) shows that humans are slightly more efficient runners than the purely rigid model in Fig. 2.1. This is not surprising given that elastic energy recovery does occur in human running.

Now that I have reviewed the main characteristics of the identified optimal gaits and their comparison with human gaits, I discuss some insights that can be obtained from the above results.

3.4.3 Walking and Running; Different Solutions of the Same Problem

Despite the *apparent* differences between the optimal continuous-support gait (walking) and the optimal intermittent-support gait (running), they have fundamental *functional* similarities. In both of these gaits there is a portion that is relatively cost-free. For walking the low-cost portion occurs during the single-support phase when the mass of the body spontaneously vaults over the stance leg. In running the low-cost portion of the step cycle occurs when both feet are in the air and the body mass moves ballistically. For both walking and running, these low-cost (quasi-passive and smooth) portions of the step cycle are interspersed between the (less smooth) high-cost portions during which the CoM motion is redirected from downward to upward (entire support phase in running and support transfer between legs in walking). This high-cost down-to-up transition is actively mediated by the action of stance leg(s), which involves ‘costs’ associated with energy loss to impact and actuator work expended to decelerate and accelerate the CoM. In both walking and running the main activity of the swing hip occurs around this down-to-up transition. This involves ‘costs’ associated with work spent to start the leg swing just after foot-clearance and then prepare it for a proper landing (reduced relative foot-ground speed) just before the foot-contact.

One important point that should be noted here is that both these optimal gaits (walking and running) are generated using the *same* bipedal model¹, and both are subject to the *same* physics principles for the interaction of body with its physical environment (gravity and the substrate). In both cases the decision on the optimal gait coordination is made based on minimizing the *same* energetic cost function. Therefore, both of these gaits should be influenced by the same determinant factors for effective gait coordination. The difference between walking and running comes only from the *different strategies available* to minimize the energetic cost at different forward speeds. In other words, they are different optimal solutions of the same problem for different circumstances. Thus, to identify the determinant factors for effective locomotion we should focus our attention on the functional similarities between the gaits and not the apparent descriptive differences. The similarities reflect the common governing principles, whereas the differences only reflect the different strategies available.

3.4.4 Determinant Factors in Effective Legged Locomotion

There are two energetic-cost factors that interplay to determine the most cost-effective movement pattern:

1. The cost of stance-leg work to redirect the CoM motion from downward to upward at each step. This cost is influenced by
 - the energy dissipations at (extended) foot-ground collision², including (i) the energy lost passively at foot-ground impact, and (ii) the dissipative stance-leg work to decelerate the downward motion of the CoM,

¹unlike many studies that use different models for walking and running, *e.g.* inverted pendulum model for walking and spring-mass model for running

²In practice collisions are not instantaneous but extended over a short period of time. In this context, the collision loss (dissipation) includes all passive and active energy dissipations that occur at early foot-ground contact, when the CoM has a decelerating motion.

- the generative work of the (trailing) stance-leg to make-up for the energy dissipations and accelerate the CoM to move upward.

Note, if the above dissipations did not occur, there was no need for the generative stance-leg work, and this cost would not exist. The dissipations come into play because of the action (pull) of gravity and that the mechanism can move only by making intermittent foot-ground contacts. The collisional dissipations² could be eliminated by, say, moving the CoM in a horizontal path and taking steps with zero foot-ground speed at touch-down. In this case, however, both legs should do substantial positive and negative work to simultaneously extend and contract as the body moves smoothly across the substrate. Unfortunately, such motion requires more work from the legs than is saved in eliminating energy loss at collisions. The optimization finds that the best strategy is to appropriately use the stance leg to adjust the CoM redirection to first help reduce collisional dissipations and then replace the loss that remains – appropriately timed thrust (*e.g.* pre-emptive push-off) that reduces energy loss and replaces any that remains.

2. The cost of swinging the limbs, including the cost of accelerating the leg at the beginning of swing to regulate the step length and step frequency, and the cost of decelerating and retracting the leg before touch-down to reduce the collision loss and prepare the leg for support transfer.

The above factors that largely determine the best coordination strategy for legged locomotion are inter-related: the initial dissipation associated with the step-to-step CoM transition from downward to upward (a loss determined by collision events) is modified and compensated for by the costs involved with support and swing leg work. Numerous other lesser costs also impact locomotion strategy (those related to stability, for instance), but under steady-state conditions the major determinants of an effective movement strategy will arise

from managing and repaying loss incurred from the interaction of the mechanism's mass with its supporting substrate.

3.4.5 Applications to Understanding Human Locomotion

As mentioned previously, many characteristics of the energy-optimal gaits generated by the *minimally constrained* bipedal model match those of human locomotion. Note that the resulting similarities here are obtained *spontaneously* based on the natural energy-optimal response of the model. In other words, unlike many other gait optimization approaches, no human data were used to train ('teach') the model to have a human-like behavior. This suggests that human gait coordination is mainly influenced by energy minimization through the interaction of the same determinant factors responsible for the model's optimal gaits. If this hypothesis is correct then the optimization model should be able to correctly predict the natural response of human gait coordination to unusual circumstances. Verification of this hypothesis is the subject of the next chapter.

3.5 Summary

This chapter uses the framework developed in Chapter 2 to investigate the characteristics of energy efficient gaits at different average forward speeds and ground slopes. Two types of gait have been considered; continuous-support gait with alternating single and double support phases, and intermittent-support gaits with alternating single support and flight phases.

For relatively slow speeds the continuous-support (no flight phase) gait is more efficient. The optimal gait in this case is the pendular walk with zero-duration DS phase and collisional TDs. In this gait the stance leg length is held constant during most of the single support phase, while the swing leg moves passively during most of its motion. The CoM moves on

an arc-shape trajectory dictated by the stance leg, and reaches its highest point when it is directly over the supporting leg. In optimal level-ground continuous-support gaits almost all complex ankle³ activity is during push-off at final portions of the support phase, prior to the following touch-down. Due to the collisional heel-strike and the preemptive push-off, vertical GRF has a double-hump shape.

By increasing the forward speed the intermittent-support (support and flight phase) gait becomes more efficient. The optimal gait at higher speeds is the impulsive run with collisional TDs, near vertical landing leg, and pulse-shaped vertical GRFs. The CoM is at its lowest point in the step cycle when it is directly over the support leg. The main contribution of the complex ankle joint is to redirect the body motion from downward to upward and provide the required velocity for take-off.

Swing-leg retraction and some residual TD impact, determined by the balance between the potential energy saving at heel-strike impact and the energetic cost of swing-leg deceleration/acceleration, are identified as important characteristics of all energy efficient gaits for many ground slopes. The contribution of the stance-ankle torque in manipulating the angular momentum of the biped is negligible (or unimportant for non-level-ground gaits). For uphill gaits the step length is shorter than for level-ground gaits, and the torso leans forward to compensate for the stance-hip torque.

³The complex ankle includes both the revolute joint between the foot and the leg and the telescoping joint along the leg

Chapter 4

WALKING AND RUNNING IN REDUCED GRAVITY

Many characteristics of the energy-optimal gaits calculated in the previous chapter match those of human gaits; supporting the hypothesis that human gait coordination is mainly governed by energy minimization. Thus, gait optimization might correctly predict the natural response of human gait coordination to unusual circumstances, such as altered gravity. In this chapter, I verify this property by comparing the energetics of human gait in reduced gravity with those predicted by energy-optimal gaits of the minimally constrained bipedal model under similar conditions.

This chapter is organized as follows. In Section 4.1, Farley and McMahon’s experiment [87] for studying simulated reduced gravity influences on human gait energetics is reviewed. The model predictions for the dependency of gait energetics and kinematics on gravity are presented in Section 4.2. The insights achieved by comparing the model predictions and the experimental observations are discussed in Section 4.3. Finally, the chapter is summarized in Section 4.4.

4.1 Reduced Gravity Effects on Human Gait Energetics

Two decades ago, Farley and McMahon [87] conducted an experiment to measure the energetics of walking and running under *approximate* reduced gravity conditions. They used a simple apparatus, shown in Fig. 4.1, to ‘simulate’ reduced gravity conditions on human subjects walking and running on a motorized treadmill. Using a series of pre-stretched springs,

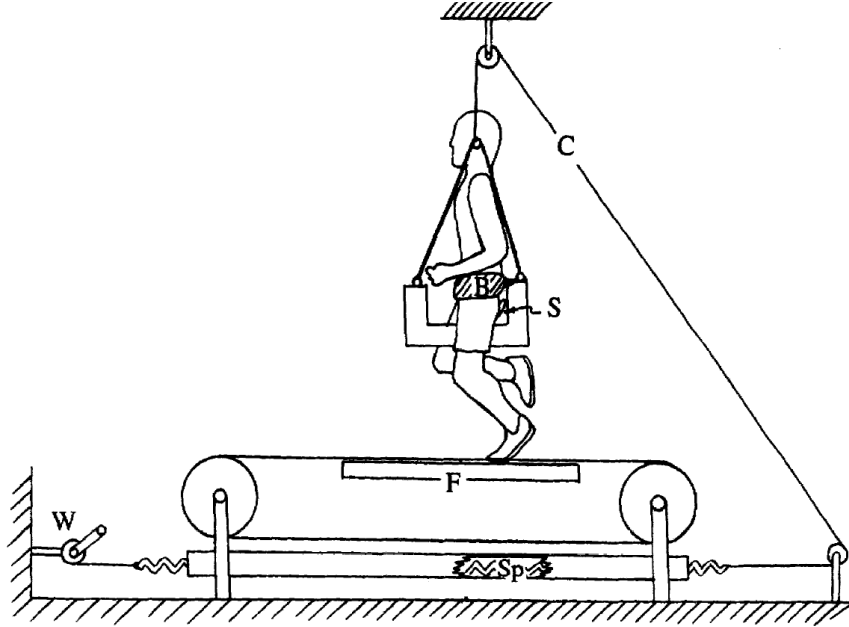


Figure 4.1: **Reduced gravity apparatus** used by Farley and McMahon [87]. It consists of “a series of springs (Sp), which applied a nearly constant upward force to the body through a bicycle saddle (S). Magnitude of force was increased by stretching springs with a winch (W). Motorized treadmill included a strain gauge force platform (F) under the tread”. The figure and the quoted text are reproduced from [87] with permission.

they could apply an almost constant upward force to the subject’s body to reduce his/her effective weight. This apparatus allowed a realistic simulation of reduced gravity in terms of the motions of the CoM but not in terms of the motions of the swinging limbs¹. By measuring the subject’s rate of Oxygen consumption during the experiment, they estimated the energetic cost of walking and running, quantified by the net metabolic energy expenditure per unit body mass and unit distance travelled (*i.e.* $E_{\text{step,metabolic}}/m_{\text{tot}} D_{\text{step}}$). Although, in their paper [87] this quantity is called the cost of transport, in order to maintain consistency with the rest of the thesis and to distinguish this quantity from the COT in (2.2), I refer to it as the *dimensional metabolic cost of transport* (DMet-COT). It is dimensional since it is not divided by the gravitational acceleration, and has the dimension [m/s²]

With the above procedure, Farley and McMahon demonstrated that the DMet-COT in

¹Although the partial reduced gravity condition provided with this technique is not realistic and does not equally affect all body segments, other studies [86, 88, 89] show that it is a good approximation for true reduced gravity in which all body segments experience the same reduced gravity level.

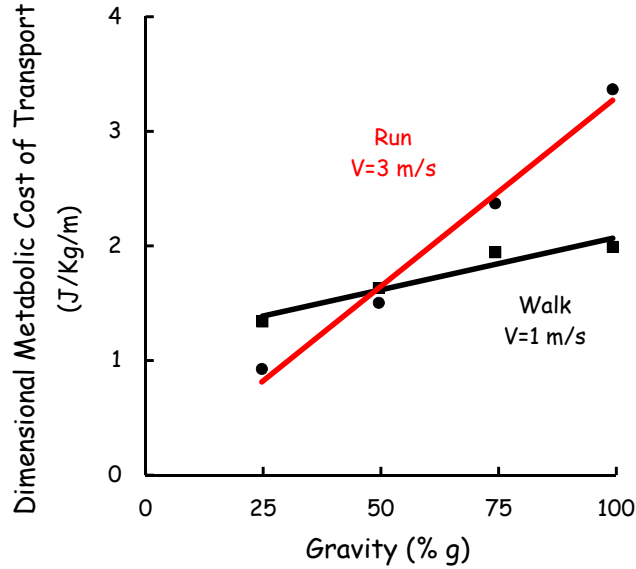


Figure 4.2: **Dimensional metabolic cost of transport (DMet-COT) of walking and running in partially reduced gravity conditions** (*i.e.* reduced effective gravity only on the CoM), measured by Farley and McMahon [87]. They calculated the DMet-COT (in the original work it is called the cost of transport) as the net metabolic energy consumption per unit body mass and unit distance travelled. As the figure shows, the DMet-COT in running declines with decreases in gravity faster than in walking.

running decreases with reduced gravity more dramatically than in walking, as shown in Fig. 4.2. In normal gravity, walking is more cost-effective than running. However, due to the greater influence of gravity reduction on energetic cost for running than for walking, the scenario is reversed at low gravity levels (*e.g.* on the Moon), and running becomes energetically more favorable.

Farley and McMahon [87] hypothesized that the difference in dependency of walking and running energetics to gravity is due to the different “energy-saving mechanisms associated with each of these gaits”: elastic energy storage and recovery in running *versus* kinetic and potential energy exchange in walking. Based on this hypothesis, spring-like elements in the human body (such as tendons, ligaments, etc.) that can store and release elastic energy have a determinant role in the mechanics of running. They concluded that “the links between the mechanics of locomotion and energetic cost is fundamentally different for running and for walking” [87].

4.2 Predictions of the Minimally Constrained Bipedal Model

With the bipedal model in Fig. 2.1, and using the gait optimization framework presented in Chapter 2, I found the optimal walking and running gaits that minimized the mechanical COT \mathcal{C}_{mt} (see Section 2.1.2) at different gravity levels and speeds. Other than the gravity level and the average forward speed, all other gait parameters including the step length, step frequency, joint angles, and joint torques/forces were determined by the optimization.

4.2.1 Predictions of Gait Energetics

The resulting *dimensional mechanical COT* (DMec-COT = $\mathcal{C}_{\text{mt}} g_{\text{red}}$, where g_{red} is the reduced gravity level) for walking and running at different speeds and gravity levels is shown in Fig. 4.3. As can be seen, the model predictions are consistent with the experimental ob-

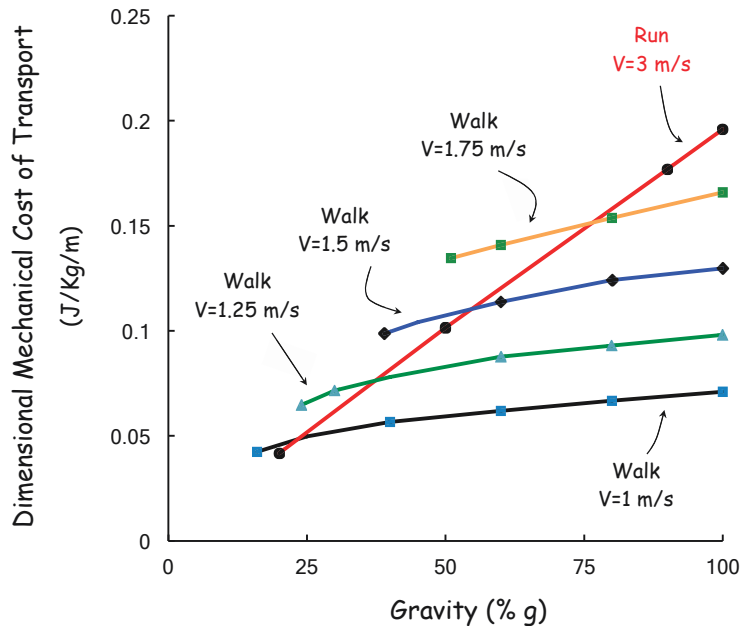


Figure 4.3: **Dimensional mechanical cost of transport (DMec-COT) of energy-optimal gaits of the model.** The optimal gaits were obtained by minimizing the mechanical COT \mathcal{C}_{mt} (see Section 2.1.2) for given speed V and gravity level g_{red} . DMec-COT was then calculated from $\mathcal{C}_{\text{mt}} g_{\text{red}}$. No curve fitting is used in this figure (lines connect the raw data points), but for more clarity some of data points are not marked. The gait optimization correctly predicts the cost trends of human gaits shown in Fig. 4.2.

servations by Farley and McMahon [87]: *the energetics of both gaits decrease with gravity, but the effect in running is much more pronounced than in walking, leading to intersection of walking and running cost curves. Consequently, the more energetically demanding gait at greater gravity levels (i.e. running) becomes the less costly at lower gravity levels.*

The cost values determined in Fig. 4.3 change slightly if specific COT \mathcal{C}_{et} (see Section 2.1.2) is used instead of mechanical COT \mathcal{C}_{mt} for the optimization objective function. This is also the case if a different number of discretization grids (*i.e.* N_{ss} , N_{ds} , and N_{fl} ; see Section 2.3.2) is employed in the optimization. However, independent of the resulting cost values, the cost trends remain the same. I also repeated the optimizations for ‘partially’ reduced gravity conditions, *i.e.* instead of changing the gravitational acceleration in the EoM for all body segments, a constant upward force at the hip was added to the model, equivalent to Farley and McMahon’s experiment). Even in this case the results remained qualitatively the same, with slight changes in cost levels and slopes.

Interestingly, the agreement between the experimental observations and model predictions is obtained even though no elastic components are used in the model. The use of springs in the model for running gaits could decrease the cost of running, improving the estimation of cross-over gravity levels (cross-overs in walking and running costs in Fig. 4.3 will occur at slightly higher gravity levels, closer to those observed in Fig. 4.2), but they will not influence the form of the result or the fact that the two gaits respond differently to a reduction in gravity level.

4.2.2 Gait Kinematics

To explore the model response in order to understand why the optimization dictates these effects due to altered gravity, I also calculated the step length of the optimal gaits associated with Fig. 4.3. The results for walking at $V = 1$ m/s and for running at $V = 3$ m/s are shown in Fig. 4.4. For walking at the other speeds used in Fig. 4.3 the optimal step length is not

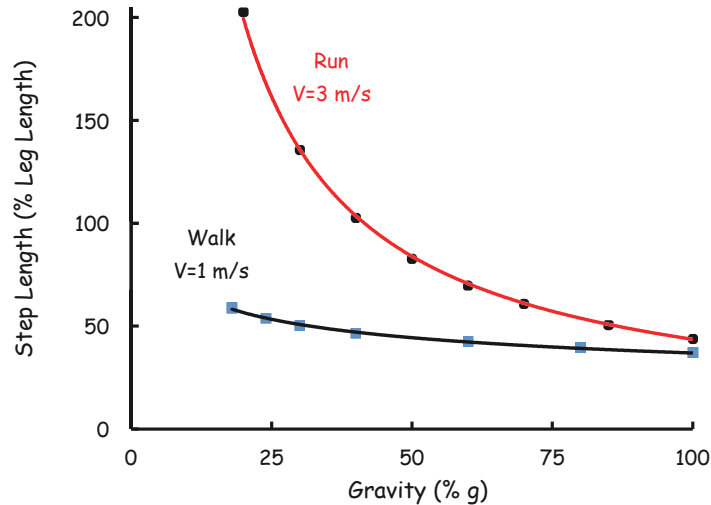


Figure 4.4: **Step length changes with gravity**, as predicted by energy-optimal gaits of the minimally constrained bipedal model presented in Chapter 2. For both walking and running, step length increases with reduced gravity, but the changes for running are substantially greater than for walking. The red line (running) corresponds to the $1/g_{\text{red}}$ trend, where g_{red} is the reduced gravity acceleration. The step length data in this figure correspond to the optimal gaits in Fig. 4.3. For more clarity, the results for walking at the other speeds used in Fig. 4.3 are not shown.

considerably different from the one shown in Fig. 4.4, and thus to improve clarity of the figure they are not shown in this figure. As can be seen, the step length for both energy-optimal walking and running increases with reduced gravity, but the changes for running are substantially greater than for walking.

Unfortunately, Farley and McMahon did not report the step length data for their experiments [87]. I have used a novel reduced gravity apparatus and collected some preliminary data from a few human subjects that verify the model predictions for gait kinematics [32]. Because more data have to be collected in order to characterize these relationships with adequate statistical confidence, the preliminary results are not reported here, and the full verification of the optimization model's ability to predict the spontaneous response of human subjects to altered gravity will be left to my future studies.

4.3 Discussion

The analyses in this chapter were performed to examine whether gait optimization can correctly predict the variations in human gait coordination in unusual circumstances. The predictive capacity of the optimization model was demonstrated through the agreement between the energetics (and kinematics, based on the preliminary data) of the optimization-generated movements and the observed subject gaits for simulated reduced gravity. Now, what can we learn from this agreement?

4.3.1 Energy Storage and Recovery Is Helpful, But Not Determinant

As mentioned previously, Farley and McMahon hypothesized that the different dependency of walking and running energetics to gravity is due to the different “energy-saving mechanisms associated with each of these gaits”. This hypothesis has originated from a prevailing perspective in studying legged locomotion [2]. According to this perspective, the coordination in walking and running occurs to maximize energy storage and recovery within the stride cycle, *e.g.* [20, 22, 27, 28, 90, 91]. In other words, the best gait coordination is the one that in one part of the gait cycle stores kinetic energy in some form of potential energy (potential gravitational energy in walking through an inverted pendulum-like motion, and potential elastic energy in running through compliant elements in the body) and then recovers it in another part of the gait cycle.

This perspective, and thus Farley and McMahon’s hypothesis for reduced gravity effects, does not match the gait optimization results in this thesis. In the previous chapter, both walking and running emerged from the gait optimization of a rigid model, with no direct or indirect reference to elasticity. In this chapter, the dependency of the energetics of both gaits to gravity was correctly predicted by the same model, without any effort to maximize energy storage and recovery. These results lead us to question the ‘energy storage and recovery’

perspective in explaining the human and animal gait coordination.

Note that disagreement with the recovery perspective does not imply questioning the occurrence or advantage of energy storage and recovery in locomotion. The exchanges between kinetic and various potential energy forms unequivocally occur in human and animal gaits *via* different energy-saving mechanisms. It is also undeniable that these passive energy exchanges reduce the energetic cost of locomotion by storing and reusing the energy at different phases of the gait. However, it seems that these exchanges are more descriptive characteristics of the expression of each gait, rather than the determinant factors of the appropriate gait coordination in each circumstance.

4.3.2 An Alternate Perspective

If not maximizing energy storage and recovery, what is a better perspective to explain the observed human gait coordination?

It seems that energy minimization has a substantial influence in both walking and running coordination (*e.g.* [14, 26, 72, 73, 92, 93], and also the results in Chapter 3). As discussed in the previous chapter, for gait optimization with a minimally constrained bipedal model energy minimization is determined by the balance between the cost of swing-leg work and the cost and loss associated with redirecting the CoM motion from downward to upward at each foot-ground contact (passive energy loss at heel-strike collision, and the cost of dissipative and generative stance-leg work). The agreement between the experimental observations and model predictions in both usual (normal gravity cases in the previous chapter) and unusual circumstances (reduced gravity in this chapter) suggests that the same determinant factors (leg work costs and collision loss) are responsible for human gait coordination as well. Based on this perspective, both walking and running are mainly influenced by *similar* determinant factors and mechanisms, not the different ones as proposed by the recovery perspective.

Now, If this is the case, how can we explain the different influence of gravity on energetics

and kinematics of walking and running? The answer is in the different characteristics of these gaits, where each gait is viewed as a movement strategy appropriate for the conditions under which it operates.

In energy-optimal gaits the energetic cost associated with redirecting the CoM motion from downward to upward is mainly influenced by energy dissipation at collisional foot-ground contact [26]. This in turn, depends on the collision angle (the relative leg-surface angle) and the velocity of the CoM prior to collision [26]. For running, collisional dissipation at foot-ground contact is minimized by landing on a near-vertical leg (see the previous chapter), regardless of the gravity level. Thus, for running at a given speed, collision loss does not change with gravity, resulting in an almost constant energetic cost per step. On the other hand, as gravity decreases, the duration of the quasi-passive flight phase, and consequently the step length, increases in reverse proportion to g (see Fig. 4.4). This results in a linear reduction in the dimensional COT with gravity, as can be seen in Fig. 4.2 and Fig. 4.3.

For walking, however, the collision angle completely depends on the step length. With a given pre-collision CoM speed, increasing the step length directly increases the collision loss and thus the energetic cost of the gait [26, 47]. However, at lower gravity levels the pre-collision CoM speed can be slightly decreased while maintaining the same average forward speed². This allows for a small increase in the step length without increasing the collision loss. Therefore, with a constant energetic cost per step, the step length slightly increases leading to a small reduction in the dimensional COT, as shown in Fig. 4.2 and Fig. 4.3.

The above discussion suggests that, unlike what was hypothesized by Farley and McMahon [87], the links between the mechanics of locomotion and energetic cost are basically similar for running and for walking. The analyses in this chapter and Chapter 3 show that

²In inverted pendular walking, the CoM speed decreases as the CoM rises to the top and then increases as it falls forward. Decreasing gravity decreases the fluctuations in CoM speed, so to maintain a given average forward speed, the CoM speed at the beginning and end of the inverted pendulum motion should be decreased.

a relatively simple model is able to predict substantial human-like behavior, even in quite unnatural circumstances. This suggests that much of the locomotory behavior displayed by humans originates with optimization of fundamental dynamics.

4.4 Summary

Motivated by the results in the previous chapter, in which many characteristics of the optimization-generated gaits matched those of human gaits, I used gait optimization to predict human gait adjustments in reduced gravity. These predictions were evaluated using the experimental data for energetics of walking and running in ‘partially’ reduced gravity conditions (where the effective gravity is reduced only on the CoM, and not on all body segments). Interestingly, the model predictions matched the experimental observations: the cost of running decreased with a reduction in effective gravity, while the cost of walking was, surprisingly, much less sensitive to the gravity level. The agreement between the model predictions and experimental observations supports the hypothesis that gait coordination in humans (and animals) is mainly influenced by energy minimization. It also solidifies the hypothesis suggested in Section 3.4.5; that the same cost factors identified in gait optimization (*i.e.* the cost of stance-leg work associated with redirecting the CoM motion from downward to upward, and the cost to move the swing leg forward and prepare it for support transfer) are determinant in human gait coordination as well.

Chapter 5

A SIMPLE BIPEDAL MODEL TO STUDY SWING-LEG RETRACTION

One of the characteristics found for many optimization-generated gaits in Chapter 3 is swing-leg retraction, the rearward rotation of the swing leg prior to foot-ground contact. This is also a well-known characteristic of human walking and running, e.g. [51], and is also observed in different gaits of many terrestrial legged animals (e.g. [52, 56, 57]). In Chapter 1 some of the advantages of swing-leg retraction were presented. In the rest of this thesis, some model-based advantages of swing-leg retraction will be discussed in detail. These advantages either have been discovered for the first time in this thesis, or were known before but not as thoroughly analyzed and for as many cases as discussed here. The technical background and modeling for this study is presented in this chapter and the following two. The advantages will be discussed in Chapter 8.

To study the advantages of swing-leg retraction, the bipedal model and numerical techniques introduced in Chapter 2 can still be used, but in this case we will be limited to our interpretation of numerical results. To gain more insight into the influence of different parameters, a simpler model that enables us to find closed-form approximate analytic solutions is more preferable. Later, these approximate solutions can be verified using numerical methods. For this purpose, I introduce a new simple model in Section 5.1. The energy optimal walking gait and the governing dynamics of this model are described in Section 5.2 and Section 5.3. Section 5.4 describes the requirements to achieve a periodic gait. These requirements lead to the definition of an ‘admissible region’ that constitutes the parameter space for step angle and speed. Finally, the chapter is summarized in Section 5.5.

5.1 Bipedal Model

The planar bipedal model used for studying swing-leg retraction is shown in Fig. 5.1. The head, arms, and trunk are represented by a point mass m_H at the hip. Each rigid leg has length ℓ and distributed mass m_{leg} , with the CoM G_{leg} located at distance b from the hip. Because each human leg is about 16% of total body mass [80], it is assumed here that m_{leg} is relatively small compared to the total mass $m_{\text{tot}} = 2m_{\text{leg}} + m_H$.

The leg moment of inertia about the hip joint is $I_{\text{leg}/H}$. To simplify later calculations I write $I_{\text{leg}/H} = \delta m_{\text{leg}} \ell b$, where dimensionless δ represents the spread of the leg mass relative to G_{leg} . It is shown in Section 5.1.1 that always $b/\ell \leq \delta \leq 1$.

The simple model presented here is modified from the powered simplest walking model used by Kuo [47] in that (i) the present model has an arbitrary distribution of mass on the leg, (ii) it has no hip spring, and (iii) in this model the mass of the leg, although generally assumed small for some purposes, needs *non*-negligible energetic cost to be accelerated.

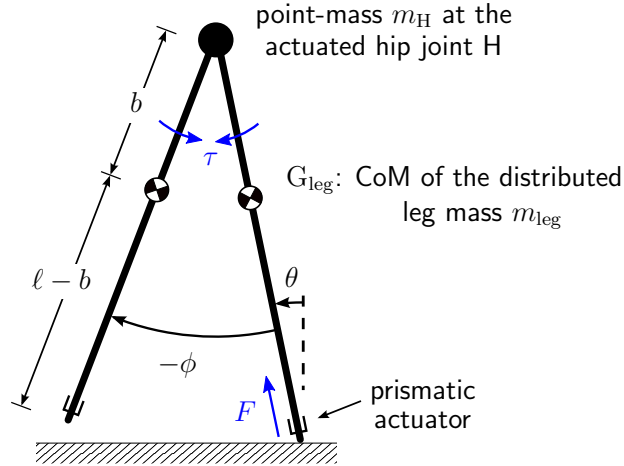


Figure 5.1: **Biped model without torso.** Two rigid legs with lengths ℓ and distributed mass m_{leg} . The leg center of mass is at G_{leg} located at distance b from the hip. The leg moment of inertia about the hip is $I_{\text{leg}/H} = \delta m_{\text{leg}} \ell b$. A point mass at the hip m_H represents the upper body. There is a motor at the hip applying torque τ between the legs, and a prismatic actuator that extends and applies push-off force F along the stance leg.

Table 5.1: Model Parameter Values of The Biped in Fig. 5.1

| Parameter | Symbol | Value | Unit |
|---------------------------|------------------|-----------------------|------|
| total body mass | m_{tot} | 75 | [Kg] |
| leg mass | m_{leg} | $0.16 m_{\text{tot}}$ | [Kg] |
| leg length | ℓ | 90.1 | [cm] |
| leg CoM proximal distance | b | 0.41ℓ | [cm] |
| leg mass spread constant | δ | 0.62 | - |

The new model in Fig.5.1 is different from the one in Fig.2.1 in that (i) the extended torso is replaced with a point mass at the hip, thus $I_{\text{trs}/G_{\text{trs}}} = I_{\text{trs}/H} = 0$; (ii) due to the removal of the extended torso, there is only one hip joint and one possible hip actuator between the legs; (iii) the new model has no extended feet and thus no revolute actuator between the feet and the legs; (iv) there is no massless part in the legs.

Unless otherwise noted, the numerical calculations in the rest of the thesis are based on the values listed in Table 5.1 from [80], as an approximation of a human with 75 Kg total mass and 170 cm body height. These values are equivalent to those listed in Table 3.1, but are adjusted according to the specifications of the new model. For example, m_{trs} is now m_H but with no moment of inertia, and $\ell = h_{\text{tot}} - h_{\text{trs}} = 0.53 h_{\text{tot}}$.

The model is powered by a hip motor and a prismatic leg-extension actuator, active on the stance leg. The leg-extending prismatic actuator on the stance leg represents all mechanisms that extend the distance from the body to the toes on the ground (e.g., ankle extension, hip tilting, and knee straightening). Unlike models that use flat feet on the ground, this model has no ankle actuator for a torque on the leg from the foot (or ground), though its inclusion in the model besides the leg prismatic actuator would have no noticeable effect in our analysis in any case (see Section 3.2.1).

This study is focused only on periodic gaits; that is, two consecutive steps are identical

with the leg roles exchanged. By assumption, friction is adequate to avoid foot slipping at all instants during the gait. As is standard in compass biped models [39, 46, 47], any possible foot scuffing during mid-swing is ignored.

5.1.1 Some Mathematical Properties of the Model

Limits of the Parameter δ :

If $I_{\text{leg}/G_{\text{leg}}}$ represents the leg moment of inertia about G_{leg} , it is always valid that

$$I_{\text{leg}/H} = \delta m_{\text{leg}} \ell b = I_{\text{leg}/G_{\text{leg}}} + m_{\text{leg}} b^2 \geq m_{\text{leg}} b^2. \quad (5.1)$$

In a stick model the maximum leg moment of inertia about the hip is achieved when all leg mass is concentrated at two ends of the leg. In this case, respecting the leg CoM at a distance b from the hip requires the point mass $m_1 = m_{\text{leg}} b/\ell$ at the toe, and the rest of the leg mass at the top of the leg, next to the hip. Thus

$$I_{\text{leg}/H} = \delta m_{\text{leg}} \ell b \leq m_1 \ell^2 = m_{\text{leg}} b \ell. \quad (5.2)$$

The above two equations imply that in all circumstances $b/\ell \leq \delta \leq 1$. Although the upper bound of δ is calculated using a stick model, in practical cases δ is even smaller. For example, for Cornell Ranger [12] $\delta = 0.72$, and for a typical human $\delta = 0.62$ (using the anthropomorphic model parameters in Table 5.1).

Invariance to Hip Mass:

In Fig. 5.1 the hip mass m_H represents the humans' upper body which is separate from the legs. Interestingly, in this model any portion of m_H can be placed on the legs without any change in forces, motion, or energetics. Assume that mass $2\Delta m$ is subtracted from m_H and Δm is added to the top of each leg, next to the hip joint H. The distance of each displaced mass Δm from the hip is $d_{\Delta m/H} = 0$, but now they move with the legs. The new biped

parameters after this mass displacement are:

$$m'_H = m_H - 2\Delta m, \quad (5.3)$$

$$m'_{\text{leg}} = m_{\text{leg}} + \Delta m, \quad (5.4)$$

$$b' = d_{G'_{\text{leg}}/H} = \frac{d_{G_{\text{leg}}/H} m_{\text{leg}} + d_{\Delta m/H} \Delta m}{m'_{\text{leg}}} = b \frac{m_{\text{leg}}}{m'_{\text{leg}}}, \quad (5.5)$$

$$I'_{\text{leg}/H} = I_{\text{leg}/H} + \Delta m d_{\Delta m/H}^2 = I_{\text{leg}/H}, \quad (5.6)$$

$$\delta' = \frac{I'_{\text{leg}/H}}{m'_{\text{leg}} b' \ell} = \frac{I_{\text{leg}/H}}{m_{\text{leg}} b \ell} = \delta, \quad (5.7)$$

where $d_{A/B}$ denotes the distance of point A from point B. Despite the change in leg mass and leg CoM, the biped CoM does not change, as the distance of each displaced mass Δm from the hip is still zero (similar to when it was on the hip), and the spatial mass distribution has not changed. Because the biped CoM and the leg moment of inertia about the hip, $I_{\text{leg}/H}$, remain unchanged, the rotation of the swing leg about the hip joint and the motion/rotation of the whole biped about the stance foot will not change. Thus, the new biped is mechanically identical to the one before the mass displacement. Furthermore, as we will see later in this chapter, m_{leg} does not appear alone in the equations, and is always multiplied by b . Because $m'_{\text{leg}} b' = m_{\text{leg}} b$ the change in m_{leg} and b does not change the system behavior.

5.2 Energy-Optimal Gaits

If we allow arbitrary actuator force and torque profiles (arbitrary functions of time), this model has an infinite number of periodic walking gaits. Of these, this study focuses on energy optimal gaits because they may have explanatory value for describing human and animal gaits, and also may be useful for efficient robot design. Energy-optimization of the model is a problem in Calculus of Variations or Dynamic Programming of the type discussed in Chapter 2, or *e.g.* in [25, 67]. This optimization can be simplified, perhaps with no loss of

accuracy (as discussed below), by guessing an appropriate low-dimensional parameterization of the force and torque profiles that uses impulses.

5.2.1 Observations of Energy Optimal Gaits

I motivate the reduction of the actuator profiles to impulses by the results presented in Chapter 3, as well as by some observations of human gait and other optimal gait studies.

- When walking, humans start extending their trailing leg’s ankle (plantar flexion) and knee joints at the end of single stance [47]. The peak muscle activity of this push-off starts just before heel-strike. Consistently, mechanical-work optimization calculations using models with different levels of complexity indicate that the stance leg length should be constant during most of the stance phase and extended (*i.e.* push-off) just before the swing leg hits the ground (*e.g.* see Chapter 3 of this thesis and [25, 26, 47, 67]).
- Experimental data from human walking show that during swing phase the leg motion is almost ballistic (*i.e.* driven only by gravity) [36] except for the beginning and end of the swing phase where hip muscles have burst activities [33, 47, 94]. Assuming that the leg swing should be faster than a passive swing, again consistently, models show that the work-minimizing torque profile for the hip consists of peak torques at the beginning and end of the swing, and no activity in between (the ‘bang-coast-bang’ profile discussed in Chapter 3).
- In general, work minimization tends to lead to concentrating actuator activity into impulses at the start and end of the various phases of the motion of various body parts (see Chapter 3, and [25]).
- The role of the ankle actuators in push-off, when the ankle extension effectively extends the legs, is well-modeled by the leg-extension prismatic actuator (see

Chapter 3). This substitution of prismatic leg extension for ankle joint extension (instead of a revolute joint with foot-roll) seems to have little effect on work-based walking energetics (see Chapter 3).

Based on the above observations and optimization results, it is expected that the mechanical-work optimized gaits in the new model typically have (i) a burst extensional push-off force applied just prior to heel-strike by the stance leg's prismatic actuator, and (ii) burst torques applied at the hip at the beginning of the swing and again at the end of the swing. The first burst torque (referred to as *swing thrust*) is to increase the swing speed, above a purely passive swing, to achieve a shorter step period at a given walking speed. The second hip burst (referred to as *swing-leg retraction*, or simply *retraction*) brakes and/or reverses the leg swing rotation prior to heel-strike.

5.2.2 Simplification to Impulsive Forces and Torques

The burst push-off force and the burst swing thrust and swing retraction torques are applied over a short period of time. So, the biped configuration changes a little, or not at all, during their application, while the velocity changes are more noticeable. For example, while the measured hip angle in human walking shows a clear sign change in leg angular velocity during swing-leg retraction [51], the associated change in leg orientation is not large enough, or its duration is too short, to be easily seen on motion-pictures and videos of human or animal walking, e.g. [52, 54]. This characteristic that velocity changes occur in an almost fixed joint configuration is approximately similar to that of exact impulsive (infinitesimal duration with infinite magnitude) forces/torques that cause discontinuous velocity jumps in an exactly fixed biped configuration. Hence, to simplify the analysis, the burst push-off force and the burst swing thrust and swing retraction torques are approximated as exactly impulsive actuations. It is expected that a full dynamic programming solution would yield this impulsive result. Although impulsive actuation is an extreme idealization, the insights

from analysis of simplified impulsive models can be an important step in improving our understanding of legged locomotion, as those discussed in [2, 26, 48].

5.2.3 Parameterization by Impulses

As motivated by the optimization and observational results above, the actuation can be reduced to one impulsive force and two impulsive torques: (i) the impulsive swing thrust torque just after toe-off to start the swing, (ii) the impulsive swing retraction torque at the end of of swing phase (just before heel-strike) to stop or reverse the swing, and (iii) the impulsive push-off force at the end of stance phase (just before heel-strike). These infinite-magnitude forces and torques are quantified by their net impulse, *i.e.* the time integral of the force/torque. If (t_s^-, t_s^+) denotes the infinitesimal period during which the impulsive swing thrust torque is applied, and (t_{pr}^-, t_{pr}^+) denotes the infinitesimal period at the end of swing where the impulsive push-off force and the impulsive retraction torque are applied, then the swing thrust impulse \mathcal{S} , the swing retraction impulse \mathcal{R} , and the push-off impulse \mathcal{P} are defined as

$$\mathcal{S} = \int_{t_s^-}^{t_s^+} \tau(t) dt, \quad (5.8)$$

$$\mathcal{R} = \int_{t_{pr}^-}^{t_{pr}^+} -\tau(t) dt, \quad (5.9)$$

$$\mathcal{P} = \int_{t_{pr}^-}^{t_{pr}^+} F(t) dt, \quad (5.10)$$

where $\tau(t)$ is the hip torque, and $F(t)$ is the stance leg's actuator force. Note that the positive directions of \mathcal{S} and \mathcal{R} are opposite.

5.2.4 Impulsive Heel-Strike and Instantaneous Support Transfer

Motivated by the gait optimization results in Chapter 3 and consistent with the assumption of impulsive actuations, heel-strike is modeled as an instantaneous and dissipative passive

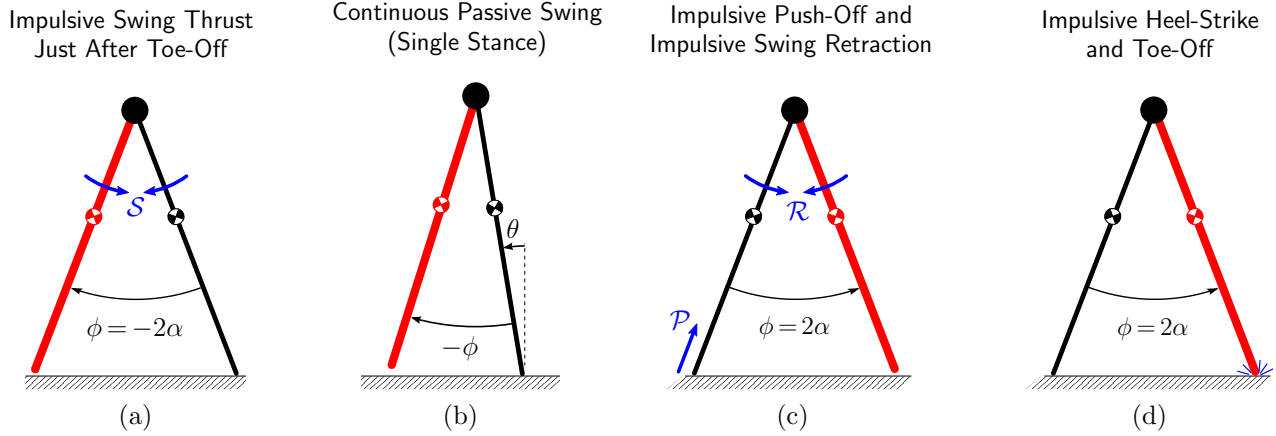


Figure 5.2: **A single gait cycle.** The initial swing leg is *thick* red, the initial stance leg is *thin* black. The four phases of one walking step are as follows. **a)** Just after the thick leg has lifted from the ground at toe-off, the impulsive *swing thrust* \mathcal{S} starts the swing with proper initial swing velocity; **b)** The passive swing of the thick leg continues until $\phi = 2\alpha$. During passive swing the thin leg’s extension actuator (not shown) is locked; **c)** Then, nearly simultaneously the *thin* black leg has an impulsive push-off \mathcal{P} and the hip has an impulsive swing retraction \mathcal{R} . The thin leg’s extension actuator is unlocked only at this phase; Finally, immediately after retraction and push-off, **d)** the thick leg collides with the ground with a sticking (heel-strike) collision.

collision in which the landing (forward) leg neither rebounds (*i.e.* inelastic collision) nor slips. At heel-strike the trailing leg is pulled off the ground (toe-off) by the advancing hip, leading to an instantaneous double-support phase. This instantaneous double-support, obviously an extreme idealization of human walking (human walking has a brief, but non-instantaneous, double-support) also minimizes work in some simple models (see Chapter 3, and [67]).

5.2.5 Gait Cycle

Based on the assumptions and simplifications made, a complete gait cycle can be shown as in Fig. 5.2. Just after the previous stance leg has lifted from the ground at toe-off, the impulsive swing thrust \mathcal{S} starts the swing with proper initial swing velocity. Then the legs move passively until $\phi = 2\alpha$. During this passive phase the stance leg’s extension actuator (not shown in the figure) is locked, and the hip moves along an arc-shape trajectory determined by the fix-length stance leg. Then, nearly simultaneously the stance leg has an

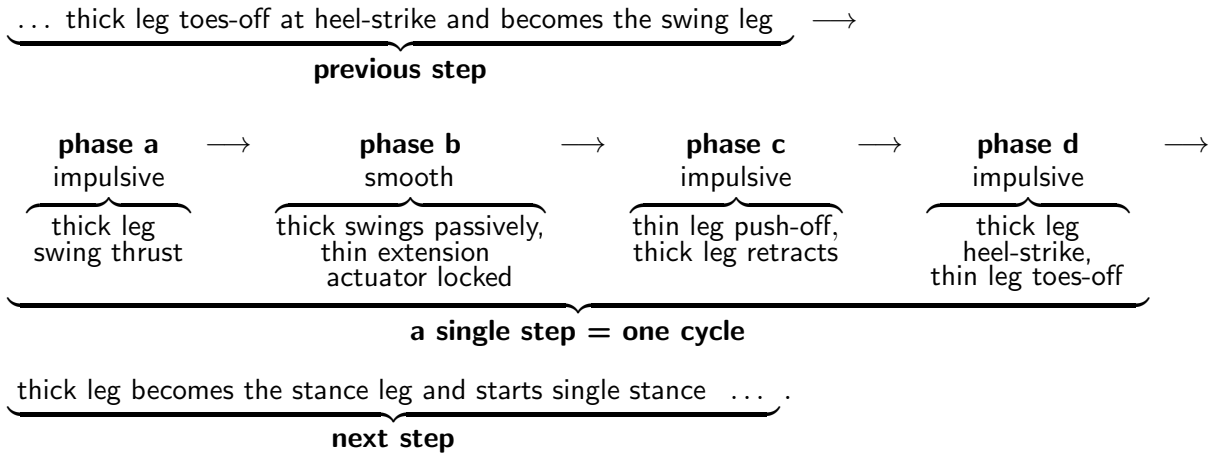


Figure 5.3: **Four phases of a gait cycle.** The phase and the leg labelings are in accordance with Fig. 5.2. ‘thick’ = swing leg, ‘thin’ = stance leg.

impulsive push-off \mathcal{P} and the hip has an impulsive swing retraction \mathcal{R} . The stance leg’s extension actuator is unlocked only during the impulsive push-off and retraction. Finally, immediately after retraction and push-off, the leading leg collides with the ground with a sticking (heel-strike) collision, and simultaneously the trailing leg is lifted from the ground.

The whole gait cycle consists of a sequence of smooth (continuous) and impulsive phases, some passive and some actuated. During the smooth passive swing, all velocities and positions are continuous functions of time, whereas at impulsive phases positions are continuous, but velocities are discontinuous. The biped state (positions and velocities) at the end of one phase is determined by the state at the start of that phase, the impulsive action at that phase, if any, and the dynamics through the phase. For example, the state at the end of passive swing is determined by the state at the beginning of the swing phase (just after the swing thrust) and the dynamics of swing. Thus, the whole step can be analyzed in terms of a sequence of state mappings of the phases shown in Fig. 5.2. In reference to this figure, the two legs are called ‘thin’ and ‘thick’, and the four phases of one step are labeled as phase (a)-(d), as shown in Fig. 5.3.

Note that phase (c) has two impulses, the push-off impulse \mathcal{P} and the retraction impulse

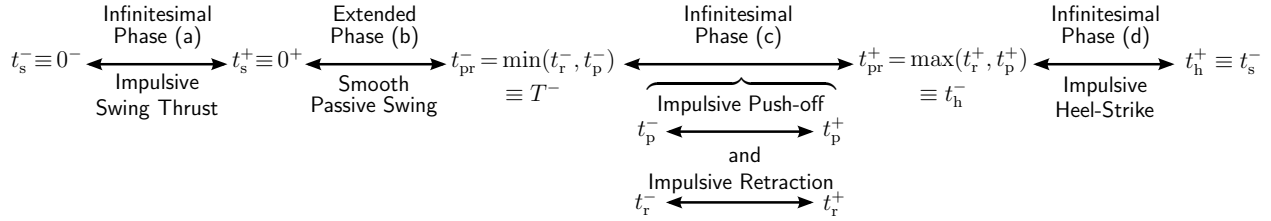


Figure 5.4: **Labels of the time instants between the phases.** In phase (c) the impulsive push-off and retraction can have any (specified) order or overlap.

\mathcal{R} , both of which happen at the same biped configuration (Fig. 5.2c). Although this phase has infinitesimal duration, one can treat \mathcal{P} and \mathcal{R} as isolated in time (with one before the other) or as having some (specified) overlap in time. As will be discussed later, the relative timing of these impulses has no influence on biped states at heel-strike and thereafter, but is relevant for gait energetics.

5.3 Details of The Dynamics

To simplify the presentation, the time instants between consecutive phases are labeled individually. A quick reference of these labels is provided in Fig. 5.4. Following the definition of swing thrust impulse \mathcal{S} in (5.8), the time instant just before \mathcal{S} is called t_s^- , and the time instant just after \mathcal{S} (the beginning of single stance) is called t_s^+ . Similarly, t_r^- and t_r^+ denote the time instants just before and just after the impulsive \mathcal{R} , and t_p^- and t_p^+ denote the time instants just before and just after the impulsive \mathcal{P} . Also, t_h^- is the time instant just before instantaneous heel-strike (after both \mathcal{P} and \mathcal{R}), and t_h^+ is the time instant just after it (= after toe-off). In (5.9) and (5.10) the impulsive push-off and retraction are defined in the infinitesimal interval (t_{pr}^-, t_{pr}^+) . Thus, $t_{pr}^- = \min(t_r^-, t_p^-)$ is the time instant just before both \mathcal{P} and \mathcal{R} (the end of the passive swing), and $t_{pr}^+ = \max(t_r^+, t_p^+) \equiv t_h^-$ is the end of single stance. In reference to Fig. 5.2, a step cycle starts just after the previous heel-strike, at t_s^- , where $\theta = -\phi/2 = \alpha$, and ends just after the next toe-off, at t_h^+ . Therefore, we can assign: $t_s^- \equiv 0^-$, $t_s^+ \equiv 0^+$, and $t_{pr}^- \equiv T^-$, where T is the step period. The gait is periodic, so $t_h^+ \equiv t_s^-$.

In the next section the modeling and state mapping of the various phases are described, continuous phase (b) first, then impulsive transitions (c), (d), and (a).

5.3.1 Continuous Dynamics

Passive Continuous Single Stance - Phase (b):

In the smooth single stance phase, starting just after the swing thrust impulse (at t_s^+) and ending just before the retraction and push-off impulses (at t_{pr}^-), the leg-extension actuator is locked and the hip joint is free. In this phase the model is a passive semi-inverted double pendulum (see Fig. 5.2b) forced by gravity and supported by the ground. The equations of motion can be found using angular momentum balance of the entire mechanism about the support foot and of the swing leg about the hip joint. After simplification, we can arrange these equations in the following standard form:

$$\mathbf{M}(\mathbf{q}) \ddot{\mathbf{q}} + \mathbf{c}(\mathbf{q}, \dot{\mathbf{q}}) = \mathbf{0}, \quad (5.11)$$

where \mathbf{M} is the inertia matrix, and the time-dependent configuration vector $\mathbf{q} = [\theta, \phi]^T$ consists of the stance-leg and hip-joint angles. The velocity dependent column vector \mathbf{c} contains Coriolis, centrifugal, and gravity terms. These quantities are expanded in Appendix B.1.1. Equation (5.11) is used when t is in the interval $(t_s^+, t_{pr}^-) = (0^+, T^-)$ with the boundary conditions: $\theta(0) = -\phi(0)/2 = \phi(T)/2 = -\theta(T) = \alpha$ (Fig. 5.2a & 5.2c).

For given step angle α and average walking speed V , the step period is calculated as $T = 2\ell \sin\alpha/V$. With information on α and T , the solution of (5.11) subject to the above boundary conditions (a two-point boundary value problem) fully determines the stance-leg and hip-joint angles $\theta(t)$ and $\phi(t)$ during passive swing, and thus the corresponding angular velocities $\dot{\theta}(t)$ and $\dot{\phi}(t)$. Therefore, the angular velocities at the beginning of the passive swing ($\dot{\theta}_{0^+}$ and $\dot{\phi}_{0^+}$) and the resulting velocities at the end of the passive swing ($\dot{\theta}_{t_{pr}^-}$ and $\dot{\phi}_{t_{pr}^-}$) are implicitly defined by the step angle α and average forward speed V . This mapping

will be determined below. Because $\dot{\theta}_{0+}$ and $\dot{\phi}_{0+}$ frequently appear in this study, for the sake of simplicity they are denoted by $\dot{\theta}_0$ and $\dot{\phi}_0$ hereafter.

No Centripetal Flight:

The solution of (5.11) is valid only if the stance foot remains on the ground throughout the passive swing, *i.e.* for $0^+ \leq t \leq T^-$. If the calculated motion requires a tensional (pulling by the substrate) GRF along the stance leg, the conditions for maintaining stance are lost. Such loss is due to the centripetal acceleration of the hip going in a circle around the foot. This limits the maximum average walking speed [95, 96]. Detailed analyses are provided in Sections 5.4.4 and 7.7.2.

Symmetric Passive Single Stance Is More Favorable:

For any given step length and average walking speed, the numerical solutions of (5.11) include at least one exact symmetric solution in which the angles have *odd symmetry* and the angular velocities have *even symmetry* about mid-stance. These symmetry properties also hold for the approximate analytic solution of this phase (see Section 7.3). Asymmetric solutions of passive single stance, if they exist, naturally have a larger maximum swing angle (or equivalently maximum hip-joint angle) in one direction, as can be seen in Fig. 5.5. In almost all cases, this implies a larger swing-leg angular rate at the start and end of the passive swing compared to the symmetric solutions. For example, in Fig. 5.5 the initial and final slopes of the asymmetric solutions are larger than those of the symmetric one. The larger initial angular rate is possible through pumping more energy to the swing leg by the swing thrust impulse. Also, the larger final angular rate causes more energy dissipation through heel-strike collision or braking at retraction. Hence, gaits with symmetric passive swing are less energetically costly.

Furthermore, similar to the swing leg, the stance leg has larger initial and final angular rates in asymmetric solutions. This is possible with a larger centripetal force and results in

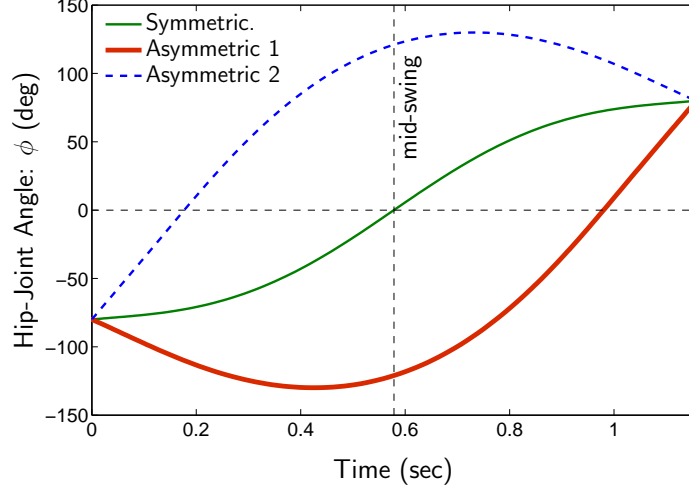


Figure 5.5: **Symmetric and asymmetric solutions of passive swing.** The three numerical solutions of the hip angle ϕ for $V = 1$ m/s and $\alpha = 40^\circ$. For the sake of visibility, the stance leg angle is not plotted here. One of the solutions (thin green) is symmetric and the other two (thick red and dashed blue) are asymmetric but cross-symmetric with each other.

a smaller GRF along the stance leg (see Section 5.4.4). Thus, gaits with asymmetric swing have a smaller maximum walking speed (see Sections 5.4.4 and 7.7.2).

Due to the above reasons, this study is limited to gaits with a symmetric passive single stance. Because of this symmetry, as far as the initial and final velocities matter, the passive single stance can be replaced with an identity mapping that maps the angular rates $\dot{\theta}_0$ and $\dot{\phi}_0$ at $t = 0^+$ to the same values at $t = t_{\text{pr}}^-$; that is to say $\dot{\theta}_{t_{\text{pr}}^-} = \dot{\theta}_0$, and $\dot{\phi}_{t_{\text{pr}}^-} = \dot{\phi}_0$.

Summarizing the dynamics of passive single stance: given the step angle α and average walking speed V , the initial and final velocities in passive swing are uniquely determined by the low-cost symmetric solution of (5.11). That is to say

$$\dot{\theta}_0 = \dot{\theta}_{t_{\text{pr}}^-} = f_1(\alpha, V), \quad (5.12)$$

$$\dot{\phi}_0 = \dot{\phi}_{t_{\text{pr}}^-} = f_2(\alpha, V). \quad (5.13)$$

These functions are numerically calculated and shown in Fig. 5.6 for some range of α and V . The shaded region in this figure is called the ‘admissible region’ and is defined later in Section 5.4.4. As this figure shows, $|\dot{\theta}_0|$ increases with both α and V . At any given α or V , the maximum $|\dot{\theta}_0|$ is achieved when the GRF along the stance leg becomes zero. Increasing

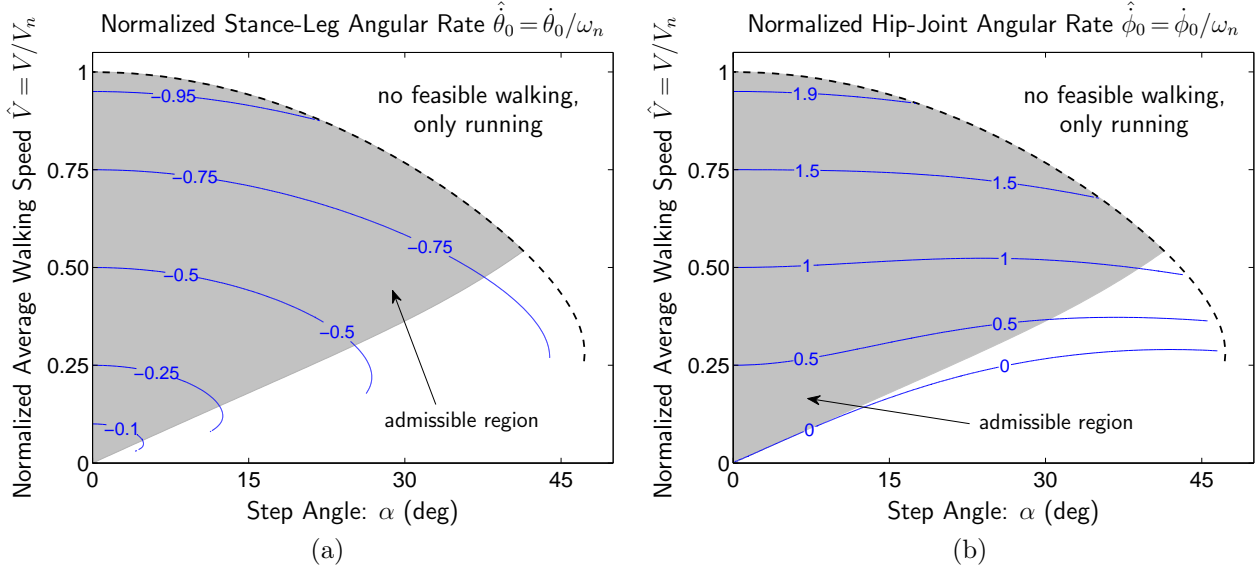


Figure 5.6: **Contour lines of the normalized angular rates at both ends of the symmetric passive swing** for some range of step angle and average walking speed. Panel (a) represents the stance-leg angular rate, and panel (b) represents the hip-joint angular rate. In both panels, angular velocities are normalized relative to $\omega_n = V_n/\ell$, where V_n is the GRF-based maximum walking speed at $\alpha = 0$ and is defined in (5.36). This maximum speed is also used to normalize the vertical axis. For the numerical values used for this figure (Table 5.1) $V_n = 3.18$ m/s, and $\omega_n = 3.53$ rad/s. Above the dashed line no walking is feasible without a pull from the ground (the gait switches to a run on non-sticking surfaces). The shaded region represents the ‘admissible region’, defined in Section 5.4.4. This region constitutes the parameter space and is the focus of this study. Panel (b) shows that the hip rate is positive (extending) for all α and V inside the admissible region.

$|\dot{\theta}_0|$ beyond that limit causes the biped to take-off (switch to run). The hip-joint angular rate $\dot{\phi}_0$ is also an increasing function of V . But, its dependency to step angle changes at different speeds. Note that for the entire admissible region, $\dot{\phi}_0 > 0$. This has relevance in calculating retraction work and optimal swing retraction impulse in Section 6.5. In Chapter 7 approximate analytic solutions are provided for (5.12) and (5.13).

5.3.2 Impulsive Transitions

Now, the three impulsive phases —push-off and retraction, heel-strike, and swing thrust— are considered. Throughout these impulsive phases the biped configuration remains unchanged, but velocities undergo discontinuous jumps in each phase. Algebraic velocity maps relate

the velocities at the end of each phase to the velocities at the beginning of that phase.

Impulsive Push-off and Swing Retraction – Phase (c):

At the end of passive single stance (at t_{pr}^-) and just before the swing foot hits the ground, the push-off impulse \mathcal{P} and the retraction impulse \mathcal{R} are applied (Fig. 5.2c). Due to the impulsive push-off, the stance leg extension rate is positive after push-off, *i.e.* $\dot{\ell} > 0$. During these impulses the stance foot is free to move along the leg, but not orthogonal to the leg, respecting no-slip ground contact of the prismatic-actuator model. To keep the prismatic assumption that the perpendicular (orthogonal to the leg) foot velocity after push-off is zero, an induced perpendicular constraint impulse is applied to the foot at the this phase.

Although the force magnitudes are infinite, causing a step change in the velocity of the hip, the biped does not take-off from the ground if the leading foot (the swing foot) immediately makes ground contact. This is possible if the retraction impulse is large enough to force the swing foot to move downward at $t_{\text{h}}^- \equiv t_{\text{pr}}^+$, allowing the next heel-strike. Later in this chapter, this condition is used to quantify the lower bound on the retraction impulse.

The velocities at t_{pr}^- were determined by the smooth dynamics during passive swing. To find the velocities immediately after \mathcal{P} and \mathcal{R} (at $t_{\text{h}}^- \equiv t_{\text{pr}}^+$) we can use linear and angular momentum balance equations over the infinitesimal interval $(t_{\text{pr}}^-, t_{\text{pr}}^+)$: (i) angular momentum of the whole mechanism about the stance foot is conserved, (ii) angular momentum of the swing leg about the hip joint jumps by \mathcal{R} , and (iii) linear momentum of the whole biped along the stance leg increases by \mathcal{P} . The corresponding expressions of these three relations map the late-passive-swing velocities $\dot{\theta}_{t_{\text{pr}}^-}$ and $\dot{\phi}_{t_{\text{pr}}^-}$ to the pre-heel-strike velocities $\dot{\theta}_{t_{\text{pr}}^+}$, $\dot{\phi}_{t_{\text{pr}}^+}$, and $\dot{\ell}_{t_{\text{pr}}^+}$:

$$\begin{bmatrix} \dot{\theta}_{t_{\text{pr}}^+} \\ \dot{\phi}_{t_{\text{pr}}^+} \\ \dot{\ell}_{t_{\text{pr}}^+} \end{bmatrix} = \begin{bmatrix} \dot{\theta}_{t_{\text{pr}}^-} \\ \dot{\phi}_{t_{\text{pr}}^-} \\ 0 \end{bmatrix} + \begin{bmatrix} J_{\dot{\theta}/\mathcal{P}} \\ J_{\dot{\phi}/\mathcal{P}} \\ J_{\dot{\ell}/\mathcal{P}} \end{bmatrix} \mathcal{P} + \begin{bmatrix} J_{\dot{\theta}/\mathcal{R}} \\ J_{\dot{\phi}/\mathcal{R}} \\ J_{\dot{\ell}/\mathcal{R}} \end{bmatrix} \mathcal{R}. \quad (5.14)$$

The configuration-dependent *impulse-influence* coefficients J_{\cdot} relate jumps in joint velocities to the force/torque impulses and are calculated in Appendix B.1.2. Note, the above mapping is independent of the relative timing of \mathcal{P} and \mathcal{R} .

Due to the mechanical coupling, the stance leg extension rate $\dot{\ell}$ in (5.14) is indirectly influenced by the retraction impulse \mathcal{R} , besides its direct influence from the push-off impulse \mathcal{P} . Likewise, the hip angular velocity $\dot{\phi}$ has a direct influence from \mathcal{R} and an indirect influence from \mathcal{P} . The indirect influence of these impulses is relevant for the gait energetics.

In Appendix B.1.2 the impulse-influence coefficients in the above velocity mapping are related to the mass-inertia matrix. Using symmetry and positive definiteness of this matrix, it is also shown there that, independent of the step angle α and the average walking speed V , the impulse-influence coefficients always satisfy:

$$J_{\dot{\ell}/\mathcal{P}} > 0, \tag{5.15}$$

$$J_{\dot{\phi}/\mathcal{R}} < 0, \tag{5.16}$$

$$J_{\dot{\phi}/\mathcal{P}} = -J_{\dot{\ell}/\mathcal{R}} < 0, \tag{5.17}$$

$$J_{\dot{\ell}/\mathcal{R}} J_{\dot{\phi}/\mathcal{P}} - J_{\dot{\ell}/\mathcal{P}} J_{\dot{\phi}/\mathcal{R}} > 0. \tag{5.18}$$

These properties are key in finding the optimal relative timing of the impulsive push-off force and retraction torque, as well as the optimal retraction impulse \mathcal{R} , studied in Chapter 6.

Note that to derive (5.14) no assumption was made on the order or percentage overlap (relative timing) of the impulsive push-off force and retraction torque. However, there is a subtle point to consider in this equation. Since $J_{\dot{\ell}/\mathcal{R}} \geq 0$, a retracting hip torque ($\mathcal{R} \geq 0$) always results in $\dot{\ell} \geq 0$, whereas an *extending*¹ hip torque ($\mathcal{R} \leq 0$) tends to decrease $\dot{\ell}$. Thus, there

¹In this thesis the ‘extension’ of the hip joint means increasing the inter-leg angle which, in-part, is achieved by moving the swing leg forward, opposite to ‘retraction’. This is opposite to what is commonly used in Anatomy, where the extension (opposite to flexion) of the hip moves the leg backward (towards the posterior side of the body). The difference in the resulting leg motion comes from the difference in the hip joints. In the model presented here the hip joint is between the legs, whereas in humans the hip joint is between the leg and the trunk, so extending the human’s hip joint (increases the angle between the leg and the trunk) moves the leg backward.

are cases in which $\dot{\ell}$ is negative for some period during the infinitesimal push-off-retraction interval $(t_{\text{pr}}^-, t_{\text{pr}}^+)$. For example, if an extending \mathcal{R} starts before \mathcal{P} (when the leg-extension joint is unlocked) it will push the foot into the ground. For simplicity, that is, to avoid considering many different cases and possibly different velocity maps, the foot is allowed to penetrate to the ground, or the leg length to shorten, if it is forced to do so. Because it turns out that a contracting stance leg (*i.e.* $\dot{\ell} < 0$) is either not energetically advantageous or can be avoided without influencing the optimal gait energetics (see Section 6.4.3) that case is neglected here. That is, for energy optimal gaits we can assume $\dot{\ell} \geq 0$ at all times, including during the impulsive phases. This post-hoc justifies the use of a general velocity map for impulsive push-off and retraction in (5.14), independent of the relative timing of \mathcal{P} and \mathcal{R} , or without concern for ground penetration in some unusual cases.

Impulsive Heel-Strike – Phase (d):

Provided that some condition holds (see ‘Instantaneous support transfer’ below), the leading foot hits the ground immediately after completion of push-off and retraction (at $t_{\text{h}}^- \equiv t_{\text{pr}}^+$). By assumption, heel-strike occurs as an instantaneous and totally plastic collision with enough friction that the new stance foot comes to a complete stop. This implies an impulsive GRF on the biped, and a discontinuous jump in the velocities of all parts of the system. The angular momentum of the trailing leg about the hip, and of the whole mechanism about the new stance foot are conserved through the heel-strike collision. These conservation laws determine the relation between the velocities at t_{pr}^+ and the post-heel-strike velocities ($\dot{\theta}_{t_{\text{h}}^+}$ and $\dot{\phi}_{t_{\text{h}}^+}$). Combining these relations with (5.14), $\dot{\theta}_{t_{\text{h}}^+}$ and $\dot{\phi}_{t_{\text{h}}^+}$ can be expressed in terms of \mathcal{P} , \mathcal{R} , and the velocities at the end of passive swing. That is

$$\begin{bmatrix} \dot{\theta}_{t_{\text{h}}^+} \\ \dot{\phi}_{t_{\text{h}}^+} \end{bmatrix} = \mathbf{A}_{\text{h}} \begin{bmatrix} \dot{\theta}_{t_{\text{pr}}^-} \\ \dot{\phi}_{t_{\text{pr}}^-} \end{bmatrix} + \mathbf{h}_{\mathcal{P}} \mathcal{P} + \mathbf{h}_{\mathcal{R}} \mathcal{R}. \quad (5.19)$$

The components of the transition matrix \mathbf{A}_{h} and the impulse-influence vectors $\mathbf{h}_{\mathcal{P}}$ and $\mathbf{h}_{\mathcal{R}}$ are given in Appendix B.1.3.

Instantaneous Support Transfer:

Support transfer includes the heel-strike and toe-off events. If the swing foot has a downward motion immediately after the impulsive push-off and retraction (at t_{pr}^+), the leading foot hits the ground and heel-strike occurs. Otherwise, there is a flight phase before the leading leg becomes the new stance leg, and thus no walking solution is achieved. Therefore, heel-strike is ensured only if the vertical swing foot velocity at t_{pr}^+ is negative:

$$\dot{y}_{f_{\text{swing}}}(t_{\text{pr}}^+) < 0. \quad (5.20)$$

It is shown in Section 7.5.1 and Section 8.2 that the above condition translates to a lower bound on the retraction impulse.

If the velocity of the trailing foot immediately after heel-strike is directed upward, *i.e.*

$$\dot{y}_{f_{\text{trailing}}}(t_{\text{h}}^+) > 0, \quad (5.21)$$

the trailing leg loses its contact with the ground (toe-off) and becomes the new swing leg. Otherwise the solution is not accepted here. The approximate analytic solution in Section 7.6 and the accurate numerical analysis show that the above toe-off condition is not a limiting constraint for a large range of biped parameters, including the model parameters in Table 5.1. More precisely, in most bipedal models, the range of step lengths and speeds for which periodic walking is feasible is not influenced by the toe-off condition in (5.21).

The above two inequalities express the conditions for the instantaneous support transfer. After toe-off (at $t_{\text{s}}^- \equiv t_{\text{h}}^+$) a new step cycle starts. The exchange of leg roles after the support transfer imposes that

$$\begin{bmatrix} \dot{\theta}_{t_{\text{s}}^-} \\ \dot{\phi}_{t_{\text{s}}^-} \end{bmatrix} = \begin{bmatrix} 0 & 1 \\ 1 & 0 \end{bmatrix} \begin{bmatrix} \dot{\theta}_{t_{\text{h}}^+} \\ \dot{\phi}_{t_{\text{h}}^+} \end{bmatrix}. \quad (5.22)$$

Impulsive Swing-Leg Thrust – Phase (a):

Immediately after toe-off, the impulsive swing thrust torque \mathcal{S} is applied at the hip to accelerate the motion of the new swing leg. The new velocities after swing thrust (at $t_{\text{s}}^+ \equiv 0^+$)

can be calculated using the conservation of angular momentum of the whole biped about the new stance foot, and of the trailing leg about the hip. The associated expressions provide the velocity transition mapping, which can be rearranged as

$$\begin{bmatrix} \dot{\theta}_{t_s^+} \\ \dot{\phi}_{t_s^+} \end{bmatrix} = \begin{bmatrix} \dot{\theta}_{t_s^-} \\ \dot{\phi}_{t_s^-} \end{bmatrix} + \begin{bmatrix} J_{\dot{\theta}/S} \\ J_{\dot{\phi}/S} \end{bmatrix} \mathcal{S}. \quad (5.23)$$

The configuration-dependent impulse-influence coefficients $J_{\dot{\theta}/S}$ and $J_{\dot{\phi}/S}$ are presented in Appendix B.1.4.

5.4 Periodic Walking

As mentioned previously, the focus of this work is on periodic gaits, in which two consecutive steps are identical with the role of each leg exchanged. In this section the conditions required to achieve a periodic walking on a level surface are discussed.

5.4.1 Periodic Gait as a Cyclic Sequence of Discrete Velocity Transitions

In Section 5.2.5 the gait cycle was described as a sequence of four continuous and impulsive phases (a)-(d). In the previous section each of these phases was modeled with a velocity transition equation that relates the velocities at the beginning of the phase to the velocities at the end of that phase (the beginning of next phase). Starting at the beginning of passive single stance, with $\dot{\theta}_0$ and $\dot{\phi}_0$, we can sequentially calculate those velocity transitions in order to find the velocities at the beginning of next passive single stance, *i.e.* $\dot{\theta}_{t_s^+}$ and $\dot{\phi}_{t_s^+}$. For a periodic gait these should match, giving

$$\dot{\theta}_{t_s^+} = \dot{\theta}_0, \quad (5.24)$$

$$\dot{\phi}_{t_s^+} = \dot{\phi}_0. \quad (5.25)$$

Summarizing (5.12)-(5.25), the energy-optimal periodic walk of the impulsive bipedal model can be illustrated as a cyclic sequence of *discrete* velocity transitions, shown in Fig. 5.7.

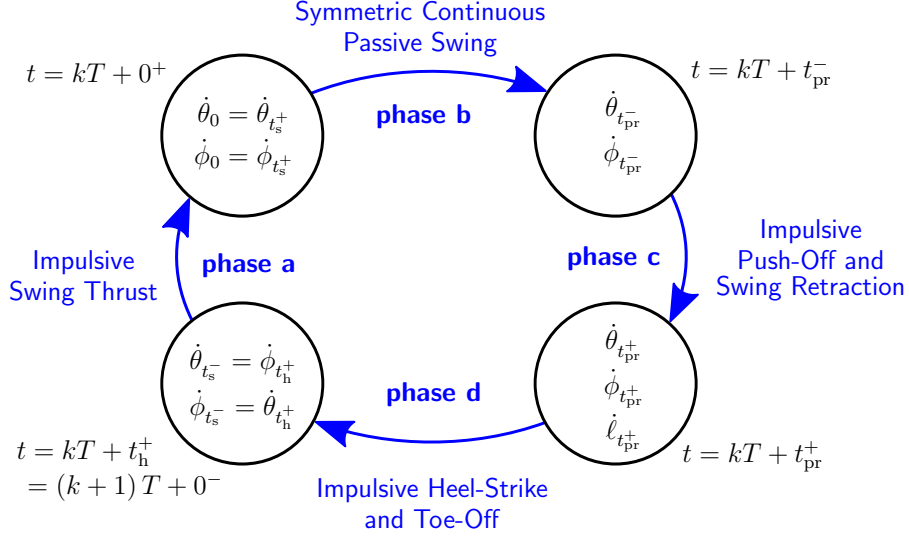


Figure 5.7: **Velocity transitions in a periodic gait cycle.** A gait cycle can be considered as a sequence of continuous and impulsive phases (blue arrows). This phase sequence can be replaced with a sequence of *discrete* velocity transitions (black circles) relating the velocities at the beginning of each phase to the velocities at the end of that phase (the beginning of the next phase). The velocity mapping of phase (a) is given by (5.23), and of phase (b) is given by (5.12) and (5.13). Equation (5.14) corresponds to the velocity mapping of phase (c), while (5.19) and (5.22) give the velocities at the end of phase (d). The symmetry in this figure does not imply the symmetry of the gait, though the passive swing is considered to be symmetric.

5.4.2 Periodicity Restricts the Actuator Impulses

Using the discontinuous velocity transitions above, we can find the required impulses for a periodic gait subject to given step length and average walking speed. Substituting (5.19)-(5.23) into (5.24) and (5.25), and the use of (5.12) and (5.13) give two equations that the three impulses, *i.e.* \mathcal{S} , \mathcal{R} , and \mathcal{P} , must obey. We can solve these to express \mathcal{P} and \mathcal{S} in terms of \mathcal{R} . This results in

$$\mathcal{S} = h_1(\alpha, V) + J_{S/\mathcal{R}}(\alpha) \mathcal{R}, \quad (5.26)$$

$$\mathcal{P} = h_2(\alpha, V) + J_{\mathcal{P}/\mathcal{R}}(\alpha) \mathcal{R}. \quad (5.27)$$

The impulse-influence coefficients $J_{S/\mathcal{R}}$ and $J_{\mathcal{P}/\mathcal{R}}$ and the functions h_1 and h_2 are given in Appendix B.2. Using (5.26) and (5.27), all the velocities at different time instants can also

be expressed solely in terms of α , V , and \mathcal{R} . Therefore, for given α and V , the thrust impulse \mathcal{S} , the push-off impulse \mathcal{P} , and all the velocities become a one-parameter family of solutions, parameterized by the retraction impulse \mathcal{R} . As for (5.14), this family of solutions does not depend on the relative timing of \mathcal{P} and \mathcal{R} .

5.4.3 Maximum Retraction Impulse

In Sections 7.4 and 8.1 we will see that $J_{\mathcal{P}/\mathcal{R}}$ in (5.27) is negative, and the push-off impulse \mathcal{P} decreases with the retraction impulse \mathcal{R} . On the other hand, the push-off impulse cannot be negative, by definition. Therefore, given the step angle α and average walking speed V , we can use (5.27) to find the maximum retraction impulse, \mathcal{R}_{\max} , for which $\mathcal{P} \geq 0$:

$$\mathcal{R} \leq \mathcal{R}_{\max}(\alpha, V) \quad \text{such that} \quad \mathcal{P}(\alpha, V, \mathcal{R}_{\max}) = 0. \quad (5.28)$$

In Sections 7.11 and 8.3.1 we will see that the above upper bound on \mathcal{R} is not an active constraint for energetic cost minimization purposes, and (5.28) is spontaneously satisfied for energy optimal gaits.

5.4.4 Admissible Combinations of Step Length and Speed

I intend to study the effects of active swing-leg retraction for all possible walking gaits, at least to the extent that can be covered by the simplified impulsive model. In this section, the range of step lengths and average walking speeds for which the model exhibits a near-human-like walking gait is calculated.

Minimum Allowed Average Walking Speed:

Examining (5.26) with different retraction impulse \mathcal{R} , step angle α , and average forward speed V shows that the required swing-thrust impulse \mathcal{S} for slow speeds or very long steps is negative, *i.e.* it pushes the swing-leg rearward. However, in normal walking, humans do

not push their swing-leg backward at the beginning of swing. The resulting non-human-like swing thrust impulse for the impulsive model is an artifact of the passive swing assumption. Due to this assumption, for gaits with slow average forward speed or very long steps the swing leg has to initially move backwards in order to match the step length and step frequency requirements. However, when walking slowly or taking long steps, humans continuously control their leg motion using accelerating and decelerating hip torques throughout the swing phase. So, the near-passive-swing assumption is not valid in this regime. For this reason, I would rather to limit my study to step lengths and speeds for which the passive swing assumption is almost valid, and the model exhibits near-human-like gaits. In mathematical terms, I limit the parameter space to the set of α , V , and \mathcal{R} for which $\mathcal{S} \geq 0$, where \mathcal{S} is given by (5.26).

The above constraint on parameter space imposes a lower bound on V , the minimum allowed walking speed V_{\min} , for each pair of α and \mathcal{R} . On the other hand, as we will see in Sections 7.4 and 8.1, the dependency of \mathcal{S} on \mathcal{R} is negligible. So, to simplify the analyses, I use V_{\min} at $\mathcal{R} = 0$ for all possible \mathcal{R} . That is to say, V is admissible if

$$V \geq V_{\min}(\alpha) \quad \text{such that} \quad \mathcal{S}(\alpha, V_{\min}, \mathcal{R}) \Big|_{\mathcal{R}=0} = 0. \quad (5.29)$$

This minimum allowed average speed is a function of step angle α . For biped parameter values given in Table 5.1, the above lower bound excludes (α, V) pairs that fall below the shaded regions in Fig. 5.8. In this figure, the vertical axis is the normalized average walking speed $\hat{V} = V/V_n$, where V_n is defined in (5.32) below.

GRF-Based Maximum Average Walking Speed:

In Section 5.3.1, the equations of motion in passive swing were derived based on the assumption that the stance foot remains on the ground during the entire nominal single stance, *i.e.* during the interval $(0^+, T^-)$. This is met only if the calculated GRF along the stance leg ($= \text{GRF}_a$) is not negative for the entire interval. That is, during the entire passive single

stance we should have

$$\text{GRF}_a = m_{\text{tot}} g \cos \theta - m_{\text{tot}} \ell \dot{\theta}^2 + m_{\text{leg}} b \left(\dot{\theta}^2 + \cos \phi (\dot{\theta} + \dot{\phi})^2 + \sin \phi (\ddot{\phi} + \ddot{\theta}) \right) \geq 0. \quad (5.30)$$

At any given step angle α , increasing the average forward speed increases the centripetal force, which in turn decreases GRF_a . The maximum average walking speed $V_{\text{max}}(\alpha)$ is, therefore, the one that results in $\text{GRF}_a = 0$ for a few instants in passive single stance and $\text{GRF}_a > 0$ for the rest of this phase. Hence, given the step angle α , the condition of feasible walking is expressed as:

$$V \leq V_{\text{max}}(\alpha) \quad \text{such that} \quad \min_{0+ \leq t \leq T-} \text{GRF}_a(t, V_{\text{max}}) = 0. \quad (5.31)$$

In this thesis, the step-angle-dependent maximum walking speed $V_{\text{max}}(\alpha)$, obtained from (5.31), is called the ‘GRF-based speed limit’. For biped parameter values given in Table 5.1, constraining $V \leq V_{\text{max}}(\alpha)$ excludes (α, V) pairs that are above the shaded region in Fig. 5.8. The vertical axis in this figure is the normalized average walking speed $\hat{V} = V/V_n$, where

$$V_n = \max_{\alpha} V_{\text{max}}(\alpha). \quad (5.32)$$

From Fig. 5.8 it is clear that

$$\max_{\alpha} V_{\text{max}}(\alpha) = V_{\text{max}}(0). \quad (5.33)$$

In fact, at $\alpha = 0$ the gravity-pull along the stance leg, *i.e.* $m_{\text{tot}} g \cos \alpha$, and the reaction of the swing-leg centripetal force on the stance leg, *i.e.* $m_{\text{leg}} b (\dot{\theta}_0^2 + \dot{\phi}_0^2) \cos 2\alpha$, are maximum. The resultant downward force allows for the maximum stance-leg angular rate, or equivalently the maximum achievable walking speed.

To calculate this maximum speed, *i.e.* $V_n = V_{\text{max}}(0)$, we can evaluate (5.30) and (5.31) at $\alpha = 0$. For $\alpha = 0$: $\theta = \phi = 0$, $\dot{\theta} = \dot{\theta}_0$, and $\dot{\phi} = \dot{\phi}_0$. On the other hand, when α approaches zero, the passive swing becomes instantaneous, and $\dot{\theta}$ and $\dot{\phi}$ approach their average value $\bar{\dot{\theta}}$ and $\bar{\dot{\phi}}$. Because always $\bar{\dot{\phi}} = -2\bar{\dot{\theta}}$, we get $\dot{\theta}_0 = \dot{\theta} = -\dot{\phi}/2$ for $\alpha = 0$. These simplify (5.30) to

$$\text{GRF}_a \Big|_{\alpha=0} = m_{\text{tot}} \ell \left(\omega_1^2 + (2\lambda - 1) \dot{\theta}_0^2 \right) \geq 0, \quad (5.34)$$

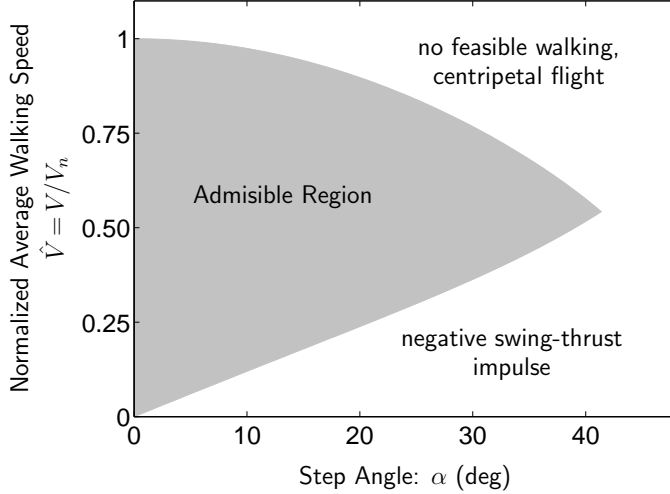


Figure 5.8: **Admissible region.** The shaded region corresponds to the *admissible combinations of step angle and speed*. Above this region, walking is not feasible as the calculated centripetal GRF during passive swing becomes negative, which requires an unrealistic sucking foot-ground contact to avoid a flight. Below the shaded region the swing-thrust impulse is applied backwards (pushes the swing leg backward) opposite to that seen in human-like gaits. The lower boundary of the region is set by (5.29), and the upper boundary is calculated using (5.31). The vertical axis is normalized relative to $V_n = V_{\max}(0)$, which is the GRF-based maximum walking speed at $\alpha = 0$, defined in (5.36). For the numerical values used for this figure (see Table 5.1), $V_n = 3.18$ m/s.

where $\omega_1 = \sqrt{g/\ell}$ and $\lambda = m_{\text{leg}} b / (m_{\text{tot}} \ell)$. It is shown in Section 7.1 that $\lambda \leq 0.5$. Thus, (5.34) results in

$$|\dot{\theta}_0| \leq \frac{\omega_1}{\sqrt{1 - 2\lambda}} = \omega_n, \quad (5.35)$$

and

$$V_n = V_{\max}(0) = \ell \max |\dot{\theta}_0| = \ell \omega_n = \frac{\ell \omega_1}{\sqrt{1 - 2\lambda}}. \quad (5.36)$$

Most literatures, if not all, calculate the maximum walking speed using a simple inverted pendulum model without considering the effect of a non-massless swing leg, *e.g.* [14, 95]. With this common approach the maximum walking speed is calculated as $\ell \omega_1$, which can be obtained from (5.36) with $\lambda = 0$ ($m_{\text{leg}} = 0$). My calculation here provides a more realistic prediction and shows that by increasing λ the maximum walking speed increases.

Note that the average walking speed V can increase up to the GRF-based speed limit $V_{\max}(\alpha)$ if no other constraints limit the motion. It is shown in Section 7.5.1 (analytically)

and Section 8.2 (numerically) that if the retraction impulse \mathcal{R} is not large enough to ensure heel-strike, maximum average walking speed should be less than the GRF-based $V_{\max}(\alpha)$.

Admissible Region:

The step-angle-dependent minimum and maximum walking speeds in (5.29) and (5.31) define the set of α and V combinations for which periodic powered walking with passive single stance and non-rearward swing-thrust impulse can be formulated with the impulsive model. This set is frequently used in the rest of this thesis and will be referred to as the ‘admissible region’. It corresponds to the shaded area in Fig. 5.8.

5.5 Summary

In this chapter a simple bipedal model was introduced to study swing-leg retraction in walking. The model is the modified version of the powered simplest walking model in [47]. It consists of a point-mass hip and two rigid legs with arbitrarily distributed mass. The model is powered by a motor (revolute actuator) at the hip and a telescoping (prismatic) actuator along the stance leg. The energy-optimal walking gait of this model was predicted based on the results of Chapter 3, previous optimal gait studies, and human gait observations. This optimal gait consists of three infinitesimal-duration impulsive phases and one extended smooth phase. Immediately after toe-off an impulsive torque, swing-thrust, is applied at the hip to accelerate the swing leg motion. Then the extended passive swing phase starts, where the hip motor is off and the stance leg extension actuator is locked. In this phase the hip moves on an arc-shape path dictated by the fixed-length stance leg. At the end of passive swing, an impulsive extensional force, push-off, is applied along the stance leg, and an impulsive hip torque, swing-leg retraction, is applied at the hip. The late-swing impulsive force and torque can be applied with any relative timing (any order or overlap). Finally, the collisional heel-strike occurs, followed by an instantaneous double-support. This phase

sequence was modeled as a series of discrete velocity mappings, relating the velocities at the beginning of each phase to those at the start of the previous phase. Using these mappings and given the step angle and average walking speed, it was shown that all gait parameters of a periodic gait can be expressed as a one-parameter family of solutions parameterized by the swing-leg retraction impulse. This set of solutions will be used in the following chapters to find the energy-optimal retraction impulse.

Chapter 6

ENERGETICS OF IMPULSIVE WALKING GAITS

In the previous chapter a bipedal model with impulsive actuation was introduced to study the consequences of swing-leg retraction in walking. In this chapter the energetics of the model are formulated, and the conditions to achieve an energy-optimal gait are calculated.

The ultimate goal of this chapter is to find the optimal retraction impulse \mathcal{R}^* that minimizes the net energetic cost for given gait parameters (such as step angle α , and average walking speed V). In order to achieve this goal, the following steps are taken: First, in Section 6.1, the work-based energetic cost equation introduced in Chapter 2 is reformulated, and the total energetic cost of walking is expressed in terms of the cost of each impulsive actuation. In Section 6.2, the work of the impulsive swing-thrust torque and its energetic cost is found. The work performed by the impulsive push-off force and the impulsive retraction torque depends on their relative timing. These work quantities are calculated in Section 6.3 through introducing the so-called *overlap parameter* that quantifies the relative timing of impulsive push-off force and retraction torque. The optimal relative timing of these impulsive actuations that minimizes the net energetic cost of walking for given gait parameters is found in Section 6.4. Finally, in Section 6.5, the problem of calculating the energy-minimizing retraction impulse is formulated as a simple single-variable optimization problem using the results of Sections 6.1-6.4. The chapter is summarized in Section 6.6.

6.1 Work-Based Energetic Cost of Step

In the context of energetics, the most natural option for the cost of an action is the energy supplied to the actuator(s) during that action. The input energy to an actuator depends

on the mechanical work done, and the actuator efficiency. In general, the efficiencies of an actuator for doing positive and negative work can be different¹. For example, human muscles have about 25% and 120% efficiency for positive and negative² work, respectively [26, 73]. If the positive quantities $1/c_1$ and $1/c_2$ are the efficiencies of positive and negative² work, respectively, or equivalently c_1 and c_2 are the cost of unit positive and unit negative work, then the net energetic cost of doing W^+ positive work and W^- negative work ($W^- < 0$) is:

$$E = c_1 W^+ - c_2 W^-. \quad (6.1)$$

The above definition is consistent with the cost model defined in (2.1). Using (6.1), we can define the energetic cost *per step* for swing thrust, push-off, and swing retraction, respectively denoted by E_S , E_P , and E_R . The total energetic cost of walking per step is then given by

$$E_{\text{step}} = E_P + E_S + E_R. \quad (6.2)$$

In the above equation it is assumed that dissipative collisional heel-strike is totally passive. This does not mean that heel-strike does not cost for the system. The energy loss at collisional heel-strike indirectly increases the net energetic cost, as the same amount of positive work has to be done during the rest of the gait to compensate for it. Later in this thesis, I modify the assumption of passive heel-strike and consider a more general scenario in which some negative actuator work is also done during heel-strike. In that case, heel-strike will have both direct and indirect costs.

In order to calculate E_S , E_R , and E_P , the positive and negative work done by each impulse should be calculated. The work of an impulsive force/torque depends on whether it is *overlapping* in time with other impulsive *active* forces and torques [26], or not. An

¹In most actuators negative mechanical work at the output acts as an energy source that partially or entirely compensates for the losses. So, less input energy is required for doing negative work compared to doing the same amount of positive work. Consequently, the efficiency of negative work is normally greater than that of positive work.

²Here, efficiency is defined as the ratio of the absolute-value of output work to the input energy. In this case, the efficiency of negative work is a positive number. Sometimes, the work itself (without using the absolute-value function) is used to calculate the efficiency, so the efficiency of negative work becomes a negative number. Based on the second definition, human muscles have -120% negative work efficiency.

impulsive force/torque is *isolated*, if during its application all other impulsive active forces and torques are zero. Therefore, in the model under study, the impulsive swing thrust torque is always isolated, whereas the impulsive push-off force and the impulsive swing retraction torque can be arbitrarily overlapping.

6.2 Energetic Cost of Isolated Impulsive Swing Thrust Torque

Consider an isolated impulsive force/torque with impulse \mathcal{I} applied to a joint, where the joint velocity jumps from \dot{q}^- to \dot{q}^+ by that impulse. As stated in [97], the net work performed by this impulsive force/torque is calculated as

$$W = \frac{1}{2} \mathcal{I} (\dot{q}^+ + \dot{q}^-), \quad (6.3)$$

and the corresponding positive work is given by

$$W^+ = \begin{cases} [W]^+ & \text{if } \dot{q}^+ \dot{q}^- \geq 0 \\ \frac{1}{2} \mathcal{I} \frac{(\dot{q}^+)^2}{\dot{q}^+ - \dot{q}^-} & \text{if } \dot{q}^+ \dot{q}^- < 0 \end{cases}, \quad (6.4)$$

where the positive-value function $[\cdot]^+$ is defined as $[x]^+ = x$ if $x \geq 0$, otherwise $[x]^+ = 0$. With the above equations, the negative work is calculated from

$$W^- = W - W^+. \quad (6.5)$$

Given the step angle α , average walking speed V , and retraction impulse \mathcal{R} , equations (6.3)-(6.5) can be used to calculate the positive and negative work $W_{\mathcal{S}}^+$ and $W_{\mathcal{S}}^-$ performed by the impulsive swing thrust torque, where $\mathcal{I} = \mathcal{S}$ is given by (5.26), $\dot{q}^+ = \dot{\phi}_{t_s^+} = \dot{\phi}_0$ is given by (5.12) and (5.13), and $\dot{q}^- = \dot{\phi}_{t_s^-} = \dot{\phi}_0 - J_{\phi/\mathcal{S}} \mathcal{S}$ is given by (5.23) and (5.25). Finally, according to the general energetic cost equation in (6.1), the energetic cost of impulsive swing thrust is calculated as

$$E_{\mathcal{S}} = c_1 W_{\mathcal{S}}^+ - c_2 W_{\mathcal{S}}^-. \quad (6.6)$$

6.3 Energetic Cost of Impulsive Push-off Force and Retraction Torque

If the impulsive push-off force and the impulsive swing retraction torque are isolated, *i.e.* one comes completely after the other, equations (6.3)-(6.5) can be used to calculate their work. However, in general, they can be arbitrarily overlapped. In a multibody system, when overlapping impulsive forces/torques are applied at different joints, the velocity jump at each joint is influenced not only by the impulsive force/torque at that joint, but also by other overlapping forces/torques in other joints. In this case, a special technique should be used to exclude the mechanical energy involved in the interaction between the overlapping forces/torques. This technique was originally developed by Ruina *et. al.* [26] to study the simultaneous impulsive forces on particles, where each force does only positive or negative work. Here, I modify and extend that technique to multibody systems, and to episodes where an impulsive force/torque does both positive and negative work.

Using the definition of retraction impulse in (5.9) and of push-off impulse in (5.10), I define the *partial* retraction impulse $\mathcal{R}(t)$ and the *partial* push-off impulse $\mathcal{P}(t)$ as below

$$\mathcal{R}(t) = - \int_{t_{\text{pr}}^-}^t \tau(t') dt' = r(t) \mathcal{R}, \quad (6.7)$$

$$\mathcal{P}(t) = \int_{t_{\text{pr}}^-}^t F(t') dt' = p(t) \mathcal{P}, \quad (6.8)$$

where the integral's upper limit t satisfies $t_{\text{pr}}^- \leq t \leq t_{\text{pr}}^+$. The time-dependent non-decreasing parameters p and r express the degree of impulse completeness (or equivalently the fraction of the impulse applied), and satisfy $0 \leq p \leq 1$ and $0 \leq r \leq 1$. For example, at $t = t_{\text{p}}^-$, when the impulsive push-off force is going to start, we have $p(t_{\text{p}}^-) = 0$ and $\mathcal{P}(t_{\text{p}}^-) = 0$, and at $t = t_{\text{p}}^+$, when the impulsive push-off force has completed, we have $p(t_{\text{p}}^+) = 1$ and $\mathcal{P}(t_{\text{p}}^+) = \mathcal{P}$.

Fig. 6.1 visualizes the partial push-off and retraction impulses as the partial area under the force/torque curves in an arbitrary scenario. In this figure the infinitesimal retraction and push-off intervals $(t_{\text{r}}^-, t_{\text{r}}^+)$ and $(t_{\text{p}}^-, t_{\text{p}}^+)$ are exaggerated for clarity of illustration.

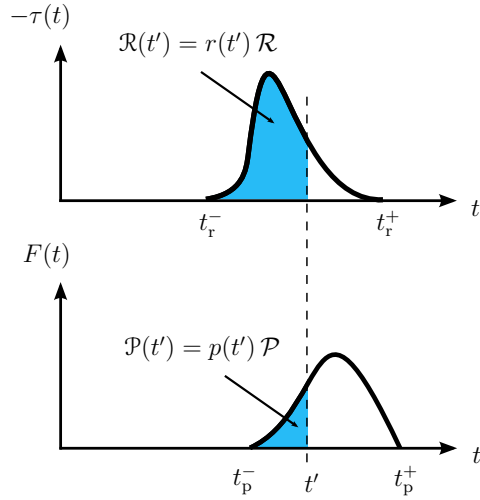


Figure 6.1: **Partial impulses.** The partial retraction impulse \mathcal{R} and the partial push-off impulse \mathcal{P} as the partial area under the force/torque curves for the arbitrary impulsive retraction torque and push-off force profiles. The timing between the two impulses is also arbitrary. The length of the periods over which the impulsive push-off force and retraction torque are applied is infinitesimal, but is exaggerated here for clarity of illustration.

6.3.1 Net Swing-Leg Retraction Work

Using the push-off and retraction velocity mapping in (5.14), and the partial impulses in (6.7) and (6.8), the *instantaneous* hip-joint angular rate for $t_{\text{pr}}^- \leq t \leq t_{\text{pr}}^+$ is defined as

$$\begin{aligned} \dot{\phi}(t) &= \dot{\phi}_{t_{\text{pr}}^-} + J_{\dot{\phi}/\mathcal{R}} \mathcal{R}(t) + J_{\dot{\phi}/\mathcal{P}} \mathcal{P}(t) \\ &= \dot{\phi}_0 + J_{\dot{\phi}/\mathcal{R}} r(t) \mathcal{R} + J_{\dot{\phi}/\mathcal{P}} p(t) \mathcal{P}. \end{aligned} \quad (6.9)$$

In the second line, the substitution of $\dot{\phi}_{t_{\text{pr}}^-}$ with $\dot{\phi}_0$ follows (5.13). Now, consider an arbitrary instant t in the interval $(t_{\text{pr}}^-, t_{\text{pr}}^+)$. The *partial* retraction work is defined as the work done by the impulsive retraction torque τ from its beginning until t , and is given by

$$\mathcal{W}_{\mathcal{R}}(t) = \int_{t_{\text{pr}}^-}^t \dot{\phi}(t') \tau(t') dt', \quad (6.10)$$

where $\dot{\phi}(t)$ is given by (6.9). The definition of the partial retraction impulse in (6.7) implies $d\mathcal{R} = -\tau(t') dt'$. Using this equality, and assigning $\mathcal{P}(t) = p_t \mathcal{P}$ and $\mathcal{R}(t) = r_t \mathcal{R}$ based on (6.7)

and (6.8), we can simplify $\mathcal{W}_{\mathcal{R}}(t)$ as

$$\begin{aligned}\mathcal{W}_{\mathcal{R}}(t) &= - \int_0^{r_t \mathcal{R}} \left(\dot{\phi}_0 + J_{\dot{\phi}/\mathcal{R}} \mathcal{R} + J_{\dot{\phi}/\mathcal{P}} \mathcal{P} \right) d\mathcal{R} \\ &= - \int_0^{r_t} \left(\dot{\phi}_0 + J_{\dot{\phi}/\mathcal{R}} r \mathcal{R} + J_{\dot{\phi}/\mathcal{P}} p \mathcal{P} \right) \mathcal{R} dr \\ &= -\dot{\phi}_0 r_t \mathcal{R} - \frac{1}{2} J_{\dot{\phi}/\mathcal{R}} r_t^2 \mathcal{R}^2 - s_t J_{\dot{\phi}/\mathcal{P}} \mathcal{R} \mathcal{P},\end{aligned}\tag{6.11}$$

where

$$s_t = \int_0^{r_t} p dr.\tag{6.12}$$

The *partial overlap* parameter s_t quantifies the overlap between the impulsive push-off force and the impulsive retraction torque during the interval (t_{pr}^-, t) . This concept is clarified below, when explaining (6.15) and Fig. 6.2. Because $0 \leq p \leq p_t$ for $0 \leq r \leq r_t$, s_t always satisfies

$$0 \leq s_t \leq p_t r_t.\tag{6.13}$$

For $t = t_{\text{pr}}^+$ the impulsive retraction torque is complete ($r_{t_{\text{pr}}^+} = 1$), and $\mathcal{W}_{\mathcal{R}}(t_{\text{pr}}^+)$ gives the net work $W_{\mathcal{R}}$ done by the impulsive retraction torque, as

$$W_{\mathcal{R}} = -\dot{\phi}_0 \mathcal{R} - \frac{1}{2} J_{\dot{\phi}/\mathcal{R}} \mathcal{R}^2 - s J_{\dot{\phi}/\mathcal{P}} \mathcal{R} \mathcal{P},\tag{6.14}$$

where

$$s = s_{t_{\text{pr}}^+} = \int_0^1 p dr.\tag{6.15}$$

The *overlap parameter* s satisfies $0 \leq s \leq 1$, and quantifies the percentage overlap between the impulsive push-off force and retraction torque. In Fig. 6.2b the overlap parameter s is visualized as the area under the cross-plots of p versus r for different relative timings of the impulsive push-off force $F(t)$ and retraction torque $\tau(t)$ shown in Fig. 6.2a. When $s = 0$, the impulsive retraction torque occurs completely before the impulsive push-off force (episode iv), whereas $s = 1$ corresponds to the case where the impulsive retraction torque starts completely after the impulsive push-off force (episode ii). In both of these cases the push-off and retraction impulses are isolated. Two impulses are ‘synchronous’ if they are proportional (episode i), resulting in $p = r$ and $s = 0.5$.

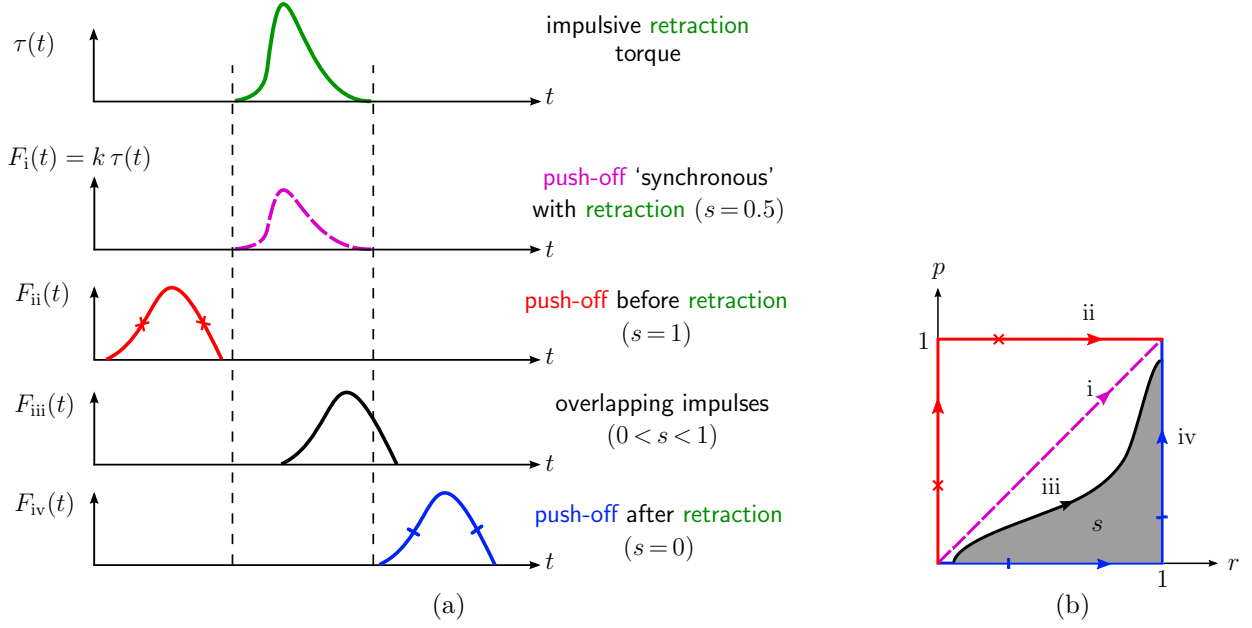


Figure 6.2: **Visualization of the overlap parameter s .** (a) As the impulsive push-off force F moves relative to the impulsive retraction torque τ , the overlap parameter s changes from 0 to 1. (b) The overlap parameter s can be considered as the area under the cross-plot of p vs. r . Different paths in (b) correspond to different episodes in (a). Impulsive F and τ are ‘synchronous’ if they are proportional, and thus $s = 0.5$.

In the formula of the net retraction work $W_{\mathcal{R}}$ in (6.14), $J_{\dot{\phi}/\mathcal{R}}$, $J_{\dot{\phi}/\mathcal{P}}$, $\dot{\phi}_0$, and \mathcal{P} are known when the step angle α , average speed V , and retraction impulse \mathcal{R} are given (see Sections 5.3.1, 5.3.2, and 5.4.2). Thus, $W_{\mathcal{R}}$ is fully resolved by knowing α , V , \mathcal{R} , and s .

Equivalent Isolated Impulses for Net Retraction Work:

Equation (6.14) can also be rearranged as

$$W_{\mathcal{R}} = -\frac{1}{2} \mathcal{R} \left(\dot{\phi}_{t_r^-}^\dagger + \dot{\phi}_{t_r^+}^\dagger \right), \quad (6.16)$$

where $\dot{\phi}_{t_r^-}^\dagger = \dot{\phi}_0 + J_{\dot{\phi}/\mathcal{P}} s \mathcal{P}$, and $\dot{\phi}_{t_r^+}^\dagger = \dot{\phi}_{t_r^-}^\dagger + J_{\dot{\phi}/\mathcal{R}} \mathcal{R}$. Comparing (6.16) with (6.3), we can interpret $W_{\mathcal{R}}$ as the work of an isolated retraction impulse \mathcal{R} that starts completely after an *equivalent* isolated push-off impulse $\mathcal{P}^\dagger = s \mathcal{P}$. The role of \mathcal{P}^\dagger is to change the hip angular velocity from $\dot{\phi}_0$ to an *equivalent* pre-retraction velocity $\dot{\phi}_{t_r^-}^\dagger$, which is then changed by \mathcal{R} to the *equivalent* post-retraction velocity $\dot{\phi}_{t_r^+}^\dagger$.

6.3.2 Positive and Negative Swing-Retraction Work

Assuming that the impulsive hip torque $\tau(t)$ has no sign change during $(t_{\text{pr}}^-, t_{\text{pr}}^+)$, a *retracting* torque ($\mathcal{R} \geq 0$) does positive work when the hip joint is *retracting*, *i.e.* $\dot{\phi}(t) < 0$, otherwise it does negative work. Conversely, an *extending* hip torque ($\mathcal{R} \leq 0$) does positive work when the hip joint is *extending*, *i.e.* $\dot{\phi} > 0$, otherwise it does negative work.

If the instantaneous hip rate $\dot{\phi}(t)$ has no zero-crossings during the impulsive retraction torque, the impulse \mathcal{R} does only positive or negative work, given by $W_{\mathcal{R}}^+ = [W_{\mathcal{R}}]^+$, and $W_{\mathcal{R}}^- = W_{\mathcal{R}} - W_{\mathcal{R}}^+$, where $W_{\mathcal{R}}$ is calculated from (6.14).

If $\dot{\phi}(t)$ has zero-crossings during the application of \mathcal{R} , then the impulsive retraction torque does both positive and negative work. In this case, the span of the retraction torque can be divided into consecutive sub-intervals connected to each other at the zero-crossings of $\dot{\phi}(t)$. During each of these sub-intervals the retraction torque does only positive or negative work. By sequentially evaluating $\mathcal{W}_{\mathcal{R}}(t)$, given by (6.11), at the end of all sub-intervals and calculating the differences, we can find the work done during each sub-interval, and ultimately calculate the total positive or negative work done by the impulsive retraction torque. For example, consider a case where an impulsive retraction torque starts with doing negative work, and $\dot{\phi}(t)$ has two zero-crossings at t_1 and t_2 , where $t_1 \leq t_2$. The positive retraction torque in this case is given by $W_{\mathcal{R}}^+ = \mathcal{W}_{\mathcal{R}}(t_2) - \mathcal{W}_{\mathcal{R}}(t_1)$, and the negative retraction torque by $W_{\mathcal{R}}^- = W_{\mathcal{R}} - W_{\mathcal{R}}^+ = W_{\mathcal{R}} + \mathcal{W}_{\mathcal{R}}(t_1) - \mathcal{W}_{\mathcal{R}}(t_2)$.

As mentioned for (5.16) and (5.17), the impulse-influence coefficients $J_{\dot{\phi}/\mathcal{R}}$ and $J_{\dot{\phi}/\mathcal{P}}$ are both negative. Thus, for $\mathcal{R} \geq 0$ the instantaneous hip rate $\dot{\phi}(t)$, given by (6.9), decreases throughout push-off and retraction, and cannot have more than one zero-crossing, if any. Assume that this possible zero-crossing is at t_0 . Then, the retraction torque does only negative work before t_0 , and only positive work after it. Thus, $W_{\mathcal{R}}^- = \mathcal{W}_{\mathcal{R}}(t_0)$, and $W_{\mathcal{R}}^+ = W_{\mathcal{R}} - W_{\mathcal{R}}^-$.

6.3.3 Net Push-Off Work

Equivalent to the instantaneous hip rate given by (6.9), the *instantaneous* leg extension rate during the infinitesimal interval $(t_{\text{pr}}^-, t_{\text{pr}}^+)$ is defined as

$$\begin{aligned}\dot{\ell}(t) &= J_{\dot{\ell}\mathcal{P}} \mathcal{P}(t) + J_{\dot{\ell}\mathcal{R}} \mathcal{R}(t) \\ &= J_{\dot{\ell}\mathcal{P}} p(t) \mathcal{P} + J_{\dot{\ell}\mathcal{R}} r(t) \mathcal{R}.\end{aligned}\tag{6.17}$$

The *partial* push-off work $\mathcal{W}_{\mathcal{P}}(t)$ is defined as the net work done by the impulsive push-off force F from its beginning until an arbitrary instant t in $(t_{\text{pr}}^-, t_{\text{pr}}^+)$. Following the same procedure that led to the calculation of $\mathcal{W}_{\mathcal{R}}(t)$ in (6.11), we can calculate $\mathcal{W}_{\mathcal{P}}(t)$ as

$$\begin{aligned}\mathcal{W}_{\mathcal{P}}(t) &= \int_{t_{\text{pr}}^-}^t \dot{\ell}(t') F(t') dt' \\ &= \frac{1}{2} J_{\dot{\ell}\mathcal{P}} p_t^2 \mathcal{P}^2 + (p_t r_t - s_t) J_{\dot{\ell}\mathcal{R}} \mathcal{R} \mathcal{P},\end{aligned}\tag{6.18}$$

where s_t follows (6.12). For $t = t_{\text{pr}}^+$ the push-off impulse is complete ($r_{t_{\text{pr}}^+} = p_{t_{\text{pr}}^+} = 1$), and $\mathcal{W}_{\mathcal{P}}(t_{\text{pr}}^+)$ gives the net work $W_{\mathcal{P}}$ done by the push-off impulse as

$$W_{\mathcal{P}} = \frac{1}{2} J_{\dot{\ell}\mathcal{P}} \mathcal{P}^2 + (1 - s) J_{\dot{\ell}\mathcal{R}} \mathcal{R} \mathcal{P},\tag{6.19}$$

where the overlap parameter s is given by (6.15). Note that $J_{\dot{\ell}\mathcal{P}}$, $J_{\dot{\ell}\mathcal{R}}$, and \mathcal{P} are known if the step angle α , average speed V , and retraction impulse \mathcal{R} are given (see Sections 5.3.2 and 5.4.2), so the net push-off work $W_{\mathcal{P}}$ is fully resolved by knowing α , V , \mathcal{R} , and s .

Equivalent Isolated Impulses for Net Push-Off Work:

Equivalent to (6.16), $W_{\mathcal{P}}$ can be rearranged as

$$W_{\mathcal{P}} = \frac{1}{2} \mathcal{P} \left(\dot{\ell}_{t_{\text{pr}}^-}^{\dagger} + \dot{\ell}_{t_{\text{pr}}^+}^{\dagger} \right),\tag{6.20}$$

where $\dot{\ell}_{t_{\text{pr}}^-}^{\dagger} = (1 - s) J_{\dot{\ell}\mathcal{R}} \mathcal{R}$, and $\dot{\ell}_{t_{\text{pr}}^+}^{\dagger} = \dot{\ell}_{t_{\text{pr}}^-}^{\dagger} + J_{\dot{\ell}\mathcal{P}} \mathcal{P}$. In other words, $W_{\mathcal{P}}$ can be viewed as the work of the *isolated* push-off impulse \mathcal{P} when it follows the *equivalent isolated* retraction

impulse $\mathcal{R}^\dagger = (1 - s) \mathcal{R}$. The role of \mathcal{R}^\dagger is to change the leg extension rate from $\dot{\ell}_{t_{\text{pr}}}^- = 0$ to an *equivalent* pre-push-off extension rate $\dot{\ell}_{t_{\text{p}}}^\dagger$, which is then changed by \mathcal{P} to the *equivalent* post-push-off extension rate $\dot{\ell}_{t_{\text{p}}}^\dagger$.

6.3.4 Positive and Negative Push-Off Work

Because the extensional push-off force $F(t)$ is always positive, it does positive work when the leg is extending, *i.e.* $\dot{\ell}(t) \geq 0$, and does negative work when the leg is contracting, *i.e.* $\dot{\ell}(t) < 0$. For $\dot{\ell}(t)$ given in (6.17) the impulse-influence coefficients $J_{i/\mathcal{R}}$ and $J_{i/\mathcal{P}}$ are always positive, as mentioned in Section 5.3.2. Thus, independent of the relative timing of \mathcal{P} and \mathcal{R} , $\dot{\ell}(t) \geq 0$ for any $\mathcal{R} \geq 0$. In other words, when \mathcal{R} is *retracting*, $W_{\mathcal{P}}^+ = W_{\mathcal{P}}$ and $W_{\mathcal{P}}^- = 0$.

As given by (5.17), $J_{i/\mathcal{R}} > 0$, so an extending retraction torque ($\mathcal{R} < 0$) tends to decrease the leg extension rate $\dot{\ell}(t)$. Thus, depending on the relative timing of the impulsive push-off force and extensional retraction torque, $\dot{\ell}(t)$ can become negative for some period of time, causing the push-off force to do negative work during that period. The same procedure explained in Section 6.3.2 (for calculating positive and negative retraction work) can be used to calculate the positive and negative work done by the impulsive push-off force when the leg extension rate $\dot{\ell}(t)$ has zero-crossings during push-off.

6.3.5 Energetic Cost of Impulsive Push-Off and Swing-Leg Retraction

Given the positive and negative work performed by the impulsive push-off force and retraction torque, the individual energetic costs of these impulsive actions are given by

$$E_{\mathcal{P}} = c_1 W_{\mathcal{P}}^+ - c_2 W_{\mathcal{P}}^-, \quad (6.21)$$

$$E_{\mathcal{R}} = c_1 W_{\mathcal{R}}^+ - c_2 W_{\mathcal{R}}^-. \quad (6.22)$$

Unlike the *net* push-off work $W_{\mathcal{P}}$ and the *net* retraction work $W_{\mathcal{R}}$, the energetic cost $E_{\mathcal{P}}$ and $E_{\mathcal{R}}$ can not be calculated, in a general case, by knowing only the step angle α , average

speed V , retraction impulse \mathcal{R} , and overlap parameter s . In fact, we also need to make assumptions on zero-crossings of $\dot{\ell}(t)$ and $\dot{\phi}(t)$ in order to calculate $W_{\mathcal{P}}^+$, $W_{\mathcal{P}}^-$, $W_{\mathcal{R}}^+$, and $W_{\mathcal{R}}^-$.

Although, in general, an infinite number of cases is possible for the zero-crossings of $\dot{\ell}(t)$ and $\dot{\phi}(t)$, I am only interested in those that result in a minimum energetic cost E_{step} . In the next section, I show that the minimum E_{step} always can be achieved with $\dot{\ell}(t) \geq 0$ (no zero-crossing of $\dot{\ell}$, implying all-positive push-off work). With this result, and using the optimal relative timing of push-off and retraction that will be found in the next section, the possible zero-crossings of $\dot{\phi}(t)$ are limited to a single case, so we will be able to calculate $E_{\mathcal{P}}$ and $E_{\mathcal{R}}$ of an optimal gait using only α , V , and \mathcal{R} .

6.4 Optimal Relative Timing of Impulsive Push-off and Retraction

The impulsive push-off \mathcal{P} and the impulsive retraction \mathcal{R} are applied during the late-swing infinitesimal interval $(t_{\text{pr}}^-, t_{\text{pr}}^+)$, called the *push-off-retraction* interval. The relative timing of these two impulsive force and torque, quantified by the overlap parameter s defined in (6.15), can influence the gait energetics. The optimal relative timing of \mathcal{P} and \mathcal{R} , quantified by s^* , is the one that minimizes the energetic cost E_{step} , given by (6.2), for given gait parameters.

Among the different terms in E_{step} , the cost of impulsive swing thrust does not depend on the overlap parameter s . Thus, s^* can also be determined by minimizing the net energetic cost of push-off and retraction, given by

$$\begin{aligned} E_{\mathcal{P}\mathcal{R}} &= E_{\mathcal{P}} + E_{\mathcal{R}} \\ &= c_1 (W_{\mathcal{P}}^+ + W_{\mathcal{R}}^+) - c_2 (W_{\mathcal{P}}^- + W_{\mathcal{R}}^-). \end{aligned} \quad (6.23)$$

The second line in the above equation is obtained by substituting for $E_{\mathcal{P}}$ and $E_{\mathcal{R}}$ from (6.21) and (6.22).

As mentioned in the previous section, calculating $E_{\mathcal{P}\mathcal{R}}$ in a general case requires assump-

tions on the zero-crossings of the instantaneous joint velocities $\dot{\ell}(t)$ and $\dot{\phi}(t)$. Thus, I first assume that the stance leg is always non-contracting, *i.e.* $\dot{\ell}(t) \geq 0$, and find the optimal overlap parameter s^* that minimizes $E_{\mathcal{P}\mathcal{R}}$ subject to this assumption. Then I show that this is not a limiting assumption and does not affect the minimum achievable energetic cost $E_{\mathcal{P}\mathcal{R}}$. Now, as the first step of this procedure, let us determine how the constraint $\dot{\ell}(t) \geq 0$ limits the possible range of s .

6.4.1 Range of Overlap Parameter for a Non-Contracting Stance Leg

According to the formula of the instantaneous leg extension rate $\dot{\ell}(t)$, given by (6.17), the condition of a non-contracting stance leg can be expressed as

$$\dot{\ell}(t) \geq 0 \quad \iff \quad p(t) \geq -\frac{J_{\dot{\ell}\mathcal{R}} \mathcal{R}}{J_{\dot{\ell}\mathcal{P}} \mathcal{P}} r(t). \quad (6.24)$$

On the other hand, the impulse completeness parameter $p(t)$ always satisfies $0 \leq p \leq 1$ (see Section 6.3). The latter can be combined with the above equivalence relation to find the following bounds on $p(t)$ that ensure $\dot{\ell}(t) \geq 0$:

$$p_{\min} \leq p(t) \leq 1, \quad (6.25)$$

where

$$p_{\min} = \max \left(0, -\frac{J_{\dot{\ell}\mathcal{R}} \mathcal{R}}{J_{\dot{\ell}\mathcal{P}} \mathcal{P}} r \right). \quad (6.26)$$

Evaluating the overlap parameter s , defined in (6.15), with the above bounds on p , gives

$$s_{\min}(\mathcal{R}) \leq s \leq 1, \quad (6.27)$$

where

$$s_{\min}(\mathcal{R}) = \max \left(0, -\frac{J_{\dot{\ell}\mathcal{R}} \mathcal{R}}{2 J_{\dot{\ell}\mathcal{P}} \mathcal{P}} \right). \quad (6.28)$$

Therefore, respecting $\dot{\ell}(t) \geq 0$ limits the overlap parameter s within the range given by (6.27).

According to Fig. 6.2, $s = 1$ corresponds to the case where the isolated impulsive push-off force is followed by the isolated impulsive retraction torque (push-off then retraction).

For $\mathcal{R} > 0$, equation (6.28) results in $s_{\min} = 0$ which, according to Fig. 6.2, corresponds to applying the impulsive push-off force completely before the impulsive retraction torque.

For $\mathcal{R} < 0$, $s_{\min} = -J_{\dot{\ell}\mathcal{R}} \mathcal{R} / (2 J_{\dot{\ell}\mathcal{P}} \mathcal{P})$, which is achieved if $p = p_{\min} = -J_{\dot{\ell}\mathcal{R}} \mathcal{R} r / (J_{\dot{\ell}\mathcal{P}} \mathcal{P})$ for all $0 \leq r \leq 1$. This is equivalent to the case that satisfies the following three conditions: (i) both the impulsive push-off force and the impulsive *extending* retraction torque ($\mathcal{R} < 0$) start simultaneously and immediately after the passive swing at t_{pr}^- , (ii) the *partial* impulses of push-off force and retraction torque increase proportionally until the retraction impulse is complete (*i.e.* $r = 1$), and (iii) based on (6.24), the impulsive push-off force is applied at a minimum level during the impulsive retraction torque just to ensure $\dot{\ell}(t) = 0$. With this relative timing, some portion of the push-off impulse, *i.e.* $\mathcal{P}(t_{\text{r}}^+) = -J_{\dot{\ell}\mathcal{R}} \mathcal{R} / J_{\dot{\ell}\mathcal{P}}$, is already applied by the time the impulsive retraction torque is complete. Typically, the retraction impulse \mathcal{R} is much smaller than the push-off impulse \mathcal{P} (the retraction impulse is scaled with the leg mass and inertia, whereas the push-off force is scaled with the total body mass). Thus, typically $p_{t_{\text{r}}^+} = \mathcal{P}(t_{\text{r}}^+) / \mathcal{P} \ll 1$, implying that for $s = s_{\min}$ only a negligible fraction of the push-off impulse, *i.e.* $\mathcal{P}(t_{\text{r}}^+)$, is applied during the advancing extensional retraction torque, and the rest, *i.e.* $\mathcal{P} - \mathcal{P}(t_{\text{r}}^+)$, is applied after it.

The range of overlap parameter s found in this section is used in the next section to find the optimal relative timing of push-off and retraction subject to the constraint $\dot{\ell}(t) \geq 0$.

6.4.2 Optimal Overlap Parameter for Gaits With a Non-Contracting Stance Leg

For gaits with a non-contracting stance-leg, *i.e.* $\dot{\ell}(t) \geq 0$, the push-off impulse does only positive work, and the energetic cost $E_{\mathcal{P}\mathcal{R}}$ in (6.23) can be simplified as

$$E_{\mathcal{P}\mathcal{R}} = c_1 (W_{\mathcal{P}} + W_{\mathcal{R}}^+) - c_2 W_{\mathcal{R}}^-. \quad (6.29)$$

In this equation the net push-off work $W_{\mathcal{P}}$ is given by (6.19), and the positive and negative retraction work $W_{\mathcal{R}}^+$ and $W_{\mathcal{R}}^-$ satisfy $W_{\mathcal{R}}^+ + W_{\mathcal{R}}^- = W_{\mathcal{R}}$, where the net retraction work $W_{\mathcal{R}}$ is

given by (6.14).

Now, given the step angle α , push-off impulse \mathcal{P} , and retraction impulse \mathcal{R} ³, and with the constraint $\dot{\ell}(t) \geq 0$, the optimal relative timing of impulsive \mathcal{P} and \mathcal{R} is given by the overlap parameter s^* that minimizes $E_{\mathcal{P}\mathcal{R}}$ given in (6.29), when s^* is bounded within (6.27). At the optimum the following three different cases are possible for the retraction work:

1) The impulsive retraction torque does only negative work (braking the leg swing): In this case $W_{\mathcal{R}}^+ = 0$, and $W_{\mathcal{R}}^- = W_{\mathcal{R}}$. Thus, equation (6.29) gives

$$\frac{\partial E_{\mathcal{P}\mathcal{R}}}{\partial s} = c_1 \frac{\partial W_{\mathcal{P}}}{\partial s} - c_2 \frac{\partial W_{\mathcal{R}}}{\partial s} = -c_1 J_{\dot{\ell}\mathcal{R}} \mathcal{R} \mathcal{P} + c_2 J_{\dot{\phi}\mathcal{P}} \mathcal{R} \mathcal{P}. \quad (6.30)$$

Using $J_{\dot{\ell}\mathcal{R}} = -J_{\dot{\phi}\mathcal{P}}$ from (5.17), we can simplify the above equation as

$$\frac{\partial E_{\mathcal{P}\mathcal{R}}}{\partial s} = -(c_1 + c_2) J_{\dot{\ell}\mathcal{R}} \mathcal{P} \mathcal{R}. \quad (6.31)$$

According to (5.17), $J_{\dot{\ell}\mathcal{R}}$ is always positive. Therefore, with $\mathcal{R} > 0$ (retracting hip torque), $\partial E_{\mathcal{P}\mathcal{R}}/\partial s < 0$, implying that the energetic cost monotonically decreases with s . Thus, energy expenditure is minimized when s is maximized within the range of (6.27), *i.e.* $s^* = 1$. With $\mathcal{R} < 0$, however, $\partial E_{\mathcal{P}\mathcal{R}}/\partial s > 0$, implying that the cost monotonically increases with s . So, energy expenditure is minimized when s is at the lower bound of (6.27), *i.e.* $s^* = s_{\min}(\mathcal{R})$.

Interestingly, for this case, where $\dot{\ell}(t) \geq 0$ and the impulsive \mathcal{R} does only negative work, both the push-off cost, *i.e.* $E_{\mathcal{P}} = c_1 W_{\mathcal{P}}$, and the retraction cost, *i.e.* $E_{\mathcal{R}} = -c_2 W_{\mathcal{R}}$, simultaneously decrease when s approaches s^* ($\partial E_{\mathcal{P}}/\partial s$ and $\partial E_{\mathcal{R}}/\partial s$ are the first and the second terms in (6.30), respectively). This suggests that for given retraction impulse \mathcal{R} and push-off impulse \mathcal{P} , and as long as $\dot{\ell}(t) \geq 0$, the energy minimizing policy is to avoid performing negative retraction work as much as possible (leading to a reduction in push-off work as well).

³For periodic gaits the push-off impulse is fully resolved when the step angle α , average speed V , and retraction impulse \mathcal{R} are known [see (5.27)]. Thus in those cases α , V , and \mathcal{R} can be the given parameters. However, the analysis in this section is not limited to only periodic gaits, so the given parameters are α , V and \mathcal{P} .

2) The impulsive retraction torque does only positive work (accelerating the swing leg): In this case $W_{\mathcal{R}}^- = 0$, and $W_{\mathcal{R}}^+ = W_{\mathcal{R}}$. Thus, equation (6.29) gives

$$\frac{\partial E_{\mathcal{P}\mathcal{R}}}{\partial s} = c_1 \left(\frac{\partial W_{\mathcal{P}}}{\partial s} + \frac{\partial W_{\mathcal{R}}}{\partial s} \right) = -c_1 \left(J_{\dot{\ell}/\mathcal{R}} + J_{\dot{\phi}/\mathcal{P}} \right) \mathcal{R} \mathcal{P}. \quad (6.32)$$

Now, based on (5.17), $J_{\dot{\ell}/\mathcal{R}} = -J_{\dot{\phi}/\mathcal{P}}$, so

$$\frac{\partial E_{\mathcal{P}\mathcal{R}}}{\partial s} = 0. \quad (6.33)$$

In other words, for gaits with $\dot{\ell}(t) \geq 0$ as far as the impulsive retraction torque does only positive work the optimal overlap parameter s^* does not have a unique solution, and energy minimization has no preference on the relative timing of impulsive push-off and retraction. Now, let us find the range of s^* for which the condition of all-positive retraction work is met.

For $\mathcal{R} > 0$ the impulsive retraction torque does only positive work when the instantaneous hip rate $\dot{\phi}(t)$ is negative (the hip joint is retracting), or equivalently when the impulse completeness parameters defining $\dot{\phi}(t)$ in (6.9) satisfy

$$\max(0, p^\dagger(r)) \leq p \leq 1 \quad \text{for } 0 \leq r \leq 1, \quad (6.34)$$

where

$$p^\dagger(r) = -\frac{\dot{\phi}_0 + r \mathcal{R} J_{\dot{\phi}/\mathcal{R}}}{J_{\dot{\phi}/\mathcal{P}} \mathcal{P}}. \quad (6.35)$$

Using the definition of s in (6.15), the above bound on p translates to the following bounds of s^* :

$$\max(0, s^\dagger(\mathcal{R})) \leq s^* \leq 1, \quad (6.36)$$

where

$$s^\dagger(\mathcal{R}) = -\frac{\dot{\phi}_0 + J_{\dot{\phi}/\mathcal{R}} \mathcal{R}/2}{J_{\dot{\phi}/\mathcal{P}} \mathcal{P}}. \quad (6.37)$$

For all s^* in (6.36) a given $\mathcal{R} > 0$ does only positive work. Within this range, $s^* = 1$ is applicable for all $\mathcal{R} > 0$, and also matches the optimal solution in the previous case (case 1 above). So, I choose $s^* = 1$ as the optimal solution here.

Equivalently, if $\mathcal{R} < 0$ (extending hip torque) the retraction impulse does only positive work when $\dot{\phi}(t) > 0$. This condition is met when

$$p_{\min}(r) \leq p \leq \min(1, p^\dagger(r)) \quad \text{for } 0 \leq r \leq 1, \quad (6.38)$$

where $p_{\min}(r)$ is given by (6.26). The above bound on p gives the following range of s^* for the cases where a given $\mathcal{R} < 0$ does only positive work at the optimum.

$$s_{\min}(\mathcal{R}) \leq s^* \leq \min(1, s^\dagger(\mathcal{R})) \quad (6.39)$$

Here, $s_{\min}(\mathcal{R})$ and $s^\dagger(\mathcal{R})$ are given by (6.28) and (6.37), respectively. To be consistent with case 1 above, where \mathcal{R} does only negative work, I choose $s^* = s_{\min}(\mathcal{R})$ as the optimal solution in this case.

When a given retraction impulse \mathcal{R} does only positive work, the retraction work $W_{\mathcal{R}}$ continuously increases as s approaches the selected s^* ($s^* = 1$ for $\mathcal{R} > 0$ and $s^* = s_{\min}$ for $\mathcal{R} < 0$). However, with $\dot{\ell}(t) \geq 0$ this increase in $W_{\mathcal{R}}$ is entirely compensated by an equal decrease in the push-off work performed by the given impulse \mathcal{P} , so the net positive work $W_{\mathcal{P}} + W_{\mathcal{R}}$ remains constant (*i.e.* becomes independent of s). Consequently, any increase in the retraction cost $E_{\mathcal{R}} = c_1 W_{\mathcal{R}}$, as s approaches s^* , is cancelled by an equal decrease in the push-off cost $E_{\mathcal{P}} = c_1 W_{\mathcal{P}}$, so the net cost $E_{\mathcal{P}\mathcal{R}}$ remains constant.

3) The impulsive retraction torque does both positive and negative work: According to the above two cases, the optimal policy in this case is to do less negative and more positive retraction work, as much as possible. Note that with $\dot{\ell}(t) \geq 0$, any decrease [increase] in negative [positive] retraction work reduces the all-positive push-off work. Thus, with this policy the cost of negative retraction work and the cost of push-off work decrease but the cost of positive retraction work increases. However, any increase in the cost of positive retraction work is cancelled by a partial reduction of push-off cost, so the net cost decreases. Thus, similar to the other two cases, the optimal overlap parameter in this is $s^* = 1$ for $\mathcal{R} > 0$ and $s^* = s_{\min}$ for $\mathcal{R} < 0$.

The above result can be also verified by directly minimizing the net energetic cost $E_{\mathcal{P}\mathcal{R}}$. To save the space, this procedure is described below only for $\mathcal{R} \geq 0$.

Equation (6.9) expresses the instantaneous hip rate $\dot{\phi}(t)$ in terms of the partial push-off and retraction impulses. Because $\mathcal{R} > 0$, and $J_{\dot{\phi}/\mathcal{P}}$ and $J_{\dot{\phi}/\mathcal{R}}$ are both negative (see Section 5.3.2), $\dot{\phi}(t)$ continuously decreases during the push-off-retraction interval, and can have only one zero-crossing in this interval. Assume that the only zero-crossing of the hip angular rate $\dot{\phi}(t)$ occurs at $t = t_0$. Then, there exist $r_{t_0} = r(t_0)$ and $p_{t_0} = p(t_0)$ where $0 \leq r_{t_0} \leq 1$ and $0 \leq p_{t_0} \leq 1$, and

$$\dot{\phi}(t_0) = \dot{\phi}_0 + r_{t_0} J_{\dot{\phi}/\mathcal{R}} \mathcal{R} + p_{t_0} J_{\dot{\phi}/\mathcal{P}} \mathcal{P} = 0. \quad (6.40)$$

The impulsive retraction torque does negative work before t_0 , and positive work after it. The negative retraction work $W_{\mathcal{R}}^-$ can be calculated by the partial work $\mathcal{W}_{\mathcal{R}}(t_0)$, given by evaluating (6.11) at $t = t_0$. This gives

$$W_{\mathcal{R}}^- = -\dot{\phi}_0 r_{t_0} \mathcal{R} - \frac{1}{2} J_{\dot{\phi}/\mathcal{R}} r_{t_0}^2 \mathcal{R}^2 - s_{t_0} J_{\dot{\phi}/\mathcal{P}} \mathcal{R} \mathcal{P}, \quad (6.41)$$

where the partial overlap parameter s_{t_0} is given by (6.12). The positive retraction work then becomes $W_{\mathcal{R}}^+ = W_{\mathcal{R}} - W_{\mathcal{R}}^-$.

Fig. 6.3 visualizes the partial overlap parameter s_{t_0} in the r - p plane for an arbitrary scenario. From this figure, and also from the definition of the partial overlap parameter in (6.12), it is clear that

$$0 \leq s_{t_0} \leq p_{t_0} r_{t_0}. \quad (6.42)$$

The partial overlap parameter s_{t_0} limits the *total* overlap parameter s by constraining it between the following lower and upper bounds, corresponding respectively to paths i and ii in Fig. 6.3.

$$s_{t_0} + (1 - r_{t_0}) p_{t_0} \leq s \leq s_{t_0} + 1 - r_{t_0} \quad (6.43)$$

With the positive and negative retraction work given above, and by knowing $J_{\dot{\phi}/\mathcal{R}} = -J_{\dot{\phi}/\mathcal{P}}$ (see Section 5.3.2), it is a simple practice to verify that the energetic cost $E_{\mathcal{P}\mathcal{R}}$, given by

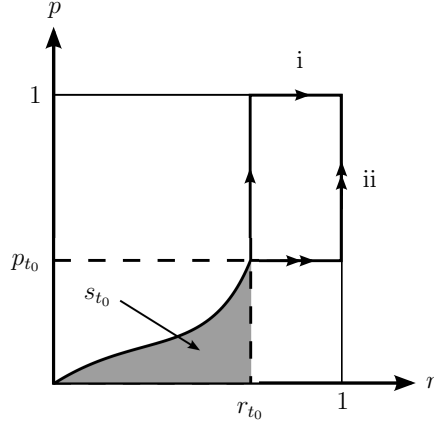


Figure 6.3: **The partial overlap parameter** s_{t_0} . The path i and ii determine the upper and lower bounds of the total overlap parameter s , respectively.

(6.29), is not a direct function of s . In other words, $\partial E_{\mathcal{P}\mathcal{R}}/\partial s = 0$. Now, according to (5.17),

$J_{\dot{\phi}/\mathcal{P}} < 0$, so we get

$$\frac{\partial E_{\mathcal{P}\mathcal{R}}}{\partial s_{t_0}} = (c_1 + c_2) J_{\dot{\phi}/\mathcal{P}} \mathcal{R} \mathcal{P} \leq 0. \quad (6.44)$$

The above equation implies that $E_{\mathcal{P}\mathcal{R}}$ decreases with increasing s_{t_0} , and becomes minimum when s_{t_0} is maximized within its bounds. Thus, according to (6.42), the optimum s_{t_0} is

$$s_{t_0}^* = p_{t_0} r_{t_0}. \quad (6.45)$$

On the other hand,

$$\frac{\partial E_{\mathcal{P}\mathcal{R}}}{\partial r_{t_0}} = -(c_1 + c_2) p_{t_0} J_{\dot{\phi}/\mathcal{P}} \mathcal{R} \mathcal{P} \geq 0, \quad (6.46)$$

implying that at the optimum, r_{t_0} should be minimum while respecting the constraints.

With the zero-crossing constraint in (6.40), and because $J_{\dot{\phi}/\mathcal{P}}$ and $J_{\dot{\phi}/\mathcal{R}}$ are both negative (see Section 5.3.2), the minimum r_{t_0} is achieved when $p_{t_0} = 1$. Finally, substituting the latter and (6.45) into (6.43) results in $s^* = 1$. (End of Proof)

Summarizing the cases 1-3 above, I showed that independent of the step length, walking speed, or the actuator work efficiencies, when the stance leg is constrained to be non-contracting, *i.e.* $\dot{\ell}(t) \geq 0$, the optimal overlap parameter is $s^* = 1$ for $\mathcal{R} > 0$ (retracting hip torque) and $s^* = -J_{\dot{\phi}/\mathcal{R}} \mathcal{R}/(2 J_{\dot{\phi}/\mathcal{P}} \mathcal{P})$ for $\mathcal{R} < 0$ (extending hip torque).

In the next section, I show that the minimum energetic cost can be achieved with $\dot{\ell}(t) \geq 0$, so the above optimality result still holds even if the constraint $\dot{\ell}(t) \geq 0$ is lifted.

6.4.3 Optimal Overlap Parameter With Leg Contraction Allowed

As mentioned in Section 6.3.4, for all gaits in which the retraction torque is *retracting*, *i.e.* $\mathcal{R} \geq 0$, the stance leg is always non-contracting. Thus, for all $\mathcal{R} \geq 0$ the optimality result obtained in the previous section holds even if the constraint $\dot{\ell}(t) \geq 0$ is not imposed. However, with an *extending* retraction torque ($\mathcal{R} < 0$), and depending on the relative timing of the impulsive push-off force and retraction torque, the leg extension rate $\dot{\ell}(t)$ can become negative for some period during the push-off-retraction interval (see Section 6.3.4), causing the push-off force to do negative work during that period. Because minimizing the energetic cost limits the overlap parameter and thus the relative timing of push-off and retraction, it can potentially limit $\dot{\ell}(t)$ as well. So, let us find how $\dot{\ell}(t)$ should change inside the push-off-retraction interval of a minimum-energy gait with given \mathcal{P} and $\mathcal{R} < 0$.

For the impulsive model under study, the leg extension rate is always zero at the start of the push-off-retraction interval, *i.e.* $\dot{\ell}_{t_{\text{pr}}}^- = 0$. Also, given the push-off impulse \mathcal{P} and the retraction impulse \mathcal{R} , the leg extension rate at the end of the push-off-retraction interval, *i.e.* $\dot{\ell}_{t_{\text{pr}}}^+$, is known and is given by (5.14). In energy-optimal gaits $\dot{\ell}_{t_{\text{pr}}}^+ > 0$, as the stance leg should be extending immediately prior to heel-strike to reduce the collision loss [26, 47]. Thus, all possible candidate profiles for $\dot{\ell}(t)$ in the push-off-retraction interval should connect $\dot{\ell}_{t_{\text{pr}}}^- = 0$ to a given $\dot{\ell}_{t_{\text{pr}}}^+ > 0$.

Among an infinite number of possible profiles for $\dot{\ell}(t)$, starting at $\dot{\ell}_{t_{\text{pr}}}^- = 0$ and ending at $\dot{\ell}_{t_{\text{pr}}}^+ > 0$, consider the arbitrary profile shown in Fig. 6.4, in which an impulsive extending retraction torque has caused $\dot{\ell}(t)$ to be negative (contracting) for $t_1 \leq t \leq t_2$. By varying t_1 , t_2 , or the magnitude of $\dot{\ell}(t)$ we can get different functions for the leg extension rate. Now, to find the best $\dot{\ell}(t)$, let us minimize the energetic cost of the gait for this arbitrary profile.

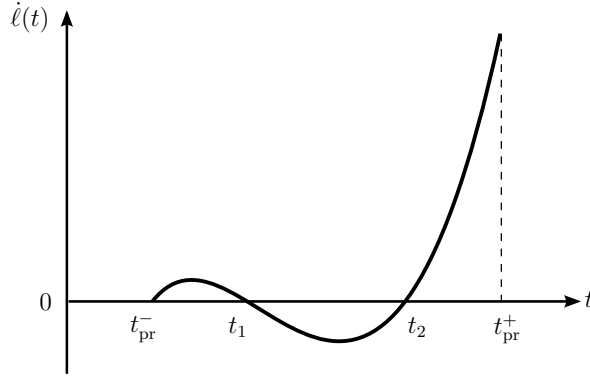


Figure 6.4: **Instantaneous stance leg extension rate** during an arbitrary scenario of impulsive extensional push-off force and impulsive extending retraction torque ($\mathcal{R} < 0$). The extending retraction torque tends to decrease the leg extension rate, and results in $\dot{\ell}(t) < 0$ for $t_1 \leq t \leq t_2$. During this period the impulsive push-off force does negative work.

Note that because the cost of swing thrust impulse is not influenced by $\dot{\ell}(t)$ during the push-off-retraction interval ($\dot{\ell}_{t_{pr}^-}$ and $\dot{\ell}_{t_{pr}^+}$ are fixed for given \mathcal{P} and \mathcal{R}) minimizing E_{step} , given by (6.2), and $E_{\mathcal{P}\mathcal{R}}$, given by (6.23), has the same consequences on $\dot{\ell}(t)$.

In order to calculate $E_{\mathcal{P}\mathcal{R}}$, we need to calculate the positive and negative work performed by the push-off and retraction impulses. For the case shown in Fig. 6.4 the impulsive push-off force performs negative work for $t_1 \leq t \leq t_2$, and positive work during the rest of the interval (t_{pr}^-, t_{pr}^+). Using the technique described in Section 6.3.4, these positive and negative work quantities are given by

$$W_{\mathcal{P}}^- = \mathcal{W}_{\mathcal{P}}(t_2) - \mathcal{W}_{\mathcal{P}}(t_1), \quad (6.47)$$

$$W_{\mathcal{P}}^+ = \mathcal{W}_{\mathcal{P}} - \mathcal{W}_{\mathcal{P}}^-, \quad (6.48)$$

where $\mathcal{W}_{\mathcal{P}}$ is the net push-off work, given by (6.19), and $\mathcal{W}_{\mathcal{P}}(t_1)$ and $\mathcal{W}_{\mathcal{P}}(t_2)$ are the partial work quantities performed by the impulsive push-off force from t_{pr}^- until t_1 and t_2 . These partial work quantities can be calculated from (6.18) as below.

$$\mathcal{W}_{\mathcal{P}}(t_1) = \frac{1}{2} J_{\dot{\ell}\mathcal{P}} p_{t_1}^2 \mathcal{P}^2 + (p_{t_1} r_{t_1} - s_{t_1}) J_{\dot{\ell}\mathcal{R}} \mathcal{R} \mathcal{P} \quad (6.49)$$

$$\mathcal{W}_{\mathcal{P}}(t_2) = \frac{1}{2} J_{\dot{\ell}\mathcal{P}} p_{t_2}^2 \mathcal{P}^2 + (p_{t_2} r_{t_2} - s_{t_2}) J_{\dot{\ell}\mathcal{R}} \mathcal{R} \mathcal{P} \quad (6.50)$$

In the above, s_{t_1} and s_{t_2} are the partial overlap parameters corresponding to $t = t_1$ and $t = t_2$ [see (6.12)], and p_{t_1} , r_{t_1} , p_{t_2} , and r_{t_2} are the impulse completeness parameters (see Section 6.3) at t_1 and t_2 and satisfy $\dot{\ell}(t_1) = \dot{\ell}(t_2) = 0$, where $\dot{\ell}(t)$ is given by (6.17).

The impulsive retraction torque does net work $W_{\mathcal{R}}$, negative work $W_{\mathcal{R}}^-$, and positive work $W_{\mathcal{R}}^+ = W_{\mathcal{R}} - W_{\mathcal{R}}^-$. The net work $W_{\mathcal{R}}$ is given by (6.14), and is a function of the net overlap parameter s , but not s_{t_1} and s_{t_2} . In general, $W_{\mathcal{R}}^-$ and $W_{\mathcal{R}}^+$ depend on $W_{\mathcal{R}}$ and possible zero-crossings of the instantaneous hip rate (see Section 6.3.2). Thus, they are also independent of s_{t_1} and s_{t_2} , but have dependency in s .

Using the above positive and negative work quantities, and given the step angle α , push-off impulse \mathcal{P} , and retraction impulse \mathcal{R} , the net energetic cost $E_{\mathcal{P}\mathcal{R}}$ can be calculated from (6.23) as a function of a few free parameters (the partial and net overlap parameters s_{t_1} , s_{t_2} , and s , as well as the impulse completeness parameters p_{t_1} , p_{t_2} , r_{t_1} , and r_{t_2}). Now given α , \mathcal{P} , and $\mathcal{R} < 0$, I investigate the minimum $E_{\mathcal{P}\mathcal{R}}$ for the following three possible cases:

1) The extending retraction torque does only positive work (accelerating the forward leg rotation): In this case $W_{\mathcal{R}}^- = 0$, and $W_{\mathcal{R}}^+ = W_{\mathcal{R}}$. Thus,

$$\begin{aligned} E_{\mathcal{P}\mathcal{R}} &= c_1 (W_{\mathcal{P}}^+ + W_{\mathcal{R}}^+) - c_2 (W_{\mathcal{P}}^- + W_{\mathcal{R}}^-) \\ &= c_1 (W_{\mathcal{P}} + W_{\mathcal{R}}) - (c_1 + c_2) W_{\mathcal{P}}^-. \end{aligned} \quad (6.51)$$

According to the work-energy principle, the net push-off and retraction work $W_{\mathcal{P}\mathcal{R}} = W_{\mathcal{P}} + W_{\mathcal{R}}$ is equal to the change in kinetic energy of the biped from t_{pr}^- to t_{pr}^+ . Because the velocities (\equiv kinetic energy) at these two instants are independent of the relative timing of impulsive push-off and retraction (see Section 5.3.2), $W_{\mathcal{P}\mathcal{R}}$ does not depend on s , s_{t_1} , and s_{t_2} . This can be also verified by inspecting $W_{\mathcal{P}\mathcal{R}}$, calculated from (6.14) and (6.19), and recognizing that $J_{\dot{\phi}/\mathcal{P}} = -J_{\dot{\phi}/\mathcal{R}}$ [see (5.17)].

With a constant $W_{\mathcal{P}\mathcal{R}}$, the energetic cost $E_{\mathcal{P}\mathcal{R}}$ in (6.51) is minimized only if $W_{\mathcal{P}}^- = 0$ or equivalently when $\dot{\ell}(t) \geq 0$ for the entire push-off and retraction interval. Therefore, when

the retraction torque does only positive work, the constraint $\dot{\ell}(t) \not\leq 0$ imposed in Section 6.4.2 is not active at the optimum, implying that the optimal overlap parameter s^* found for the case 2 of the previous section does not change if the constraint $\dot{\ell}(t) \geq 0$ is not imposed.

2) The extending retraction torque does only negative work (decelerating the rearward leg rotation): In this case $W_{\mathcal{R}}^+ = 0$, and $W_{\mathcal{R}}^- = W_{\mathcal{R}}$. Thus,

$$E_{\mathcal{P}\mathcal{R}} = (c_1 + c_2) W_{\mathcal{P}}^+ - c_2 (W_{\mathcal{P}} + W_{\mathcal{R}}). \quad (6.52)$$

Because $W_{\mathcal{P}} + W_{\mathcal{R}}$ is constant for any given α , \mathcal{P} , and \mathcal{R} (see the previous case), $E_{\mathcal{P}\mathcal{R}}$ is minimized only when $W_{\mathcal{P}}^+$ is minimized. Unlike $W_{\mathcal{P}}^-$ in the previous case, $W_{\mathcal{P}}^+$ can not be reduced to zero for any given retraction impulse \mathcal{R} , as doing so requires a very large $\mathcal{R} < 0$ to make $\dot{\ell}(t) < 0$ for the entire push-off and retraction interval. Moreover, this very large $\mathcal{R} < 0$ can not be energetically optimal as it results in a large retraction cost.

In order to find the minimum possible $W_{\mathcal{P}}^+$ for any given $\mathcal{R} < 0$, we can examine its variations with respect to its free parameters. Using the work equations in (6.47)-(6.50), and recognizing that $J_{\dot{\ell}\mathcal{R}} > 0$ [see (5.17)], we can get

$$\frac{\partial W_{\mathcal{P}}^+}{\partial s} = \frac{\partial W_{\mathcal{P}}^+}{\partial s_{t_1}} = -J_{\dot{\ell}\mathcal{R}} \mathcal{P} \mathcal{R} > 0. \quad (6.53)$$

The above relations imply that $W_{\mathcal{P}}^+$ monotonically decreases with decreasing s_{t_1} and s . Thus, $W_{\mathcal{P}}^+$ is minimized only if both s_{t_1} and s are minimized subject to their corresponding lower bounds. These bounds are calculated in the following.

Using the instantaneous leg extension rate formula in (6.17), and that $\dot{\ell}(t) \geq 0$ for $t_1 \leq t \leq t_2$, we get

$$p(t) \geq -\frac{J_{\dot{\ell}\mathcal{R}} \mathcal{R}}{J_{\dot{\ell}\mathcal{P}} \mathcal{P}} r(t) \quad \text{for } 0 \leq r(t) \leq r_{t_1}. \quad (6.54)$$

For $t = t_1$, $\dot{\ell}(t_1) = 0$, and the above relation holds with the equality sign:

$$p_{t_1} = -\frac{J_{\dot{\ell}\mathcal{R}} \mathcal{R}}{J_{\dot{\ell}\mathcal{P}} \mathcal{P}} r_{t_1}. \quad (6.55)$$

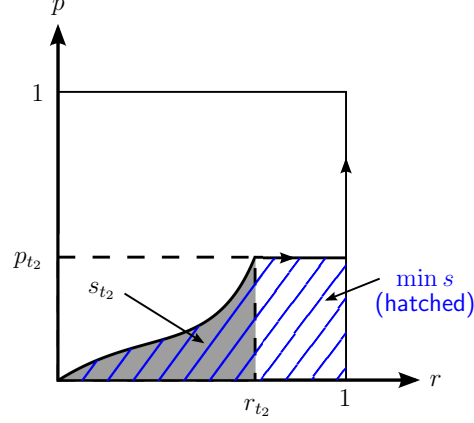


Figure 6.5: **The partial overlap parameter s_{t_2} and the minimum net overlap parameter s** for an arbitrary scenario. The area of the shaded (solid gray) region corresponds to s_{t_2} . Given s_{t_2} , the net overlap parameter s becomes minimum if the push-off impulse completeness parameter $p(t)$ does not change during (t_2, t_r^+) , *i.e.* from t_2 until $r(t) = 1$. In this case s is given by the area of the hatched region.

Now, using the above two equations and the definition of the partial overlap parameter s_t in (6.12), we can get

$$s_{t_1} = \int_0^{r_{t_1}} p dr \geq -\frac{J_{i/R} \mathcal{R}}{2 J_{i/P} \mathcal{P}} r_{t_1}^2 = \frac{p_{t_1} r_{t_1}}{2}. \quad (6.56)$$

Therefore, the lower bound of the partial overlap parameter s_{t_1} is $p_{t_1} r_{t_1}/2$.

Fig.6.5 can be used to find the lower bound of the net overlap parameter s as a function of the partial overlap parameter s_{t_2} . In this figure the partial overlap parameter s_{t_2} is visualized in the r - p plane for an arbitrary scenario. Given s_{t_2} , the net overlap parameter s is minimized if the impulse completeness parameter $p(t)$ does not change during the interval (t_2, t_r^+) , *i.e.* from t_2 until when $r(t) = 1$. In this case, s is given by the area of the hatched region. Thus, the lower bound of s is calculated as

$$s \geq s_{t_2} + p_{t_2} (1 - r_{t_2}). \quad (6.57)$$

As mentioned above, $W_{\mathcal{P}}^+$ (and equivalently $E_{\mathcal{P}\mathcal{R}}$) is minimized when s and s_{t_1} become minimum. These minimums are determined by (6.56) and (6.57). Thus, at the optimum

$$s_{t_1} = p_{t_1} r_{t_1}/2, \quad (6.58)$$

$$s_{t_2} = s - p_{t_2} (1 - r_{t_2}). \quad (6.59)$$

Substituting these optimal values in the work equations (6.47)-(6.50) and simplifying the results using the zero-crossing condition in (6.55) gives the optimal push-off work values as

$$W_{\mathcal{P}}^- = \frac{1}{2} J_{\dot{\ell}\mathcal{P}} p_{t_2}^2 \mathcal{P}^2 + (p_{t_2} - s) J_{\dot{\ell}\mathcal{R}} \mathcal{R} \mathcal{P}, \quad (6.60)$$

$$W_{\mathcal{P}}^+ = \frac{1}{2} J_{\dot{\ell}\mathcal{P}} (1 - p_{t_2}^2) \mathcal{P}^2 + (1 - p_{t_2}) J_{\dot{\ell}\mathcal{R}} \mathcal{R} \mathcal{P}. \quad (6.61)$$

Note that the above optimal work values do not depend on p_{t_1} and r_{t_1} . In fact, it can be simply verified that with optimal s_{t_1} given in (6.58) the push-off work performed in $t_{\text{pr}}^- \leq t \leq t_1$ is zero, *i.e.* $W_{\mathcal{P}}(t_1) = 0$, regardless of the value of r_{t_1} and p_{t_1} . Therefore, without any change in the minimum energetic cost, we can assume that at the optimum

$$p_{t_1}^* = r_{t_1}^* = s_{t_1}^* = 0, \quad (6.62)$$

or equivalently $t_1^* = t_{\text{pr}}^-$.

Now, according to (6.61), the minimum $W_{\mathcal{P}}^+$ (corresponding to the minimum $E_{\mathcal{P}\mathcal{R}}$) is obtained where $\partial W_{\mathcal{P}}^+ / \partial p_{t_2} = 0$, resulting in

$$p_{t_2}^* = -\frac{J_{\dot{\ell}\mathcal{R}} \mathcal{R}}{J_{\dot{\ell}\mathcal{P}} \mathcal{P}}. \quad (6.63)$$

Substituting this optimal value in the zero-crossing condition $\dot{\ell}(t_2) = J_{\dot{\ell}\mathcal{P}} p_{t_2} \mathcal{P} + J_{\dot{\ell}\mathcal{R}} r_{t_2} \mathcal{R} = 0$ gives

$$r_{t_2}^* = 1. \quad (6.64)$$

Finally, the latter simplifies (6.59) to

$$s^* = s_{t_2}. \quad (6.65)$$

Because s_{t_2} is a free parameter, the above equation implies that the optimal overlap parameter s^* does not have a unique solution when a given extending retraction torque ($\mathcal{R} < 0$) does only negative work. In fact, as it is shown below, s^* can take any value within the range

$$0 \leq s^* \leq -\frac{J_{\dot{\ell}\mathcal{R}} \mathcal{R}}{2 J_{\dot{\ell}\mathcal{P}} \mathcal{P}}. \quad (6.66)$$

If s exceeds the above upper bound, we get $\dot{\ell}(t) > 0$ for the entire push-off-retraction interval (see Section 6.4.1), and the above work and energetic cost calculations are not valid. Notwithstanding, according to the case 1 in the previous section, decreasing energetic cost in this case requires to reduce s to the above upper bound. On the other hand, for all s within the range given by (6.66), $\dot{\ell}(t) \leq 0$ for some period in the push-off-retraction interval, and the above work and energetic cost calculations are valid. In this case, independent of the value of s , and as long as (6.62)-(6.66) hold, the positive push-off work $W_{\mathcal{P}}^+$, given by (6.61), and consequently the energetic cost $E_{\mathcal{P}\mathcal{R}}$, given by (6.52), are at their minimum. Thus, (6.66) represents the range of all valid optimal s^* when a given extending retraction torque ($\mathcal{R} < 0$) does only negative work.

Note that unlike the minimum $W_{\mathcal{P}}^+$, given by (6.61), the resulting negative push-off work $W_{\mathcal{P}}^-$, given by (6.60), does depend on s and increases with it ($-J_{\dot{\ell}\mathcal{R}} \mathcal{R} \mathcal{P} > 0$ because $\mathcal{R} < 0$ and $J_{\dot{\ell}\mathcal{R}} > 0$). However, this increase is cancelled by an equal decrease in all-negative retraction work ($\partial W_{\mathcal{R}}/\partial s = -\partial W_{\mathcal{P}}^-/\partial s$), so the net negative work is independent of the value of s .

Among all possible s^* given by (6.66), $s^* = -J_{\dot{\ell}\mathcal{R}} \mathcal{R}/(2 J_{\dot{\ell}\mathcal{P}} \mathcal{P})$ results in a special case. With this specific s^* and while (6.62)-(6.64) hold, $\dot{\ell}(t) = 0$ for $t_{\text{pr}}^- \leq t \leq t_2$, or equivalently $\dot{\ell}(t) \geq 0$ for the entire push-off-retraction interval. In other words, a non-contracting stance leg is a possible optimal policy in this case. Imposing the constraint $\dot{\ell}(t) \geq 0$ only limits s^* to one solution (among a range of possible solutions), but does not influence the minimum achievable net energetic cost.

3) The extending retraction torque does both positive and negative work: In this case we can divide the push-off and retraction interval, *i.e.* $(t_{\text{pr}}^-, t_{\text{pr}}^+)$, into subintervals within each the retraction torque does only positive or negative work. According to the previous two cases, $\dot{\ell}(t) \geq 0$ is energetically optimal for all of these subintervals. Therefore, $\dot{\ell}(t) \geq 0$ is also a possible optimal policy when a given extending \mathcal{R} does both positive and negative work. This implies that we can use the constraint $\dot{\ell}(t) \geq 0$ without influencing the minimum

achievable energetic cost for given \mathcal{P} , \mathcal{R} and α .

Summarizing the cases 1-3 above, I used the leg extension profile shown in Fig. 6.4 to show that a non-contracting stance leg, *i.e.* $\dot{\ell}(t) \geq 0$, can always result in the minimum energetic cost. Repeating the analyses for any arbitrary profile of $\dot{\ell}(t)$, with any number of zero-crossings, will give the same result. Thus, the constraint $\dot{\ell}(t) \geq 0$ that was imposed in Section 6.4.2 to calculate the optimal s^* does not influence the minimum achievable energetic cost, and the resulting s^* represents the unconstrained optimal solutions as well.

6.4.4 Optimal Relative Timing of Impulsive Push-off and Retraction

Summarizing Sections 6.4.1-6.4.3, I showed that independent of the step length, walking speed, or the actuator work efficiencies, the minimum energetic cost in all cases can be achieved with

$$s^* = \begin{cases} 1 & \text{if } \mathcal{R} > 0, \\ s_{\min}(\mathcal{R}) = -\frac{J_{\dot{\ell}/\mathcal{R}} \mathcal{R}}{2 J_{\dot{\ell}/\mathcal{P}} \mathcal{P}} & \text{if } \mathcal{R} < 0. \end{cases} \quad (6.67)$$

As discussed in Section 6.4.1, $s^* = 1$ corresponds to the push-off-then-retraction scenario. In other words, when the impulsive retraction torque is retracting, *i.e.* $\mathcal{R} > 0$, the optimal relative timing is to apply the impulsive retraction torque completely after the impulsive push-off force (no overlap). For $\mathcal{R} < 0$, where the retraction torque is extending, $s^* = s_{\min}(\mathcal{R})$ corresponds to the case when the impulsive retraction torque and the impulsive push-off force start simultaneously, but with a minimal push-off activity just to avoid $\dot{\ell}(t) < 0$ during the extending retraction torque. In this case the main portion of the push-off impulse is applied completely after the impulsive retraction torque.

6.4.5 Intuitive Justification of the Optimal Relative Timing

The optimal relative timing of the impulsive push-off \mathcal{P} and impulsive retraction \mathcal{R} can be intuitively justified as follows. The velocities just after both \mathcal{P} and \mathcal{R} , given by (5.14), are independent of the relative timing of these two impulses. Therefore, the net change in kinetic energy of the system made by the impulsive push-off and retraction, and consequently the total work done by them (*i.e.* $W_{\mathcal{P}\mathcal{R}} = W_{\mathcal{P}} + W_{\mathcal{R}}$), is also independent of this relative timing. On the other hand, the push-off force accelerates the hip along the stance leg, inducing an (inertial) torque on the swing leg. This induced torque tends to brake the forward swing of the leg and/or accelerate its rotation in the rearward direction. This push-off-mediated brake/retraction is in concert with the action of a retracting hip torque ($\mathcal{R} > 0$), but is opposite to that of an extending hip torque ($\mathcal{R} < 0$). As the hip torque is delayed relative to the push-off force, more push-off-mediated braking/retraction takes place before the hip torque. Therefore, the later [sooner] a given retracting [extending] hip torque starts (relative to the push-off force, and within the push-off-retraction interval), the less negative work (braking) and the more positive work (rearward acceleration) it does. Now, because the net work $W_{\mathcal{P}\mathcal{R}}$ is constant, the increase in positive retraction work $W_{\mathcal{R}}^+$ is accompanied by an equal decrease in all-positive push-off work $W_{\mathcal{P}}$. Thus, the total positive work $W_{\mathcal{P}} + W_{\mathcal{R}}^+$ is not influenced by the changes in $W_{\mathcal{R}}^+$. However, the decrease in negative retraction work (decrease in $|W_{\mathcal{R}}^-|$) should be accompanied by an equal decrease in push-off work to keep $W_{\mathcal{P}\mathcal{R}}$ constant. Thus, both the total negative work and the total positive work decrease by this change, which result in a reduced net energetic cost. This cost reduction is maximized when the negative retraction work is minimized for a given \mathcal{R} , or equivalently when an impulsive retracting hip torque is applied completely after the impulsive push-off force, and an extending hip torque starts immediately after the passive swing phase. In the latter, avoiding leg contraction, *i.e.* $\dot{\ell} \neq 0$, results in a minimal push-off activity during the extending hip torque.

The above reasoning is valid for both periodic and aperiodic gaits, as well as for any biped model in which the push-off force acts in concert with the retracting hip torque in braking/retracting the leg swing, including human-like models with torso and articulated legs. In the next section this generality is shown with a more direct mathematical method.

6.4.6 Generality of the Optimal Relative Timing Result

The resulting optimal relative timing is achieved mainly based on the characteristic that: $J_{\dot{\phi}/\mathcal{P}} = -J_{\dot{\theta}/\mathcal{R}} < 0$. As shown in Appendix B.1.2, the equality relation here is guaranteed by the symmetry of the mass-inertia matrix, and the inequality comes from the fact that the push-off force tends to retract the swing leg. Because the symmetry of the mass-inertia matrix is a general property, the optimal relative timing found in this section holds for any walking model in which the push-off force acts in concert with the retracting hip torque in braking/retracting the leg swing; a result that was also intuitively justified in the previous section.

For example, consider the more realistic models in Fig.6.6. In these models the retraction impulse \mathcal{R} is applied by the swing hip actuator (both models have two hip actuators, each acting between the torso and the corresponding leg) and pushes the swing leg toward the stance leg (decreasing the swing hip angle ϕ). In the model with straight legs the push-off impulse \mathcal{P} is directly applied by the prismatic actuator along the stance leg, whereas in the model with articulated legs the resultant push-off impulse \mathcal{P} is provided indirectly by the knee impulse \mathcal{K} and the ankle impulse \mathcal{A} that extend the corresponding joint angles. Following the procedure used in Appendix B.1.2, the impulse-influence coefficients of the push-off-retraction velocity maps in these models can be related to their mass-inertia matrix. Thus, the symmetry of the mass-inertia matrix guarantees $J_{\dot{\phi}/\mathcal{P}} = -J_{\dot{\theta}/\mathcal{R}}$ for the straight-leg biped, and $J_{\dot{\phi}/\mathcal{K}} = -J_{\dot{\psi}/\mathcal{R}}$ and $J_{\dot{\phi}/\mathcal{A}} = -J_{\dot{\theta}/\mathcal{R}}$ for the articulated-leg biped. On the other hand, in both models the (directly/indirectly generated) push-off impulse \mathcal{P} accelerates the hip

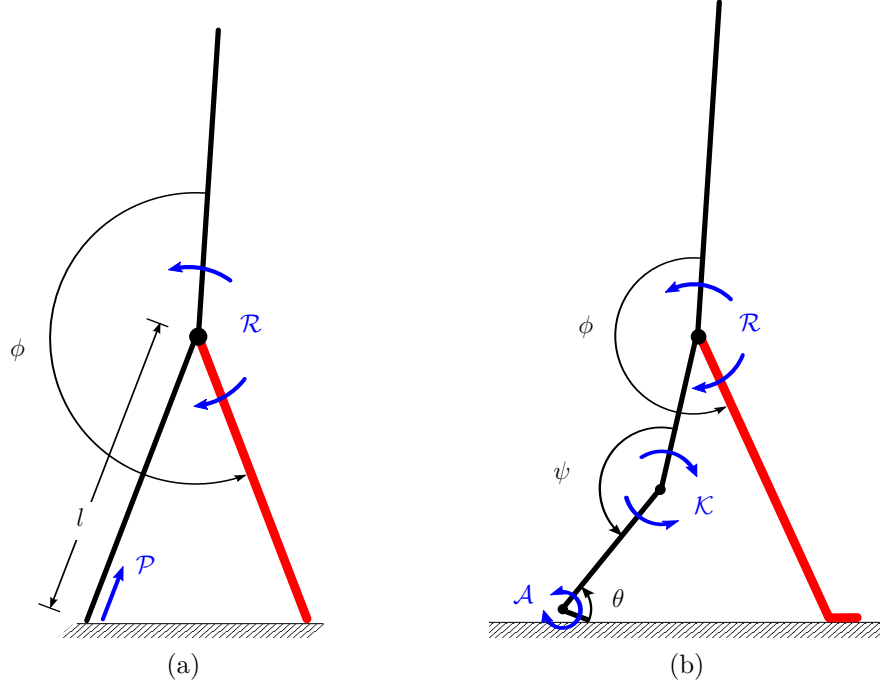


Figure 6.6: **Two bipedal models with torso.** Each model has two hip actuators, each acting between the torso and the corresponding thigh. The swing retraction torque, quantified by the impulse \mathcal{R} , decreases ϕ and pushes the swing leg toward the stance leg. **(a)** The straight-leg model: the push-off impulse \mathcal{P} is provided by a prismatic actuator along the stance leg. **(b)** The articulated-leg model: the resultant push-off is provided by the knee and ankle torques, quantified by their impulses \mathcal{K} and \mathcal{A} , which tend to extend the corresponding angles (consequently extending the leg).

forward, which in a normal configuration tends to decrease the swing hip angle ϕ . This implies $J_{\dot{\phi}/\mathcal{P}} < 0$ for the straight-leg model, and $J_{\dot{\phi}/\mathcal{K}} < 0$ and $J_{\dot{\phi}/\mathcal{A}} < 0$ for the articulated-leg model. Therefore, the optimality conditions resulting to (6.67) are also satisfied for both of these models, so the same optimal relative timing of push-off and retraction holds for both.

6.4.7 Application for Practical Non-Impulsive Systems

Although the analysis in this section is based on impulsive functions, arguably the results are still applicable to many practical cases in which the (optimal) gait includes burst forces/torques. Although realistic forces/torques have bounded magnitudes and are applied over an extended period of time, the duration of the burst forces/torque is relatively short, so the biped configuration does not change much during their application. Therefore, these

burst forces/torques effectively change the velocities while the biped configuration is approximately constant, similar to the effect of theoretically impulsive actions.

The analysis in the previous section shows that for given push-off force impulse and late-swing extending hip torque impulse, energetic cost is minimized when the overlap parameter is minimized while respecting $\dot{\ell}(t) \geq 0$. Similar to the theoretical impulsive cases, this optimal relative timing can be achieved with practical burst forces/torques when the extending hip torque is applied at the end of passive swing and practically before the pre-emptive push-off.

When the late-swing hip torque is retracting, however, there is a small difference between the theoretical and practical cases. With a retracting hip torque the minimum cost is obtained when the overlap parameter s is maximized. In the case of impulsive forces/torques this can be achieved when the retracting torque is completely isolated and applied between the push-off and heel-strike ($s^* = 1$). However, for practical non-impulsive cases, this isolation of the actions will degrade the gait efficiency by inserting a non-infinitesimal gap between the push-off and heel-strike (for efficient walking push-off should be applied just before heel-strike [47]). Hence, maximizing the overall energy efficiency in practical cases can be achieved by postponing the retracting hip torque until the *final* portion of the pre-emptive push-off before heel-strike. Verification of this strategy in human walking and in practical robots can be a possible extension to the current work.

6.5 Energy Optimal Swing Retraction Impulse

Given the step angle α , average walking speed V , and unit-work costs c_1 and c_2 , the optimal retraction impulse \mathcal{R}^* is the one that minimizes the net energetic cost E_{step} , given by (6.2).

Among the different terms contributing in E_{step} , the swing thrust cost $E_{\mathcal{S}}$ is given by (6.6) as a function of α , V , and \mathcal{R} . In general, the push-off cost $E_{\mathcal{P}}$ is given by (6.21). However, as shown in Section 6.4.3, we can limit our study to $\dot{\ell}(t) \geq 0$ without influencing

the minimum possible E_{step} . In this case, the push-off impulse does only positive work and

$$E_{\mathcal{P}} = c_1 W_{\mathcal{P}}, \quad (6.68)$$

where the net push-off work $W_{\mathcal{P}}$ is given by (6.19). Using the optimal overlap parameter s^* , given by (6.67), $W_{\mathcal{P}}$ and thus $E_{\mathcal{P}}$ can be calculated for any given α , V , and \mathcal{R} .

Another contributing term in E_{step} is the retraction cost $E_{\mathcal{R}}$, given by (6.22). However, so far we have not been able to calculate $E_{\mathcal{R}}$ without any assumptions on the zero-crossings of the instantaneous hip rate $\dot{\phi}(t)$. Fortunately, this problem is resolved by using the energy optimal relative timing of \mathcal{P} and \mathcal{R} found in the previous section.

As discussed in the previous section, for $\mathcal{R} > 0$ the energetic cost is minimized when \mathcal{P} and \mathcal{R} are isolated, and \mathcal{R} comes completely after \mathcal{P} . Using this relative timing and the instantaneous hip rate $\dot{\phi}(t)$ given in (6.9), the hip rates immediately before and after the impulsive \mathcal{R} become

$$\dot{\phi}_{t_r^-} = \dot{\phi}(t) \Big|_{\substack{p=1 \\ r=0}} = \dot{\phi}_0 + J_{\dot{\phi}/\mathcal{P}} \mathcal{P}, \quad (6.69)$$

$$\dot{\phi}_{t_r^+} = \dot{\phi}(t) \Big|_{\substack{p=1 \\ r=1}} = \dot{\phi}_{t_r^-} + J_{\dot{\phi}/\mathcal{R}} \mathcal{R} = \dot{\phi}_0 + J_{\dot{\phi}/\mathcal{P}} \mathcal{P} + J_{\dot{\phi}/\mathcal{R}} \mathcal{R}. \quad (6.70)$$

Because the impulses are isolated in this case, the formula of the work done by an isolated impulsive force/torque, given by (6.3) and (6.4), can be used to calculate the positive and negative retraction work, where $\mathcal{I} = \mathcal{R}$, and $\dot{q}^- = \dot{\phi}_{t_r^-}$ and $\dot{q}^+ = \dot{\phi}_{t_r^+}$ are given by (6.69) and (6.70).

For $\mathcal{R} < 0$ the optimal relative timing of push-off and retraction does not represent isolated impulses ($0 < s^* = s_{\min}(\mathcal{R}) < 1$). However, in this case, the impulsive extending retraction torque does only positive work for all α and V within the admissible region (defined in section 5.4.4). To verify this characteristic, recall from Section 6.4.1 that for $s = s^* = s_{\min}(\mathcal{R})$ the impulsive push-off force is applied minimally during the extending retraction torque. This

minimal level is given by $p(t) = p_{\min} = -J_{\dot{\ell}/\mathcal{R}} \mathcal{R} r(t) / (J_{\dot{\ell}/\mathcal{P}} \mathcal{P})$. With this $p(t)$, the instantaneous hip rate during the impulsive retraction torque ($t_r^- \leq t \leq t_r^+$) can be calculated from (6.9) as

$$\begin{aligned}
\dot{\phi}(t) &= \dot{\phi}_0 + J_{\dot{\phi}/\mathcal{R}} r(t) \mathcal{R} + J_{\dot{\phi}/\mathcal{P}} p(t) \mathcal{P} \\
&= \dot{\phi}_0 + J_{\dot{\phi}/\mathcal{R}} r(t) \mathcal{R} - J_{\dot{\phi}/\mathcal{P}} \frac{J_{\dot{\ell}/\mathcal{R}}}{J_{\dot{\ell}/\mathcal{P}}} r(t) \mathcal{R} \\
&= \dot{\phi}_0 + \frac{J_{\dot{\phi}/\mathcal{R}} J_{\dot{\ell}/\mathcal{P}} - J_{\dot{\phi}/\mathcal{P}} J_{\dot{\ell}/\mathcal{R}}}{J_{\dot{\ell}/\mathcal{P}}} r(t) \mathcal{R}.
\end{aligned} \tag{6.71}$$

As shown in Fig. 5.6b, inside the admissible region and even for some area below it $\dot{\phi}_0 > 0$. On the other hand, according to the sign properties of the impulse-influence coefficients, indicated in (5.15) and (5.18), the last fraction in (6.71) is always negative. Also, for an extensional retraction torque, \mathcal{R} is negative. Thus, throughout the impulsive extensional hip torque, *i.e.* for $0 \leq r(t) \leq 1$, the instantaneous hip rate $\dot{\phi}(t)$ remains positive inside the admissible region, and \mathcal{R} does only positive work (extending the hip joint). In other words, with $\mathcal{R} < 0$ and $s = s^*$, and for any given step angle α and average speed V in the admissible region, $W_{\mathcal{R}}^- = 0$ and $W_{\mathcal{R}}^+$ is calculated from the net work $W_{\mathcal{R}}$, given by (6.14), as below:

$$\begin{aligned}
W_{\mathcal{R}}^+ &= W_{\mathcal{R}} \Big|_{s=s^*} = -\dot{\phi}_0 \mathcal{R} - \frac{1}{2} J_{\dot{\phi}/\mathcal{R}} \mathcal{R}^2 - s^* J_{\dot{\phi}/\mathcal{P}} \mathcal{R} \mathcal{P} \\
&= -\dot{\phi}_0 \mathcal{R} - \frac{1}{2} J_{\dot{\phi}/\mathcal{R}} \mathcal{R}^2 + \frac{J_{\dot{\ell}/\mathcal{R}} \mathcal{R}}{2 J_{\dot{\ell}/\mathcal{P}} \mathcal{P}} J_{\dot{\phi}/\mathcal{P}} \mathcal{P} \mathcal{R} \\
&= -\dot{\phi}_0 \mathcal{R} - \frac{J_{\dot{\phi}/\mathcal{R}} J_{\dot{\ell}/\mathcal{P}} - J_{\dot{\phi}/\mathcal{P}} J_{\dot{\ell}/\mathcal{R}}}{2 J_{\dot{\ell}/\mathcal{P}}} \mathcal{R}^2.
\end{aligned} \tag{6.72}$$

Thus, given α , V , and \mathcal{R} , we can calculate the positive and negative retraction work subject to $s = s^*$. Finally, the retraction cost $E_{\mathcal{R}}(s^*)$ can be calculated from (6.22) as a function of α , V , and \mathcal{R} .

Now, given a pair of step angle α and average walking speed V in the admissible region, as well as the unit-work costs c_1 and c_2 , we can calculate the net energetic cost E_{step} subject to $s = s^*$, solely in terms of the retraction impulse \mathcal{R} . Thus, the optimal impulse \mathcal{R}^* that

minimizes E_{step} for given admissible α and V can be found by solving

$$\mathcal{R}^* = \min_{\mathcal{R}} E_{\text{step}}(\alpha, V, \mathcal{R}, s^*), \quad (6.73)$$

subject to the

- heel-strike constraint in (5.20),
- toe-off constraint in (5.21),
- required push-off and swing-thrust impulse constraints in (5.26) and (5.27),
and
- maximum retraction impulse constraint in (5.28).

This optimization can be accurately solved using simple numerical methods. However, to gain more insight, an approximate analytic solution is preferable. Calculating this analytic solution is the subject of the next chapter.

6.6 Summary

In this chapter the energetics of the simple bipedal model with impulsive actuation was studied. A work-based cost model was used to calculate the net energetic cost of the gait. For many actuators, including human muscles, this cost model is a good simple choice, as it directly uses the energy supplied to the actuator for doing mechanical work. By including the actuator work efficiencies in the cost formulation, this cost model indirectly takes into account the cost of generating force/torque as well as the cost of internal losses, including energy conversion losses. The net energetic cost per step was formulated as the total sum of the cost of individual impulsive force and torques in one step. The work (and the cost) of the isolated impulsive swing-thrust torque can be simply calculated using the change in kinetic energy of the biped before and after the swing-thrust. This method, however, does not apply in general for the impulsive push-off force and swing retraction torque, as they can have overlap. This problem was overcome by introducing some novel concepts,

such as a partial overlap parameter and partial work done by each impulse. Consequently, I showed that for given push-off and retraction impulses, reducing the negative retraction work or increasing its positive work reduces the push-off work and can also reduce the net energetic cost. If the impulsive retraction torque is retracting ($\mathcal{R} > 0$), the minimum cost is achieved if it is applied completely after the impulsive push-off force. However, if the impulsive retraction torque is extending ($\mathcal{R} < 0$) the minimum cost is achieved when the impulsive push-off force is applied almost completely after the extending hip torque. Using this relative timing, the net energetic cost can be expressed in terms of only the step angle α , average walking speed V , and swing retraction impulse \mathcal{R} . So, a simple single-variable parameter optimization can be used to find the energy-optimal retraction impulse for any given step angle α and average walking speed V .

Chapter 7

APPROXIMATE ANALYTIC ANALYSIS OF THE IMPULSIVE WALKING MODEL

Although all the equations in Chapters 5 and 6 can be solved numerically, in order to gain more insight, I have found simple closed-form analytic solutions based on some approximations. Although approximate, these simple analytic solutions are very useful in predicting the influence of different parameters on the kinematics or energetics of a gait. In fact, most of the non-approximate analyses presented in Chapters 5, 6, and 8 were motivated by the observations from the approximate analytic solutions in this chapter. These solutions can also serve as a very good initial guess for accurate numerical optimizations. Moreover, they can be used to verify whether the results found by numerical optimization are indeed global optimums, and not just local minima/maxima.

The content of this chapter can be divided into four groups: Group 1) In Section 7.1 the main approximation used to simplify the governing equations is explained. With this approximation, the nonlinear and coupled equations of motion in passive single stance are simplified in Section 7.2, and then solved in Section 7.3. These solutions are key for the rest of the analyses in this chapter, since through them all gait variables can be related to the step angle and average walking speed. Group 2) Using the results of the sections in Group 1, the approximate constraints required to achieve a periodic walking gait are found in next four sections: First, the approximate swing-thrust and push-off impulses required for a periodic walk are calculated in Section 7.4. The range of possible retraction impulses for feasible periodic walking is approximated in Section 7.5, and the conditions for instantaneous support transfer are approximated in Section 7.6. In Section 7.7 the approximate minimum and

maximum walking speeds, and the approximate maximum step angle are derived. Group 3) The goal of the next two sections is to calculate the required parameters to approximate the energetic cost of the gait. Section 7.8 provides the approximate solutions for the velocities before and after the impulsive events. These solutions will be used in Section 7.9 to approximate the work and cost of each impulse. Group 4) Finally, using the results of the previous sections, the optimal retraction impulse that minimizes the energetic cost per step is derived. First, in Section 7.10 it is shown that the *extensional* retraction torque is not energetically optimal in the entire admissible region. Then, the optimal retraction impulse and retraction rates are calculated in Sections 7.11 and 7.12. At the end, the chapter is summarized in Section 7.13.

All the approximate analytic solutions presented in this chapter, except for the approximate stance leg dynamics in Section 7.2 are the contributions of this work. In fact, based on the best of my knowledge, this is the first time that approximate analytic solutions are provided for almost all gait parameters of a bipedal model with non-massless legs.

7.1 Small-Leg Mass Approximation

In this study, I partially adopt the approximation $\beta = m_{\text{leg}}/m_{\text{tot}} \ll 1$ from Garcia *et. al.* [46] to simplify the governing equations. This approximation is based on the fact that in many practical bipedal systems, including humans, the leg mass constitutes a small fraction of the total mass. For example, in humans only 16% of the total body mass is distributed in each leg. In [46] the above approximation was used for a model in which legs mass is concentrated at the feet. Although we can use the same approximation for the biped model in Fig. 5.1, the differences between the models motivate some modifications in the approximation. In particular, in Fig. 5.1 the leg mass can be arbitrarily distributed and the leg CoM is at an arbitrary distance b from the hip. Since b can vary among different models, any proposed

modifications in ‘ $\beta \ll 1$ ’ should somehow take this variability into account.

For the biped shown in Fig. 5.1, a candidate parameter equivalent to $\beta = m_{\text{leg}}/m_{\text{tot}}$ is

$$\lambda = \frac{m_{\text{leg}} b}{m_{\text{tot}} \ell}. \quad (7.1)$$

Because $m_{\text{tot}} \geq 2 m_{\text{leg}}$ and $\ell \geq b$, the range of λ is

$$0 \leq \lambda \leq 0.5. \quad (7.2)$$

$\lambda = 0$ corresponds to the case where the legs are massless ($m_{\text{leg}} = 0$), or the leg mass is concentrated at the top of the legs ($b = 0$). The maximum value of λ occurs when all the biped mass is equally concentrated at both feet ($m_{\text{tot}} = 2 m_{\text{leg}}$, and $b = \ell$). For humans and many robots λ is typically very small. For example, for the Cornell Ranger $\lambda = 0.07$ [12], and for the human subject data in Table 5.1, $\lambda \approx 0.06$.

The parameter λ determines the degree to which the motion of the biped’s CoM (or equivalently the motion of the stance leg) is influenced by the swing leg. For example, as mentioned above, for $\lambda = 0$ the legs either are massless or have their mass concentrated next to the hip. In either case, the motion of the biped’s CoM is completely decoupled from that of the swing leg. Since λ is typically small in many practical systems, including humans, it is reasonable to use $\lambda \approx 0$ to simplify the governing dynamics. This is equivalent to ignoring the small effects of the swing leg motion on CoM (stance leg) dynamics.

The advantage of using $\lambda \approx 0$ instead of $m_{\text{leg}}/m_{\text{tot}} \approx 0$ is that λ is typically smaller than $m_{\text{leg}}/m_{\text{tot}}$, so neglecting it provides more accurate approximations. For example, for the model parameters in Table 5.1, $\lambda = 0.06$, whereas $m_{\text{leg}}/m_{\text{tot}} = 0.16$.

7.2 Approximate Dynamics in Passive Single Stance

The governing dynamics in passive single stance is described by the EoM in (5.11) with details provided by (B.1) and (B.2). These equations are coupled and nonlinear, and cannot

be solved analytically in the general case. In order to find closed-form solutions for the stance leg and hip joint angles, *i.e.* $\theta(t)$ and $\phi(t)$, these equations are simplified in a few steps, explained below.

The parameter λ appears in the first row of (B.1) and (B.2), and, as explained in Section 7.1, quantifies the small coupling effects of the swing leg motion on stance leg dynamics. Using $\lambda \approx 0$, we can ignore these small coupling effects and focus on only the dominant behavior of the stance leg dynamics. In mathematical terms, because $\lambda \ll 1$, the terms in the EoM that include λ are much smaller than the others, and can be neglected. Note that in (B.1) the non-dimensional parameter δ is multiplied by λ . However, because δ is not a large number (typically smaller than 1, as shown in Section 5.1.1), it does not cause problems for the approximation above.

In the next step, I partially linearize the governing equations using first-order small angle approximations, e.g., $\sin \theta = \theta$, and $\cos \theta = 1$.

With the above small-leg mass and small angle approximations the simplified EoM can be expressed as

$$\ddot{\tilde{\theta}} - \frac{g}{\ell} \tilde{\theta} = 0, \quad (7.3)$$

$$\ddot{\tilde{\phi}} + \frac{g/\ell - \dot{\tilde{\theta}}^2}{\delta} \tilde{\phi} = -\frac{g}{\ell} \tilde{\theta}, \quad (7.4)$$

where the first equation is also used to simplify the second one. In this chapter, the accent ‘ \sim ’ is used over the approximate variables to distinguish them from non-approximate ones.

Equation (7.3) represents the approximate stance leg dynamics and describes the (linearized) motion of an isolated inverted pendulum. Equation (7.4) represents the approximate swing leg dynamics and describes the (linearized) motion of a non-inverted pendulum with a moving support. The centripetal acceleration of the hip along the vertical reduces the effective gravity on this pendulum (the coefficient of $\tilde{\phi}$), and the horizontal acceleration of the hip (the right hand side of (7.4)) acts as a forcing function for swing dynamics.

7.3 Approximate Analytic Solution of Passive Single Stance

7.3.1 Stance Leg Motion

As expected, the stance leg approximate dynamics are decoupled from the swing leg motion. Equation (7.3) is an ordinary differential equation subject to the boundary conditions defined at both ends of the passive swing: $\tilde{\theta}(0) = -\tilde{\theta}(T) = \alpha$ (see Section 5.3.1). The solution of this equation for $0 \leq t \leq T$ is:

$$\tilde{\theta}(t) = -\frac{\alpha}{\sinh(\omega_1 T/2)} \sinh(\omega_1(t - T/2)), \quad (7.5)$$

where

$$\omega_1 = \sqrt{g/\ell} \quad (7.6)$$

is the stance leg's approximate characteristic frequency. As for the exact solutions, $\tilde{\theta}(t)$ only depends on α and T , which are uniquely calculated from the step length and average forward speed ($\alpha = \sin^{-1}(0.5 D_{\text{step}}/\ell)$ and $T = D_{\text{step}}/V$). Interestingly, the approximate stance leg angle $\tilde{\theta}(t)$ has *odd symmetry* about mid-stance. This implies the *even symmetry* of the stance leg angular rate $\dot{\tilde{\theta}}(t)$ during passive single stance.

Verifying the accuracy of the approximate solution in (7.5), Fig. 7.1 compares the approximate analytic and the non-approximate numerical solutions of the stance leg angle, *i.e.* $\tilde{\theta}(t)$ and $\theta(t)$, for $V = 1.24$ m/s and $\alpha = 31.61^\circ$. The model parameters are those in Table 5.1. The evident accuracy of the approximate analytic solution in this figure holds for almost all other step angles and speeds in the admissible region (defined in Section 5.4.4), but degrades outside this region (which is not the focus of this work). Fig. 7.1 also shows that the odd symmetry of the stance leg leg angle in passive single stance is also valid for the non-approximate numerical solution.

Given the step angle α and average walking speed V (or the step period T), we can differentiate (7.5) to calculate $\dot{\tilde{\theta}}(t)$ and get the following approximate solution for the stance

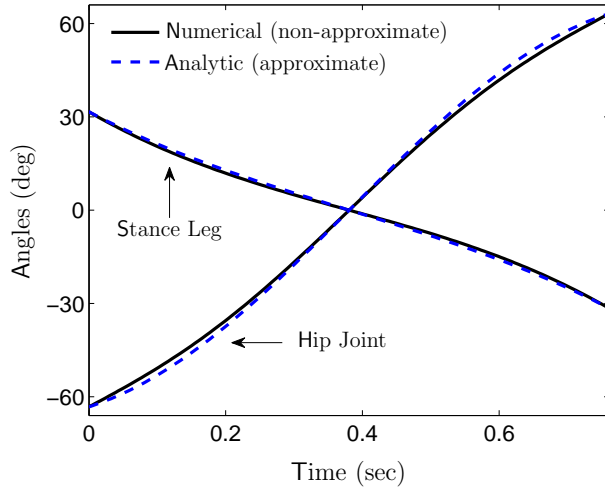


Figure 7.1: **Stance-leg and hip-joint angles** for walking at $V = 1.24$ m/s and $\alpha = 31.61^\circ$. The model parameters are those listed in Table 5.1. The evident accuracy of the approximate analytical solution in this figure holds also for almost all other step angles and speeds in the admissible region (defined in Section 5.4.4).

leg angular rate at the beginning and end of the symmetric passive swing:

$$\tilde{\theta}_0 = \tilde{\theta}_{t_{pr}^-} = -\frac{\omega_1 \alpha}{\tanh(\omega_1 T/2)} = -\frac{\omega_1 \alpha}{\tanh(\ell \omega_1 \sin \alpha / V)}. \quad (7.7)$$

This equation is the approximate closed-form version of (5.12).

In Fig. 7.2a, the approximate angular rate $\tilde{\theta}_0$ is compared to the original non-approximate $\dot{\theta}_0$ for different step angles and average walking speeds in the admissible region (see Section 5.4.4). The non-approximate $\dot{\theta}_0$ is calculated from the numerical solution of the original EoM, given in (5.11). As it is seen, the accuracy of the approximate solution is very good at small step angles and fast speeds, but it degrades at slower speeds and long steps. In this figure V_n is the maximum GRF-based speed limit, given by (5.36).

7.3.2 Swing Leg Motion

Although (7.4) is linear in $\tilde{\phi}$, it has a time-varying coefficient ($\tilde{\theta}$ is a function of time), which makes it difficult to solve. To overcome this difficulty I use another approximation: As seen in Fig 7.1, the variations of $\dot{\theta}(t)$ during single stance is small, so $\theta(t)$ can also be

approximated as a line: $\theta(t) \approx \rho t + \alpha$, where

$$\rho = -\frac{2\alpha}{T} = -\frac{\alpha V}{\ell \sin \alpha} \quad (7.8)$$

is the average angular rate of the stance leg. Now, by approximating $\tilde{\theta}$ with ρ (neglecting the small variations of $\tilde{\theta}$) the swing leg dynamics are simplified as

$$\ddot{\tilde{\phi}} + \omega_2^2 \tilde{\phi} = \omega_1^2 \tilde{\theta}, \quad (7.9)$$

where

$$\omega_2 = \sqrt{\frac{\omega_1^2 - \rho^2}{\delta}}. \quad (7.10)$$

Equivalent to ω_1 , the quantity ω_2 is the approximate effective characteristic frequency of the swing leg. Equation (7.10) is defined for $\omega_1^2 \geq \rho^2$, or equivalently when

$$V \leq V^\dagger(\alpha) = \ell \omega_1 \frac{\sin \alpha}{\alpha}. \quad (7.11)$$

We will see in Section 7.7.2 that the above condition is met for all feasible walking gaits (for all V less than the GRF-based maximum walking speed). Now, because $\tilde{\theta}$ is already known from (7.5), we can solve (7.9) subject to the boundary conditions $\tilde{\phi}(0) = -\tilde{\phi}(T) = -2\alpha$ (see Section 5.3.1). This results in

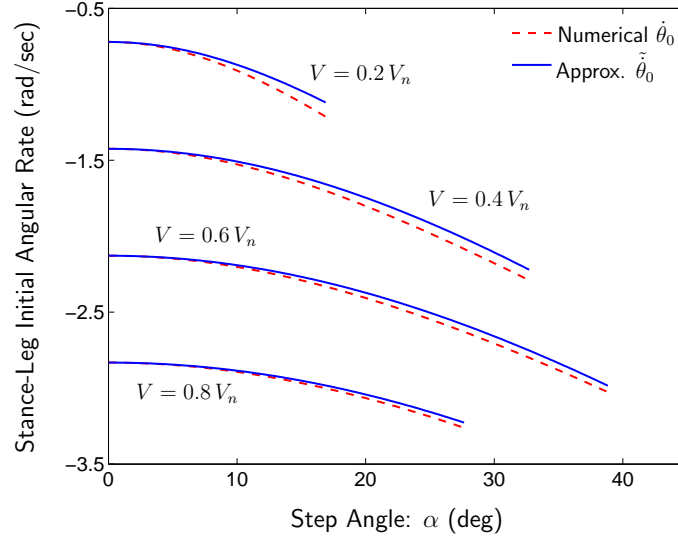
$$\tilde{\phi}(t) = (\eta - 1)\tilde{\theta}(t) + \frac{(1 + \eta)\alpha}{\sin(\omega_2 T/2)} \sin(\omega_2(t - T/2)), \quad (7.12)$$

where

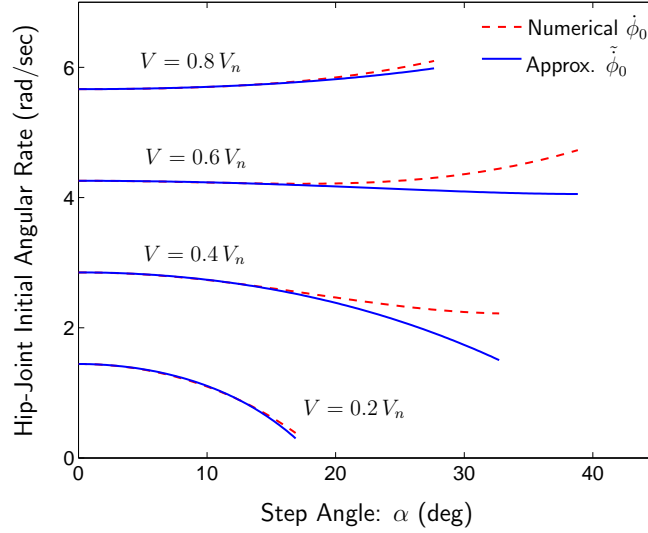
$$\eta = \frac{\omega_2^2}{\omega_1^2 + \omega_2^2}. \quad (7.13)$$

Similar to the stance leg angle, $\tilde{\phi}(t)$ has *odd symmetry* about mid-stance. Therefore, the hip rate $\dot{\tilde{\phi}}(t)$ has *even symmetry* in passive single stance. These symmetry properties were also observed for the numerical low-energy solution in Fig. 5.5.

Fig. 7.1 verifies the accuracy of the above approximate solution for $V = 1.24$ m/s and $\alpha = 31.61^\circ$, where $\tilde{\phi}(t)$ is compared against the corresponding symmetric numerical solution



(a)



(b)

Figure 7.2: **Comparison of the approximate (analytic) and the accurate (numerical) angular rates** at the beginning of the passive swing for different step angles and average walking speeds in the admissible region (see Fig. 5.8). The approximate angular rates $\tilde{\theta}_0$ and $\tilde{\phi}_0$ are calculated from the analytic solutions in (7.7) and (7.14). The non-approximate angular rates $\dot{\theta}_0$ and $\dot{\phi}_0$ are calculated using the numerical solution of the original EoM, given by (5.11). For clarity, the results for only four selected average speeds are shown. The calculations are based on the numerical values listed in Table 5.1. V_n is the maximum GRF-based speed limit, given by (5.36). For the respecting parameter set $V_n = 3.18$ m/s. The figures show that the accuracy of the approximate solutions is very good at small step angles, but it degrades at long steps and slow speeds.

of the original (non-approximate) EoM in (5.11). The accuracy of the approximate analytic solution observed in this figure holds for almost all other step angles and walking speeds in the admissible region, with some degradations at very long steps (where the small angle approximation used to derive (7.4) does not hold much).

Using $\tilde{\phi}(t)$ given by (7.12) and symmetry of the solution, the approximate hip rate at the beginning and end of the passive swing is calculated as

$$\tilde{\dot{\phi}}_0 = \tilde{\dot{\phi}}_{t_{\text{pr}}} = (\eta - 1) \tilde{\dot{\theta}}_0 + (1 + \eta) \frac{\omega_2 \alpha}{\tan(\omega_2 T/2)}, \quad (7.14)$$

where $\tilde{\dot{\theta}}_0$ is given by (7.7). This equation is the approximate closed-form version of (5.13).

Fig. 7.2b compares the approximate angular rate $\tilde{\dot{\phi}}_0$ with the non-approximate $\dot{\phi}_0$ at different step angles and average walking speeds in the admissible region (defined in Section 5.4.4). $\dot{\phi}_0$ is calculated using the numerical solution of the original EoM, given by (5.11). Other conditions are explained in the figure caption. As this figure shows, the accuracy of the approximate solution is very good at small step angles and fast speeds, but it degrades at slower speeds and long steps. This is not surprising, as the small-angle approximation used to linearize the dynamics does not hold much for large step angles.

The approximate analytic solutions of $\tilde{\dot{\theta}}_0$ and $\tilde{\dot{\phi}}_0$, given by (7.7) and (7.14), are key for the analyses in the rest of this chapter. In fact, all other gait parameters are related to the step angle α and average walking speed V *via* these solutions. In the next four sections, the approximate constraints required to achieve a periodic walking gait are calculated.

7.4 Approximate Swing-Thrust and Push-Off Impulses

The non-approximate swing-thrust and push-off impulses required for a periodic gait are given by (5.26) and (5.27). Simplifying those equations by neglecting small terms that

involve λ gives the corresponding approximate impulses:

$$\tilde{\mathcal{S}} = \delta m_{\text{leg}} \ell b \tilde{\Omega}, \quad (7.15)$$

$$\tilde{\mathcal{P}} = - \left(m_{\text{tot}} \ell \tilde{\dot{\theta}}_0 + \frac{\mathcal{R}}{\ell} \right) \tan \alpha, \quad (7.16)$$

where

$$\tilde{\Omega}(\alpha, V) = \tilde{\dot{\phi}}_0 + \frac{2 \sin^2 \alpha}{\delta} \tilde{\dot{\theta}}_0 \quad (7.17)$$

is the approximate change in the hip rate due to the swing-thrust impulse [see equation (7.38)]. In the above equations $\tilde{\dot{\theta}}_0$ and $\tilde{\dot{\phi}}_0$ are given by (7.7) and (7.14). The accuracy of the above approximate solutions will be verified in Chapter 8.

For given biped parameters, the approximate swing-thrust impulse in (7.15) is solely a function of step angle α and average forward speed V ($\tilde{\dot{\theta}}_0$ and $\tilde{\dot{\phi}}_0$ are fully determined by α and V). Although $\tilde{\mathcal{S}}$ is not a function of retraction impulse \mathcal{R} , there would be a small dependency between them if λ was not neglected.

Using (7.16) we can find

$$\frac{\partial \tilde{\mathcal{P}}}{\partial \mathcal{R}} = - \frac{\tan \alpha}{\ell} < 0. \quad (7.18)$$

In other words, the approximate push-off impulse decreases with the retraction impulse. This observation motivates further investigations with non-approximate equations and leads to the discovery of one of the novel advantages of active swing-leg retraction, which will be presented in Chapter 8.

The push-off impulse calculated using the powered simplest walking model [47] (effectively massless legs) is $\mathcal{P} = -m_{\text{tot}} \ell \dot{\theta}_0 \tan \alpha$. Although $\tilde{\mathcal{P}}$ in (7.16) gives the same value if the legs are massless ($\mathcal{R} = 0$ for massless legs), it provides a more accurate prediction for realistic models with non-negligible leg mass.

7.5 Approximate Minimum and Maximum Retraction Impulse

In this section the approximate range of possible retraction impulses for feasible periodic walking is calculated. The lower and upper bounds calculated here will be used in Section 7.11 in the search for the optimal retraction impulse.

7.5.1 Ensuring Heel-Strike and the Minimum Required Retraction Impulse

As discussed in Section 5.3.2, ensuring heel-strike immediately after the impulsive push-off and retraction, *i.e.* at t_{pr}^+ , requires that the swing foot moves downward at t_{pr}^+ . This condition was expressed by (5.20) as a negative swing foot velocity prior to heel-strike:

$$\dot{y}_{f_{\text{swing}}}(t_{\text{pr}}^+) = \dot{\ell}_{t_{\text{pr}}^+} \cos \alpha + \ell \sin \alpha \left(2 \dot{\theta}_{t_{\text{pr}}^+} + \dot{\phi}_{t_{\text{pr}}^+} \right) \leq 0. \quad (7.19)$$

In a periodic walk with given step angle α and average speed V , we can use the push-off-retraction velocity map in (5.14), the push-off impulse in (5.27), and $\lambda \approx 0$ to simplify and approximate the above equation as

$$\dot{y}_{f_{\text{swing}}}(t_{\text{pr}}^+) \approx \left(-\frac{\mathcal{R}}{\delta m_{\text{leg}} b \ell} + \tilde{\Omega} + \tilde{\theta}_0 \right) \ell \sin \alpha \leq 0. \quad (7.20)$$

Thus, the approximate condition for ensuring heel-strike in a periodic gait is

$$\mathcal{R} \geq \delta m_{\text{leg}} \ell b \left(\tilde{\Omega} + \tilde{\theta}_0 \right) = \tilde{\mathcal{R}}_{\text{min}}(\alpha, V), \quad (7.21)$$

where $\tilde{\theta}_0$ and $\tilde{\Omega}$ are given by (7.7) and (7.17). At $\mathcal{R} = \tilde{\mathcal{R}}_{\text{min}}$ the leading leg touches the ground with (approximately) zero vertical velocity, but since its horizontal velocity is still non-zero the foot-ground contact is collisional and includes energy loss.

Equation (7.21) gives the approximate minimum retraction impulse required for periodic walking. Fig. 7.3 shows the contour lines of $\tilde{\mathcal{R}}_{\text{min}}$ for step angles and speeds in the ‘approximate admissible region’ (defined in Section 7.7.3). If the maximum *available* retraction impulse is not large enough to satisfy (7.21) for some range of α and V , periodic walking

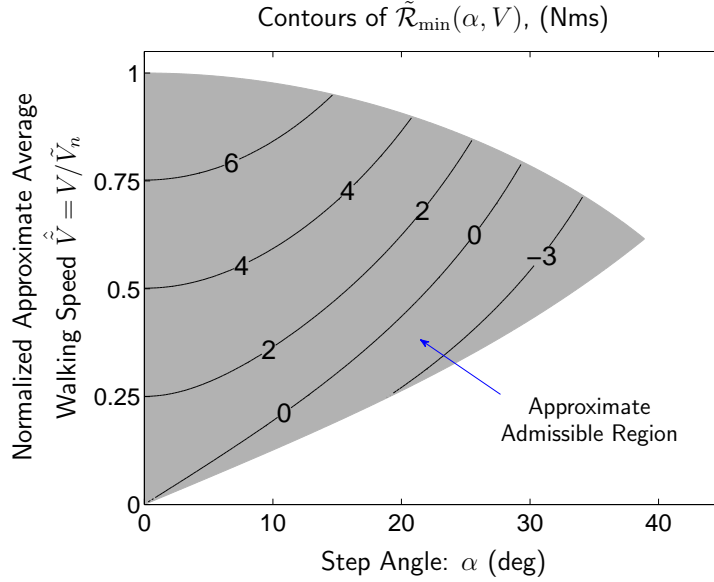


Figure 7.3: **Contour lines of the approximate minimum retracting impulse, $\tilde{\mathcal{R}}_{\min}$, required to enforce heel-strike.** The shaded area is the approximate admissible region, defined in Section 7.7.3. The approximate solution predicts that for step angles and speeds above the contour line $\tilde{\mathcal{R}}_{\min} = 0$ a retracting hip torque ($\mathcal{R} > 0$) is required at the end of swing phase to ensure heel-strike. The vertical axis is the normalized average walking speed $\hat{V} = V/\tilde{V}_n$, where \tilde{V}_n is given by (7.32). The model parameter values are those in Table 5.1.

may not be achieved in some portion of the admissible region. In particular, the approximate solution *predicts* that for step angles and speeds above the contour line $\tilde{\mathcal{R}}_{\min} = 0$ in Fig. 7.3, a retracting hip torque ($\mathcal{R} > 0$) is necessary at the end of swing phase to ensure heel-strike. In other words, periodic walking is likely not feasible in that region without a retracting hip torque, at least to the extent that is predicted by the approximate solution. This observation leads to discovering one of the important advantages of swing-leg retraction which is discussed in the next chapter.

7.5.2 Approximate Maximum Allowed Retraction Impulse

Since the push-off impulse cannot be negative, we can use the constraint $\tilde{\mathcal{P}} \geq 0$ with $\tilde{\mathcal{P}}$ given by (7.16), to find the approximate maximum retraction impulse at any given step angle α

and average walking speed V . This results in

$$\mathcal{R} \leq \tilde{\mathcal{R}}_{\max}(\alpha, V) = -m_{\text{tot}} \ell^2 \tilde{\theta}_0, \quad (7.22)$$

where $\tilde{\theta}_0$ is given by (7.7). This equation is the approximate closed-form version of (5.28). In Section 7.11 we will see that the above upper bound on \mathcal{R} is not an active constraint for energetic cost minimization purposes, and (7.22) is spontaneously satisfied for energy optimal gaits.

7.6 Approximate Condition for Instantaneous Support Transfer

The impulsive walking gait includes an instantaneous support transfer (instantaneous double-support) in which the previous support leg (the trailing leg) loses its contact with the ground immediately after the collisional heel-strike, and the support is transferred to the leading leg. As discussed in Section 5.3.2 and stated in (5.21), this is met only if the vertical velocity of the trailing foot immediately after heel-strike is positive:

$$\dot{y}_{f_{\text{trailing}}}(t_{\text{h}}^+) = -\ell \sin \alpha \left(2\dot{\theta}_{t_{\text{h}}^+} + \dot{\phi}_{t_{\text{h}}^+} \right) > 0. \quad (7.23)$$

In order to find the approximate requirements that satisfy this condition, we can use the heel-strike velocity mapping in (5.19), the push-off impulse relation in (5.27), and $\lambda \approx 0$ to approximate $\dot{y}_{f_{\text{trailing}}}(t_{\text{h}}^+)$ as below:

$$\dot{y}_{f_{\text{trailing}}}(t_{\text{h}}^+) \approx -\frac{2\ell \sin \alpha (\delta - \sin^2 \alpha)}{\delta} \tilde{\theta}_0. \quad (7.24)$$

In the above equation, $\tilde{\theta}_0$ is always negative [see (7.7)]. Thus, the condition of instantaneous double-support can be approximately expressed as the following upper bound on the step angle:

$$\alpha \leq \sin^{-1} \sqrt{\delta}. \quad (7.25)$$

For model parameter data in Table 5.1, this upper bound becomes 0.91^{rad} (52°) which is greater than the maximum possible step angle ($0.72^{\text{rad}} = 41.39^\circ$) in the admissible region

(see Section 7.7.4). Thus for this data set the toe-off condition in (7.23) is not a limiting constraint, and instantaneous double-support is spontaneously obtained for all α and V in the admissible region. In other words, in the process of calculating the optimal retraction impulse in (6.73) or in Section 7.11, the toe-off constraint can be dropped from the optimization problem. If for some models δ is too small (leg mass is concentrated close to the leg CoM that is close to the hip) the constraint in (7.25) may reduce the size of admissible region.

7.7 Approximate Admissible Region

In Section 5.4.4, the admissible region was defined as the area in the α - V plane that is enclosed between the step-angle dependent minimum and maximum average walking speeds, given by (5.29) and (5.31). In the following, approximate solutions for those boundaries are provided. These solutions will be used to define the ‘approximate admissible region’, the focus of the analyses in this chapter.

7.7.1 Approximate Minimum Allowed Average Walking Speed

In (5.29) the minimum allowed walking speed was defined based on the condition of non-negative swing-thrust impulse \mathcal{S} . Rewriting (5.29) by substituting $V_{\min}(\alpha)$ and \mathcal{S} with their approximate versions $\tilde{V}_{\min}(\alpha)$ and $\tilde{\mathcal{S}}$, where $\tilde{\mathcal{S}}$ is given by (7.15), the approximate minimum allowed average walking speed $\tilde{V}_{\min}(\alpha)$ can be calculated from

$$V \geq \tilde{V}_{\min}(\alpha) \quad : \quad \tilde{\Omega}(\alpha, \tilde{V}_{\min}) = 0, \quad (7.26)$$

where $\tilde{\Omega}(\alpha, V)$ is given by (7.17). Therefore, in the approximate admissible region $\tilde{\Omega} \geq 0$.

7.7.2 Approximate GRF-Based Maximum Average Walking Speed

In (5.31) the upper bound of the average walking speed is defined based on the condition of non-negative centripetal GRF, given by (5.30). Rewriting (5.30) in terms of λ gives:

$$\text{GRF}_a = m_{\text{tot}} \ell \left(\omega_1^2 \cos \theta - \dot{\theta}^2 \right) + m_{\text{tot}} \ell \lambda \left(\dot{\theta}^2 + \cos \phi (\dot{\theta} + \dot{\phi})^2 + \sin \phi (\ddot{\phi} + \ddot{\theta}) \right), \quad (7.27)$$

where ω_1 is given by (7.6). For $\lambda \approx 0$ the condition $\text{GRF}_a \geq 0$ is approximated as

$$\tilde{\theta}^2(t) \leq \omega_1^2 \cos \tilde{\theta}(t) \quad \text{for all } t \text{ in } 0 < t < T. \quad (7.28)$$

Although this inequality should be held during the entire passive single stance, it is only necessary to check it at either end of this period. This is because of the symmetry of the stance leg motion, and that for all t in passive single stance the following are valid:

1. $\dot{\theta}(t)^2 \leq \dot{\theta}_0^2$, since the stance leg moves slower as it approaches vertical, and speeds up as it falls.
2. $|\theta(t)| \leq \alpha$, and thus $\cos \alpha \leq \cos \theta(t)$.

Based on the above, equation (7.28) can be reduced to

$$\tilde{\theta}_0^2 \leq \omega_1^2 \cos \alpha. \quad (7.29)$$

The above inequality can be combined with the closed-form solution of $\tilde{\theta}_0$ in (7.7) to find

$$V \leq \tilde{V}_{\text{max}}(\alpha) = \frac{\sin \alpha}{\tanh^{-1}(\alpha/\sqrt{\cos \alpha})} \ell \omega_1. \quad (7.30)$$

The step-angle dependent $\tilde{V}_{\text{max}}(\alpha)$ is the approximate GRF-based walking speed limit.

Defining $\tilde{\omega}_n$ and \tilde{V}_n respectively as the maximum $|\tilde{\theta}_0(\alpha, V)|$ and maximum $\tilde{V}_{\text{max}}(\alpha)$ for all feasible walking gaits, we can use (7.29) and (7.30) to find:

$$\tilde{\omega}_n = \max_{\alpha, V} |\tilde{\theta}_0| = \omega_1, \quad (7.31)$$

$$\tilde{V}_n = \max_{\alpha} \tilde{V}_{\text{max}}(\alpha) = \tilde{V}_{\text{max}}(0) = \ell \omega_1 = \ell \tilde{\omega}_n. \quad (7.32)$$

Recognizing that the above results are achieved using $\lambda \approx 0$, $\tilde{\omega}_n$ and \tilde{V}_n are consistent with their non-approximate versions, *i.e.* $\omega_n = \max |\dot{\theta}_0| = \omega_1 / \sqrt{1 - 2\lambda}$ and $V_n = \max V_{\max}(\alpha) = \ell \omega_n$, found in (5.35) and (5.36).

Finally, it can be easily verified that for all $\alpha > 0$: $\alpha \leq \tanh^{-1}(\alpha / \sqrt{\cos \alpha})$. Thus, the approximate GRF-based walking speed limit $\tilde{V}_{\max}(\alpha)$, given in (7.30), always satisfies:

$$\tilde{V}_{\max}(\alpha) \leq V^\dagger(\alpha), \quad (7.33)$$

where $V^\dagger(\alpha)$ is given by (7.11) and is the maximum speed for which the approximate swing leg frequency ω_2 , given by (7.10), is defined. In other words, for all α and V for which periodic walking is feasible, ω_2 exists, and all the above approximate solutions that include $\tilde{\phi}(t)$ or $\tilde{\phi}_0$ are valid.

7.7.3 Approximate Admissible Region

Equivalent to the original admissible region, defined in Section 5.4.4, the approximate admissible region is defined as the set of step angles α and average walking speeds V that satisfy

$$\tilde{V}_{\min}(\alpha) \leq V \leq \tilde{V}_{\max}(\alpha), \quad (7.34)$$

where $\tilde{V}_{\min}(\alpha)$ and $\tilde{V}_{\max}(\alpha)$ are given by (7.26) and (7.30).

Fig. 7.4 compares the approximate and the non-approximate admissible regions, calculated for the model parameters in Table 5.1. According to this figure, the approximate admissible region (hatched region) covers the majority of the non-approximate (solid gray) admissible region, and thus has a good accuracy. The upper boundary of the admissible region is the GRF-based walking speed limit, given by (5.31). According to Fig. 7.4 this speed limit is well approximated by the corresponding analytic solution given by (7.30).

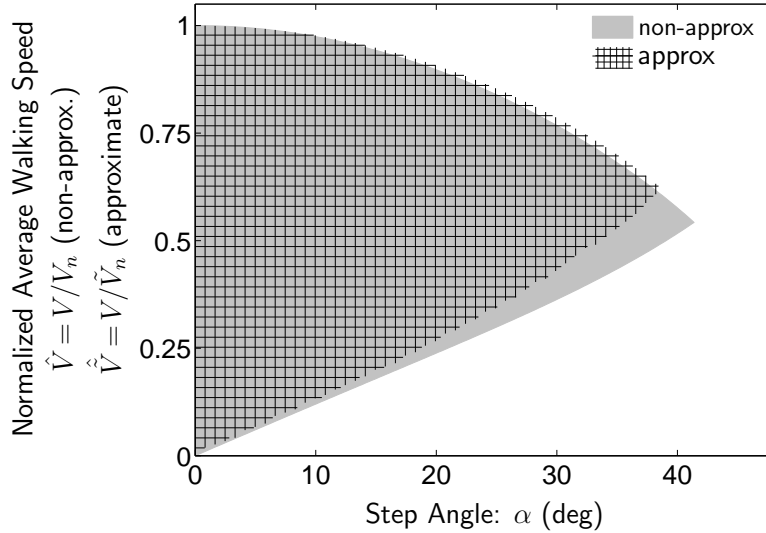


Figure 7.4: **Comparison of the approximate and non-approximate admissible regions.** The shaded area corresponds to the numerically calculated admissible region, defined in Section 5.4.4. The hatched area is the approximate admissible region defined by (7.26) and (7.30). The vertical axis is the normalized average walking speed. For the non-approximate numerical solution, the normalizing speed \hat{V}_n is given by (5.36). For the approximate solution, the normalizing speed \tilde{V}_n is given by (7.32). For the numerical values used for this figure (see Table 5.1), $V_n = 3.18$ m/s, and $\tilde{V}_n = 2.97$ m/s

7.7.4 Approximate Maximum Walking Step Angle

The approximate maximum walking speed in (7.30) can also be used to estimate the maximum possible step angle in periodic walking. That equation is valid only for $\alpha \leq \sqrt{\cos \alpha}$. Solving the latter for the equality case gives the approximate maximum possible step angle as $\tilde{\alpha}_{\max} \cong 0.82^{\text{rad}}$ (47.2°). This value is very close to the accurate maximum step angle of a biped with *massless* legs, which is $\alpha_{\max} \Big|_{m_{\text{leg}}=0} = \cos^{-1}(2/3) \cong 0.84^{\text{rad}}$ (48.2°) [95]. At both these step angles the corresponding average walking speed V is zero. Note that this can be accepted only if the defined lower bound of walking speed, given by (5.29) or (7.26), is not considered. In fact, the above (unconstrained) maximum step angles $\tilde{\alpha}_{\max}$ and $\alpha_{\max} \Big|_{m_{\text{leg}}=0}$ are bigger than the one achievable in the admissible region, which is $\alpha_{\max} = 0.72^{\text{rad}}$ (41.39°) (see Fig. 7.4).

Now, I intend to approximate the energetic cost of the gait to calculate the approximate

energy-optimal retraction impulse. For this purpose, the approximate work of each impulse should be calculated. This, in turn, requires to calculate the approximate velocities at phase transitions. This velocity and work calculation is the subject of the next two sections.

7.8 Approximate Velocities Before and After the Impulsive Actions

In this section the approximate analytic solutions for the velocities before and after the impulsive swing thrust torque, push-off force, and swing retraction torque are calculated.

7.8.1 Approximate Angular Rates Before and After the Impulsive Swing-Thrust Torque

According to the periodicity conditions in (5.24) and (5.25), the angular velocities after the impulsive swing thrust, *i.e.* at t_s^+ , is equal to those at the beginning of the passive swing. This equality also holds for the approximate velocities. Thus

$$\tilde{\theta}_{t_s^+} = \tilde{\theta}_0, \quad (7.35)$$

$$\tilde{\phi}_{t_s^+} = \tilde{\phi}_0, \quad (7.36)$$

where $\tilde{\theta}_0$ and $\tilde{\phi}_0$ are given by (7.7) and (7.14). The velocity mapping of the impulsive swing-thrust is given by (5.23). Approximating this equation with $\lambda \approx 0$, and replacing \mathcal{S} , $\dot{\theta}_{t_s^+}$, and $\dot{\phi}_{t_s^+}$ with their approximations, *i.e.* $\tilde{\mathcal{S}}$, $\tilde{\theta}_{t_s^+}$, and $\tilde{\phi}_{t_s^+}$ given by (7.15), (7.35), and (7.36), we can find the approximate angular rates before the impulsive swing thrust as

$$\tilde{\theta}_{t_s^-} = \tilde{\theta}_0 - \frac{1 - \cos 2\alpha/\delta}{m_{\text{tot}} \ell^2} \tilde{\mathcal{S}} \Big|_{\lambda \approx 0} = \tilde{\theta}_0, \quad (7.37)$$

$$\tilde{\phi}_{t_s^-} = \tilde{\phi}_0 - \frac{\tilde{\mathcal{S}}}{\delta m_{\text{leg}} b \ell} = \tilde{\phi}_0 - \tilde{\Omega}, \quad (7.38)$$

Using the definition of $\tilde{\Omega}$ in (7.17), equation (7.38) can also be written as

$$\tilde{\phi}_{t_s^-} = -\frac{2 \sin^2 \alpha}{\delta} \tilde{\theta}_0. \quad (7.39)$$

Examining the expression of $\tilde{\theta}_0$ in (7.7) shows that in all cases $\tilde{\theta}_0 < 0$, leading to $\tilde{\phi}_{t_s^-} > 0$. On the other hand, in the approximate admissible region $\tilde{\Omega} \geq 0$ (see Section 7.7.1). These last two inequalities, together with (7.38) result in $\tilde{\phi}_0 > 0$. Thus, in the entire approximate admissible region $\tilde{\phi}_{t_s^+} > 0$ and also $\tilde{\phi}_{t_s^-} > 0$. This result will help us calculate the positive swing-thrust work in Section 7.9.1.

7.8.2 Approximate Velocities Before and After the Impulsive Push-Off Force

As discussed in the previous chapter, in energy optimal gaits the impulsive push-off force always starts immediately after the passive swing, at t_{pr}^- . In this case, the approximate velocities before the impulsive push-off force, *i.e.* at t_p^- , are equal to those at the end of passive swing, which are given by (7.7), (7.14), and

$$\tilde{\ell}_{t_p^-} = \dot{\ell}_{t_{pr}^-} = 0. \quad (7.40)$$

The velocities after the impulsive push-off force depends on the relative timing of the push-off and retraction impulses. As discussed in Section 6.4, for a *retracting* \mathcal{R} , *i.e.* $\mathcal{R} > 0$, energetic cost is minimized when the impulsive push-off force completely precedes the impulsive retraction torque. With this optimal relative timing, the velocities immediately after \mathcal{P} (at t_p^+) can be calculated by substituting $\mathcal{R} = 0$ in the push-off-retraction velocity mapping, given by (5.14). Now, using $\lambda \approx 0$, we can find

$$\tilde{\theta}_{t_p^+} = \tilde{\theta}_0, \quad (7.41)$$

$$\tilde{\phi}_{t_p^+} = \tilde{\phi}_0 - \frac{\sin 2\alpha}{\delta m_{tot} \ell} \tilde{\mathcal{P}}, \quad (7.42)$$

$$\tilde{\ell}_{t_p^+} = \frac{\tilde{\mathcal{P}}}{m_{tot}}, \quad (7.43)$$

where the approximate push-off impulse $\tilde{\mathcal{P}}$ is given by (7.16), and the angular velocities $\tilde{\theta}_0$ and $\tilde{\phi}_0$ are given by (7.7) and (7.14). To simplify the calculations of the retraction work in Section 7.9.3, it is better to express $\tilde{\phi}_{t_p^+}$ in terms of the retraction impulse \mathcal{R} . Substituting

for $\tilde{\mathcal{P}}$ from (7.16), and using the formula of $\tilde{\Omega}$ in (7.17), equation (7.42) is further simplified as

$$\dot{\phi}_{t_p^+}^{\tilde{}} = \tilde{\Omega} + \frac{2 \sin^2 \alpha}{\delta m_{\text{tot}} \ell^2} \mathcal{R}. \quad (7.44)$$

Note that with the optimal relative timing of impulsive push-off force and *retracting* hip torque (*i.e.* push-off then retraction) the impulsive retraction torque has not started at t_p^+ . However, from (7.44) it appears that \mathcal{R} can change velocities even before the retraction torque begins! This is because in a periodic gait the required push-off impulse \mathcal{P} changes with \mathcal{R} , as shown in (5.27). So, even when \mathcal{R} is applied completely after t_p^+ , it can indirectly influence $\dot{\phi}_{t_p^+}^{\tilde{}}$ *via* the impulse \mathcal{P} .

The post-push-off leg extension rate calculated using the powered simplest walking model [47] (effectively massless legs) is $\dot{\ell}_{t_p^+} = \mathcal{P}/m_{\text{tot}}$. Equation (7.43) gives the same result if the legs are massless (for massless legs $\tilde{\mathcal{P}}$ is equal to the push-off impulse \mathcal{P} of the powered simplest walking model; see Section 7.4 for more details). However, with $\tilde{\mathcal{P}}$ given by (7.16), equation (7.43) provides a more accurate prediction for realistic models with non-negligible distributed leg mass.

Following the procedure used to derive (7.41)-(7.43), we can also find the approximate post-push-off velocities for an extensional impulsive retraction torque, *i.e.* $\mathcal{R} < 0$. However, as it will be shown in Section 7.10, the extensional retraction torque is not energetically optimal in the admissible region, and thus no effort is made here to calculate those velocities.

7.8.3 Approximate Velocities Before and After the Impulsive Retraction Torque

Similar to the previous section, only a *retracting* hip torque, *i.e.* $\mathcal{R} > 0$, is considered here, and the analysis of an *extensional* retraction torque, *i.e.* $\mathcal{R} < 0$, is left for Section (7.10).

For energy optimal gaits, in which impulsive $\mathcal{R} > 0$ is applied completely after impulsive \mathcal{P} , the velocities immediately before \mathcal{R} , *i.e.* at t_p^- , are equal to those in (7.41)-(7.44).

Using the same relative timing of \mathcal{P} and \mathcal{R} as above, the velocities immediately after the impulsive *retracting* hip torque, *i.e.* at $t_r^+ \equiv t_{pr}^+$, are given by the push-off-retraction velocity mapping in (5.14). Approximating this equation using $\lambda \approx 0$ results in

$$\tilde{\theta}_{t_r^+} = \tilde{\theta}_{t_{pr}^+} = \tilde{\theta}_0 + \frac{1 - \cos 2\alpha/\delta}{m_{\text{tot}} \ell^2} \mathcal{R}, \quad (7.45)$$

$$\tilde{\phi}_{t_r^+} = \tilde{\phi}_{t_{pr}^+} = \tilde{\phi}_0 - \frac{\sin 2\alpha}{\delta m_{\text{tot}} \ell} \tilde{\mathcal{P}} - \frac{\mathcal{R}}{\delta m_{\text{leg}} \ell b}, \quad (7.46)$$

$$\tilde{\ell}_{t_r^+} = \tilde{\ell}_{t_{pr}^+} = \frac{\tilde{\mathcal{P}}}{m_{\text{tot}}} + \frac{\sin 2\alpha}{\delta m_{\text{tot}} \ell} \mathcal{R}, \quad (7.47)$$

where the approximate push-off impulse $\tilde{\mathcal{P}}$ is given by (7.16), and the angular velocities $\tilde{\theta}_0$ and $\tilde{\phi}_0$ are given by (7.7) and (7.14). To simplify the work calculations in Section 7.9.3, it is better to express $\dot{\phi}_{t_r^+}$ in terms of the retraction impulse \mathcal{R} . After substituting for $\tilde{\mathcal{P}}$ from (7.16), we can further simplify (7.46) using $\lambda \approx 0$ and the formula of $\tilde{\Omega}$ in (7.17). This results in

$$\tilde{\phi}_{t_r^+} = \tilde{\phi}_{t_{pr}^+} = \tilde{\Omega} - \frac{\mathcal{R}}{\delta m_{\text{leg}} b \ell}. \quad (7.48)$$

7.9 Approximate Work and Energetic Costs

As shown in the previous chapter, for $\mathcal{R} > 0$ energetic cost is minimized when the impulsive retraction torque is isolated from the impulsive push-off force and is applied after it is completed. With this relative timing, all three impulsive actuations, *i.e.* the impulsive swing thrust and swing retraction torques and the impulsive push-off force, are isolated, and the work equations in (6.3) and (6.4) can be used for all the three impulses. For $\mathcal{R} < 0$, however, energy optimal gaits include overlapping impulses. But, as will be shown in Section 7.10, $\mathcal{R} < 0$ is never energetically optimal inside the admissible region. Hence, in this section, the approximate work and energetic cost calculations are only provided for gaits with $\mathcal{R} \geq 0$, and subject to the optimal push-off-then-retraction sequence.

7.9.1 Approximate Work and Energetic Cost of Impulsive Swing Thrust Torque

Using (6.3) with $\mathcal{I} = \tilde{\mathcal{S}}$ from (7.15), $\dot{q}^+ = \tilde{\phi}_{t_s^+}$ from (7.36), and $\dot{q}^- = \tilde{\phi}_{t_s^-}$ from (7.39), the approximate net swing-thrust work is calculated as

$$\begin{aligned}\tilde{W}_S &= \frac{1}{2} \tilde{\mathcal{S}} \left(\tilde{\phi}_{t_s^-} + \tilde{\phi}_{t_s^+} \right) \\ &= \frac{1}{2} \delta m_{\text{leg}} b \ell \tilde{\Omega} \left(\tilde{\phi}_0 - \frac{2 \sin^2 \alpha}{\delta} \tilde{\theta}_0 \right),\end{aligned}\quad (7.49)$$

where $\tilde{\theta}_0$, $\tilde{\phi}_0$, and $\tilde{\Omega}$ are given by (7.7), (7.14), and (7.17). Using the formula of $\tilde{\Omega}$ in (7.17), the above equation can be further simplified as

$$\tilde{W}_S = \frac{1}{2} \delta m_{\text{leg}} b \ell \left(\tilde{\phi}_0^2 - \frac{4 \sin^4 \alpha}{\delta^2} \tilde{\theta}_0^2 \right). \quad (7.50)$$

To approximate the energetic cost, we also need to find the positive and negative work. As discussed in Sections 7.7.1 and 7.8.1, in the approximate admissible region (i) $\tilde{\mathcal{S}} \geq 0$, and (ii) the approximate hip rate before and after the impulsive swing-thrust torque (and therefore throughout it) is positive. Therefore, the impulsive $\tilde{\mathcal{S}}$ does only positive work in the approximate admissible region. This implies $\tilde{W}_S^+ = \tilde{W}_S$, and $\tilde{W}_S^- = 0$.

Now, using the cost equation in (6.6), the approximate cost associated with $\tilde{\mathcal{S}}$ is

$$\tilde{E}_S = c_1 \tilde{W}_S. \quad (7.51)$$

Because \tilde{W}_S does not depend on the retraction impulse \mathcal{R} , \tilde{E}_S is also independent of \mathcal{R} . This result will be used in Sections 7.10 and 7.11 to simplify the derivation of the approximate optimal retraction impulse.

7.9.2 Approximate Work and Energetic Cost of Impulsive Push-Off Force

Since the optimal gaits with $\mathcal{R} > 0$ include isolated impulses, we can use (6.3), with $\mathcal{I} = \tilde{\mathcal{P}}$ from (7.16), $\dot{q}^- = \tilde{\ell}_{t_p^-}$ from (7.40), and $\dot{q}^+ = \tilde{\ell}_{t_p^+}$ from (7.43), to calculate the approximate net

push-off work as

$$\begin{aligned}\tilde{W}_{\mathcal{P}} &= \frac{\tilde{\mathcal{P}}^2}{2 m_{\text{tot}}} \\ &= \frac{\left(m_{\text{tot}} \ell \tilde{\theta}_0 + \mathcal{R}/\ell\right)^2}{2 m_{\text{tot}}} \tan^2 \alpha.\end{aligned}\quad (7.52)$$

It was shown in the previous chapter that in energy optimal gaits the impulsive push-off force does only positive work. Thus, the approximate energetic cost of push-off is calculated according to (6.68) as

$$\tilde{E}_{\mathcal{P}} = c_1 \tilde{W}_{\mathcal{P}}. \quad (7.53)$$

7.9.3 Approximate Work and Energetic Cost of Impulsive Swing Retraction Torque

With the optimal push-off-then-retraction sequence (isolated impulses), the work formula in (6.3) can be used with $\mathcal{I} = -\mathcal{R}$ (the positive directions of \mathcal{R} and $\dot{\phi}$ are opposite), $\dot{q}^- = \tilde{\phi}_{t_r^-} = \tilde{\phi}_{t_p^+}$ from (7.44), and $\dot{q}^+ = \tilde{\phi}_{t_r^+}$ from (7.48), to calculate the approximate net retraction work as

$$\tilde{W}_{\mathcal{R}} = -\frac{1}{2} \mathcal{R} \left(\tilde{\phi}_{t_r^-} + \tilde{\phi}_{t_r^+} \right) \quad (7.54)$$

$$= -\mathcal{R} \tilde{\Omega} + \frac{\mathcal{R}^2}{2 \delta m_{\text{leg}} b \ell}. \quad (7.55)$$

Note that another round of approximation with $\lambda \approx 0$ was used to simplify (7.54) to (7.55).

In the approximate admissible region $\tilde{\Omega} \geq 0$, so the pre-retraction hip rate $\tilde{\phi}_{t_r^-}$ ($= \tilde{\phi}_{t_p^+}$), given by (7.44), is positive for all $\mathcal{R} > 0$. This implies that for any step angle α and average walking speed V in the approximate admissible region the impulsive retraction torque always *starts with doing negative work*. For $0 \leq \mathcal{R} < \tilde{\mathcal{R}}^\ddagger$, where

$$\tilde{\mathcal{R}}^\ddagger = \delta m_{\text{leg}} \ell b \tilde{\Omega}, \quad (7.56)$$

the post-retraction hip rate $\tilde{\phi}_{t_r^+}$, given by (7.48), is also positive, and the impulsive retraction torque does *only negative work*. For $\mathcal{R} > \tilde{\mathcal{R}}^\ddagger$, however, the impulsive retraction torque does

some positive work at the end, which can be calculated using (6.4) with the same substitutions used for (7.54). Therefore, both approximate positive and negative retraction works are fully resolved in the entire approximate admissible region. That is to say, given the step angle α and average walking speed V in the approximate admissible region

$$\tilde{W}_{\mathcal{R}}^+ = \begin{cases} 0 & \text{if } 0 \leq \mathcal{R} \leq \tilde{\mathcal{R}}^\ddagger, \\ \tilde{W}_{\mathcal{R}} + \frac{\delta m_{\text{leg}} b \ell}{2} \tilde{\Omega}^2 & \text{if } \mathcal{R} > \tilde{\mathcal{R}}^\ddagger, \end{cases} \quad (7.57)$$

and $\tilde{W}_{\mathcal{R}}^- = \tilde{W}_{\mathcal{R}} - \tilde{W}_{\mathcal{R}}^+$, where $\tilde{W}_{\mathcal{R}}$ is given by (7.55). Interestingly, except for the case where $\tilde{W}_{\mathcal{R}}^+ = 0$, $\tilde{W}_{\mathcal{R}}$ and $\tilde{W}_{\mathcal{R}}^+$ have the same dependency in \mathcal{R} , and the approximate negative retraction work does not depend on \mathcal{R} .

Finally, the approximate energetic cost of retraction can be calculated using (6.22) as

$$\tilde{E}_{\mathcal{R}} = c_1 \tilde{W}_{\mathcal{R}}^+ - c_2 \tilde{W}_{\mathcal{R}}^-. \quad (7.58)$$

Now, by adding the approximate energetic cost of individual impulsive force and torques, given by (7.51), (7.53), and (7.58), we can calculate the approximate net energetic cost of the gait. By minimizing this approximate net cost, subject to the approximate constraints found in Sections 7.4 -7.7, we can calculate the approximate optimal retraction impulse. This is the subject of the following sections.

7.10 Extensional Retraction Torque Is Not Energetically Efficient in the Admissible Region

In order to investigate the energetic consequences of the extensional retraction torque, we can examine $\partial E_{\text{step}}/\partial \mathcal{R}$ for $\mathcal{R} < 0$, where E_{step} is the net energetic cost per step, given by (6.2). Among different terms in E_{step} , the energetic cost of swing-thrust impulse, *i.e.* $E_{\mathcal{S}}$, has a negligible dependency on \mathcal{R} . This can be verified by noticing that the approximate work

and energetic cost of impulsive swing thrust, *i.e.* \tilde{W}_S and \tilde{E}_S given by (7.50) and (7.51), are independent of \mathcal{R} . Thus, the variations of E_{step} with respect to \mathcal{R} can be approximated as

$$\frac{\partial E_{\text{step}}}{\partial \mathcal{R}} \approx \frac{\partial E_{\mathcal{P}\mathcal{R}}}{\partial \mathcal{R}}, \quad (7.59)$$

where $E_{\mathcal{P}\mathcal{R}}$ is the net cost of push-off and retraction, given by (6.29).

In energy-optimal gaits, with any given step angle α and average walking speed V in the admissible region, both the impulsive push-off force and the impulsive extensional retraction torque ($\mathcal{R} < 0$) do only positive work (see Sections 6.4.3 and 6.5). In this case, $E_{\mathcal{P}\mathcal{R}} = c_1 (W_{\mathcal{R}} + W_{\mathcal{P}})$, where the net retraction work $W_{\mathcal{R}}$ and the net push-off work $W_{\mathcal{P}}$ are given by (6.14) and (6.19). Now, using $J_{\dot{\phi}/\mathcal{P}} = -J_{\dot{\ell}/\mathcal{R}}$ from (5.17), we can write

$$\begin{aligned} \frac{\partial E_{\mathcal{P}\mathcal{R}}}{\partial \mathcal{R}} &= c_1 \frac{\partial (W_{\mathcal{R}} + W_{\mathcal{P}})}{\partial \mathcal{R}} \\ &= c_1 \frac{\partial}{\partial \mathcal{R}} \left(-\dot{\phi}_0 \mathcal{R} - \frac{1}{2} J_{\dot{\phi}/\mathcal{R}} \mathcal{R}^2 + \frac{1}{2} J_{\dot{\ell}/\mathcal{P}} \mathcal{P}^2 + J_{\dot{\ell}/\mathcal{R}} \mathcal{R} \mathcal{P} \right) \\ &= c_1 \left(-\dot{\phi}_0 - J_{\dot{\phi}/\mathcal{R}} \mathcal{R} + J_{\dot{\ell}/\mathcal{P}} \mathcal{P} \frac{\partial \mathcal{P}}{\partial \mathcal{R}} + J_{\dot{\ell}/\mathcal{R}} \mathcal{P} + J_{\dot{\ell}/\mathcal{R}} \mathcal{R} \frac{\partial \mathcal{P}}{\partial \mathcal{R}} \right) \\ &= c_1 \left(-\dot{\phi}_0 - J_{\dot{\phi}/\mathcal{R}} \mathcal{R} - J_{\dot{\phi}/\mathcal{P}} \mathcal{P} + \left(J_{\dot{\ell}/\mathcal{P}} \mathcal{P} + J_{\dot{\ell}/\mathcal{R}} \mathcal{R} \right) \frac{\partial \mathcal{P}}{\partial \mathcal{R}} \right). \end{aligned} \quad (7.60)$$

Using the push-off-retraction velocity mapping, given by (5.14), and the velocity mapping of passive swing, given by (5.13), the above equation can be simplified as

$$\begin{aligned} \frac{\partial E_{\mathcal{P}\mathcal{R}}}{\partial \mathcal{R}} &= c_1 \left(-\dot{\phi}_{t_{\text{pr}}^+} + \dot{\ell}_{t_{\text{pr}}^+} \frac{\partial \mathcal{P}}{\partial \mathcal{R}} \right) \\ &\approx c_1 \left(-\tilde{\phi}_{t_{\text{pr}}^+} + \dot{\ell}_{t_{\text{pr}}^+} \frac{\partial \tilde{\mathcal{P}}}{\partial \mathcal{R}} \right) \end{aligned} \quad (7.61)$$

$$= \frac{\partial \tilde{E}_{\mathcal{P}\mathcal{R}}}{\partial \mathcal{R}}. \quad (7.62)$$

Now consider the following three facts:

- In optimal gaits with $\mathcal{R} < 0$ the impulsive push-off force continues until the end of the push-off-retraction interval (see Section 6.4), *i.e.* until t_{pr}^+ . This implies that the stance leg is extending at t_{pr}^+ , and $\dot{\ell}_{t_{\text{pr}}^+} > 0$.

- For all gait parameters $\partial\tilde{\mathcal{P}}/\partial\mathcal{R} < 0$, as shown in (7.18).
- In the approximate admissible region, any extensional \mathcal{R} , *i.e.* $\mathcal{R} < 0$, results in $\tilde{\phi}_{t_{\text{pr}}^+} > 0$. To verify this, use the formula of $\tilde{\phi}_{t_{\text{pr}}^+}$ in (7.48) and recall that $\tilde{\Omega}$ is non-negative in the entire approximate admissible region (see Section 7.7.1).

Therefore, for any given step angle α and average walking speed V in the approximate admissible region, and for any given $\mathcal{R} < 0$, all the terms in (7.61) are negative, and

$$\frac{\partial\tilde{E}_{\text{step}}}{\partial\mathcal{R}} = \frac{\partial\tilde{E}_{\mathcal{P}\mathcal{R}}}{\partial\mathcal{R}} < 0. \quad (7.63)$$

This equation implies that in the approximate admissible region the net energetic cost \tilde{E}_{step} monotonically decreases as \mathcal{R} increases in $\mathcal{R} < 0$ (*i.e.* $\mathcal{R} \rightarrow 0^-$). In other words, the approximate optimal retraction impulse $\tilde{\mathcal{R}}^*$ that minimizes \tilde{E}_{step} in the approximate admissible region follows $\mathcal{R}^* \geq 0$.

7.11 Approximate Energy Optimal Swing-Retraction Impulse

The approximate total energetic cost per step is given by

$$\tilde{E}_{\text{step}} = \tilde{E}_S + \tilde{E}_P + \tilde{E}_R, \quad (7.64)$$

where the individual approximate energetic costs \tilde{E}_S , \tilde{E}_P , and \tilde{E}_R are given by (7.51), (7.53), and (7.58). Given the step angle α and average walking speed V in the approximate admissible region, the approximate optimal retraction impulse $\tilde{\mathcal{R}}^*$ is determined by minimizing $\tilde{E}_{\text{step}}(\alpha, V)$ subject to $\tilde{\mathcal{R}}_{\text{min}} \leq \tilde{\mathcal{R}}^* \leq \tilde{\mathcal{R}}_{\text{max}}$, where the lower bound $\tilde{\mathcal{R}}_{\text{min}}$ is imposed by (7.21) to ensure heel-strike, and the upper bound $\tilde{\mathcal{R}}_{\text{max}}$ is imposed by (7.22) to ensure a positive push-off impulse. Because in the admissible region $\tilde{\mathcal{R}}^* \geq 0$ (see the previous section) the range of approximate optimal retraction impulse is reduced to

$$\max(0, \tilde{\mathcal{R}}_{\text{min}}) \leq \tilde{\mathcal{R}}^* \leq \tilde{\mathcal{R}}_{\text{max}}. \quad (7.65)$$

Among the cost terms in \tilde{E}_{step} , the swing-thrust cost \tilde{E}_S does not depend on \mathcal{R} (see Section 7.9.1). Thus, the optimal retraction impulse $\tilde{\mathcal{R}}^*$ that minimizes \tilde{E}_{step} also minimizes $\tilde{E}_{\mathcal{P}\mathcal{R}} = \tilde{E}_{\mathcal{P}} + \tilde{E}_{\mathcal{R}}$.

Using the approximate push-off cost $\tilde{E}_{\mathcal{P}}$ in (7.53), the approximate push-off work in (7.52), and the formula of $\tilde{\mathcal{R}}_{\text{max}}$ in (7.22), we get

$$\frac{\partial \tilde{E}_{\mathcal{P}}}{\partial \mathcal{R}} = c_1 \tilde{\theta}_0 \left(1 + \frac{\mathcal{R}}{m_{\text{tot}} \ell^2 \tilde{\theta}_0} \right) \tan \alpha \quad (7.66)$$

$$= c_1 \tilde{\theta}_0 \left(1 - \mathcal{R}/\tilde{\mathcal{R}}_{\text{max}} \right) \tan \alpha, \quad (7.67)$$

where $\tilde{\theta}_0$ is given by (7.7). Because $\tilde{\theta}_0$ is always negative, respecting $\mathcal{R} \leq \tilde{\mathcal{R}}_{\text{max}}$ results in

$$\frac{\partial \tilde{E}_{\mathcal{P}}}{\partial \mathcal{R}} \leq 0. \quad (7.68)$$

In the above equation, the equality occurs only when $\mathcal{R} = \tilde{\mathcal{R}}_{\text{max}}$. Thus, the push-off cost $\tilde{E}_{\mathcal{P}}$ monotonically decreases with \mathcal{R} in $\mathcal{R} < \tilde{\mathcal{R}}_{\text{max}}$.

Using the approximate retraction work and cost, given by (7.55)-(7.58), we get

$$\frac{\partial \tilde{E}_{\mathcal{R}}}{\partial \mathcal{R}} = \begin{cases} c_2 \tilde{\Omega} \left(1 - \mathcal{R}/\tilde{\mathcal{R}}^\ddagger \right) & \text{if } 0 \leq \mathcal{R} \leq \tilde{\mathcal{R}}^\ddagger \\ -c_1 \tilde{\Omega} \left(1 - \mathcal{R}/\tilde{\mathcal{R}}^\ddagger \right) & \text{if } \mathcal{R} \geq \tilde{\mathcal{R}}^\ddagger \end{cases} \quad (7.69)$$

where $\tilde{\Omega}$ and $\tilde{\mathcal{R}}^\ddagger$ are given by (7.17) and (7.56). In the approximate admissible region $\tilde{\Omega} \geq 0$, so for the both cases in the above equation

$$\frac{\partial \tilde{E}_{\mathcal{R}}}{\partial \mathcal{R}} \geq 0. \quad (7.70)$$

Now, with (7.66)-(7.70), consider the following three facts.

- $\tilde{E}_{\mathcal{P}\mathcal{R}}$ is a smooth (differentiable) function of \mathcal{R} . Therefore, its minimum in the region $\tilde{\mathcal{R}} \geq \max(\tilde{\mathcal{R}}_{\text{min}}, 0)$ is either at the boundary of this region, *i.e.* at $\mathcal{R} = \max(\tilde{\mathcal{R}}_{\text{min}}, 0)$, or at the *stationary* points ($\partial \tilde{E}_{\mathcal{P}\mathcal{R}}/\partial \mathcal{R} = 0$) that are *local* minima ($\partial^2 \tilde{E}_{\mathcal{P}\mathcal{R}}/\partial \mathcal{R}^2 > 0$).

- $\tilde{E}_{\mathcal{P}\mathcal{R}}$ has only one local minimum ($\partial\tilde{E}_{\mathcal{P}\mathcal{R}}/\partial\mathcal{R}=0$ has only one solution for which $\partial^2\tilde{E}_{\mathcal{P}\mathcal{R}}/\partial\mathcal{R}^2 > 0$) in $\mathcal{R} \geq \tilde{\mathcal{R}}^\ddagger$, which, after using $\lambda \approx 0$, is calculated as

$$\tilde{\mathcal{R}}_1^* = \delta m_{\text{leg}} \ell b \left(\tilde{\Omega} - \tilde{\theta}_0 \tan^2 \alpha \right). \quad (7.71)$$

Recognizing that $\tilde{\theta}_0 < 0$ [see (7.7)] and that $\tilde{\Omega} \geq 0$ in the approximate admissible region, it is easy to verify that $\tilde{\mathcal{R}}_1^* > \tilde{\mathcal{R}}^\ddagger > \max(\tilde{\mathcal{R}}_{\min}, 0)$, where $\tilde{\mathcal{R}}_{\min}$ and $\tilde{\mathcal{R}}^\ddagger$ are given by (7.21) and (7.56). Moreover, using $\lambda \approx 0$, one can easily show that $\tilde{\mathcal{R}}_{\max} > \tilde{\mathcal{R}}_1^*$, where $\tilde{\mathcal{R}}_{\max}$ is given by (7.22). Thus $\tilde{\mathcal{R}}_1^*$ satisfies the bounds in (7.65).

- If $\tilde{E}_{\mathcal{P}\mathcal{R}}$ has a stationary point in $0 < \mathcal{R} \leq \tilde{\mathcal{R}}^\ddagger$, it can be only a local *maximum*. This can be explained as follows: $\partial\tilde{E}_{\mathcal{P}\mathcal{R}}/\partial\mathcal{R} = \partial\tilde{E}_{\mathcal{P}}/\partial\mathcal{R} + \partial\tilde{E}_{\mathcal{R}}/\partial\mathcal{R}$ is a piecewise-linear function of \mathcal{R} , so it can become zero (stationary point) at most in one point in the region $0 < \mathcal{R} \leq \tilde{\mathcal{R}}^\ddagger$. On the other hand, at the end of this region, *i.e.* at $\mathcal{R} = \tilde{\mathcal{R}}^\ddagger$, we have $\partial\tilde{E}_{\mathcal{P}\mathcal{R}}/\partial\mathcal{R} < 0$ (since $\partial\tilde{E}_{\mathcal{P}}/\partial\mathcal{R} < 0$ and $\partial\tilde{E}_{\mathcal{R}}/\partial\mathcal{R} = 0$), implying that $\tilde{E}_{\mathcal{P}\mathcal{R}}$ decreases after the stationary point, if that point exists. This feature is only consistent with a local maximum.

Therefore, the minimum of $\tilde{E}_{\mathcal{P}\mathcal{R}}$ subject to (7.65) is at either $\tilde{\mathcal{R}}_1^*$, or $\max(\tilde{\mathcal{R}}_{\min}, 0)$. By comparing the value of $\tilde{E}_{\mathcal{P}\mathcal{R}}$ at these two candidate points, we can find the minimum point. Based on the sign of $\tilde{\mathcal{R}}_{\min}$ the following two cases are possible:

1. $\tilde{\mathcal{R}}_{\min} < 0$, resulting in $\max(\tilde{\mathcal{R}}_{\min}, 0) = 0$. In this case, if

$$\tilde{E}_{\mathcal{P}\mathcal{R}}(\tilde{\mathcal{R}}_1^*) > \tilde{E}_{\mathcal{P}\mathcal{R}} \Big|_{\mathcal{R}=0^+}, \quad (7.72)$$

or equivalently if (after simplifying (7.72) using $\lambda \approx 0$)

$$\frac{c_2}{c_1} \geq \left(\frac{\tilde{\theta}_0}{\tilde{\Omega}} \tan^2 \alpha - 2 \right) \frac{\tilde{\theta}_0}{\tilde{\Omega}} \tan^2 \alpha, \quad (7.73)$$

the optimal retraction impulse is $\tilde{\mathcal{R}}^* = 0$, otherwise $\tilde{\mathcal{R}}^* = \tilde{\mathcal{R}}_1^*$.

2. $\tilde{\mathcal{R}}_{\min} > 0$, giving: $\max(\tilde{\mathcal{R}}_{\min}, 0) = \tilde{\mathcal{R}}_{\min}$. In this case, if

$$\tilde{E}_{\mathcal{P}\mathcal{R}}(\tilde{\mathcal{R}}_{\min}) < \tilde{E}_{\mathcal{P}\mathcal{R}}(\tilde{\mathcal{R}}_1^*), \quad (7.74)$$

or equivalently if (after simplifying (7.74) using $\lambda \approx 0$)

$$\frac{c_2}{c_1} \geq -1 + \cos^{-4}\alpha, \quad (7.75)$$

the optimal retraction impulse is $\tilde{\mathcal{R}}^* = \tilde{\mathcal{R}}_{\min}$, otherwise $\tilde{\mathcal{R}}^* = \tilde{\mathcal{R}}_1^*$.

In summary, for any given step angle α and average walking speed V in the approximate admissible region, defined by (7.34), the approximate energy minimizing retraction impulse is

$$\tilde{\mathcal{R}}^* = \begin{cases} 0 & \text{if } \tilde{\mathcal{R}}_{\min} \leq 0, \text{ and (7.73) holds,} \\ \tilde{\mathcal{R}}_{\min} & \text{if } \tilde{\mathcal{R}}_{\min} \geq 0, \text{ and (7.75) holds,} \\ \tilde{\mathcal{R}}_1^* & \text{Otherwise.} \end{cases} \quad (7.76)$$

where $\tilde{\theta}_0$, $\tilde{\Omega}$, $\tilde{\mathcal{R}}_{\min}$ and $\tilde{\mathcal{R}}_1^*$ are given by (7.7), (7.17), (7.21), and (7.71).

Interestingly, the above result predicts that the swing-leg retraction torque is not always energetically efficient. In fact, depending on the positive and negative work efficiencies, there might be a range of α and V for which $\tilde{\mathcal{R}}^*$ is either zero or $\tilde{\mathcal{R}}_{\min}$. In the latter case, energy minimization still favors not applying a retraction torque, but to ensure heel-strike at least $\mathcal{R} = \tilde{\mathcal{R}}_{\min}$ has to be applied (see Section 7.5.1).

Depending on the ratio of the positive and negative work efficiencies of the actuators involved (*i.e.* c_2/c_1), the approximate optimal retraction impulse $\tilde{\mathcal{R}}^*$ can divide the approximate admissible region into three areas corresponding to $\tilde{\mathcal{R}}^* = 0$, $\tilde{\mathcal{R}}^* = \tilde{\mathcal{R}}_{\min}$, and $\tilde{\mathcal{R}} = \tilde{\mathcal{R}}_1^*$. However, *within each of these areas the optimal retraction impulse is independent of the work efficiencies*. In the next chapter, we will see that these areas also depend on the contribution of actuator work to heel-strike energy loss.

An important point that should be noted here is that for

$$\frac{c_2}{c_1} \geq -\frac{\tilde{\theta}_0}{\tilde{\Omega}} \tan^2 \alpha \quad (7.77)$$

$\left. \frac{\partial \tilde{E}_{\text{step}}}{\partial \mathcal{R}} \right|_{\mathcal{R}=0^+} > 0$, implying that the net cost increases as \mathcal{R} grows from zero. This result, as well as the observation that \tilde{E}_{step} monotonically decreases as $\mathcal{R} < 0$ approaches zero (shown in the previous section), indicates that the energetic cost \tilde{E}_{step} can potentially have a local minimum at $\mathcal{R} = 0$. In other words, when (7.77) holds, \tilde{E}_{step} has two local minima: one at $\mathcal{R} = \mathcal{R}_1^*$, and the other at $\mathcal{R} = 0$ (provided that the constraint associated with $\tilde{\mathcal{R}}_{\text{min}}$ is not considered, otherwise the second local minimum is at $\max(\tilde{\mathcal{R}}_{\text{min}}, 0)$). Moreover, if these local minima result in equal energetic costs, then $\tilde{\mathcal{R}}^*$ has two distinct solutions. This occurs when either (7.73) or (7.75) is satisfied with equality.

The above problem is caused by the non-smooth positive-value function used to calculate the energetic cost (for calculating the positive and negative work). Thus, the same problem can also exist in the non-approximate solution. In fact, this is the case and will be discussed in detail in the next chapter.

The existence of two local minima causes discontinuous jumps in \mathcal{R}^* when varying the step length or speed. This jump occurs as the global minimum switches from one local minimum to the other. This can have consequences in numerical optimization, so extra care should be practiced to ensure that the solution is not trapped by the non-optimal local minimum. Also note that while the local minimum at \mathcal{R}_1^* is smooth (the objective function is differentiable), the one at $\mathcal{R} = 0$ has different left and right derivatives, and thus is not smooth. This can cause difficulty for numerical optimizations, but can be overcome using smoothing techniques, such as the square-root smoothing technique used in Chapter 2.

7.12 Approximate Energy-Optimal Swing Retraction Rates

Different researchers have used different definitions for the ‘swing retraction rate’. In [61, 62] it is defined as the angular speed of the hip joint (angular rate of the swing leg *relative* to the stance leg) prior to heel-strike, whereas in [59, 63, 65] it is defined as the *absolute* angular speed of the swing leg prior to heel-strike (relative to the inertial reference). To avoid confusion, I refer to these respective speeds as the *hip-joint* retraction rate, denoted by $\dot{\psi}_{\text{hip}}$, and the *swing-leg* retraction rate, denoted by $\dot{\psi}_{\text{leg}}$. These retraction rates are given by

$$\dot{\psi}_{\text{hip}} = -\dot{\phi}_{t_{\text{pr}}^+} \quad (7.78)$$

$$\dot{\psi}_{\text{leg}} = -\left(\dot{\phi}_{t_{\text{pr}}^+} + \dot{\theta}_{t_{\text{pr}}^+}\right). \quad (7.79)$$

Note that the positive direction of the retraction rates is opposite to that of the hip rate and the swing leg angular rate, to comply with the term ‘retraction’.

Given the above definitions, we can use the approximate optimal retraction impulse $\tilde{\mathcal{R}}^*$, found in the previous section, to calculate the energy-optimal swing retraction rates. Evaluating the approximate hip rate $\tilde{\phi}_{t_{\text{pr}}^+}$, given by (7.48), at $\mathcal{R} = \tilde{\mathcal{R}}^*$, and simplifying the result with $\lambda \approx 0$, gives the following approximations for the optimal hip-joint retraction rate:

$$\tilde{\psi}_{\text{hip}}^* = \begin{cases} -\tilde{\Omega} & \text{if } \tilde{\mathcal{R}}^* = 0, \\ \tilde{\theta}_0 & \text{if } \tilde{\mathcal{R}}^* = \tilde{\mathcal{R}}_{\text{min}}, \\ -\tilde{\theta}_0 \tan^2 \alpha & \text{if } \tilde{\mathcal{R}}^* = \tilde{\mathcal{R}}_1^*. \end{cases} \quad (7.80)$$

Similarly, the optimal swing-leg retraction rate takes the following three approximate values:

$$\tilde{\psi}_{\text{leg}}^* = \begin{cases} -\left(\tilde{\Omega} + \tilde{\theta}_0\right) & \text{if } \tilde{\mathcal{R}}^* = 0, \\ 0 & \text{if } \tilde{\mathcal{R}}^* = \tilde{\mathcal{R}}_{\text{min}}, \\ -\tilde{\theta}_0 / \cos^2 \alpha & \text{if } \tilde{\mathcal{R}}^* = \tilde{\mathcal{R}}_1^*. \end{cases} \quad (7.81)$$

In the above equations, $\tilde{\theta}_0$ and $\tilde{\Omega}$ are given by (7.7) and (7.17).

Interestingly, the above approximations predict that swing-leg retraction is not always energetically advantageous. In fact, for the pairs of (α, V) for which $\tilde{\mathcal{R}}^* = \tilde{\mathcal{R}}_{\min}$, or equivalently when (7.75) holds, energy optimal gaits exhibit neither a retracting hip joint nor a retracting swing leg (corresponding approximate retraction rates are not positive). Furthermore, a retracting hip-joint is also not observed in energy optimal gaits with $\tilde{\mathcal{R}}^* = 0$. These results suggest that the positive and negative work efficiencies of the actuator plays an important role in energy-optimality of retraction.

7.13 Summary

In this chapter, approximate analytic solutions were found for many gait variables. The main approximation used in this process was $\lambda = m_{\text{leg}} b / (m_{\text{tot}} \ell) \approx 0$. Almost all the analytic solutions found in this chapter are parts of the contributions of this work. The importance of these simple closed-form analytic solutions is that they provide very useful insights into how different aspects of a gait are influenced by each other and by different gait parameters. For example, the approximate analytic solutions *predict* that

- The swing-thrust impulse has a negligible dependency on the retraction impulse.
- The push-off impulse decreases with the retraction impulse.
- Without a large enough retraction impulse, walking is not feasible for some range of walking speeds and step lengths.
- Swing retraction is not always energetically efficient, and its optimality depends highly on the ratio of positive and negative work efficiencies of the actuator.

These *predictions* are only based on the approximate analyses and should be confirmed using the accurate numerical calculations. This will be studied in the next chapter.

Chapter 8

ADVANTAGES OF SWING-LEG RETRACTION

One of the characteristics that are common among different gaits of many legged organisms is *swing-leg retraction*, the rearward rotation of the swing leg prior to heel-strike. Chapter 1 discusses some of the advantages of swing retraction that have been discovered by other researchers. These include

1. improving stability of the gait,
2. improving disturbance rejection,
3. enabling a better state estimation,
4. facilitating foot clearance prior to heel-strike, and
5. reducing the risk of slippage at heel-strike.

There might be other advantages to this motion that have not yet been discovered, or that are currently not well understood. For example, the numerical results in Chapter 3 showed that swing-leg retraction can reduce the net energetic cost by reducing the relative foot-ground speed at touch-down; at least for the model parameters used in the corresponding gait optimization. However, that is not necessarily the entire picture. In the previous chapter, the approximate analytic solutions showed that there might be some cases in which retraction is not energetically favorable. Other possible advantages were also suggested by the approximate analyses in the previous chapter, and motivate more detailed investigations using non-approximate equations. These investigations are the subject of this chapter.

In this chapter three more benefits of swing-leg retraction are added to the list of 5 advantages above. Among those, the two advantages explained in Sections 8.1 and 8.2 were not known before, at least to the best of my knowledge. The last advantage, presented in

Section 8.3, was known before, but the complete picture of it and its determinant factors are parts of the contributions of this work.

This chapter is organized as follows. First, in Section 8.1 the dependency of the push-off impulse on the swing-retraction impulse is studied. Section 8.2 describes the influence of retraction on walking speed limit and step length. Finally, the energy optimality of swing retraction is examined in details in Section 8.3. At the end, the chapter is summarized in Section 8.4.

8.1 Less Push-Off Force Is Required With Swing-Leg Retraction

It was shown in the previous chapter that the approximate swing thrust impulse $\tilde{\mathcal{S}}$ is independent of the retraction impulse \mathcal{R} , whereas the approximate push-off impulse $\tilde{\mathcal{P}}$ does depend on \mathcal{R} and decreases with it. Motivated by this observation, I numerically examined the influence of \mathcal{R} on the *non-approximate* swing-thrust and push-off impulses, *i.e.* \mathcal{S} and \mathcal{P} given by (5.26) and (5.27). Fig. 8.1 shows the percentage change of these impulses with \mathcal{R} for a walking gait with $V = 1.38$ m/s and $T = 0.54$ s (typical humans' preferred walking speed and step period). As this figure shows, both \mathcal{S} and \mathcal{P} decrease with \mathcal{R} , but the reduction of \mathcal{S} is so small that it can be neglected (\mathcal{S} decreases less than 1% as \mathcal{R} increases from 0 to 10 Nms). In contrast, the changes in \mathcal{P} are more substantial and should not be neglected. The slope of the variations of \mathcal{P} with respect to \mathcal{R} is approximated by the analytic solution in (7.18) as $\partial\mathcal{P}/\partial\mathcal{R} \approx -\tan\alpha/\ell$, where α is the step angle and ℓ is the leg length.

The different dependencies of swing-thrust and push-off impulses to the retraction impulse can be explained as follows. The negligible influence of the retraction impulse on the required thrust impulse is because the swing thrust is isolated from retraction by heel-strike. After heel-strike, the motion of the new stance leg (the previous swing leg) is constrained by the hip motion, and the effect of retraction torque on leg velocity does not transfer much to the

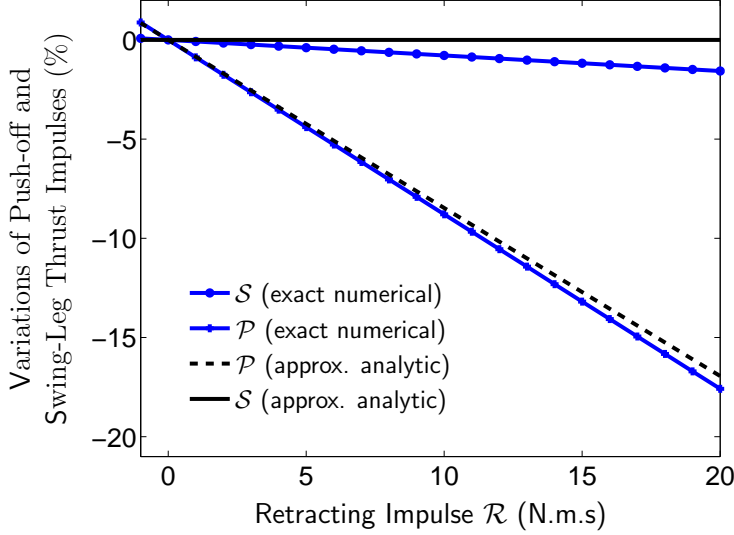


Figure 8.1: **Percentage variations of the required swing thrust impulse \mathcal{S} and push-off impulse \mathcal{P} with the retracting impulse \mathcal{R} .** The graph is plotted for the average walking speed and the step period of $V = 1.38$ m/s and $T = 0.54$ s. The variation of each impulse is calculated relative to its corresponding value at $\mathcal{R} = 0$. The model data are those in Table 5.1. The numerical results are calculated using the non-approximate equations in (5.26) and (5.27), whereas the approximate analytic results are calculated using (7.15) and (7.16). Consistent with the predictions of approximate analytic solutions, the exact numerical results show that the push-off impulse \mathcal{P} decreases with the retraction impulse \mathcal{R} , whereas the swing thrust impulse \mathcal{S} has a small dependency in \mathcal{R} which has been ignored in the approximate analytic solution.

next step. However, this is not the case for push-off and retraction, which occur at the same phase of the gait cycle. More importantly, the mechanical coupling in the system links the push-off and retraction impulses to each other. The retraction torque (force) applied by the hip actuator on the swing leg induces a reaction force on the hip. This reaction force pulls the hip up and tends to extend the stance leg, so less push-off impulse is required for a given pre-heel-strike leg extension rate $\dot{\ell}$.

Arguably, the push-off reduction effect of the retraction torque is not limited only to the simple model used in this study. As shown in Fig. 8.2, the same action-reaction and mechanical coupling should be valid for realistic bipedal systems as well. Therefore, in these systems active swing-leg retraction can have the same influence on push-off force.

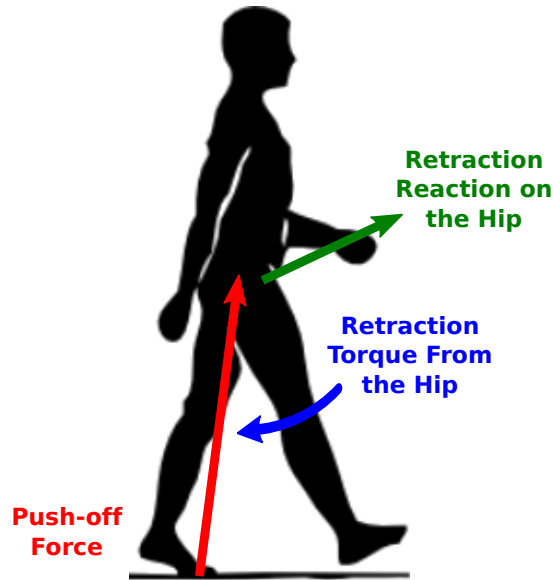


Figure 8.2: **Retraction torque and its reaction on the hip.** The hip applies a retracting force (torque) on the swing leg and pushes it back. In reverse, a reaction force is applied to the hip by the swing leg. This reaction force pulls the hip forward and reduces the required push-off force for given step length and walking speed.

Thus, the 6th advantage of swing retraction is:

the swing retraction torque reduces the required push-off force for a periodic walk.

The advantage of a reduced push-off force can be twofold:

- First, less cost is involved with generating a reduced force/torque. For example, in DC motors the armature loss (the energy loss in armature resistance) is proportional to torque-squared. So, a smaller torque implies less energy loss, and thus less input power per unit output torque.
- The second benefit of a reduced push-off force is that it does less mechanical work (see the push-off work equations in Section 6.3.3). Therefore, with a work-based energetic cost, the reduced push-off work can potentially decrease the net energetic cost, if the increase in retraction cost does not exceed the decrease in push-off cost. This potential advantage will be closely examined in Section 8.3.

8.2 Swing-Leg Retraction Enables Faster Walking Speeds and Shorter Steps

In order to walk with a desired step length and speed, the swing foot should move downward at the end of the step to make a new foot-ground contact (heel-strike) and become the new stance leg. For the impulsive gait shown in Fig. 5.2, this condition is expressed as $\dot{y}_{f_{\text{swing}}}(t_{\text{pr}}^+) < 0$ (see Section 5.3.2), where $\dot{y}_{f_{\text{swing}}}$ is the vertical swing foot velocity. In the previous chapter, using the approximate equations, this condition imposed an approximate lower bound on the retraction impulse, given by (7.21). This led to the prediction that periodic walking is not feasible in some areas in the admissible region if the available maximum retraction impulse is not large enough to ensure heel-strike. This observation motivates examining the problem with non-approximate numerical solutions.

Equivalent to the approximate $\tilde{\mathcal{R}}_{\text{min}}$ defined in Section 7.5.1, $\mathcal{R}_{\text{min}}(\alpha, V)$ is the *exact* minimum retraction impulse required to ensure heel-strike in a periodic walk with step angle α and average speed V . According to the foot velocity condition stated above, \mathcal{R}_{min} satisfies

$$\mathcal{R} \geq \mathcal{R}_{\text{min}}(\alpha, V) \quad \iff \quad \dot{y}_{f_{\text{swing}}}(t_{\text{pr}}^+, \alpha, V, \mathcal{R}) \leq 0, \quad (8.1)$$

and is given by

$$\mathcal{R}_{\text{min}}(\alpha, V) = \mathcal{R} \Big|_{\dot{y}_{f_{\text{swing}}}(t_{\text{pr}}^+, \alpha, V, \mathcal{R}) = 0}, \quad (8.2)$$

where $\dot{y}_{f_{\text{swing}}}$ is calculated from (7.19), after substituting for $\dot{\ell}_{t_{\text{pr}}^+}$, $\dot{\theta}_{t_{\text{pr}}^+}$, $\dot{\phi}_{t_{\text{pr}}^+}$, and \mathcal{P} from (5.14), and (5.27).

Fig. 8.3 shows the contour lines of the resulting \mathcal{R}_{min} in the admissible region. This figure is the non-approximate (numerically calculated) version of Fig. 7.3. The numerical values for model parameters are those in Table 5.1. The minimum required retraction impulse, \mathcal{R}_{min} , is negative in the lighter shaded area (slow walking speeds or long steps), and is positive in the darker region (fast walking speeds and short steps). This implies that at slow speeds or long steps a *retracting* hip torque ($\mathcal{R} > 0$) is not necessary for periodic walking, and heel-strike

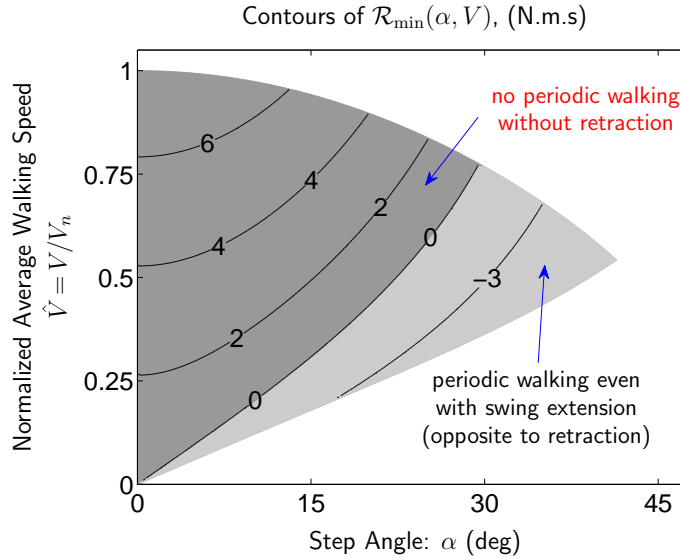


Figure 8.3: **Contour lines of the minimum retracting impulse, \mathcal{R}_{\min} , required to enforce heel-strike.** The shaded area is the admissible region, defined in Section 5.4.4. In the lower shaded area (light color) *retracting* hip torque ($\mathcal{R} > 0$) is not necessary for periodic walking, and walking is feasible even with an extensional torque ($\mathcal{R} < 0$). In the darker area, however, walking is not feasible without a *retracting* hip torque prior to heel-strike. The vertical axis is the normalized average walking speed $\hat{V} = V/V_n$, where V_n is given by (5.36). The numerical values of model parameters are taken from Table 5.1.

occurs even with an *extensional* (opposite to retracting) hip torque. For fast speeds or short steps, however, walking is not feasible without a *retracting* hip torque.

Now, let us have a look at what occurs in a physical bipedal system. The velocity of the swing foot is determined by the velocity of the hip and the angular rate of the swing leg. For an efficient periodic walk, the hip (CoM) velocity is near-horizontal at the end of the pre-emptive push-off and prior to heel-strike. Therefore, to move the swing foot downward to enforce heel-strike the swing leg should be rotating rearward at the end of the step. At slow walking speeds the swing leg velocity is small, and the braking torque induced on the swing leg by push-off¹ might be enough to stop the forward leg-swing or even reverse (retract) it, especially when taking long steps. However, for fast walks a large-enough *retracting* hip torque is required to reverse the leg rotation and ensure heel-strike. The same result is valid for walking with too-short steps, since the push-off induced torque on the swing leg is

¹The push-off force accelerates the hip along the stance leg, inducing an (inertial) torque on the swing leg. This induced torque tends to push the swing leg back, toward the stance leg.

too small (shorter steps need less push-off impulse [26, 47]; also the push-off force becomes almost parallel to the swing leg leading to a small moment arm and induced torque on the swing leg).

Based on the above results and discussion, the 7th advantage of active swing-leg retraction is discovered as

swing retracting torque significantly expands the viability region of periodic walking toward faster walking speeds and shorter steps.

8.3 Does Swing-Leg Retraction Reduce the Net Energetic Cost of Walking?

The approximate analyses in Sections 7.11 and 7.12 predict that the optimality of retraction is highly influenced by the ratio of negative and positive work efficiencies. If the efficiency of negative work (*i.e.* $1/c_2$) is smaller enough than that of positive work (*i.e.* $1/c_1$), then approximate-cost minimization favors not to use any impulsive retraction torque (*i.e.* $\tilde{\mathcal{R}}^* = 0$) unless it is required to ensure heel-strike ($\tilde{\mathcal{R}}^* \geq \tilde{\mathcal{R}}_{\min}$). This is an interesting observation and motivates a more accurate analysis using *non*-approximate equations.

8.3.1 Energy-Optimal Retraction Impulse

The non-approximate optimal retraction impulse \mathcal{R}^* can be calculated numerically by solving the minimization problem stated in (6.73). Fig. 8.4 shows the contour maps of the resulting \mathcal{R}^* in the admissible region and for different values of work efficiencies (= unit positive and negative work costs c_1 and c_2). Consistent with the predictions of approximate analysis, \mathcal{R}^* can divide the admissible region into three areas. These areas correspond to

- $\mathcal{R}^* = \mathcal{R}_1^*$ (the cyan ① region); \mathcal{R}_1^* is the impulse at which $\partial E_{\text{step}}/\partial \mathcal{R} = 0$ and $\partial^2 E_{\text{step}}/\partial \mathcal{R}^2 > 0$ (*i.e.* a local minimum stationary point). In this region energy minimization freely chooses to exploit a *retracting* hip torque;

- $\mathcal{R}^* = \mathcal{R}_{\min}$ (the gray ② region); \mathcal{R}_{\min} is the minimum retraction impulse required to ensure heel-strike, given by (8.2). In this region, energy minimization favors not to apply any retraction torque ($\mathcal{R} = 0$). However, ensuring heel-strike requires the application of at least \mathcal{R}_{\min} ;
- $\mathcal{R}^* = 0$ (the blue ③ region). In this region energy-optimal gaits do not include any retraction torque.

Therefore, only in the cyan ① area a non-zero retraction impulse is energetically advantageous (retraction is optimal by itself and is not enforced by constraints). The gray ② area would have merged with the blue ③ area if the constraint of ensuring heel-strike had been removed.

Fig. 8.4a corresponds to the case where negative work (braking and deceleration) is free, *i.e.* $c_2 = 0$, and all the energetic cost comes from the positive work. In this case, the swing retraction torque is energetically optimal in the entire admissible region. In Fig. 8.4b the work efficiencies are equal to those of human muscles [26, 73]. Due to the increase in the cost of negative work (reduced efficiency), it is more energetically advantageous not to apply any retraction torque at short steps (gray ② and blue ③ regions) if not enforced. As the cost of negative work further increases to $c_2 = c_1$ (Fig. 8.4c), the non-optimality of retraction torque is extended to a larger area, and energetic benefit of retraction is limited mainly to very long steps. Note that in all three cases (Fig. 8.4a-8.4c) the retraction torque is still applied in the majority of the admissible region (the gray ② and cyan ① regions). However, the application of retraction torque in the gray ② area is not due to being energetically advantageous, but just to enforce heel-strike.

Because \mathcal{R}_{\min} is defined based on the heel-strike condition in (8.1), its value is independent of the energetic cost coefficients c_1 and c_2 . Moreover, Fig. 8.4 shows that the value of \mathcal{R}_1^* does not depend on these coefficients (the contour lines in the cyan ① region do not change among the three panels). Thus, as predicted by the approximate analysis in Section 7.11, the

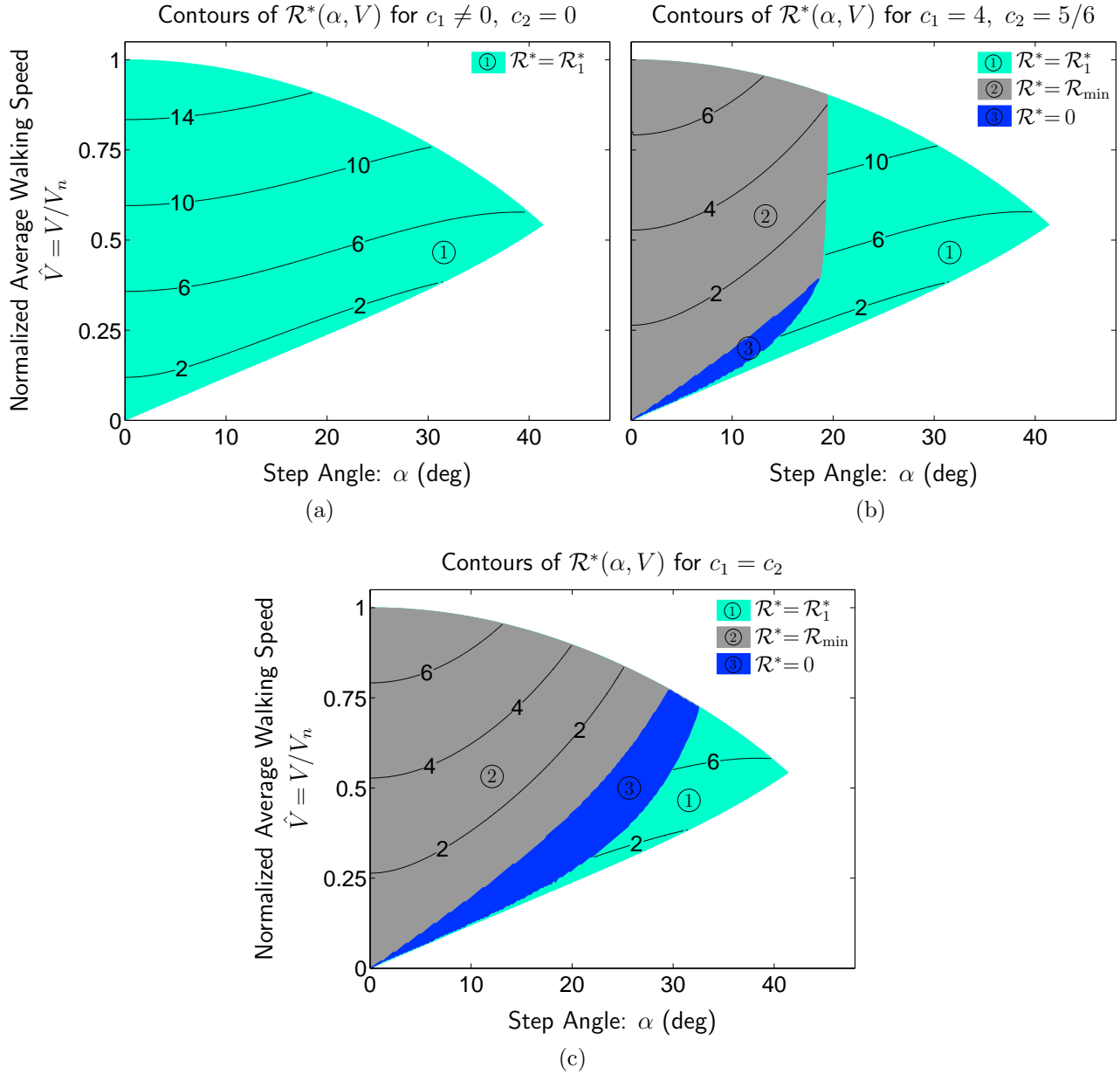


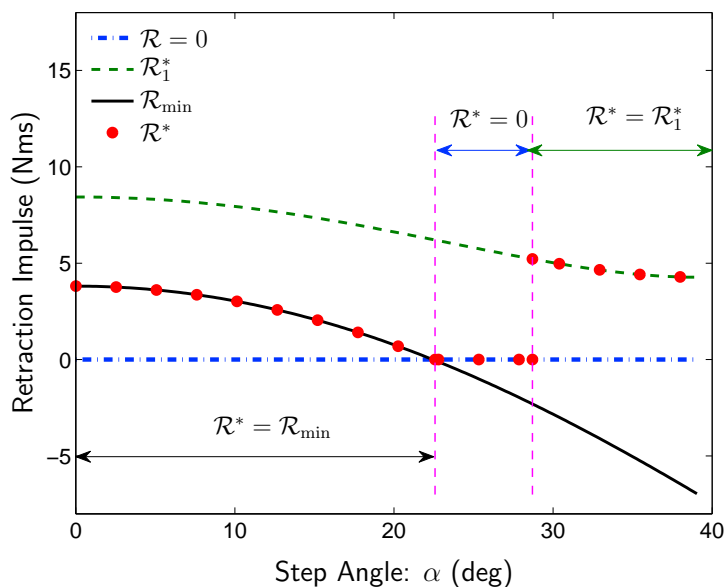
Figure 8.4: **Contour maps of the energy optimal retraction impulse \mathcal{R}^*** , calculated numerically using the minimization problem stated in (6.73). Each panel corresponds to a different set of c_1 and c_2 , *i.e.* the cost of unit positive and negative work: **a)** $c_1 \neq 0$ and $c_2 = 0$, **b)** $c_1 = 4$ and $c_2 = 5/6$ as for human muscles, and **c)** $c_1 = c_2$. In all three panels, the vertical axis is the average walking speed V normalized with V_n given by (5.36). The shaded area is the admissible region, defined in Section 5.4.4. The cyan ① area (marked with $\mathcal{R}^* = \mathcal{R}_1^*$) corresponds to the set of α and V combinations for which retraction is energetically optimal (energy minimization freely chooses to exploit retraction). \mathcal{R}_1^* is where the derivative of the net energetic cost E_{step} becomes zero (stationary point). The gray ② region (marked with $\mathcal{R}^* = \mathcal{R}_{\min}$) is where the energy minimization would prefer not to apply any retraction torque, but ensuring heel-strike requires the application of at least \mathcal{R}_{\min} (see Fig. 8.3). The blue ③ region corresponds to the zero optimal retraction impulse, *i.e.* $\mathcal{R}^* = 0$.

cost coefficients c_1 and c_2 only determine the switching conditions among $\mathcal{R}^* = 0$, $\mathcal{R}^* = \mathcal{R}_{\min}$, and $\mathcal{R}^* = \mathcal{R}_1^*$ (the borders between the cyan ①, gray ②, and blue ③ regions in Fig. 8.4), and not the value of \mathcal{R}^* in each region. These switching conditions are approximated by the inequalities (7.73) and (7.75) in the previous chapter.

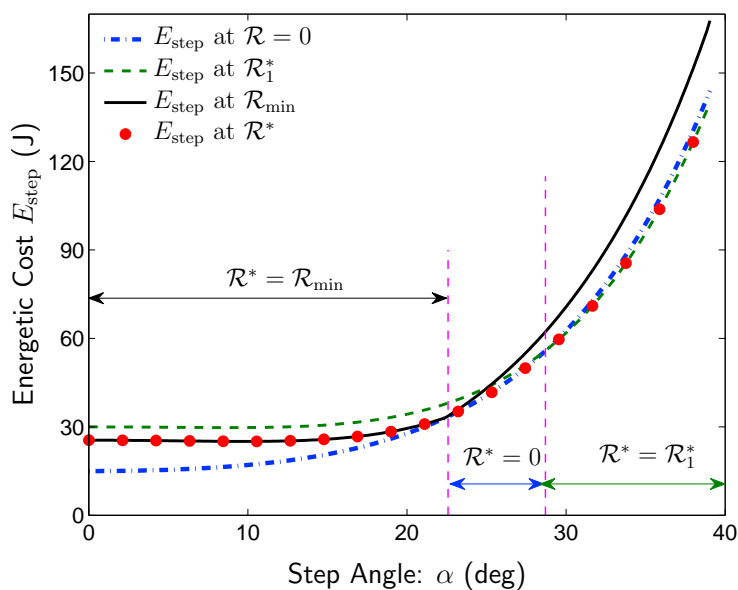
The calculated optimal retraction impulse \mathcal{R}^* has discontinuities when varying step length or speed (at the borders between the cyan ① and either the gray ② or the blue ③ regions). This fact is better shown in Fig. 8.5a. In this figure the optimal retraction impulse \mathcal{R}^* associated with $c_1 = c_2$ and $V = 1.6$ m/s (equivalent to $\hat{V} = 0.5$ in Fig. 8.4c) is plotted at different step angles. For more clarity, the corresponding \mathcal{R}_{\min} , \mathcal{R}_1^* , and $\mathcal{R} = 0$ are also shown in this figure (\mathcal{R}_1^* is the retraction impulse at which $\partial E_{\text{step}}/\partial \mathcal{R} = 0$ and $\partial^2 E_{\text{step}}/\partial \mathcal{R}^2 > 0$, and is the optimal retraction impulse in the cyan ① region in Fig. 8.4). As can be seen, \mathcal{R}^* has a discontinuous jump when it changes from $\mathcal{R}^* = 0$ to $\mathcal{R}^* = \mathcal{R}_1^*$ (at the second vertical line). As mentioned in the previous chapter, these discontinuities are due to the non-smooth positive value function used to calculate positive and negative work in the energetic cost E_{step} , given in (2.1). At the step angles and speeds in which these discontinuities occur, E_{step} becomes minimum at two different retraction impulses, and thus \mathcal{R}^* has two different solutions; similar to what was observed with the approximate solution. For example, at the border between the blue ③ and the gray ② regions in Fig. 8.4c:

$$\min E_{\text{step}} = E_{\text{step}}(\mathcal{R}_1^*) = E_{\text{step}} \Big|_{\mathcal{R}=0}, \quad (8.3)$$

implying that $\mathcal{R}^* = 0$ and $\mathcal{R}^* = \mathcal{R}_1^*$ at that point. This can be clearly seen in Fig. 8.5, or in its zoomed version, Fig. 8.6. In Fig. 8.5b the energetic cost E_{step} is calculated separately for different retraction impulses shown in Fig. 8.5a (introduced at the start of this paragraph). As it is seen, the minimum cost before the second vertical line is given by $E_{\text{step}} \Big|_{\mathcal{R}=0}$ (the dotted blue curve), but switches to $E_{\text{step}}(\mathcal{R}_1^*)$ (the dashed green curve) after it. Exactly on this switching line the two energetic cost curves are equal. As the result, the optimal retraction impulse, shown in Fig. 8.5a, has two different solutions at the switching point (marked with

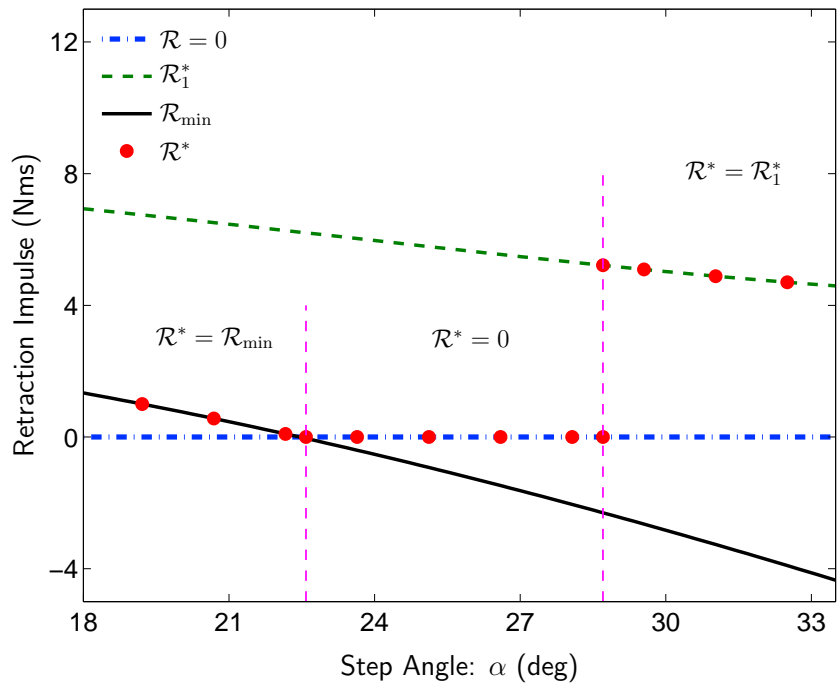


(a)

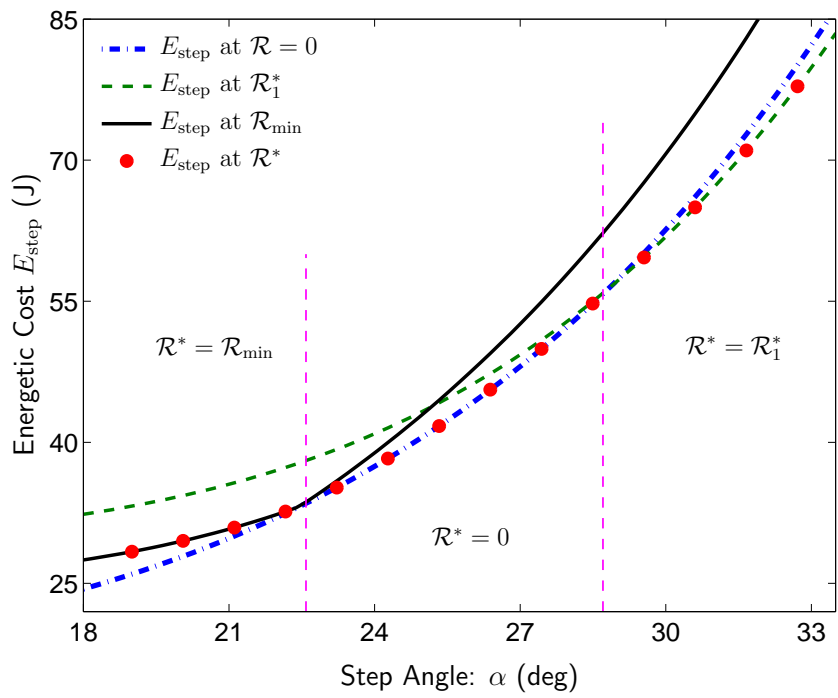


(b)

Figure 8.5: **Different retraction impulses and their energetic cost** corresponding to the cost coefficients $c_1 = c_2$ and average walking speed $V = 1.6$ m/s (equivalent to $\hat{V} = 0.5$ in Fig. 8.4c). The optimal retraction impulse \mathcal{R}^* and its energetic cost are shown with red dots. The vertical lines represent the step angles at which \mathcal{R}^* switches from \mathcal{R}_{\min} to $\mathcal{R} = 0$ and then to \mathcal{R}_1^* . Exactly on each switching line, the two cost curves associated with \mathcal{R}^* before and after the transition are equal, and the optimal retraction impulse has two solutions. Note that although $\mathcal{R} = 0$ results in the least energetic cost for step angles before the first vertical line, ensuring heel-strike in this region results in $\mathcal{R}^* = \mathcal{R}_{\min}$.



(a)



(b)

Figure 8.6: The zoomed version of Fig. 8.5.

the red dots on the second vertical line in Fig. 8.5a and Fig. 8.6a). The equality of the cost curves at switching lines implies that the energetic cost surface is always continuous (though non-smooth) for all α and V , including at the discontinuous transitions of \mathcal{R}^* .

8.3.2 Energy-Optimal Retraction Rates

Using the optimal retraction impulse \mathcal{R}^* calculated above, we can calculate the optimal hip-joint and swing-leg retraction rates, *i.e.* $\dot{\psi}_{\text{hip}}^*$ and $\dot{\psi}_{\text{leg}}^*$, defined in (7.78) and (7.79). The result is consistent with the predictions of the approximate analytic solution in Section 7.12; That is, in energy optimal gaits

- the hip joint is *retracting* ($\dot{\psi}_{\text{hip}}^* > 0$) *only* when $\mathcal{R}^* = \mathcal{R}_1^*$ (see Fig. 8.7).
- the swing leg is *retracting* ($\dot{\psi}_{\text{leg}}^* > 0$) almost only when $\mathcal{R}^* \neq \mathcal{R}_{\text{min}}$ (see Fig. 8.8).

Thus, similar to the retraction impulse \mathcal{R}^* , and depending on the ratio of work efficiencies c_2/c_1 , an *actively controlled retracting* swing leg or hip joint may not always be energetically advantageous.

Interestingly, some recent experiments with human subjects show that swing retraction does not exist in all gaits (personal communication with Dr. Maziar Sharbafi in Nov. 2013 discussing a recent study performed in Lauflabor - Locomotion Lab in TU Darmstadt in Germany). This is completely consistent with my predictions with a simple impulsive model.

8.3.3 Effect of Doing Active Negative Work During Heel-strike

All the energetic analyses performed so far are based on minimizing the total energetic cost E_{step} defined in (6.2). In that equation, no direct cost² is considered for heel-strike. This is

²In a periodic gait on a level ground each action/event has a direct cost (possibly of zero value) and an indirect cost. The direct cost is the energetic cost associated with actuator work during that action/event. The indirect cost is the energetic cost associated with other actions that compensate for the energy change made by the first action/event. This is because in a level-ground periodic gait the net energy change of the mechanism in each step should be zero to maintain the same speed. Therefore, any negative work done during the step should be cancelled by an equal positive work, and *vice versa*.

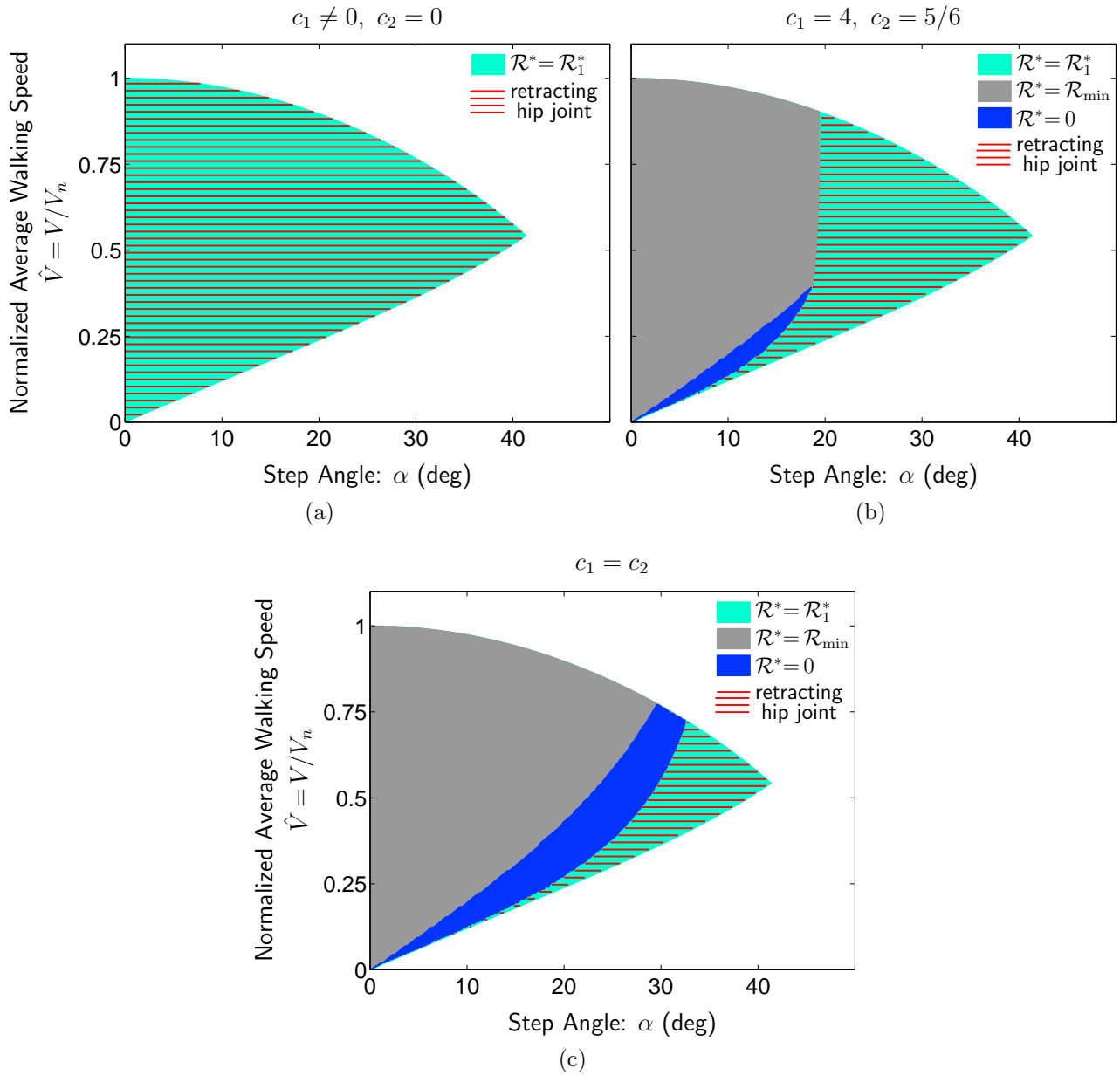


Figure 8.7: **Optimality region of a retracting hip joint at heel-strike**, corresponding to the optimal retraction impulse \mathcal{R}^* found for Fig.8.4. Each panel corresponds to a different set of c_1 and c_2 , *i.e.* the cost of unit positive and negative work: **a)** $c_1 \neq 0$ and $c_2 = 0$ (free negative work), **b)** $c_1 = 4$ and $c_2 = 5/6$ as for human muscles, and **c)** $c_1 = c_2$. A retracting hip joint (*i.e.* $\psi_{\text{hip}}^* > 0$) is energetically optimal only in the hatched region, which is where $\mathcal{R}^* = \mathcal{R}_1^*$. In all three panels, the vertical axis is the average walking speed V normalized with V_n given by (5.36). The shaded area is the admissible region, defined in Section 5.4.4.

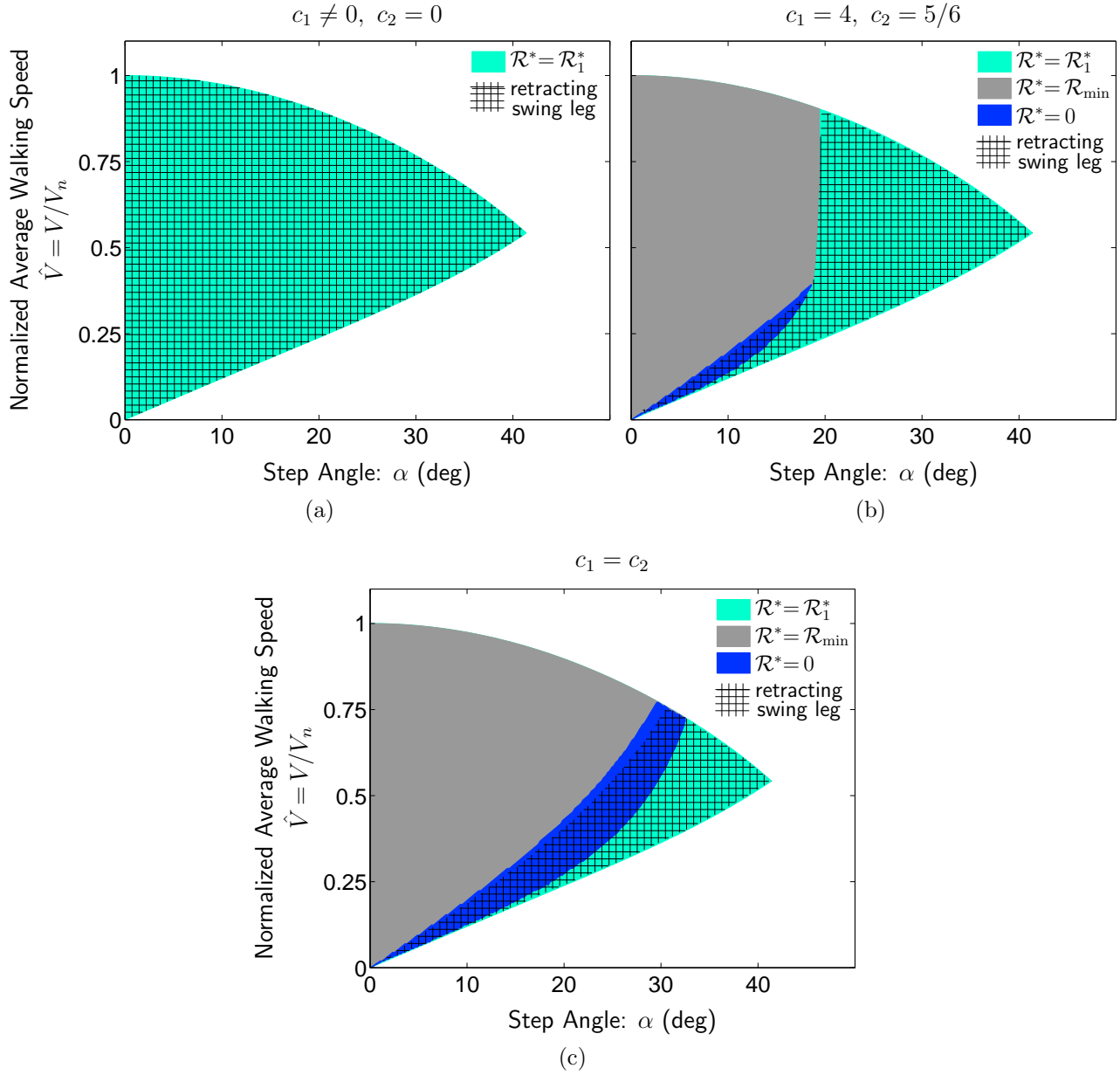


Figure 8.8: **Optimality region of a retracting *swing leg* at heel-strike**, corresponding to the optimal retraction impulse \mathcal{R}^* found for Fig.8.4. Each panel corresponds to a different set of c_1 and c_2 , *i.e.* the cost of unit positive and negative work: **a)** $c_1 \neq 0$ and $c_2 = 0$ (free negative work), **b)** $c_1 = 4$ and $c_2 = 5/6$ as for human muscles, and **c)** $c_1 = c_2$. A retracting swing leg (*i.e.* $\dot{\psi}_{\text{leg}}^* > 0$) is energetically optimal only in the hatched region, which is where $\mathcal{R}^* = \mathcal{R}_1^*$ and for most of the area corresponding to $\mathcal{R}^* = 0$. In all three panels, the vertical axis is the average walking speed V normalized with V_n given by (5.36). The shaded area is the admissible region, defined in Section 5.4.4.

based on the assumption that all the energy dissipation at heel-strike³ takes place passively in the form of loss. However, in reality some portion of that energy dissipation may occur as negative actuator work. For example, during step-to-step transitions in human walking, some negative work is done by muscles (actuators), besides the passive energy loss associated with tissue and surface deformations [48]. In order to address this possibility, I assume that k fraction ($0 \leq k \leq 1$) of the energy dissipation at heel-strike takes place actively by negative actuator work. That is to say, if $W_{\mathcal{H}}$ denotes the net energy dissipation at heel-strike, then

$$W_{\mathcal{H}} = W_{\mathcal{H},\text{active}} + W_{\mathcal{H},\text{passive}}, \quad (8.4)$$

where

$$W_{\mathcal{H},\text{active}} = k W_{\mathcal{H}}. \quad (8.5)$$

In this case the total energetic cost per step, defined in (6.2), should be modified as below to include the *direct* cost of heel-strike:

$$\check{E}_{\text{step}} = E_{\mathcal{S}} + E_{\mathcal{P}} + E_{\mathcal{R}} + E_{\mathcal{H}}. \quad (8.6)$$

To distinguish the original E_{step} with \check{E}_{step} , the latter is called the *modified* energetic cost per step. In the above equation, $E_{\mathcal{H}}$ is the energetic cost of active negative work done during heel-strike. Because heel-strike is all dissipative, $W_{\mathcal{H},\text{active}}$ is all negative work and thus

$$E_{\mathcal{H}} = -c_2 W_{\mathcal{H},\text{active}} = -c_2 k W_{\mathcal{H}}. \quad (8.7)$$

Similar to the work done by other impulsive actions in the gait, $W_{\mathcal{H}}$ can be calculated using the work formula in (6.3). However, there is a simpler way for this, which provides a very useful insight. In a periodic gait on a level ground, all the losses and performed work must sum to zero, otherwise the system will gain or lose energy in every step. Thus, we should have $W_{\mathcal{S}} + W_{\mathcal{P}} + W_{\mathcal{R}} + W_{\mathcal{H}} = 0$. From this equation, the net energy change at heel-strike is

³Due to the dissipative collisional heel-strike, the kinetic energy of the biped decreases through the heel-strike impact.

given by:

$$W_{\mathcal{H}} = -(W_{\mathcal{S}} + W_{\mathcal{P}} + W_{\mathcal{R}}). \quad (8.8)$$

Using the above equations, we can find a simpler form for the *modified* total energetic cost per step, defined in (8.6). For this purpose, first substitute for $E_{\mathcal{S}}$, $E_{\mathcal{R}}$, $E_{\mathcal{P}}$, and $E_{\mathcal{H}}$ from (6.6), (6.22), (6.68), (8.7), and (8.8), to get

$$\begin{aligned} \check{E}_{\text{step}} &= c_1 W_{\mathcal{S}}^+ - c_2 W_{\mathcal{S}}^- \\ &\quad + c_1 W_{\mathcal{P}}^+ \\ &\quad + c_1 W_{\mathcal{R}}^+ - c_2 W_{\mathcal{R}}^- \\ &\quad + c_2 k (W_{\mathcal{S}} + W_{\mathcal{P}} + W_{\mathcal{R}}). \end{aligned} \quad (8.9)$$

Because for each action the net work is $W = W^+ + W^-$, the above equation is simplified as

$$\begin{aligned} \check{E}_{\text{step}} &= \check{c}_1 W_{\mathcal{S}}^+ + \check{c}_2 W_{\mathcal{S}}^- \\ &\quad + \check{c}_1 W_{\mathcal{P}}^+ \\ &\quad + \check{c}_1 W_{\mathcal{R}}^+ + \check{c}_2 W_{\mathcal{R}}^-, \end{aligned} \quad (8.10)$$

where

$$\check{c}_1 = c_1 + k c_2, \quad (8.11)$$

$$\check{c}_2 = (1 - k) c_2. \quad (8.12)$$

The coefficients \check{c}_1 and \check{c}_2 are the *modified* costs of doing unit positive and negative work, respectively. Finally, by defining a *modified* energetic cost equation as

$$\check{E} = \check{c}_1 W^+ - \check{c}_2 W^-, \quad (8.13)$$

the *modified* total energetic cost per step can be written as

$$\check{E}_{\text{step}} = \check{E}_{\mathcal{S}} + \check{E}_{\mathcal{P}} + \check{E}_{\mathcal{R}}. \quad (8.14)$$

The modified energetic cost \check{E} , defined in (8.13), has the same form as the original energetic cost E , defined in (6.1). Similarly, the modified total energetic cost \check{E}_{step} , given by (8.14) has

the same form as the original total energetic cost E_{step} , given by (6.2). The only difference between the modified and the original versions is that c_1 and c_2 are replaced with their modified versions \check{c}_1 and \check{c}_2 . Therefore, *all the energetic analyses done so far (approximate and accurate energy-optimal retraction impulse and rates) are also valid with the inclusion of active negative work at heel-strike, if we just replace c_1 and c_2 with \check{c}_1 and \check{c}_2 .*

At one extreme, heel-strike is fully passive ($k=0$), resulting in $\check{c}_1 = c_1$ and $\check{c}_2 = c_2$. In this case, the optimality of swing retraction at any given step angle α and average walking speed V is determined, as before, by the ratio $\check{c}_2/\check{c}_1 = c_2/c_1$ (Fig. 8.4 – Fig. 8.8 do not change). At the other extreme, heel-strike is fully active ($k=1$, resulting in $\check{c}_2 = 0$, and $\check{c}_1 = c_1 + c_2 \neq 0$). In this case, the optimality condition for retraction is similar to that of free negative work shown in Fig. 8.4a. In other words, when heel-strike is fully active swing retraction is *always* energetically optimal, independent of the values of c_1 and c_2 . Therefore, by increasing the contribution of active negative work in heel-strike dissipations, swing retraction becomes energetically advantageous in a wider range of step lengths and walking speeds (the cyan ① area in Fig. 8.4 grows within the admissible region). This is because increasing k increases the direct cost of heel-strike, so the balance between the energy savings of retraction (reduced push-off work and heel-strike dissipation) and the extra effort spent by retraction (decelerating and reaccelerating the leg) is influenced by more energy saving.

8.3.4 Swing Retraction Can Reduce the Net Energetic Cost of Walking

Now, I return to the question asked in the title of Section 8.3: Does swing-leg retraction reduce the net energetic cost of walking? The answer to this question can be given as the 8th advantage of active swing-leg retraction:

*depending on the average walking speed, step length, the ratio of positive and negative work efficiencies, and the contribution of actuator work in heel-strike energy dissipation, swing retraction **can** reduce the net energetic cost of walking.*

The ratio of positive and negative work efficiencies, *i.e.* c_2/c_1 , and the contribution of actuator work in heel-strike energy dissipation, *i.e.* the quantity k in (8.5), independently influence the optimality of swing retraction: as c_2/c_1 increases, the range of step lengths and speeds for which swing retraction is energetically advantageous *decreases*, whereas increasing k *increases* this range.

Note that in this study I have only considered the level-ground walking. When walking on a slope or a staircase, gravity can passively provide a significant portion of the positive/negative work, so the results might be slightly different from what was found here. For example, the optimization results in Chapter 3 suggest that for downhill walking an *extensional* retraction torque ($\mathcal{R} < 0$) is energetically optimal in the admissible region (to increase the heel-strike impact loss as a cost-effective way for dissipating the extra kinetic energy obtained during the step). This is not the case for level-ground walking, as can be seen in Fig. 8.4 ($\mathcal{R}^* \neq 0$).

8.4 Summary

Motivated by the predictions of approximate analytic solutions in the previous chapter, I discovered new aspects of swing-leg retraction. I showed that without a retracting hip torque, heel-strike can be missed at fast speeds or short steps, and therefore periodic walking will not be possible. In other words, active swing-leg retraction enables walking at fast speeds or short steps. I also showed that, at any given step length and speed, a retraction torque can reduce the push-off impulse required for the periodic walk. This reduction facilitates the production of push-off force and also decreases the energetic cost associated with push-off work. Although this energy saving comes at an extra effort spent by the hip actuator to retract the leg, swing-leg retraction can still result in a net energetic saving. My analyses showed that depending on the step length, walking speed, relative timing of push-off and

retraction, actuator efficiencies for positive and negative work, and the contribution of actuator work in heel-strike energy dissipation, the energy saving of a reduced push-off force and heel-strike collision can exceed the extra effort spent for retraction, leading to a net energy saving.

The above mentioned advantages of active swing-leg retraction were either not known before (reducing the push-off impulse, and increasing maximum walking speed), or a very small picture of the entire scenario had been discovered (possible net energetic saving). The findings of this work, together with the previously discovered advantages reviewed at the beginning of this chapter, constitute the 8 advantages of swing-leg retraction that can potentially explain why swing retraction is a common characteristic of biological legged locomotion. These advantages can be summarized as below:

swing retraction

1. helps biped stability,
2. improves disturbance rejection,
3. improves state estimation,
4. facilitates foot-ground clearance,
5. reduces risk of slippage at heel strike,
6. enables faster walking and shorter steps,
7. makes push-off easier,
8. can reduce the net energetic cost.

Chapter 9

CONCLUSIONS

In this thesis I probed two simple bipedal models with analytic and numerical techniques in order to achieve a better understanding of the governing principles of effective legged locomotion.

The first model, shown in Fig. 2.1, consists of a torso, flat feet, and actuated telescoping legs, and is equipped with actuated hip and ankle joints. I used this model with numerical optimization to find the characteristics of energy optimal gaits, and to investigate the effective strategies for reducing the cost of locomotion in different circumstances.

In the second model, shown in Fig. 5.1, the torso is reduced to a point-mass at the hip. This reduction in the model is meant to facilitate calculating approximate analytic solutions for different gait parameters to study the consequences of swing-leg retraction in walking. The analytic solutions helped to obtain new insights into the influence of different factors in system behavior.

Energy optimality is the main criterion for most of the analyses in this thesis. I have used a work-based energetic cost model, given by (2.1) or in a simpler form by (6.1), in which positive and negative mechanical work done by an actuator have individual contributions *via* the actuator efficiency associated with each.

9.1 Insights From Energy-Optimal Gaits of a Minimally Constrained Model

In Chapters 2-4, dynamic optimization was used to investigate the energy-optimal gaits of the first model. The corresponding optimal control problem was formulated in Chapter 2. A gait was considered optimal if its COT, given by (2.2), was minimum for given gait parameters

(*e.g.* desired forward speed). In previous studies with minimalistic models, extra constraints were required to achieve practical gaits (for instance minimum step length constraint in [25]). The current work differs from the previous analyses by limiting the imposed constraints to almost only those required for a physically consistent system; allowing the optimization to freely define the appropriate gait. The minor increase in the current model complexity over previous minimalistic ones permitted the removal of unrealistic and artificial constraints.

Although simple, the model provides numerous insights into human locomotion dynamics. In particular, my minimally constrained model automatically determined that:

- Pendular walk and impulsive run are the most efficient gaits (from an energetic point of view) in, respectively, low and high forward speeds.
- Bouncing motion of the CoM is economical at higher speeds even without having elasticity in the structure.
- For work-based energetic costs, the optimal gaits are always collisional (if allowed), but the impact impulse and its dissipation varies with different parameters including the slope of terrain.
- The optimal gaits for different terrains and speeds are determined by a slope-dependent balance between heel-strike impact loss and the costs associated with its avoidance. For level-ground gaits this balance occurs when collision loss is reduced, but not avoided completely, whereas by increasing or decreasing the slope (moving on a staircase or a ramp) the balance moves respectively toward complete collision avoidance or inclusion of substantial collision loss.
- For level-ground or uphill gaits, swing-leg retraction serves as part of the optimal strategy to increase the efficiency of locomotion by reducing the impact loss (later in Chapter 8 it was shown that this energy saving results in a reduced push-off impulse and push-off work). For level-ground gaits, leg retraction is achieved actively by applying hip torque to the swing leg, while in uphill

gaits swing leg retraction is accomplished largely through the passive action of gravity. In down-hill gaits retraction is replaced with extension (moving the swing leg forward) to increase the energy-loss at heel-strike. This is a cost-effective way of dissipating the extra kinetic energy obtained during the step.

- Stance-leg push-off just before heel-strike is another important strategy to reduce the collision loss in gaits that always have a support leg on the ground.
- In gaits with an aerial phase landing on a near vertical leg reduces the momentum loss in the horizontal direction, and consequently the collision loss.
- Burst activities of swing hip torque limited to both ends of the swing period, rather than smoothly generated throughout the swing, minimizes swing work because it allows a greater contribution from passive sources.
- An extended double support phase in walking is not energetically efficient unless extra constraints are imposed.
- Pre-emptive push-off (to change the linear momentum of the CoM) is the main contribution of the ankle rather than applying torque to change the angular momentum. Therefore, if push-off is provided by another means (such as a telescoping actuator along the axis of the stance leg), then the (revolute) ankle actuator will have negligible activity in all gaits.
- For uphill or downhill gaits, the stance-hip torque (the torque between the torso and the support leg) can be large and, potentially, destabilize the torso. In order to passively stabilize the torso in this case, the upper body should be properly leaned to take advantage of gravity to compensate for the destabilizing hip torque.

Some of these observations have been recognized and reported previously based on optimization of minimal models [25, 26]. These previous observations were verified here with a

slightly more realistic model.

One of the main outcomes of this study is that despite the apparent differences between walking and running, they share the same determinant factors for effective gait coordination. The difference between walking and running comes only from the different strategies available to minimize the energetic cost at different speeds. Based on the results of the gait optimizations, two energetic cost factors were identified that interplay to determine the most efficient movement pattern. One is the cost of stance-leg work associated with deflecting the CoM motion from downward to upward at each step [48, 49]. This cost is influenced by (i) passive and active energy dissipations in the decelerating (downward) part of redirecting the CoM motion, and (ii) the generative work of the (trailing) stance-leg to make-up for the energy dissipations and accelerate the CoM to move upward. The second main energetic factor involved in the optimization of gait is the cost of swinging the legs, including the cost of accelerating the leg at the beginning of swing to regulate the step length and step frequency, and the cost of decelerating and retracting the leg before touch-down to reduce the collision loss and prepare the leg for support transfer.

These factors are strongly inter-related:

- The dissipations associated with the step-to-step CoM transition from downward to upward (a part of the 1st factor) is reduced by a proper timing of stance leg push-off (the generative part of the 1st factor) and heel-strike [26, 47].
- Accelerating the swing leg (the 2nd factor) at the beginning of the swing phase increases the step frequency beyond the natural frequency of the leg and results in a shorter step length and less collision loss (the 1st factor) [47].
- The stance-leg push-off work (the 1st factor) and the swing-hip's declarative work (negative swing-retraction work; the 2nd factor) are reduced by a proper timing of push-off force and retraction torque (see Section 6.4).
- Active swing-leg retraction (the 2nd factor) reduces the stance-leg push-off

impulse (the 1st factor) required for a given periodic gait (see Section 8.1).

- Swing-leg retraction (the 2nd factor) can reduce the relative foot-ground velocity at touch-down and result in a less heel-strike collision loss (the 1st factor).

Therefore, the effective movement strategy is the one that takes advantage of the interaction among these determinant factors to achieve the minimum energetic cost for different functional circumstances.

Many of the energetic and kinematic characteristics of the optimization model match those of human walking and running in different circumstances (Chapters 3 and 4). In particular, the model correctly predicts the changes in human gait energetics in simulated reduced gravity conditions, measured by Farley and McMahon [87]: the energetic costs of walking and running decrease with a reduction in effective gravity, but the changes in the cost of running are substantially larger than those in walking. The consistency between the model predictions and human gait observations even in these unusual circumstances (simulated reduced gravity) strongly supports the hypothesis that energy minimization is the dominant governing principle in human gait coordination [14, 26, 72, 73, 92, 93]. It also indicates that energy minimization in human gait is mainly influenced by the balance between the same determinant factors (the costs of support and swing leg) responsible for the model's optimal gaits.

9.2 Swing-Leg Retraction

Using the second bipedal model introduced in this thesis, I investigated new aspects of swing-leg retraction in bipedal walking. One of the strengths of this study is that almost all analyses have been done analytically, and the use of numerical methods have mostly been limited to verifying the predictions of the approximate analytic solutions.

After simplifying the energy-optimal walking of this model into a sequence of impulsive

and smooth phases in Chapter 5, and calculating the positive and negative work of overlapping impulsive forces and torques in Chapter 6, I showed that, for any given push-off and retraction impulses, the energy-optimal relative timing of the impulsive push-off force and retraction torque depends on whether the hip torque is *retracting* (pushing the swing leg rearward) or *extending* (pushing the swing leg forward): If it is *retracting*, the optimal timing is to apply the impulsive push-off force completely before the impulsive hip torque, otherwise it is best to apply the impulsive push-off force *almost* completely after the impulsive hip torque. In the latter, the adverb ‘almost’ refers to the negligible portion of the push-off impulse that should be applied during the extending hip torque to avoid shortening the stance leg. These relative timings improve the gait efficiency by reducing the positive and negative work done by the push-off force and retraction torque, respectively. Interestingly, the above results are valid for a large range of bipedal systems (including humans) in which the push-off force causes the swing leg to move rearward (this rearward motion is caused by the inertial forces induced on the swing leg due the coupling in the system).

Using a series of approximations, I obtained closed-form approximate analytic solutions for most of the gait parameters, such as the leg angles and velocities throughout the step, the maximum average walking speed at any possible step length, the energy-optimal retraction impulse and retraction rates, and the push-off, swing thrust, and minimum and maximum retraction impulses required for periodic walking. These approximate analytic solutions led to the following discoveries that were also verified using numerical solutions:

- Active swing-leg retraction *can increase the high-speed limit of walking*. Although the reduced ground reaction force, caused by the inverted pendulum-like motion of the CoM, can be a limiting factor in maximum walking speed, transitioning from one step to other is also important. Without active retraction, heel-strike can be missed at fast speeds or short steps, and the biped will switch from walking to running (even at speeds less than those predicted by a

single inverted pendulum, *e.g.* [95]).

- For a given walking speed and step length, active leg retraction *can reduce the push-off impulse*, and thus the actuator/muscle forces needed for push-off. When the hip actuator applies a retracting torque to the swing leg, a reaction force is applied on the hip and accelerates it forward. This reduces the push-off impulse that is required to achieve a desired hip acceleration before heel-strike. In contrast to push-off, the swing thrust impulse (the early-swing hip torque that accelerates the swing leg motion) is almost independent of the retraction impulse, and is mainly determined by the step length and average speed.
- *Active swing-leg retraction can result in a net energetic saving, but not in all cases.* My analyses showed that *the energetic utility of swing retraction depends on the*

1. *step length,*
2. *speed,*
3. *actuator efficiencies for positive and negative work, and*
4. *contribution of active work in heel-strike energy dissipation.*

As the ratio of negative work efficiency to positive work efficiency increases (the ratio c_2/c_1 decreases, where c_1 and c_2 are the costs of unit positive and negative work, respectively), or the contribution of actuator (negative) work in the dissipations of CoM motion redirection increases, swing retraction becomes energetically beneficial for a larger range of step lengths and speeds. **Note:** although a retracting hip torque might be energetically inefficient in some gaits (increases the net energetic cost), it still might be required to ensure heel-strike. In other words, the application of a retraction torque in an energy-optimal gait may not be due to its energetic advantage, but to make the gait feasible.

9.3 Future Works

9.3.1 Gait Optimization with More Realistic Models:

Although the models used in this thesis are more complex than the minimalistic models studied by other researchers (*e.g.* [25, 26, 47, 67]), they still involve many simplifications. For example, in the first bipedal model (Fig. 2.1) the feet and the lower leg segments are massless, joints are frictionless, the forces and torques can increase unboundedly at foot-ground contacts, actuator forces/torques are fully independent of the corresponding joint velocities, energy supplied to each actuator only depends on its mechanical work, etc. The second bipedal model (Fig. 5.1) involves more simplifications, since it is a simplified version of the first model.

In reality, none of the above simplifying assumptions is valid. A possible extension of the current work is to modify these assumptions and consider a more realistic model of either a robot or humans. For example, the ideal actuator model can be replaced with the model of a physical actuator, such as a muscle or motor. This will realistically limit the peak force, speed, and joint power, and will impose force-velocity constraints that are missing in the current study (in most actuators the maximum torque decreases with speed). Furthermore, with a more realistic actuator model a more accurate estimation of the energetic cost can be obtained, since the energy supplied to the actuators can be directly calculated.

9.3.2 Experimental Verification of Model Predictions:

The analysis in this thesis led to a few predictions that need to be examined with human subjects. For example, an apparatus of the type in Fig. 4.1 can be used to evaluate the model predictions of changes in human gait kinematics under simulated reduced gravity (Chapter 4). In fact, this experimental study is a part of my research plan for the near future.

Other possible experimental studies that can be inspired by this work include the explo-

ration of the range of step length and speed for which swing-leg retraction is not observed in human walking (Chapter 8), and investigating the relative timing of push-off force and retraction torque in human walking (Chapter 6). These experimental studies can be used as another validation of the hypothesis that energy minimization is the main governing principle of human gait coordination.

9.3.3 Energy-Efficient Closed-Loop Control:

The actuator forces and torques calculated for different optimal gaits in this thesis are open-loop policies and most likely do not result in any stable gait. In practice, feedback control is necessary to achieve a desired steady gait with almost any mechanism. Now, the question is how to achieve energy efficiency while guaranteeing stability/robustness?

A traditional approach to this problem is to use a given optimization-generated gait as a reference trajectory and use high bandwidth feedback controllers to stabilize the system around that trajectory. Although this technique is simple, it usually does not lead to an energy-efficient gait. Why? Because efficiency in almost all optimal gaits mainly relies on exploiting the natural dynamics of the system. Normally, the optimal policy is to let different parts of the system move passively or with minimal force during some portion of the gait cycle, and to apply the main control actions (actuator forces and torques) only at some critical intervals (Chapter 3). However, high-gain controllers do not take advantage of the natural dynamics of the system and continuously apply control actions (no passive intervals) to drive any deviation from the reference trajectory to zero.

Another approach that seems more promising is to use a given feedback control scheme, *e.g.* state feedback, with gains to be determined by the optimization. The set of the optimal gains is the one that maximizes a proper performance measure that encodes both efficiency and stability/robustness. For example, the optimization can search for the gains that result in a minimum cost of transport with N (sufficiently large) successful steps. Obviously,

the resulting efficiency (*e.g.* cost of transport) in this method depends on the implemented controller scheme. The open-loop gaits generated using trajectory optimization can be used as the baselines to evaluate the performance of a given controller in achieving efficient gaits.

Bibliography

- [1] E. R. Westervelt, J. W. Grizzle, C. Chevallereau, J. H. Choi, and B. Morris, *Feedback Control of Dynamic Bipedal Robot Locomotion*. CRC Press, 2007.
- [2] J. E. A. Bertram and S. J. Hasaneini, “Neglected losses and key costs: tracking the energetics of walking and running,” *J. Exp. Biol.*, vol. 216, no. 6, pp. 933–938, Mar. 2013.
- [3] H. Geyer, “Simple models of legged locomotion based on compliant limb behavior,” Ph.D. dissertation, Friedrich Schiller University of Jena, Germany, 2005.
- [4] J. Pratt, “Exploiting inherent robustness and natural dynamics in the control of bipedal walking robots,” Ph.D. dissertation, Massachusetts Institute of Technology, Boston, MA, USA, 2000.
- [5] P. A. Bhounsolue, “A controller design framework for bipedal robots: Trajectory optimization and event-based stabilization,” Ph.D. dissertation, Cornell University, Ithaca, NY, USA, May 2012.
- [6] A. D. Kuo, “Choosing Your Steps Carefully, Trade-offs Between Economy and Versatility in Dynamic Walking Bipedal Robots,” *IEEE Robotics and Automation Magazine*, vol. 14, no. 2, pp. 18–29, 2007.
- [7] Y. Sakagami, R. Watanabe, C. Aoyama, S. Matsunaga, N. Higaki, and K. Fujimura, “The intelligent asimo: System overview and integration,” in *Intelligent Robots and Systems, 2002. IEEE/RSJ International Conference on*, vol. 3. IEEE, 2002, pp. 2478–2483.
- [8] Honda. (2013) ASIMO The world’s most advanced humanoid robot. [Online]. Available: <http://asimo.honda.com/>

- [9] Boston Dynamics, “Petman - bigdog gets a big brother,” 2009. [Online]. Available: http://www.bostondynamics.com/robot_petman.html
- [10] —, “Atlas - The Agile Anthropomorphic Robot,” 2013. [Online]. Available: http://www.bostondynamics.com/robot_Atlas.html
- [11] A. Ruina. (2012) Reflex approximation of optimal control for an energy-efficient bipedal walking platform. [Online]. Available: http://ruina.tam.cornell.edu/research/topics/locomotion_and_robotics/NSFRuinaRobotProposal2012.pdf
- [12] P. Bhounsule, J. Cortell, B. Hendriksen, J. Karssen, C. Paul, and A. Ruina, “A robot that can walk far using little energy,” *submitted to the Int. J. Robotic Research*, 2012.
- [13] R. M. Alexander, “Mechanics of bipedal locomotion,” *In: Perspectives in Experimental Biology*, vol. 1, pp. 493–504, 1976.
- [14] —, “Optimization and gaits in the locomotion of vertebrates,” *Physiological Reviews*, vol. 69, no. 4, pp. 1199–1227, 1989.
- [15] R. Blickhan, “The spring-mass model for running and hopping,” *J. Biomechanics*, vol. 22, pp. 1217–1227, 1989.
- [16] T. A. McMahon and G. C. Cheng, “The mechanics of running: how does stiffness couple with speed?” *Journal of Biomechanics*, vol. 23, pp. 65–78, 1990.
- [17] C. T. Farley, R. Blickhan, J. Saito, and C. R. Taylor, “Hopping frequency in humans: a test of how springs set stride frequency in bouncing gaits,” *Journal of Applied Physiology*, vol. 71, no. 6, pp. 2127–2132, 1991.
- [18] R. Blickhan and R. Full, “Similarity in multilegged locomotion: bouncing like a monopode,” *Journal of Comparative Physiology A*, vol. 173, no. 5, pp. 509–517, 1993.

- [19] W. J. Schwind and D. E. Koditschek, “Characterization of monopod equilibrium gaits,” in *Robotics and Automation, 1997. Proceedings., 1997 IEEE International Conference on*, vol. 3. IEEE, 1997, pp. 1986–1992.
- [20] G. Cavagna and R. Margaria, “Mechanics of walking.” *Journal of Applied Physiology*, vol. 21, no. 1, pp. 271–278, 1966.
- [21] J. B. d. M. Saunders, V. T. Inman, and H. D. Eberhart, “The major determinants in normal and pathological gait,” *The Journal of Bone & Joint Surgery*, vol. 35, no. 3, pp. 543–558, 1953.
- [22] G. Cavagna, N. Heglund, and C. Taylor, “Mechanical work in terrestrial locomotion: Two basic mechanisms for minimizing energy expenditure,” *Am. J. Physiol.*, vol. 233, pp. 243–261, 1977.
- [23] R. M. Alexander and A. Jayes, “A dynamic similarity hypothesis for the gaits of quadrupedal animals,” *J. Zoology*, vol. 210, pp. 135–152, 1983.
- [24] R. Kram, A. Domingo, and D. P. Ferris, “Effect of reduced gravity on the preferred walk-run transition speed,” *J. Exp. Biol.*, vol. 200, pp. 821–826, 1997.
- [25] M. Srinivasan and A. Ruina, “Computer optimization of a minimal biped model discovers walking and running,” *Nature Magazine*, vol. 439, no. 7072, pp. 72–75, January 2006.
- [26] A. Ruina, J. E. A. Bertram, and M. Srinivasan, “A collisional model of the energetic cost of support work qualitatively explains leg sequencing in walking and galloping, pseudo-elastic leg behavior in running and the walk-to-run transition,” *J. Theor. Biol.*, vol. 237, no. 2, pp. 170–192, November 2005.
- [27] G. Cavagna, F. Saibene, and R. Margaria, “Mechanical work in running,” *Journal of Applied Physiology*, vol. 19, no. 2, pp. 249–256, 1964.

- [28] G. A. Cavagna and M. Kaneko, “Mechanical work and efficiency in level walking and running,” *J. Physiol.*, vol. 268, pp. 467–481, 1977.
- [29] H. Geyer, A. Seyfarth, and R. Blickhan, “Compliant leg behaviour explains basic dynamics of walking and running,” *Proc. of the Royal Society of London, Series B: Biological Sciences*, vol. 273, pp. 2861–2867, 2006.
- [30] F. Iida, J. Rummel, and A. Seyfarth, “Bipedal walking and running with spring-like biarticular muscles,” *Journal of biomechanics*, vol. 41, no. 3, pp. 656–667, 2008.
- [31] S. J. Hasaneini, C. J. B. Macnab, J. E. A. Bertram, and H. Leung, “Gravity effects on energetics and kinematics of walking and running using dynamic optimization,” in *Online Proc. of Dynamic Walking Conf.*, 2011, pp. 101–102.
- [32] —, “Dynamic optimization clearly shows the determinants of bipedal gaits: reduced gravity predictions and verification,” in *Online Proc. of Dynamic Walking Conf.*, 2012.
- [33] J. Basmajian, “The human bicycle,” *Biomechanics VA*, pp. 297–302, 1976.
- [34] G. A. Cavagna, H. Thys, and A. Zamboni, “The sources of external work in level walking and running.” *The Journal of physiology*, vol. 262, no. 3, pp. 639–657, 1976.
- [35] S. Mochon and T. A. McMahon, “Ballistic walking,” *Journal of Biomechanics*, vol. 13, no. 1, pp. 49–57, 1980.
- [36] —, “Ballistic walking: an improved model,” *Mathematical Biosciences*, vol. 52, no. 1, pp. 241–260, 1980.
- [37] T. McGeer, “Stability and control of two-dimensional biped walking,” *Center for Systems Science, Simon Fraser University, Burnaby, BC, Canada, Technical Report CSS-IS TR 88-01*, vol. 1, 1988.

- [38] —, “Passive dynamic walking,” *Center for Systems Science, Simon Fraser University, Burnaby, BC, Canada, Technical Report CSS-IS TR 88-02*, vol. 1, 1988.
- [39] —, “Passive dynamic walking,” *The Int. J. Robotic Research*, vol. 9, no. 2, pp. 62–82, 1990.
- [40] —, “Passive walking with knees,” in *Proc. of IEEE ICRA*, 1990, pp. 1640–1645.
- [41] —, “Dynamics and control of bipedal locomotion,” *Journal of Theoretical Biology*, vol. 163, no. 3, pp. 277–314, 1993.
- [42] —, “Passive dynamic biped catalogue, 1991,” in *Experimental Robotics II*. Springer, 1993, pp. 463–490.
- [43] —. (2010, Oct.) McGeer and passive dynamic bipedal walking. [Online]. Available: <http://youtu.be/WOPED7I5Lac>
- [44] S. H. Collins, M. Wisse, and A. Ruina, “A three-dimensional passive-dynamic walking robot with two legs and knees,” *The International Journal of Robotics Research*, vol. 20, no. 7, pp. 607–615, 2001.
- [45] S. Collins, A. Ruina, R. Tedrake, and M. Wisse, “Efficient bipedal robots based on passive-dynamic walkers,” *Science Magazine*, vol. 307, no. 5712, pp. 1082–1085, 2005.
- [46] M. Garcia, A. Chatterjee, A. Ruina, and M. Coleman, “The simplest walking model: Stability, complexity, and scaling,” *ASME J. Biomechanical Engineering*, vol. 120, no. 2, pp. 281–288, April 1998.
- [47] A. D. Kuo, “Energetics of actively powered locomotion using the simplest walking model,” *J. Biomedical Eng.*, vol. 124, pp. 113–120, 2002.
- [48] A. D. Kuo, J. M. Donelan, and A. Ruina, “Energetic consequences of walking like an inverted pendulum: step-to-step transitions,” *Exercise and sport sciences reviews*,

- vol. 33, no. 2, pp. 88–97, 2005.
- [49] J. M. Donelan, R. Kram, and A. D. Kuo, “Mechanical work for step-to-step transitions is a major determinant of the metabolic cost of human walking,” *Journal of Experimental Biology*, vol. 205, no. 23, pp. 3717–3727, 2002.
- [50] P. G. Adamczyk and A. D. Kuo, “Redirection of center-of-mass velocity during the step-to-step transition of human walking,” *J. Exp. Biol.*, vol. 212, pp. 2668–2678, 2009.
- [51] V. T. Inman, H. J. Ralston, and F. Todd, *Human walking*. Baltimore: Williams & Wilkins, 1981.
- [52] E. Muybridge, *Animal locomotion*. Published under the auspices of the University of Pennsylvania, 1887.
- [53] N. Eckett. (2012, Mar.) Sprint form slow motion. [Online]. Available: <http://youtu.be/PH-3cHxXAK0>
- [54] P. Brewster. (2012, Jan.) Treadmill, gait HD - halt imaging. [Online]. Available: <http://youtu.be/D0fzcDu46fM>
- [55] J. Rose and J. G. Gamble, *Human Walking*, 2nd ed. Baltimore: Williams & Wilkins, 1994.
- [56] S. J. Gray, *Animal locomotion*. Weidenfeld & Nicolson London, 1968.
- [57] National Geographic. (2012, Dec.) Cheetahs on the edge - director’s cut. [Online]. Available: http://youtu.be/THA_5cqAfCQ
- [58] R. Ghigliazza, R. Altendorfer, P. Holmes, and D. Koditschek, “A simply stabilized running model,” *SIAM Journal on Applied Dynamical Systems*, vol. 2, no. 2, pp. 187–218, 2003.

- [59] A. Seyfarth, H. Geyer, and H. Herr, “Swing-leg retraction: a simple control model for stable running,” *J. Exp. Biol.*, vol. 206, pp. 2547–2555, 2003.
- [60] H. K. Khalil, *Nonlinear Systems*. New York: Macmillan Publishing Company, 1992.
- [61] M. Wisse, C. G. Atkeson, and D. K. Kloimwieder, “Swing leg retraction helps biped walking stability,” in *Proc. 5th IEEE-RAS Int. Conf. on Humanoid Robots*, Tsukuba, Japan, Dec. 2005, pp. 295–300.
- [62] D. G. E. Hobbelen and M. Wisse, “Swing-leg retraction for limit cycle walkers improves disturbance rejection,” *Robotics, IEEE Trans. on*, vol. 24, no. 2, pp. 377–389, 2008.
- [63] J. G. D. Karssen, M. Haberland, M. Wisse, and S. Kim, “The optimal swing-leg retraction rate for running,” in *Proc. 2011 IEEE Int. Conf. on Robotics and Automation (ICRA)*, Shanghai, China, May 2011, pp. 4000–4006.
- [64] J. Grizzle. (2013, Jul.) Progress on controlling MARLO, an Atrias-series 3D underactuated bipedal robot. [Online]. Available: <http://youtu.be/qXIfHBH4ry0>
- [65] M. Haberland, J. Karssen, S. Kim, and M. Wisse, “The effect of swing leg retraction on running energy efficiency,” in *Proc. 2011 IEEE/RSJ Int. Conf. on Intelligent Robots and Systems (IROS)*, San Francisco, CA, USA, Sep 2011, pp. 3957–3962.
- [66] S. J. Hasaneini, C. J. B. Macnab, J. E. A. Bertram, and H. Leug, “The dynamic optimization approach to locomotion dynamics: human-like gaits from a minimally-constrained biped model,” *J. Advanced Robotics*, vol. 27, no. 11, pp. 845–859, Jul. 2013.
- [67] M. Srinivasan, “Fifteen observations on the structure of energy-minimizing gaits in many simple biped models,” *J. Royal Society Interface*, pp. 74–98, 2011.
- [68] M. B. Popovic, A. Goswami, and H. Herr, “Ground reference points in legged locomotion: Definitions, biological trajectories and control implications,” *The Int. J. Robotics Research*, vol. 24, no. 12, pp. 1013–1032, 2005.

- [69] J. Cleese, G. Chapman, T. Gilliam, E. Idle, T. Jones, and M. Palin. Ministry of Silly Walks. for example <http://youtu.be/IqhlQfXUk7w> or <http://youtu.be/9ZlBUglE6Hc>.
- [70] J. E. A. Bertram and A. Ruina, “Multiple walking speed-frequency relations are predicted by constrained optimization,” *J. Theor. Biol.*, vol. 209, pp. 445–453, 2001.
- [71] H. J. Ralston, “Energy-speed relation and optimal speed during level walking,” *European J. Appl. Physiol. and Occupational Physiology (Int Z Angew Physiol.)*, vol. 17, no. 4, pp. 277–283, 1958.
- [72] D. F. Hoyt and C. R. Taylor, “Gait and the energetics of locomotion in horses,” *Nature*, vol. 292, pp. 239–240, 1981.
- [73] R. Margaria, *Biomechanics and Energetics of Muscular Exercise*. Clarendon Press, UK, 1976.
- [74] Y. Hurmuzlu and D. B. Marghitu, “Rigid body collisions of planar kinematic chains with multiple contact points,” *Int. J. Robotic Research*, no. 1, pp. 82–92, 1994.
- [75] M. Ackermann and A. J. van den Bogert, “Optimality principles for model-based prediction of human gait,” *Journal of biomechanics*, vol. 43, no. 6, pp. 1055–1060, 2010.
- [76] ———, “Predictive simulation of gait at low gravity reveals skipping as the preferred locomotion strategy,” *Journal of biomechanics*, vol. 45, no. 7, pp. 1293–1298, 2012.
- [77] J. T. Betts, *Practical Methods for Optimal Control Using Nonlinear Programming*. Society for Industrial and Appl. Mathematics, 2001.
- [78] K. Taji and M. Miyamoto, “A globally convergent smoothing newton method for non-smooth equations and its application to complementarity problems,” *Computational Optimization and Applications*, vol. 22, no. 1, pp. 81–101, 2002.

- [79] M. Srinivasan, “Why walk and run: energetic costs and energetic optimality in simple mechanics-based models of a bipedal animal,” Ph.D. dissertation, Cornell University, May 2006.
- [80] D. A. Winter, *Biomechanics and motor control of human movement*. Hoboken, N.J.: John Wiley & Sons Inc., 2005.
- [81] P. E. Gill and W. Murray, “Snopt: An sqp algorithm for large-scale constrained optimization,” *SIAM J. on Optimization*, vol. 12, no. 4, pp. 979–1006, 2002.
- [82] B. M. Nigg and W. Herzog, *Biomechanics of the Musculo-Skeletal System*. John Wiley & Sons, Inc., 1994, pp. 219–220.
- [83] T. Keller, A. Weisberger, J. Ray, S. Hasan, R. Shiavi, and D. Spengler, “Relationship between vertical ground reaction force and speed during walking, slow jogging, and running,” *Clinical Biomechanics*, vol. 11, no. 5, pp. 253–259, 1996.
- [84] J. Doke, J. M. Donelan, and A. D. Kuo, “Mechanics and energetics of swinging the human leg,” *J. Exp. Biol.*, vol. 208, pp. 439–445, 2009.
- [85] A. D. Kuo, “A simple model of bipedal walking predicts the preferred speedstep length relationship,” *J. Biomech. Eng.*, vol. 123, pp. 264–269, 2001.
- [86] J. M. Donelan and R. Kram, “Exploring dynamic similarity in human running using simulated reduced gravity,” *J. Exp. Biol.*, vol. 203, pp. 2405–2415, 2000.
- [87] C. T. Farley and T. A. McMahon, “Energetics of walking and running: insights from simulated reduced-gravity experiments,” *J. Appl. Physiol.*, vol. 73, no. 6, pp. 2709–2712, 1992.
- [88] D. Newman, “Modeling reduced gravity human locomotion,” *Int. J. Appl. Sci. Comp*, vol. 3, pp. 91–101, 1996.

- [89] B. Davis and P. Cavanagh, “Simulating reduced gravity: a review of biomechanical issues pertaining to human locomotion.” *Aviation, space, and environmental medicine*, vol. 64, no. 6, pp. 557–566, 1993.
- [90] G. Cavagna, F. Saibene, and R. Margaria, “External work in walking,” *Journal of Applied Physiology*, vol. 18, no. 1, pp. 1–9, 1963.
- [91] J. He, R. Kram, and T. A. McMahon, “Mechanics of running under simulated low gravity,” *Journal of Applied Physiology*, vol. 71, no. 3, pp. 863–870, 1991.
- [92] J. A. Borelli and P. Maquet, *On the movement of animals (De Motu Animalium, Pars prima)*. Springer-Verlag, 1989, p. 152.
- [93] R. M. Alexander, “Design by numbers,” *Nature*, vol. 412, no. 6847, pp. 591–591, 2001.
- [94] T. A. McMahon, *Muscles, reflexes, and locomotion*. Princeton, NJ: Princeton University Press, 1984.
- [95] J. R. Usherwood, “Why not walk faster?” *Biol. Lett.*, vol. 1, no. 3, pp. 338–341, Sep 2005.
- [96] R. M. Alexander, *Principles of Animal Locomotion*, ser. Princeton paperbacks. Princeton University Press, 2003.
- [97] A. M. Formal’skii, “Ballistic walking design via impulsive control,” *J. of Aerospace Eng.*, vol. 23, no. 2, pp. 129–138, April 2010.
- [98] G. Strang, *Linear Algebra And Its Applications*, 3rd ed. San Diego, CA: Harcourt Brace Jovanovich, 1988.

Appendix A

Equations of Motion of the Biped With Torso

A.1 Equations of Motion of the Unpinned Biped

The equations of motion of the unpinned biped are given by (2.3) and (2.4). The details of the matrices and vectors in those equations are as below.

A.1.1 Inertia Matrix

$$\mathbf{M} = \begin{bmatrix} M_1 & M_2 \cos(\theta_1 - \theta_2) & M_3 \cos(\theta_1 - \theta_3) \\ M_2 \cos(\theta_2 - \theta_1) & M_4 & M_2 \cos(\theta_2 - \theta_3) \\ M_3 \cos(\theta_3 - \theta_1) & M_2 \cos(\theta_3 - \theta_2) & M_1 \end{bmatrix}, \quad (\text{A.1})$$

where

$$M_1 = I_{\text{leg}/G_{\text{leg}}} + m_{\text{leg}} b^2 (1 - m_{\text{leg}}/m_{\text{tot}}), \quad (\text{A.2})$$

$$M_2 = m_{\text{leg}} m_{\text{trs}} a b / m_{\text{tot}}, \quad (\text{A.3})$$

$$M_3 = -m_{\text{leg}}^2 b^2 / m_{\text{tot}}, \quad (\text{A.4})$$

$$M_4 = I_{\text{trs}/G_{\text{trs}}} + 2 m_{\text{trs}} m_{\text{leg}} a^2 / m_{\text{tot}}. \quad (\text{A.5})$$

A.1.2 Coriolis, Centrifugal, and Gravity Vector

$$\mathbf{c} = \mathbf{c}_1 + \mathbf{c}_2, \quad (\text{A.6})$$

where

$$\mathbf{c}_1 = \begin{bmatrix} (m_{\text{leg}} b - m_{\text{tot}} \ell_1(t)) g \sin(\theta_1 + \gamma) \\ -m_{\text{trs}} a g \sin(\theta_2 + \gamma) \\ m_{\text{leg}} b g \sin(\theta_3 + \gamma) \end{bmatrix}, \quad (\text{A.7})$$

and

$$\mathbf{c}_2 = \begin{bmatrix} 0 & C_1 \sin(\theta_1 - \theta_2) & C_2 \sin(\theta_1 - \theta_3) \\ C_1 \sin(\theta_2 - \theta_1) & 0 & C_1 \sin(\theta_2 - \theta_3) \\ C_2 \sin(\theta_3 - \theta_1) & C_1 \sin(\theta_3 - \theta_2) & 0 \end{bmatrix} \begin{bmatrix} \dot{\theta}_1^2 \\ \dot{\theta}_2^2 \\ \dot{\theta}_3^2 \end{bmatrix}, \quad (\text{A.8})$$

with

$$C_1 = a b m_{\text{leg}} m_{\text{trs}} / m_{\text{tot}}, \quad (\text{A.9})$$

$$C_2 = -m_{\text{leg}}^2 b^2 / m_{\text{tot}}. \quad (\text{A.10})$$

A.1.3 Jacobian Matrices

$$\mathbf{J}_{1\theta} = \begin{bmatrix} \left(\ell_1 - \frac{b m_{\text{leg}}}{m_{\text{tot}}} \right) \cos \theta_1 & \frac{a m_{\text{trs}} \cos \theta_2}{m_{\text{tot}}} & -\frac{b m_{\text{leg}} \cos \theta_3}{m_{\text{tot}}} \\ \left(\ell_1 - \frac{b m_{\text{leg}}}{m_{\text{tot}}} \right) \sin \theta_1 & \frac{a m_{\text{trs}} \sin \theta_2}{m_{\text{tot}}} & -\frac{b m_{\text{leg}} \sin \theta_3}{m_{\text{tot}}} \end{bmatrix}, \quad (\text{A.11})$$

$$\mathbf{J}_{21\theta} = \begin{bmatrix} -\ell_1 \cos \theta_1 & 0 & \ell_2 \cos \theta_3 \\ -\ell_1 \sin \theta_1 & 0 & \ell_2 \sin \theta_3 \end{bmatrix} \quad (\text{A.12})$$

A.1.4 Torque-Influence Matrix

$$\mathbf{B} = \begin{bmatrix} 1 & 1 & 0 & 0 \\ 0 & -1 & -1 & 0 \\ 0 & 0 & 1 & 1 \end{bmatrix} \quad (\text{A.13})$$

A.2 Equations of Motion in Single Support Phase

The equations of motion in single support phase are given by (2.10). The details of the matrices and vectors in that equation are as below.

A.2.1 Mass-Inertia Matrix

$$\mathbf{M}_{ss} = \begin{bmatrix} M_{ss11} & 0 & M_{ss13} & M_{ss14} \\ 0 & M_{ss22} & M_{ss23} & M_{ss24} \\ M_{ss13} & M_{ss23} & M_{ss33} & 0 \\ M_{ss14} & M_{ss24} & 0 & M_{ss44} \end{bmatrix} \quad (\text{A.14})$$

where

$$M_{ss11} = m_{\text{tot}}, \quad (\text{A.15})$$

$$M_{ss13} = m_{\text{trs}} a \sin(\theta_1 - \theta_2), \quad (\text{A.16})$$

$$M_{ss14} = -m_{\text{leg}} b \sin(\theta_1 - \theta_3), \quad (\text{A.17})$$

$$M_{ss22} = I_{\text{leg}/G_{\text{leg}}} + m_{\text{tot}} \ell_1^2 + m_{\text{leg}} b (b - 2 \ell_1), \quad (\text{A.18})$$

$$M_{ss23} = m_{\text{trs}} a \ell_1 \cos(\theta_1 - \theta_2), \quad (\text{A.19})$$

$$M_{ss24} = -m_{\text{leg}} b \ell_1 \cos(\theta_1 - \theta_3), \quad (\text{A.20})$$

$$M_{ss33} = I_{\text{trs}/G_{\text{trs}}} + m_{\text{trs}} a^2, \quad (\text{A.21})$$

$$M_{ss44} = I_{\text{leg}/G_{\text{leg}}} + m_{\text{leg}} b^2. \quad (\text{A.22})$$

A.2.2 Coriolis, Centrifugal, and Gravity Vector

$$\mathbf{c}_{ss} = \mathbf{c}_{1ss} + \mathbf{c}_{2ss}, \quad (\text{A.23})$$

where

$$\mathbf{c}_{1ss} = \begin{bmatrix} m_{\text{tot}} g \cos(\theta_1 + \gamma) \\ (m_{\text{leg}} b - m_{\text{tot}} \ell_1(t)) g \sin(\theta_1 + \gamma) \\ -m_{\text{trs}} a g \sin(\theta_2 + \gamma) \\ m_{\text{leg}} b g \sin(\theta_3 + \gamma) \end{bmatrix}, \quad (\text{A.24})$$

and

$$\mathbf{c}_{2_{ss}} = \begin{bmatrix} 0 & C_{ss12} & C_{ss13} & C_{ss14} \\ -C_{ss12} & 0 & C_{ss23} & C_{ss24} \\ -C_{ss13} & -C_{ss23} & 0 & 0 \\ -C_{ss14} & -C_{ss24} & 0 & 0 \end{bmatrix} \begin{bmatrix} 2 \dot{\ell}_1 \dot{\theta}_1 \\ \dot{\theta}_1^2 \\ \dot{\theta}_2^2 \\ \dot{\theta}_3^2 \end{bmatrix}, \quad (\text{A.25})$$

with

$$C_{ss1} = m_{\text{leg}} b - m_{\text{tot}} \ell_1, \quad (\text{A.26})$$

$$C_{ss2} = -m_{\text{trs}} a \cos(\theta_1 - \theta_2), \quad (\text{A.27})$$

$$C_{ss3} = m_{\text{leg}} b \cos(\theta_1 - \theta_3), \quad (\text{A.28})$$

$$C_{ss4} = m_{\text{trs}} \ell_1 a \sin(\theta_1 - \theta_2), \quad (\text{A.29})$$

$$C_{ss5} = -m_{\text{leg}} \ell_1 b \sin(\theta_1 - \theta_3). \quad (\text{A.30})$$

A.2.3 Torque-Influence Matrix

$$\mathbf{B}_{ss} = \begin{bmatrix} 1 & 0 & 0 & 0 \\ 0 & 1 & 1 & 0 \\ 0 & 0 & -1 & -1 \\ 0 & 0 & 0 & 1 \end{bmatrix} \quad (\text{A.31})$$

A.3 Equations of Motion in Double-Support Phase

The equations of motion in double-support phase are given by (2.14). The details of the matrices and vectors in that equation are as below.

A.3.1 Mass-Inertia Matrix

$$\mathbf{M}_{\text{ds}} = \begin{bmatrix} M_{\text{ds}11} & M_{\text{ds}12} & 0 & M_{\text{ds}14} \\ M_{\text{ds}21} & M_{\text{ds}22} & M_{\text{ds}23} & 0 \\ M_{\text{ds}31} & M_{\text{ds}32} & M_{\text{ds}33} & 0 \\ M_{\text{ds}41} & M_{\text{ds}42} & M_{\text{ds}43} & M_{\text{ds}44} \end{bmatrix}, \quad (\text{A.32})$$

where

$$M_{\text{ds}11} = -\frac{\sin(\theta_1 - \theta_3)}{\sin \theta_3}, \quad (\text{A.33})$$

$$M_{\text{ds}12} = -\frac{\ell_1 \cos(\theta_1 - \theta_3)}{\sin \theta_3}, \quad (\text{A.34})$$

$$M_{\text{ds}14} = \frac{\ell_2}{\sin \theta_3}, \quad (\text{A.35})$$

$$M_{\text{ds}21} = -\frac{m_{\text{tot}} \ell_1}{\tan(\theta_1 - \theta_3)}, \quad (\text{A.36})$$

$$M_{\text{ds}22} = I_{\text{leg}/G_{\text{leg}}} + m_{\text{leg}} b (b - 2 \ell_1) + m_{\text{tot}} \ell_1^2, \quad (\text{A.37})$$

$$M_{\text{ds}23} = \frac{m_{\text{trs}} a \ell_1 \sin(\theta_2 - \theta_3)}{\sin(\theta_1 - \theta_3)}, \quad (\text{A.38})$$

$$M_{\text{ds}31} = m_{\text{trs}} a \sin(\theta_1 - \theta_2), \quad (\text{A.39})$$

$$M_{\text{ds}32} = m_{\text{trs}} a \ell_1 \cos(\theta_1 - \theta_2), \quad (\text{A.40})$$

$$M_{\text{ds}33} = I_{\text{trs}/G_{\text{trs}}} + m_{\text{trs}} a^2, \quad (\text{A.41})$$

$$M_{\text{ds}41} = \frac{m_{\text{tot}} \ell_2 - m_{\text{leg}} b \sin^2(\theta_1 - \theta_3)}{\sin(\theta_1 - \theta_3)}, \quad (\text{A.42})$$

$$M_{\text{ds}42} = -m_{\text{leg}} \ell_1 b \cos(\theta_1 - \theta_3), \quad (\text{A.43})$$

$$M_{\text{ds}43} = \frac{m_{\text{trs}} \ell_2 a \sin(\theta_1 - \theta_2)}{\sin(\theta_1 - \theta_3)}, \quad (\text{A.44})$$

$$M_{\text{ds}44} = I_{\text{leg}/G_{\text{leg}}} + m_{\text{leg}} b (b - \ell_2). \quad (\text{A.45})$$

A.3.2 Coriolis, Centrifugal, and Gravity Vector

$$\mathbf{c}_{ds} = \mathbf{c}_{1ds} + \mathbf{c}_{2ds}, \quad (\text{A.46})$$

where

$$\mathbf{c}_{1ds} = \begin{bmatrix} 0 \\ -\frac{\cos(\theta_1 + \gamma)}{\tan(\theta_1 - \theta_3)} m_{\text{tot}} \ell_1 g + (m_{\text{leg}} b - m_{\text{tot}} \ell_1) g \sin(\theta_1 + \gamma) \\ -m_{\text{trs}} a g \sin(\theta_2 + \gamma) \\ \frac{m_{\text{tot}} \ell_2 g \cos(\theta_1 + \gamma)}{\sin(\theta_1 - \theta_3)} + m_{\text{leg}} b g \sin(\theta_3 + \gamma) \end{bmatrix}, \quad (\text{A.47})$$

and

$$\mathbf{c}_{2ds} = \begin{bmatrix} C_{ds11} & C_{ds12} & C_{ds13} & 0 & 0 \\ C_{ds21} & 0 & C_{ds23} & C_{ds24} & C_{ds25} \\ C_{ds31} & 0 & C_{ds33} & 0 & 0 \\ C_{ds41} & 0 & C_{ds43} & C_{ds44} & C_{ds45} \end{bmatrix} \begin{bmatrix} 2 \dot{\ell}_1 \dot{\theta}_1 \\ 2 \dot{\ell}_2 \dot{\theta}_3 \\ \dot{\theta}_1^2 \\ \dot{\theta}_2^2 \\ \dot{\theta}_3^2 \end{bmatrix}, \quad (\text{A.48})$$

with

$$C_{ds11} = -\frac{\cos(\theta_1 - \theta_3)}{\sin \theta_3}, \quad (\text{A.49})$$

$$C_{ds12} = \frac{1}{\sin \theta_3}, \quad (\text{A.50})$$

$$C_{ds13} = \frac{\ell_1 \sin(\theta_1 - \theta_3)}{\sin \theta_3}, \quad (\text{A.51})$$

$$C_{ds21} = m_{\text{tot}} \ell_1 - m_{\text{leg}} b, \quad (\text{A.52})$$

$$C_{ds23} = \frac{\ell_1 (m_{\text{tot}} \ell_1 - m_{\text{leg}} b)}{\tan(\theta_1 - \theta_3)}, \quad (\text{A.53})$$

$$C_{ds24} = \frac{m_{\text{trs}} \ell_1 a \cos(\theta_2 - \theta_3)}{\sin(\theta_1 - \theta_3)}, \quad (\text{A.54})$$

$$C_{ds25} = -\frac{m_{\text{leg}} \ell_1 b}{\sin(\theta_1 - \theta_3)}, \quad (\text{A.55})$$

$$C_{\text{ds31}} = m_{\text{trs}} a \cos(\theta_1 - \theta_2), \quad (\text{A.56})$$

$$C_{\text{ds33}} = -m_{\text{trs}} \ell_1 a \sin(\theta_1 - \theta_2), \quad (\text{A.57})$$

$$C_{\text{ds41}} = -m_{\text{leg}} b \cos(\theta_1 - \theta_3), \quad (\text{A.58})$$

$$C_{\text{ds43}} = \frac{m_{\text{leg}} \ell_1 b \sin^2(\theta_1 - \theta_3) - \ell_2 (m_{\text{tot}} \ell_1 - m_{\text{leg}} b)}{\sin(\theta_1 - \theta_3)}, \quad (\text{A.59})$$

$$C_{\text{ds44}} = -\frac{m_{\text{trs}} \ell_2 a \cos(\theta_1 - \theta_2)}{\sin(\theta_1 - \theta_3)}, \quad (\text{A.60})$$

$$C_{\text{ds45}} = \frac{m_{\text{leg}} \ell_2 b \cos(\theta_1 - \theta_3)}{\sin(\theta_1 - \theta_3)}. \quad (\text{A.61})$$

A.3.3 Torque-Influence Matrix

$$\mathbf{B}_{\text{ds}} = \begin{bmatrix} 0 & 0 & 0 & 0 & 0 & 0 \\ -\frac{\ell_1}{\tan(\theta_1 - \theta_3)} & -\frac{\ell_1}{\sin(\theta_1 - \theta_3)} & 1 & 1 & 0 & 0 \\ 0 & 0 & 0 & -1 & -1 & 0 \\ \frac{\ell_2}{\sin(\theta_1 - \theta_3)} & \frac{\ell_2}{\tan(\theta_1 - \theta_3)} & 0 & 0 & 1 & 1 \end{bmatrix} \quad (\text{A.62})$$

A.4 Equations of Motion in Flight Phase

A.4.1 Coriolis and Centrifugal Vector

The equations of motion in flight phase are given by (2.15). In that equation

$$\mathbf{c}_{\text{fl}} = -m_{\text{tot}} \mathbf{J}_{1\theta}^{\text{T}} \mathbf{g} + \mathbf{c}, \quad (\text{A.63})$$

where \mathbf{c} and $\mathbf{J}_{1\theta}$ are given by (A.6) and (A.11). Based on (A.6), $\mathbf{c} = \mathbf{c}_1 + \mathbf{c}_2$, where \mathbf{c}_1 and \mathbf{c}_2 are given by (A.7) and (A.8). By inspection, it can be verified that $-m_{\text{tot}} \mathbf{J}_{1\theta}^{\text{T}} \mathbf{g} + \mathbf{c}_1 = \mathbf{0}$. Therefore,

$$\mathbf{c}_{\text{fl}} = \mathbf{c}_2. \quad (\text{A.64})$$

A.4.2 Torque-Influence Matrix

$$\mathbf{B}_{fl} = \begin{bmatrix} 1 & 0 \\ -1 & -1 \\ 0 & 1 \end{bmatrix} \quad (\text{A.65})$$

A.5 Jacobian Matrices

$$\mathbf{J}_{1\theta} = \frac{\partial \mathbf{r}_{A_1/G_{tot}}}{\partial \mathbf{q}_\theta} = \begin{bmatrix} \left(\ell_1 - \frac{b m_{leg}}{m_{tot}} \right) \cos \theta_1 & \frac{a m_{trs} \cos \theta_2}{m_{tot}} & -\frac{b m_{leg} \cos \theta_3}{m_{tot}} \\ \left(\ell_1 - \frac{b m_{leg}}{m_{tot}} \right) \sin \theta_1 & \frac{a m_{trs} \sin \theta_2}{m_{tot}} & -\frac{b m_{leg} \sin \theta_3}{m_{tot}} \end{bmatrix}, \quad (\text{A.66})$$

$$\mathbf{J}_{2\theta} = \frac{\partial \mathbf{r}_{A_2/G_{tot}}}{\partial \mathbf{q}_\theta} = \begin{bmatrix} -\frac{b m_{leg} \cos \theta_1}{m_{tot}} & \frac{a m_{trs} \cos \theta_2}{m_{tot}} & \left(\ell_2 - \frac{b m_{leg}}{m_{tot}} \right) \cos \theta_3 \\ -\frac{b m_{leg} \sin \theta_1}{m_{tot}} & \frac{a m_{trs} \sin \theta_2}{m_{tot}} & \left(\ell_2 - \frac{b m_{leg}}{m_{tot}} \right) \sin \theta_3 \end{bmatrix} \quad (\text{A.67})$$

$$\mathbf{J}_{1\ell_1} = \frac{\partial \mathbf{r}_{A_1/G_{tot}}}{\partial \ell_1} = \begin{bmatrix} \sin \theta_1 \\ -\cos \theta_1 \end{bmatrix} \quad (\text{A.68})$$

$$\mathbf{J}_{2\ell_2} = \frac{\partial \mathbf{r}_{A_2/G_{tot}}}{\partial \ell_2} = \begin{bmatrix} \sin \theta_3 \\ -\cos \theta_3 \end{bmatrix} \quad (\text{A.69})$$

$$\mathbf{J}_{21\theta} = \frac{\partial \mathbf{r}_{A_2/A_1}}{\partial \mathbf{q}_\theta} = \mathbf{J}_{2\theta} - \mathbf{J}_{1\theta} = \begin{bmatrix} -\ell_1 \cos \theta_1 & 0 & \ell_2 \cos \theta_3 \\ -\ell_1 \sin \theta_1 & 0 & \ell_2 \sin \theta_3 \end{bmatrix} \quad (\text{A.70})$$

$$\mathbf{J}_{21\ell_1} = \frac{\partial \mathbf{r}_{A_2/A_1}}{\partial \ell_1} = -\mathbf{J}_{1\ell_1} \quad (\text{A.71})$$

$$\mathbf{J}_{21\ell_2} = \frac{\partial \mathbf{r}_{A_2/A_1}}{\partial \ell_2} = \mathbf{J}_{2\ell_2} \quad (\text{A.72})$$

$$\mathbf{h}_1 = \begin{bmatrix} \left(\ell_1 - b \frac{m_{\text{leg}}}{m_{\text{tot}}} \right) \sin\theta_1 \dot{\theta}_1^2 + \frac{m_{\text{trs}}}{m_{\text{tot}}} a \sin\theta_2 \dot{\theta}_2^2 - \frac{m_{\text{leg}}}{m_{\text{tot}}} b \sin\theta_3 \dot{\theta}_3^2 - 2 \cos\theta_1 \dot{\ell}_1 \dot{\theta}_1 \\ \left(b \frac{m_{\text{leg}}}{m_{\text{tot}}} - \ell_1 \right) \cos\theta_1 \dot{\theta}_1^2 - \frac{m_{\text{trs}}}{m_{\text{tot}}} a \cos\theta_2 \dot{\theta}_2^2 + \frac{m_{\text{leg}}}{m_{\text{tot}}} b \cos\theta_3 \dot{\theta}_3^2 - 2 \sin\theta_1 \dot{\ell}_1 \dot{\theta}_1 \end{bmatrix} \quad (\text{A.73})$$

$$\mathbf{h}_2 = \begin{bmatrix} -\frac{m_{\text{leg}}}{m_{\text{tot}}} b \sin\theta_1 \dot{\theta}_1^2 + \frac{m_{\text{trs}}}{m_{\text{tot}}} a \sin\theta_2 \dot{\theta}_2^2 + \left(\ell_2 - b \frac{m_{\text{leg}}}{m_{\text{tot}}} \right) \sin\theta_3 \dot{\theta}_3^2 - 2 \cos\theta_3 \dot{\ell}_2 \dot{\theta}_3 \\ \frac{m_{\text{leg}}}{m_{\text{tot}}} b \cos\theta_1 \dot{\theta}_1^2 - \frac{m_{\text{trs}}}{m_{\text{tot}}} a \cos\theta_2 \dot{\theta}_2^2 - \left(\ell_2 - b \frac{m_{\text{leg}}}{m_{\text{tot}}} \right) \cos\theta_3 \dot{\theta}_3^2 - 2 \sin\theta_3 \dot{\ell}_2 \dot{\theta}_3 \end{bmatrix} \quad (\text{A.74})$$

$$\mathbf{h}_{21} = \mathbf{h}_2 - \mathbf{h}_1 \quad (\text{A.75})$$

Appendix B

Simple Bipedal Model Without Torso

B.1 Details of the Dynamics

B.1.1 Equations of Motion in Passive Single Stance

To derive the EoM in passive single stance we can use the angular momentum balance (AMB) equation of the entire mechanism about the support foot, and of the swing leg about the hip joint. After normalizing these equations by $m_{\text{tot}} \ell^2$ and $\delta m_{\text{leg}} b \ell$, respectively, we can express them in the standard form of (5.11) with the following matrix and vectors.

$$\mathbf{M} = \begin{bmatrix} 1 + 2(\delta - 1 - \cos \phi) \lambda & (\delta - \cos \phi) \lambda \\ 1 - (1/\delta) \cos \phi & 1 \end{bmatrix} \quad (\text{B.1})$$

$$\mathbf{c} = \begin{bmatrix} \lambda \dot{\phi} (2\dot{\theta} + \dot{\phi}) \sin \phi \\ -\sin \phi \dot{\theta}^2 / \delta \end{bmatrix} + (g/\ell) \begin{bmatrix} (\sin(\phi + \theta) + \sin \theta) \lambda - \sin \theta \\ \sin(\phi + \theta) / \delta \end{bmatrix} \quad (\text{B.2})$$

Here, $\lambda = m_{\text{leg}} b / (m_{\text{tot}} \ell)$, and g is the gravitational acceleration.

B.1.2 Velocity Mapping of Impulsive Push-off and Retraction

As mentioned in section 5.3.2 the velocity mapping of the impulsive push-off and retraction can be derived using the momentum conservation/jump equations. However, to show the properties of the mapping matrix, it is preferred to derive the mapping equation using the EoM. Because the mapping is unique, both methods give the same result.

The EoM in (5.11) is not applicable during push-off and retraction, because in that equation $\tau = F = \ddot{\ell} = \dot{\ell} = 0$. The extended EoM for the more general case in which the

stance-leg length ℓ is not necessarily constant and the hip and stance-leg actuators can apply force/torque can be obtained from (i) linear momentum balance equation of the whole mechanism along the stance leg, (ii) angular momentum balance (AMB) equation of the swing leg about the hip joint, and (iii) AMB equation of the whole mechanism about the stance foot. After rearrangement, these three equations can be written in the following standard form:

$$\mathbf{M}_e(\mathbf{q}_e) \ddot{\mathbf{q}}_e + \mathbf{c}_e(\mathbf{q}_e, \dot{\mathbf{q}}_e) = \begin{bmatrix} F \\ \tau \\ 0 \end{bmatrix}, \quad (\text{B.3})$$

where $\mathbf{q}_e(t) = [\ell(t), \phi(t), \theta(t)]^T$, and \mathbf{M}_e and \mathbf{c}_e are the extended versions of \mathbf{M} and \mathbf{c} in (5.11). The extended mass-inertia matrix \mathbf{M}_e is symmetric and positive definite.

Since the velocities are always bounded, and $\mathbf{q}_e(t)$ remains unchanged during the infinitesimal period of impulsive push-off and retraction, between t_{pr}^- and t_{pr}^+ , integrating both sides of (B.3) over the infinitesimal interval $(t_{\text{pr}}^-, t_{\text{pr}}^+)$ results in

$$\mathbf{M}_{e,t_{\text{pr}}^-} \cdot \left(\dot{\mathbf{q}}_{e,t_{\text{pr}}^+} - \dot{\mathbf{q}}_{e,t_{\text{pr}}^-} \right) = \begin{bmatrix} \mathcal{P} \\ -\mathcal{R} \\ 0 \end{bmatrix}, \quad (\text{B.4})$$

where $\dot{\mathbf{q}}_{e,t_{\text{pr}}^-} = \dot{\mathbf{q}}_e(t_{\text{pr}}^-)$, $\dot{\mathbf{q}}_{e,t_{\text{pr}}^+} = \dot{\mathbf{q}}_e(t_{\text{pr}}^+)$, and

$$\mathbf{M}_{e,t_{\text{pr}}^-} = \mathbf{M}_e(\mathbf{q}_{e,t_{\text{pr}}^-}) = \begin{bmatrix} M_{11} & M_{12} & M_{13} \\ M_{12} & M_{22} & M_{23} \\ M_{13} & M_{23} & M_{33} \end{bmatrix}, \quad (\text{B.5})$$

with

$$M_{11} = m_{\text{tot}}, \quad (\text{B.6})$$

$$M_{12} = M_{13} = m_{\text{leg}} b \sin 2\alpha, \quad (\text{B.7})$$

$$M_{22} = m_{\text{leg}} b \ell \delta, \quad (\text{B.8})$$

$$M_{23} = m_{\text{leg}} \ell b (\delta - \cos 2\alpha), \quad (\text{B.9})$$

$$M_{33} = m_{\text{tot}} \ell^2 + m_{\text{leg}} \ell b (2\delta - 4 \cos^2 \alpha). \quad (\text{B.10})$$

Rearranging (B.4) gives the velocity mapping of the impulsive push-off and retraction as

$$\dot{\mathbf{q}}_{\text{e},t_{\text{pr}}^+} = \dot{\mathbf{q}}_{\text{e},t_{\text{pr}}^-} + \mathbf{M}_{\text{e},t_{\text{pr}}^-}^{-1} \begin{bmatrix} \mathcal{P} \\ -\mathcal{R} \\ 0 \end{bmatrix}. \quad (\text{B.11})$$

Now, given

$$\mathbf{M}_{\text{e},t_{\text{pr}}^-}^{-1} = \begin{bmatrix} J_{11} & J_{12} & J_{13} \\ J_{21} & J_{22} & J_{23} \\ J_{31} & J_{32} & J_{33} \end{bmatrix}, \quad (\text{B.12})$$

and considering $t_{\text{pr}}^+ \equiv t_{\text{h}}^-$, we can simplify (B.11) as

$$\begin{bmatrix} \dot{\ell}_{t_{\text{h}}^-} \\ \dot{\phi}_{t_{\text{h}}^-} \\ \dot{\theta}_{t_{\text{h}}^-} \end{bmatrix} = \begin{bmatrix} 0 \\ \dot{\phi}_{t_{\text{pr}}^-} \\ \dot{\theta}_{t_{\text{pr}}^-} \end{bmatrix} + \begin{bmatrix} J_{11} & -J_{12} \\ J_{21} & -J_{22} \\ J_{31} & -J_{32} \end{bmatrix} \begin{bmatrix} \mathcal{P} \\ \mathcal{R} \end{bmatrix} \quad (\text{B.13})$$

The above velocity mapping should be identical to (5.14), so

$$\begin{bmatrix} J_{11} & -J_{12} \\ J_{21} & -J_{22} \\ J_{31} & -J_{32} \end{bmatrix} = \begin{bmatrix} J_{\ell/\mathcal{P}} & J_{\ell/\mathcal{R}} \\ J_{\phi/\mathcal{P}} & J_{\phi/\mathcal{R}} \\ J_{\theta/\mathcal{P}} & J_{\theta/\mathcal{R}} \end{bmatrix}. \quad (\text{B.14})$$

The matrix $\mathbf{M}_{\text{e},t_{\text{pr}}^-}^{-1}$ inherits the symmetry and positive definiteness properties from the mass-inertia matrix \mathbf{M}_{e} . In a positive definite matrix all diagonal elements are positive. Also, based on the Sylvester's criterion [98], all leading principal minors of a positive definite matrix are positive. The k th leading principal minor of a matrix is the determinant of its upper-left

k by k sub-matrix. Therefore, for all walking gaits $J_{11} > 0$, $J_{22} > 0$, and $J_{11} J_{22} - J_{21} J_{12} > 0$, or equivalently

$$J_{\dot{\phi}/\mathcal{R}} < 0, \quad (\text{B.15})$$

$$J_{\dot{\ell}/\mathcal{P}} > 0, \quad (\text{B.16})$$

$$J_{\dot{\ell}/\mathcal{R}} J_{\dot{\phi}/\mathcal{P}} - J_{\dot{\ell}/\mathcal{P}} J_{\dot{\phi}/\mathcal{R}} > 0. \quad (\text{B.17})$$

Moreover, the symmetry of $\mathbf{M}_{e,t_{\text{pr}}}^{-1}$ implies $J_{12} = J_{21}$, or equivalently,

$$J_{\dot{\phi}/\mathcal{P}} = -J_{\dot{\ell}/\mathcal{R}}. \quad (\text{B.18})$$

The push-off impulse \mathcal{P} pushes the hip forward, inducing a clockwise (negative) torque on the swing leg which tends to decrease $\dot{\phi}$. This, together with (B.18) implies

$$J_{\dot{\phi}/\mathcal{P}} = -J_{\dot{\ell}/\mathcal{R}} < 0. \quad (\text{B.19})$$

Similar to the above equation, the inequalities (B.15) and (B.16) can also be derived intuitively by noticing that the push-off impulse increases $\dot{\ell}$ and a retracting hip torque ($\mathcal{R} > 0$) tends to decrease $\dot{\phi}$.

B.1.3 Heel-Strike Velocity Map

Velocities just before and just after the collisional heel-strike are related to each other by conservation of angular momentum of the swing leg about the hip and of the whole mechanism about the leading foot. These equations can be written in the following form:

$$\mathbf{H}^+ \begin{bmatrix} \dot{\theta}_{t_h^+} \\ \dot{\phi}_{t_h^+} \end{bmatrix} = \mathbf{H}^- \begin{bmatrix} \dot{\theta}_{t_h^-} \\ \dot{\phi}_{t_h^-} \\ \dot{\ell}_{t_h^-} \end{bmatrix}, \quad (\text{B.20})$$

where

$$\mathbf{H}^- = [\mathbf{h}_1^- \quad \mathbf{h}_2^- \quad \mathbf{h}_3^-], \quad (\text{B.21})$$

$$\mathbf{H}^+ = [\mathbf{h}_1^+ \quad \mathbf{h}_2^+], \quad (\text{B.22})$$

and

$$\mathbf{h}_1^- = \begin{bmatrix} m_{\text{leg}} b \ell (\delta - 1) \\ 2 m_{\text{leg}} \ell b (\delta - 2 \cos^2 \alpha) + m_{\text{tot}} \ell^2 \cos 2\alpha \end{bmatrix}, \quad (\text{B.23})$$

$$\mathbf{h}_2^- = \begin{bmatrix} 0 \\ m_{\text{leg}} b \ell (\delta - 1) \end{bmatrix}, \quad (\text{B.24})$$

$$\mathbf{h}_3^- = \begin{bmatrix} 0 \\ (m_{\text{leg}} b - m_{\text{tot}} \ell) \sin 2\alpha \end{bmatrix}, \quad (\text{B.25})$$

$$\mathbf{h}_1^+ = \begin{bmatrix} m_{\text{leg}} b \ell (\delta - \cos 2\alpha) \\ m_{\text{tot}} \ell^2 + 2 m_{\text{leg}} b \ell (\delta - 2 \cos^2 \alpha) \end{bmatrix}, \quad (\text{B.26})$$

$$\mathbf{h}_2^+ = \begin{bmatrix} -m_{\text{leg}} b \ell \cos 2\alpha \\ m_{\text{tot}} \ell^2 + m_{\text{leg}} b \ell (\delta - 2 - \cos 2\alpha) \end{bmatrix}. \quad (\text{B.27})$$

The post-heel-strike angular velocities can be directly related to the velocities at the end of passive swing using the velocity map in (5.19), where

$$\mathbf{A}_h = (\mathbf{H}^+)^{-1} \mathbf{H}^- \begin{bmatrix} 1 & 0 \\ 0 & 1 \\ 0 & 0 \end{bmatrix}, \quad (\text{B.28})$$

$$\mathbf{h}_P = (\mathbf{H}^+)^{-1} \mathbf{H}^- \mathbf{M}_{e, t_{\text{pr}}}^{-1} \begin{bmatrix} 1 \\ 0 \\ 0 \end{bmatrix}, \quad (\text{B.29})$$

$$\mathbf{h}_{\mathcal{R}} = -(\mathbf{H}^+)^{-1} \mathbf{H}^- \mathbf{M}_{e, \bar{t}_{\text{pr}}}^{-1} \begin{bmatrix} 0 \\ 1 \\ 0 \end{bmatrix}, \quad (\text{B.30})$$

and $\mathbf{M}_{e, \bar{t}_{\text{pr}}}$ is given by (B.5)-(B.10).

B.1.4 Swing Thrust Velocity Map

The mapping matrix in (5.23) associated with the impulsive swing thrust is

$$\mathbf{t} = \begin{bmatrix} J_{\dot{\theta}/S} \\ J_{\dot{\phi}/S} \end{bmatrix} = \mathbf{M}^{-1} \begin{bmatrix} 0 \\ 1 \\ \frac{1}{\delta m_{\text{leg}} b \ell} \end{bmatrix} = \begin{bmatrix} \frac{\cos 2\alpha - \delta}{m_{\text{tot}} \ell^2 (\lambda (-\cos^2(2\alpha) + \delta^2 - 2\delta) + \delta)} \\ \frac{1 + (2\delta - 4 \cos^2\alpha) \lambda}{m_{\text{leg}} \ell b (\lambda (-\cos^2(2\alpha) + \delta^2 - 2\delta) + \delta)} \end{bmatrix}, \quad (\text{B.31})$$

where the mass-inertia matrix \mathbf{M} is given by (B.1) evaluated at $\phi = -2\alpha$.

B.2 Required Swing-Thrust and Push-Off Impulse for Periodic Walking

Combining equations (5.12), (5.13), (5.19), (5.22)-(2.24) and solving for \mathcal{S} and \mathcal{P} gives (5.26)

and (5.27) where

$$\begin{bmatrix} h_1 \\ h_2 \end{bmatrix} = \begin{bmatrix} \mathbf{E} \mathbf{t} & \mathbf{h}_{\mathcal{P}} \end{bmatrix}^{-1} (\mathbf{E} - \mathbf{A}_{\text{h}}) \begin{bmatrix} f_1(\alpha, V) \\ f_2(\alpha, V) \end{bmatrix}, \quad (\text{B.32})$$

$$\begin{bmatrix} J_{S/\mathcal{R}} \\ J_{\mathcal{P}/\mathcal{R}} \end{bmatrix} = - \begin{bmatrix} \mathbf{E} \mathbf{t} & \mathbf{h}_{\mathcal{P}} \end{bmatrix}^{-1} \mathbf{h}_{\mathcal{R}}, \quad (\text{B.33})$$

where \mathbf{A}_{h} , $\mathbf{h}_{\mathcal{P}}$ and $\mathbf{h}_{\mathcal{R}}$ are given by (B.28)-(B.30), scalar functions f_1 and f_2 relate $\dot{\theta}_0$ and $\dot{\phi}_0$ to α and V and are given by (5.12) and (5.13), vector \mathbf{t} is given by (B.31), and

$$\mathbf{E} = \begin{bmatrix} 0 & 1 \\ 1 & 0 \end{bmatrix}. \quad (\text{B.34})$$

Appendix C

Copyright Permissions

The following three pages include the copyright permissions obtained through the Copyright Clearance Center (RightsLink).



Taylor & Francis
Taylor & Francis Group

Title: The dynamic optimization approach to locomotion dynamics: human-like gaits from a minimally-constrained biped model

Author: S.J. Hasaneini, C.J.B. Macnab, J.E.A. Bertram et al.

Publication: Advanced Robotics

Publisher: Taylor & Francis

Date: Aug 1, 2013

Copyright © 2013 Taylor & Francis

| |
|---|
| User ID |
| <input type="text"/> |
| Password |
| <input type="text"/> |
| <input type="checkbox"/> Enable Auto Login |
| <input type="button" value="LOGIN"/> |
| Forgot Password/User ID? |
| If you're a copyright.com user , you can login to RightsLink using your copyright.com credentials. Already a RightsLink user or want to learn more? |

Thesis/Dissertation Reuse Request

Taylor & Francis is pleased to offer reuses of its content for a thesis or dissertation free of charge contingent on resubmission of permission request if work is published.

[BACK](#)[CLOSE WINDOW](#)



RightsLink®

Home

Create Account

Help



Title: Energetics of walking and running: insights from simulated reduced-gravity experiments

Author: C. T. Farley, T. A. McMahon

Publication: Journal of Applied Physiology

Publisher: The American Physiological Society

Date: Dec 1, 1992

Copyright © 1992, The American Physiological Society

| |
|--|
| User ID |
| <input type="text"/> |
| Password |
| <input type="text"/> |
| <input type="checkbox"/> Enable Auto Login |
| LOGIN |
| Forgot Password/User ID? |

If you're a copyright.com user, you can login to RightsLink using your copyright.com credentials. Already **a RightsLink user** or want to [learn more?](#)

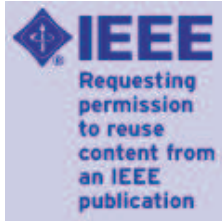
Permission Not Required

Permission is not required for this type of use.

BACK

CLOSE WINDOW

Copyright © 2014 [Copyright Clearance Center, Inc.](#) All Rights Reserved. [Privacy statement.](#) Comments? We would like to hear from you. E-mail us at customercare@copyright.com



Title: Optimal relative timing of stance push-off and swing leg retraction

Conference Proceedings: Intelligent Robots and Systems (IROS), 2013 IEEE/RSJ International Conference on

Author: Hasaneini, S.Javad; Macnab, Chris J.B.; Bertram, John E.A.; Leung, Henry

Publisher: IEEE

Date: 3-7 Nov. 2013

Copyright © 2013, IEEE

| |
|---|
| User ID |
| <input type="text"/> |
| Password |
| <input type="text"/> |
| <input type="checkbox"/> Enable Auto Login |
| <input type="button" value="LOGIN"/> |
| Forgot Password/User ID? |
| If you're a copyright.com user , you can login to RightsLink using your copyright.com credentials. Already a RightsLink user or want to learn more? |

Thesis / Dissertation Reuse

The IEEE does not require individuals working on a thesis to obtain a formal reuse license, however, you may print out this statement to be used as a permission grant:

Requirements to be followed when using any portion (e.g., figure, graph, table, or textual material) of an IEEE copyrighted paper in a thesis:

- 1) In the case of textual material (e.g., using short quotes or referring to the work within these papers) users must give full credit to the original source (author, paper, publication) followed by the IEEE copyright line © 2011 IEEE.
- 2) In the case of illustrations or tabular material, we require that the copyright line © [Year of original publication] IEEE appear prominently with each reprinted figure and/or table.
- 3) If a substantial portion of the original paper is to be used, and if you are not the senior author, also obtain the senior author's approval.

Requirements to be followed when using an entire IEEE copyrighted paper in a thesis:

- 1) The following IEEE copyright/ credit notice should be placed prominently in the references: © [year of original publication] IEEE. Reprinted, with permission, from [author names, paper title, IEEE publication title, and month/year of publication]
- 2) Only the accepted version of an IEEE copyrighted paper can be used when posting the paper or your thesis on-line.
- 3) In placing the thesis on the author's university website, please display the following message in a prominent place on the website: In reference to IEEE copyrighted material which is used with permission in this thesis, the IEEE does not endorse any of [university/educational entity's name goes here]'s products or services. Internal or personal use of this material is permitted. If interested in reprinting/republishing IEEE copyrighted material for advertising or promotional purposes or for creating new collective works for resale or redistribution, please go to http://www.ieee.org/publications_standards/publications/rights/rights_link.html to learn how to obtain a License from RightsLink.

If applicable, University Microfilms and/or ProQuest Library, or the Archives of Canada may supply single copies of the dissertation.

[BACK](#)[CLOSE WINDOW](#)